HOLOCENE VOLCANIC TEPHRA IN THE WILLAMETTE NATIONAL FOREST, WESTERN OREGON: DISTRIBUTION, GEOCHEMICAL CHARACTERIZATION, AND GEOARCHAEOLOGICAL EVALUATION

PHASE I INVESTIGATION

A FINAL REPORT SUBMITTED TO
THE WILLAMETTE NATIONAL FOREST,
EUGENE, OREGON

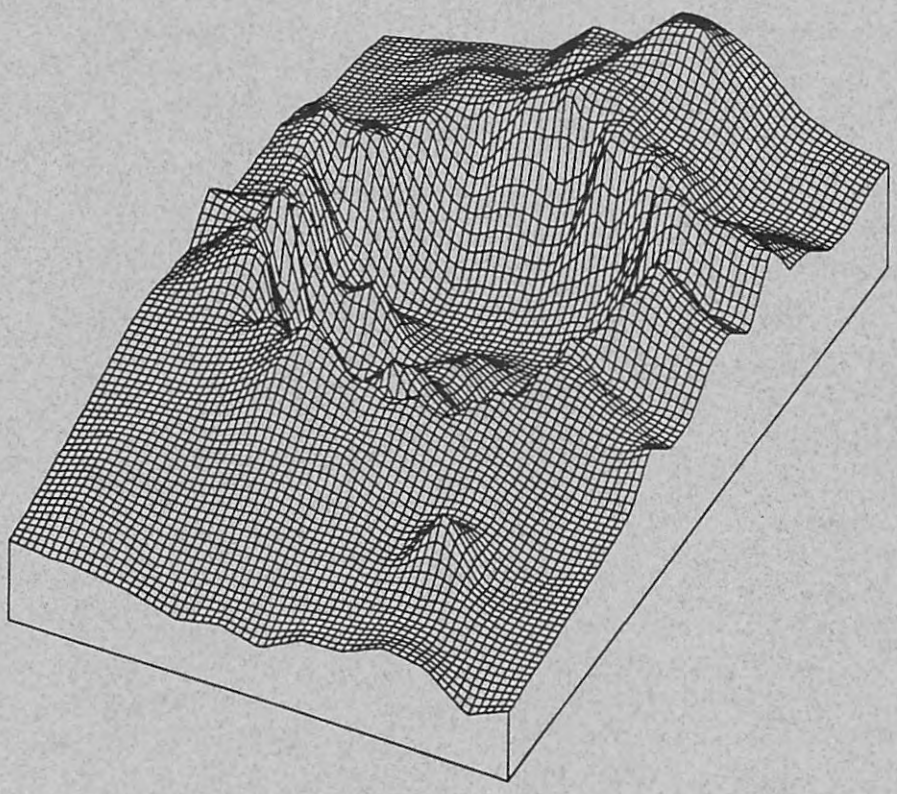

CRAIG E. SKINNER
STEFAN C. RADOSEVICH
1991

HOLOCENE VOLCANIC TEPHRA IN THE WILLAMETTE NATIONAL FOREST, LINN AND LANE COUNTIES, WESTERN OREGON: DISTRIBUTION, GEOCHEMICAL CHARACTERIZATION, AND GEOARCHAEOLOGICAL EVALUATION

PHASE I INVESTIGATION

A Final Report Submitted to the
Willamette National Forest,
Eugene, Oregon

Contract No. 53-04R4-0-2780

By

Craig E. Skinner, M.S., ED.M.
Stefan C. Radosevich, PH.D.
Northwest Research ▪ Trans-World Geology
Eugene, Oregon
1991

ABSTRACT

Many deposits of post-glacial (Holocene) volcanic tephra have been recognized within and immediately adjacent to the boundaries of the Willamette National Forest in western Oregon. Ages of these deposits range throughout much of the last 10,000 years, from as recent as about 1,000 years ago to the beginning of the Holocene Epoch.

The most widespread and voluminous of these tephra deposits originated from Mount Mazama (Crater Lake) during a series of explosive eruptions about 6,845 to 7,015 radiocarbon years ago. Ash from the Mazama eruptions covered the entire present-day Willamette National Forest and still exists in many contexts throughout the region today. It has been identified in several central western Cascades archaeological sites, though Mazama tephra has undoubtedly gone unrecognized in numerous other archaeological investigations. Explosive eruptions of silicic tephra also occurred near South Sister volcano at Rock Mesa and the Devils Hill Dome Chain about 2,000 radiocarbon years ago. Small amounts of tephra from these eruptions are found today in the eastern central periphery of the Willamette National Forest, though none has been identified in any archaeological sites to date.

Numerous Holocene cinder cones are also located within a few kilometers of the Cascade Crest. Basaltic to basaltic andesite tephra is found associated with several of these cinder cones. Although these deposits are areally-restricted (in comparison to the more widespread silicic ashes), they have been identified in a few High Cascades archaeological sites.

Several lines of evidence verify that the eruption of both the silicic and basaltic tephra deposits were coeval with human occupation in the present-day Willamette National Forest. The impact of the airfall tephra events on these prehistoric groups is thought to have been minimal because of the seasonally-utilized nature of the areas that were most affected by the ashfalls (though the effects of the eruptions may have been catastrophic to the northeast of the volcano). Observations of observed ashfalls also suggest that environmental damage caused by tephra falls is quite short-lived. Disruption of aboriginal seasonal procurement of non-critical resources would have lasted only a few years at most and it is likely that the eruption of Mount Mazama and other sources of tephra had little effect on the prehistoric populations utilizing Cascades resources. The major archaeological significance of the airfall deposits of silicic and basaltic ash appears to lie in their potential importance as chronologic tools.

A review of previous tephra-related archaeological research carried out within the Willamette National Forest reveals that the chronologic potential of volcanic ash dating has been only rarely realized. Volcanic ash from Mount Mazama and basaltic tephra sources has almost certainly gone unrecognized in excavations in many parts of the Willamette National Forest. When volcanic tephra has been identified in

archaeological sites, it has often not been used as a temporal marker and the relationship of the tephra to artifactual remains is often only sketchily-described. These problems are attributed to a lack of familiarity by archaeologists with tephrochronologic methods, with tephra identification, and with the geographic distribution of potential Holocene sources of volcanic ash in the Willamette National Forest.

The Volcanic Tephra Project was initiated in order to address several of these shortcomings. An overview of Holocene tephra deposits and tephragenic volcanic activity within the boundaries of the Willamette National Forest study area was assembled to provide background information for future geoarchaeological researchers. Tephra samples were collected from locales within the Willamette National Forest and from potential primary sources of tephra deposits that lay outside the boundaries of the study area. Major and trace element studies of these samples were used to ascertain the potential value of atomic absorption spectrophotometry (AAS) and electron microprobe analysis (EPMA) techniques in characterizing and correlating tephra deposits found at archaeological sites within the study area.

AAS characterization studies of 50 basaltic and silicic tephra samples from 12 geologic sources resulted in varied degrees of success. Low cost, ease of sample preparation, and rapid turnaround time were important criteria in selecting AAS as the primary characterization method for this study. Major and trace element abundances easily distinguished between silicic and basaltic tephra sources, as expected, as well as between the two major silicic source areas (Crater Lake and South Sister). Characterization studies of Mazama paleosols from several locations were less successful, however. These paleosols could not be clearly correlated with the Mazama eruptions, even though their geologic context verified Crater Lake as the source of the ash. Regularities in major and trace element enrichment and depletions relative to the Mazama tephra samples suggests that weathering and contamination by adjoining stratigraphic units played an important role in the differences in chemical composition. In locations where individual pumice lapillus are available for analysis, AAS characterization will be an effective characterization technique. More elaborate prepreparation of bulk samples of paleosols from secondary contexts such as archaeological sites is likely to correct most of the problems encountered. AAS characterization of basaltic tephra deposits showed some promise, though the chemical clustering of different sources was not as marked as for the silicic tephra sources. The chemical characterization of basaltic tephra deposits, however, when combined with a knowledge of the distribution of basaltic tephra sources, may be useful in identifying the geologic source of basaltic tephra in most locations. More elaborate prepreparation procedures are recommended for any future basaltic tephra AAS studies.

EPMA studies of a subset of 9 silicic tephra source samples and a single archaeological sample were used to evaluate the role of this method for future tephra studies in the

study area. EPMA, while being more expensive, requiring more elaborate sample preparation methods, and lacking in analytical precision for the trace elements, was of interest because of the very small sample sizes required for analysis. Individual shards of tephra or small lapilli from archaeological soils can be easily analyzed. Major element abundances were used to characterize pumice lapilli from three geologic sources (Mazama, Rock Mesa, and Devils Hill), paleosols from three secondary geologic contexts, and a paleosol from the Woodduck Site near Mount Jefferson. Visual and statistical analysis of the major element data from this small sample demonstrated that all three sources can be easily distinguished from one another. Additionally, the suspected Mazama paleosols from the geologic and archaeological contexts were clearly correlated with the Mazama source. Based on the success of the EPMA characterization of silicic volcanic ash in the Willamette National Forest, we recommend that further studies be undertaken with a larger geologic source sample. EPMA characterization studies of basaltic tephra remain largely unexplored. The results of AAS analyses of basaltic tephra suggest that major element composition can be used to characterize basaltic tephra and a preliminary research program is recommended if further EPMA studies are undertaken.

We conclude that the geochemical characterization of basaltic and silicic volcanic tephra deposits in the Willamette National Forest will be of further use in archaeological studies in this region. The chronologic information that these ash deposits hold should not be neglected in future archaeological research. Further geochemical studies of basaltic and silicic volcanic ashes in the Willamette National Forest are recommended. We also conclude, though, that these geochemical studies, however compelling they might be to the archaeological researcher, may be needed only on rare occasions. A familiarity with the Holocene volcanic history of the region, with basic geological field techniques, and with tephra identification methods may be all that is needed to identify the geologic sources of most tephra deposits encountered. We recommend further research not only in the chemical characterization of regional basaltic and silicic volcanic ash sources, but in the geological study of Holocene tephra sources. Of particular importance for future geoarchaeological and geological studies of volcanic tephra is the detailed identification of the areal distribution of ash from these sources and continued geochronological study of the tephragenic volcanic activity in the study region.

PREFACE

The Willamette National Forest Volcanic Tephra Project was conducted for the Willamette National Forest under contract number 53-04R4-0-2780. All field work and laboratory analysis (with the exception of the atomic absorption analyses) was conducted by Craig E. Skinner and Stefan C. Radosevich. Atomic absorption analyses of the volcanic tephra samples were performed by Christine McBirney, Center for Volcanology, University of Oregon.

During the 1990 field season, we visited nearly all the known and potential tephra sources that we had identified in the study area. We did not reach the Carver Lake vents at the South Sister - our observations about tephra at the Carver flow in that area came from earlier field work. We considered it unlikely that basaltic tephra from Horseshoe Cone (Bear Butte) would be found in the Willamette National Forest and made no attempt to sample this source.

Some of the terminology that is used throughout this report may be unfamiliar to archaeologists. We have introduced many of the terms in Part II of the report and have defined them in Appendix One, the glossary. All terms defined in the glossary (except acronyms) are italicized at their first appearance in each major section of the text.

We hope that this initial Willamette National Forest volcanic tephra study will stimulate further research and the increased use of tephrochronologic methods in future archaeological research. Though we were a little surprised by our own conclusions, we do see an important place for tephrochronologic studies in the future of archaeological research in this region.

ACKNOWLEDGEMENTS

We thank Carl Davis and Cathy Lindberg for making this project a possibility. Cathy Lindberg served as the Contracting Officer's representative and cheerfully provided her time, help, library, and cooperation throughout the project.

We would also like to extend our appreciation to: Linda Audrain, for a thorough edit of the manuscript; David Whitson, for his editing and numerous improvements to Section V of the report; Jon Silvermoon, for early conversations about volcanic tephra in the Willamette National Forest; Christine McBirney, for her excellent AAS analyses; Gordon Goles, for his productive comments and suggestions; Alexander R. McBirney, for his suggestions that aimed us toward atomic absorption analysis of the samples; Felicia Beardsley, for the archaeological samples from the Woodduck Sites, and Eric Bergland, for the literature on the McKenzie District sites.

TABLE OF CONTENTS

IV
VOLCANIC TEPHRA AND WILLAMETTE NATIONAL FOREST PREHISTORY AND ARCHAEOLOGY

V
GEOCHEMICAL CHARACTERIZATION OF TEPHRA FROM WILLAMETTE NATIONAL FOREST LOCATIONS

VI
CONCLUSIONS AND RECOMMENDATIONS

APPENDICES

FIGURES AND PLATES: COVERS AND FRONTISPIECE

1. Front Cover. Perspective diagram of the Crater Lake Caldera in the southern High Cascades of Oregon as it might have appeared immediately following the climactic eruptions of about 6850 years ago. Topographic data are from Crater Lake East and Crater Lake West 7½' U.S. Geological Survey topographic maps; bathymetric data are from Byrne (1962).

2. Page prior to Introduction. Map showing the distribution and thickness of Crater Lake pumice. This map, the first relatively accurate depiction of the distribution of airfall tephra from the Mazama eruptions, is from Howel Williams' classic 1942 study of Crater Lake National Park (Williams, 1942:70). Since then, the map has appeared in many publications.

3. Page prior to Volcanic Tephra: An Introduction. The May 18, 1980, eruption of Mount St. Helens in Washington. The plume of ash from this eruption rose to an elevation of about 63,000 feet and was spread eastward several hundred kilometers across the western United States. This Plinian eruption of volcanic tephra was not unlike the 7,000 B.P. eruptions of ash from Mount Mazama, though on a considerably smaller scale.

4. Page prior to Sources of Holocene Volcanic Tephra in the Willamette National. Mount Mazama as it might have appeared immediately before the collapse of the summit during the climactic eruptions. From a painting by Paul Rockwood.

5. Page prior to Volcanic Tephra and Willamette National Forest Prehistory. The pumice found during the 1983 excavations of Vine Rockshelter was initially attributed to a Mazama Mimic tephra source. Later reanalysis of the volcanic ash correctly identified Mount Mazama as the source of the rockshelter deposits.

6. Page prior to Geochemical Characterization of Tephra. Chernoff faces were used by Skinner and Radosevich (1989) to look for geochemical similarities between characterized volcanic tephra from the Vine Rockshelter and 35LA51 archaeological sites and potential geologic sources of ash. This graphical statistical technique, developed by Chernoff (1973), is surprisingly effective for correlating archaeological samples with tephra sources. In the pictured faces, data from 10 different trace elements are visually displayed as facial characteristics. Similarities in faces indicates similarities in multi-element composition. From left to right and top to bottom: faces 1-4 - tephra from the two archaeological sites; faces 5-10 - tephra from Mount Mazama; faces 11-13 - tephra from Newberry Volcano; faces 14-17 - tephra from the geochemically-indistinguishable Rock Mesa and Devils Hill Dome Chain eruptions; face 18 - tephra typical of that from several Holocene eruptions in the Medicine Lake Highlands, California.

7. Page prior to Conclusions and Recommendations. Perspective diagram of the Crater Lake caldera as it might have appeared shortly after the climactic eruptions of the volcano. This image was created from the same digitized topographic data as the cover illustration.

FIGURES: MAIN TEXT

PLATES

TABLES

I.
INTRODUCTION

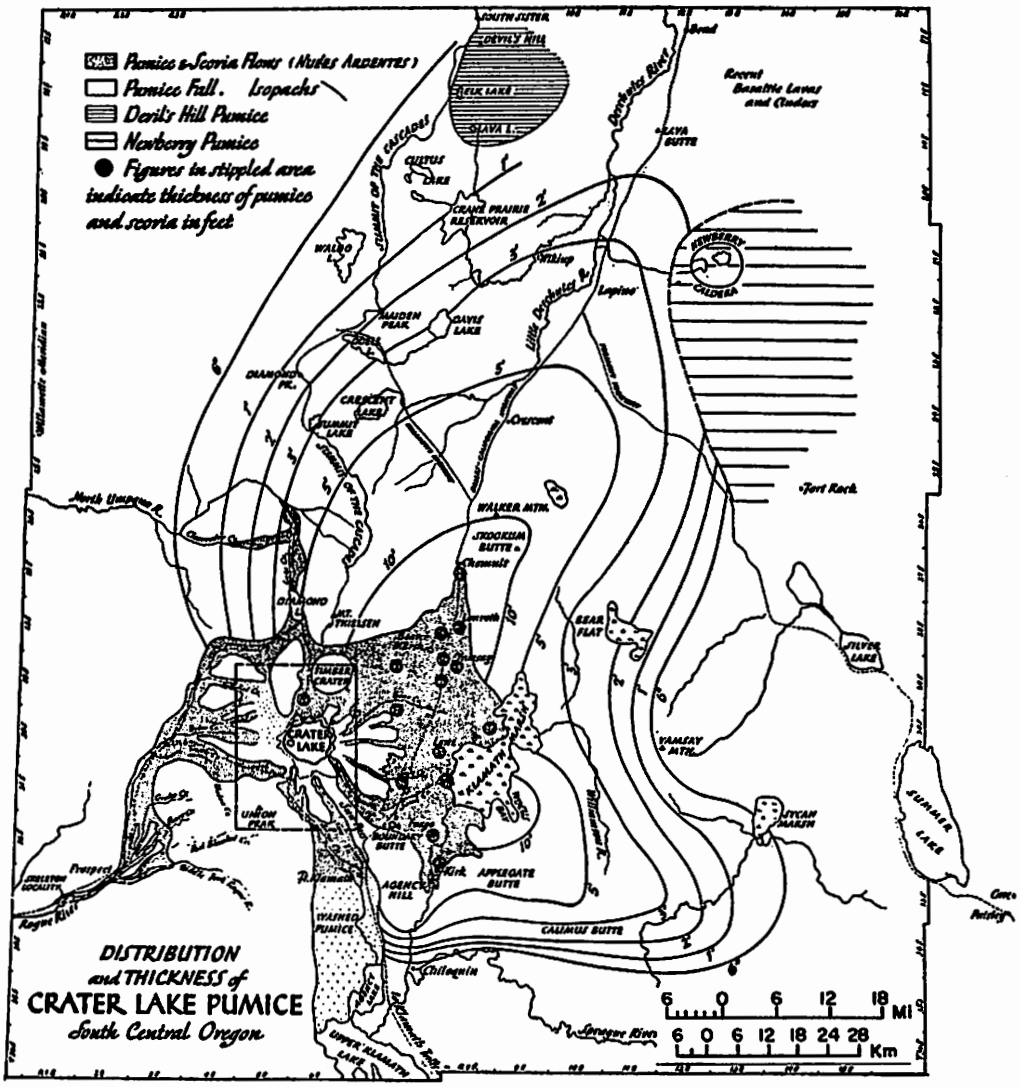

HOLOCENE VOLCANIC TEPHRA IN THE WILLAMETTE NATIONAL FOREST: DISTRIBUTION, CHARACTERIZATION AND GEOARCHAEOLOGICAL EVALUATION

INTRODUCTION

The purpose of this document is to present the results of a preliminary (Phase I) research investigation of *Holocene* (post-glacial) sources and deposits of volcanic *tephra* within and immediately peripheral to the Willamette National Forest of Oregon.

ARCHAEOLOGICAL CHRONOLOGIES IN THE WILLAMETTE NATIONAL FOREST

Prehistoric cultural chronologies are currently poorly-defined and very generalized in most areas of the Willamette National Forest of Oregon. Up to 1987, only 13 radiocarbon dates from seven archaeological sites had been recorded in the Willamette National Forest (Minor, 1987:41). Since that time, only a few additional radiocarbon dates have been added. As a result, chronological estimates have been largely dependent on the cross-dating of projectile point sequences developed in adjoining regions (Baxter, 1986a:103-126; Minor, 1987:41-42,159). Recent limited obsidian hydration studies (see Lindberg-Muir, 1988, for example) have also provided some raw data for chronologic research. Without more reliable radiocarbon and *tephrochronologic* dates with which to calibrate the rates of obsidian hydration, though, these hydration data can do little more than test for stratigraphic integrity or relative chronologies at archaeological sites.

Tephrochronologic methods, however, offer the potential of a relatively simple and cost-effective *chronostratigraphic* approach for determining relative and absolute age relationships at Willamette National Forest archaeological sites. In addition, because of the geographically widespread distribution of some volcanic ash deposits, tephrochronological methods can provide a valuable tool for the dating and regional correlation of associated materials at archaeological sites. It is absolutely essential, however, that geoarchaeological studies of tephra deposits, their sources, and the appropriate *characterization* and correlation methods precede any serious tephrochronologic archaeological applications in a given region. Archaeologists, though they may be eager to apply geological methods to archaeological problems, must give adequate attention to the crucial initial geoarchaeological research that must be carried out prior to reliable archaeological applications of these methods. The principal general objective of this overview and the tephra research that is reported here, then, is to provide the initial data needed for reliable future applications of tephrochronologic methods to archaeological problems within the Willamette National Forest.

A COMPELLING NEED FOR TEPHROCHRONOLOGIC RESEARCH IN THE WILLAMETTE NATIONAL FOREST

The area now encompassed by the Willamette National Forest was completely blanketed by *silicic* volcanic tephra during the 6,850 - 7,000 B.P. eruptions of Mount Mazama. When preserved in favorable environments, this well-dated stratigraphic horizon offers the potential to provide valuable intra- and inter-site chronologic information. The 2,000 B.P. eruptions of silicic tephra from several vents in the Rock Mesa area on the eastern border of the Willamette National Forest also offer some regional tephrochronologic potential (figure 1).

Less well-known and only moderately well-documented in the geologic literature are the Holocene *basaltic* eruptions of the central High Cascades. Basaltic tephra originating from cinder cones located within about 10 km of the Cascade Crest was erupted throughout the Holocene (figure 1). Some of the most recent basaltic volcanic activity may have ceased on the southern slopes of Mt. Jefferson only about 1,000 years ago. These basaltic vents and their associated tephra deposits are distributed within the Willamette National Forest from the upper southern slopes of Mt. Jefferson to the southern flanks of the South Sister. The archaeological and chronological significance of this basaltic tephra remains largely uninvestigated to date and only a few archaeological sites have been found in association with the tephra (see Section IV). Despite the fact that deposits of basaltic tephra are significantly more localized in their spatial distribution than the much more geographically dispersed silicic volcanic ashes, they still have considerable potential for use in the development of localized chronologies.

The identification and characterization (fingerprinting) of the many deposits of tephra in the Willamette National Forest hold chronological potential that can prove valuable for future archaeological studies in the region. The data provided in this overview are designed to form the foundations on which future tephra studies in the Willamette National Forest can rest.

RESEARCH OBJECTIVES AND STRATEGIES

Several explicit research objectives and strategies were developed as part of the Willamette National Forest tephra research project:

1. **Identification of previously distinguished and potential Holocene (post-glacial) deposits and eruptive vents of basaltic and silicic tephra within the Willamette National Forest.**

The identification of potential tephra-producing source vents and deposits in the Willamette National Forest was based on a comprehensive survey of the literature and a search of aerial photographs of the High Cascades area. This was followed by field reconnaissance investigations of most of the known and potential tephra source areas.

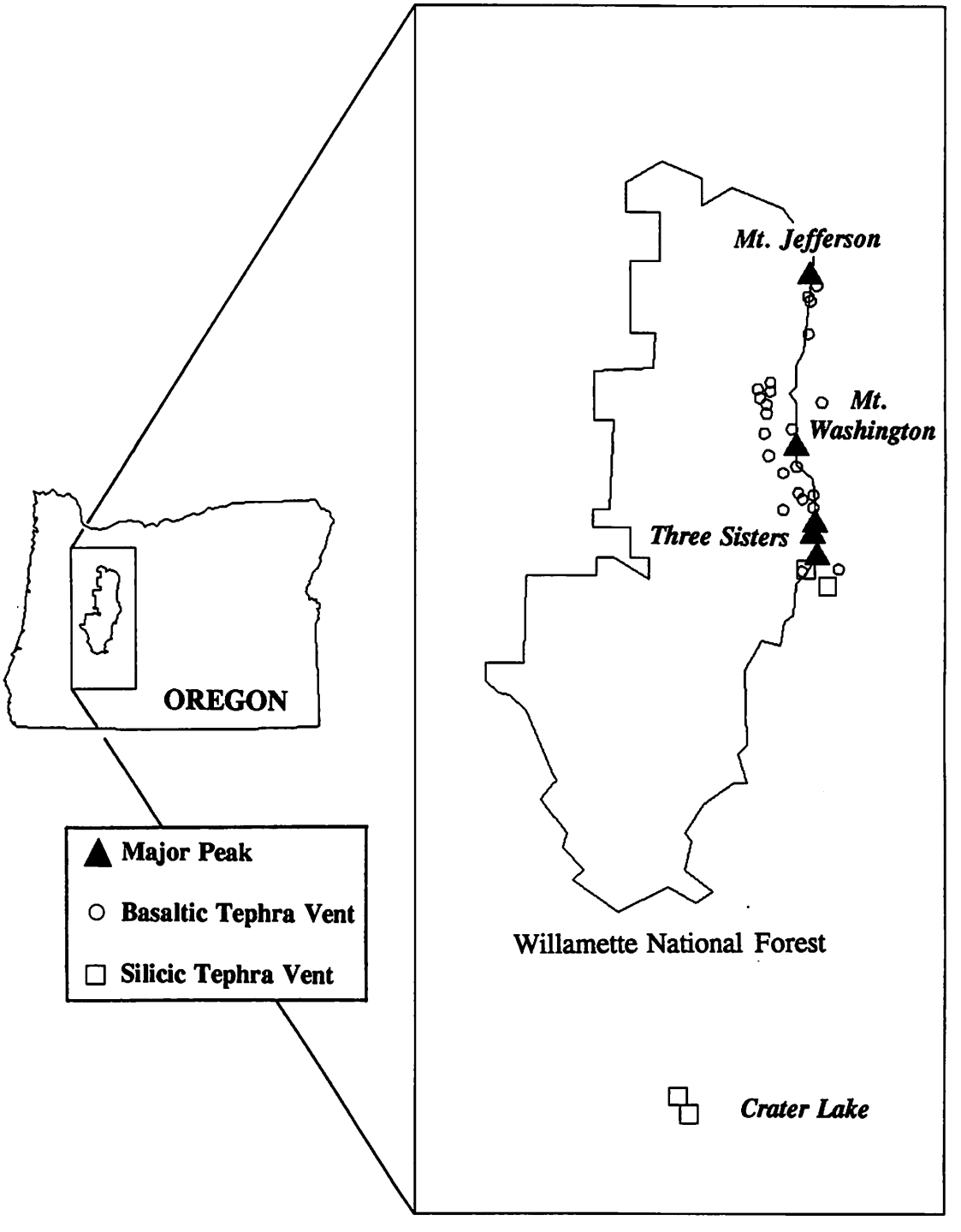

Figure 1. Distribution of Holocene volcanic vents and sources of tephra deposits within the Willamette National Forest.

2. **Preliminary description and initial determination of the areal distribution and regional stratigraphy of the tephra deposits.**

Most of the known and potential tephra sources that were identified were examined in the field. The approximate spatial distribution and stratigraphic relationships of volcanic tephra were determined by examination of natural exposures, artificial exposures such as road and trail cuts, and occasional stratigraphic test pits. These observations were incorporated into Section III of this document, a description of the sources of the tephra deposits in the Willamette National Forest.

3. **Preliminary geochemical characterization studies of the major silicic and basaltic sources of tephra.**

In this initial evaluation, samples of tephra selected to represent maximum chronological, spatial, and geochemical variation during eruptive events were collected at major tephra sources within and adjacent to the Willamette National Forest. This included tephra from Mount Mazama, Rock Mesa, the Devils Hill Dome Chain, Forked Butte, South Cinder Peak, Sand Mountain, Nash Crater, Little Nash Crater, the Lost Lake Group, Belknap Crater, Yapoah Crater, and Collier Cone (figure 1). While several analytical methods were available for the geochemical characterization of tephra samples, atomic absorption analysis (AAS) was selected for the initial primary characterization of the tephra. AAS provided a combination of low sample cost, minimal sample preparation, rapid turn-around time, and proven effectiveness. Fifty samples of tephra from geological and archaeological contexts were analyzed with AAS. An additional eleven samples of silicic tephra were also characterized using the electron microprobe (EPMA). Microprobe analysis of the ash, while entailing more detailed sample preparation, greater expense, and lower precision, was evaluated because of its potential in characterizing very small fractions of tephra. In addition, the feasibility of using already-existing published compositional data from several different analytical facilities was investigated through an interlaboratory comparison of geochemical data.

4. **Evaluation of the geoarchaeological significance and potential of tephrochronologic methods in the Willamette National Forest.**

What is the potential archaeological significance of tephrochronologic methods in the Willamette National Forest? How can tephrochronologic methods best be used in archaeological research in the study area? What techniques can be effectively utilized to identify the geologic sources of volcanic ash? What problems are archaeologists using tephrochronological methods likely to encounter? How effective have previous archaeological studies been in using tephra-related data? Are further studies of volcanic tephra within the Willamette National Forest warranted? These and similar questions were addressed in this stage of the research and are discussed throughout this overview.

5. Overview of volcanic tephra-producing activity in the Willamette National Forest.

An overview of tephrochronologic methods, tephra-producing (*tephragenic*) volcanic activity in the Willamette National Forest, the results of geochemical characterization studies, and the application of tephrochronologic methods to archaeological problems were all integrated into the final report for this project. This overview was intended to act as an initial reference source for future workers in the Willamette National Forest until further tephra studies are undertaken.

II.
VOLCANIC TEPHRA: AN INTRODUCTION

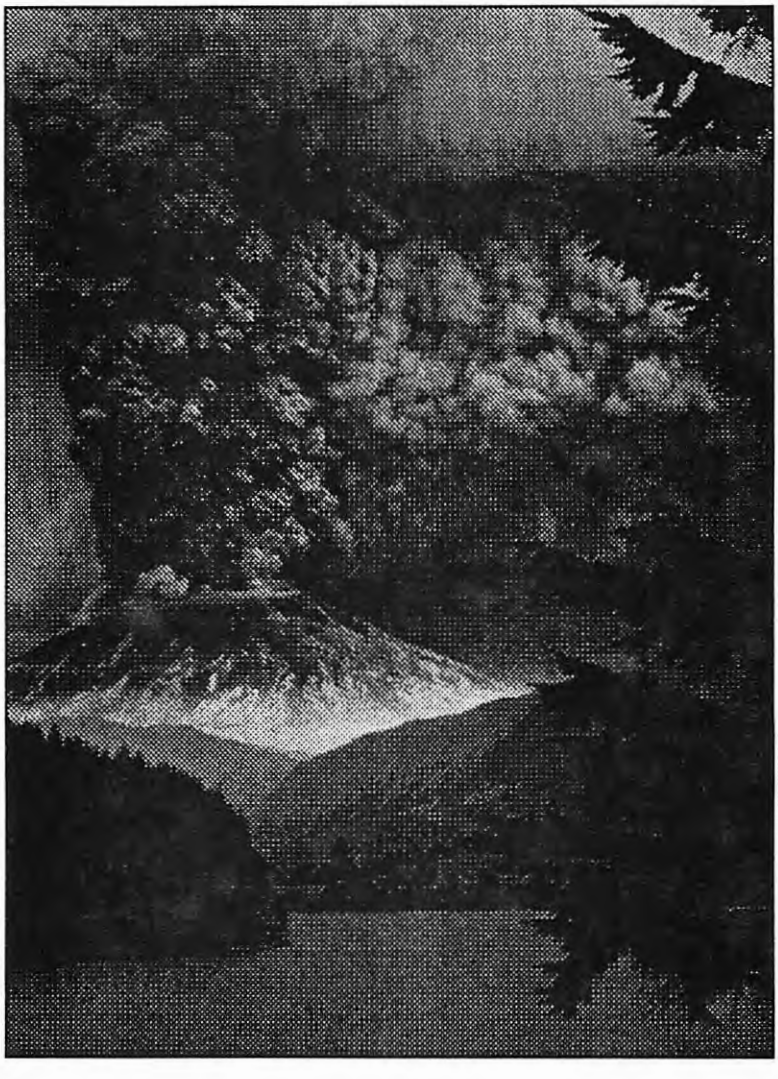

VOLCANIC TEPHRA: AN INTRODUCTION

WHAT IS VOLCANIC TEPHRA?

The term *tephra* refers to all *pyroclastic ejecta* or fragmental material that are blown into the air through explosive eruptive volcanic activity (Thorarinsson, 1981). When speaking in a non-specific way of airfall pyroclastic materials, tephra is the general term of choice. Individual tephra fragments ejected during these explosive volcanic eruptions are termed *pyroclasts*. Eruptive activity that produces volcanic tephra may be called *tephragenic* eruptions.

The chemical composition of tephras is of particular importance in understanding tephragenic volcanic activity and their deposits. It is the composition of the *magmas* from which tephras are derived, particularly the *silica* composition, that ultimately determines most of the characteristics of tephra eruptions and their resultant deposits. In the current project, tephras have been classified rather broadly on the basis of their silica composition as either *basaltic* or *silicic*. Basaltic tephras are those which have a silica composition of between 45 and 57 weight percent oxide. In this project, unless otherwise specified, the category of basaltic tephras explicitly includes tephras of a *basaltic andesite* composition, usually considered to have a silica content of between about 53 and 57 percent. The silicic category of tephras includes, for the purposes of this project, tephras of a composition described in the literature as *rhyolitic*, *dacitic*, or *rhyodacitic* (see Appendix 2). All *Holocene* tephras found within the Willamette National Forest fall within the boundaries of these two loosely-defined compositional categories. No *Holocene* tephras of an intermediate (*andesitic*) silica content were found.

Tephra fragments from terrestrial vents are generally transported in one of two different ways (figures 2 and 3):

1. They are transported through the air and fall back to the surface as *airfall* or *fallout* deposits. All the Holocene tephra deposits that are known in the Willamette National Forest are of an airfall origin. Airfall deposits are typical of tephras of both basaltic and silicic composition.

2. They are transported by ashflows to become *pyroclastic flow* deposits. These ashflows or *glowing avalanches* are created by the near-vent collapse of eruption columns, by the low-pressure "boiling over" from vents, or from directed lateral blasts from vents. Tephra suspended in hot gases is carried away from the vent as a gas-charged flow. These ash flows follow valleys and topographic lows and often move several tens of kilometers from the vent. Excellent examples of pyroclastic flow deposits can be found in the upper Umpqua River Valley immediately west of Crater Lake where they are well-exposed in highway roadcuts. No pyroclastic flow deposits have been identified within the Willamette National Forest, though ash flows from the

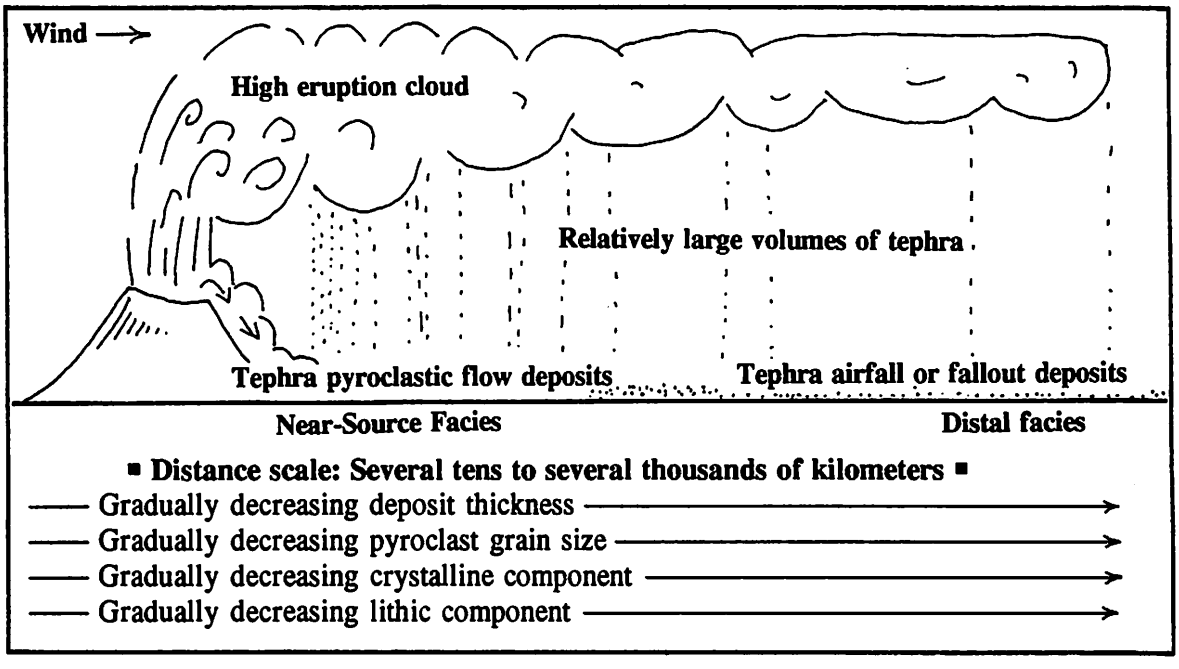

Figure 2. Typical Plinian-style eruption of silicic tephra. Examples of tephra deposits in the Willamette National Forest that originated by Plinian activity are Mazama tephra and the tephra from the vents located on the southern slopes of the South Sister Volcano.

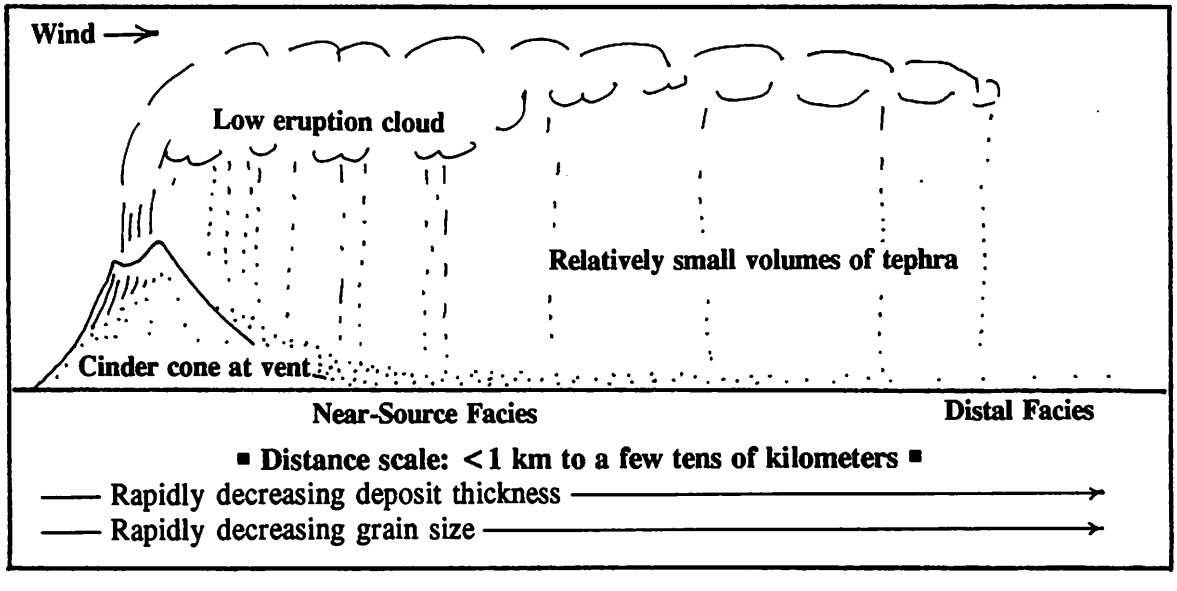

Figure 3. Typical Strombolian-style eruption of basaltic tephras. Numerous deposits of tephra associated with Holocene cinder cones can be found in the Willamette National Forest near the Cascade Crest from the southern slopes of Mount Jefferson to the southern flanks of the South Sister volcano.

climactic eruptions of Mount Mazama nearly reached the current southern boundary of the study area (figure 6). Pyroclastic flow deposits are limited almost entirely to volcanic tephras of a silicic composition.

A third type of common eruptive process, the *base surge*, has also been identified in association with tephragenic eruptions. Base surge deposits result from violently explosive eruptions such as those that result from the contact of magma and water (hydromagmatic eruptions). No base surge deposits were identified within the Willamette National Forest.

Classification of Tephra

A variety of different classification schemes exist for describing volcanic tephra. These schemes are based on grain size, chemical composition of pyroclasts and magma, genesis of the pyroclasts, environment of deposition, and mechanism of transport and deposition. A simplified classification scheme based on silica composition (there are many others; see Schmid, 1981, and LeBas et al, 1986, for some recent developments) was just outlined. The most commonly used classification scheme and the one best-suited for geoarchaeological studies of tephra deposits, though, is based on grain size (Fisher, 1961; Williams and McBirney, 1979:127-132; table 1).

GRAIN SIZE (MM)	TEPHRA FRAGMENTS (PYROCLASTS)		TEPHRA DEPOSITS (UNCONSOLIDATED)
256	Blocks and Bombs	Blocks and Bombs	Agglomerate
64	Lapilli		Lapilli layer or lapilli bed
2	Coarse		Coarse Ash
1/16	Fine	Ash	Fine Ash

Table 1. Classification of volcanic tephra by grain size (adapted from Fisher, 1961, and Schmid, 1981).

The grain size of a tephra deposit is strongly dependent on the distance of the deposit from the vent. A coarse-grained deposit, for example, is a reliable sign of the proximity of a vent. While fine-grained deposits usually signal "farness" from a vent, Walker (1971) cautions that the presence of fine-grained deposits is not always a reliable indicator of vent distance. In general, though, grain size decreases as a function of the distance of the deposit from the vent (Fisher, 1964 and Walker, 1971). This characteristic may be sometimes used to identify the primary sources of proximate deposits of tephras from different primary sources. In the South Sister area of the Oregon High Cascades, for example, *lapilli* of silicic tephra from the Mazama eruptions and from the Rock Mesa and Devils Hill eruptions co-occur in many deposits. The differences in grain size alone between the Mazama and South Sister deposits are often enough to distinguish between their sources.

Besides the previously introduced terminology relating to chemical composition, transport methods, and grain size, a few other terms useful for describing tephra are introduced here.

Three common names based on degree of vesicularity, *scoria*, *cinders*, and *pumice*, are often used in describing tephra deposits. These names do not refer to size but they most commonly describe *vesicular* pyroclasts that fall into the lapilli or larger size range. Fresh pumice is usually a white to gray or brown silicic glass (occasionally basaltic) which will often float on water. Scoria and cinders (synonymous terms) are usually of a basaltic composition, and though they are quite vesicular they will readily sink in water (Williams and McBirney, 1979:132-133; Fisher and Schmincke, 1984:92).

CHARACTERISTICS OF TEPHRAGENIC ERUPTIONS

The largest volumes and most widespread geographic dispersals of volcanic tephra are produced primarily by eruptions of a *Plinian* type, the same style of eruption that took place at Crater Lake about 7,000 years ago. Considerably lesser and more areally-restricted quantities of volcanic tephra are produced by *Strombolian* style eruptions, the style that is typical of that which produces basaltic *cinder cones*. Strombolian-style eruptive activity was responsible for the deposition of the numerous deposits of tephra of basaltic to basaltic andesite composition that lie within the present-day boundaries of the Willamette National Forest. (The reader is directed to Heiken and Wohletz, 1965; Fisher and Schmincke, 1984, and Williams and McBirney, 1979, for further discussions of other eruptive styles).

Most tephras come from new magma that rises through volcanic conduits to a surface vent. As the rising magma approaches the surface, pressure is lowered, releasing the dissolved gases (volatiles) which are an important constituent of the magmas. The release of these dissolved gases (exsolution) drives the eruptive process in a fashion similar to that of a shaken bottle of soda whose pressure is suddenly lowered by the

opening of the cap. Early in an eruptive phase, while the amount of volatiles is still high, the explosiveness of the volcanic activity is at its greatest. It is this stage that typically produces the greatest volume and widest dispersal of volcanic tephra. Later, when many of the gases have escaped from the magma, activity becomes quieter; this stage of the eruption is typified by the extrusion of flows of lava. The maximum size of pyroclasts deposited at any single location usually marks these early stages of eruptive activity.

The explosiveness of a volcanic eruption is governed in part by the amount of dissolved gases in the magma, but is also dependent on the viscosity of the magma. The thicker and more viscous the magma, the greater the potential for explosive eruptions during the release of the volatiles. The viscosity of the magmas is directly related to their chemical composition with the amount of silica (SiO^2) being the most important variable - the greater the amount of silica, the higher the viscosity, and the greater the potential for explosive eruptive activity. Eruptions of high-silica (silicic) magmas such as those produced at Crater Lake or during the 1980 activity of Mount St. Helens are those, then, that tend to produce very explosive volcanic events that distribute pyroclastic materials (tephra) great distances. It is not unusual for silicic tephra from these eruptions to travel hundreds, or even thousands of kilometers, from their sources. The eruptions of less viscous magma of much lower silica composition (basaltic to basaltic andesite), are much less explosive - tephra produced during these eruptions often travels no more than a few kilometers from their vents.

The dispersal and grain size characteristics of pyroclastic fall deposits are largely dependent on wind direction and strength, the height of the eruptive column, the style of activity (Plinian versus Strombolian), and the degree of fragmentation of the magma. Wind strength and direction, in particular, are critical in determining the shape of the tephra depth *isopachs* and the grain size *isopleths* of a tephra fall deposit (Self et al., 1974). The most characteristic pattern to a single tephra sheet is that of a fan-shaped deposit with the source somewhere near the apex (see figure 4 for some examples). Fairly symmetrical fallout patterns are also reported, particularly those resulting from low intensity basaltic eruptions with low eruptive columns. All fallout tephra sheets tend to systematically thin out along an axis radiating away from the source, though the rate at which the tephra thins in typical asymmetrical fallout sheets is dependent on the direction of the deposits from the source. These tephra sheets are best described with an isopach map constructed from many measurements of the thickness of the tephra deposits.

Unlike the horizontally-bedded deposits that result from most depositional processes, *primary* airfall tephra units are *mantle-bedded* units that follow the topographic contours of the terrain that they cover. (This mantle-bedding is illustrated in many High Cascades roadcuts where silicic and basaltic tephras mantle older glacial deposits; see plate 11 for an example). Volcanic tephra, though, is easily eroded. After the initial deposition of airfall tephra, a variety of geomorphic processes act upon the ash

to remove or transport it to new contexts. The most important of these processes are fluvial and aeolian transport. Volcanic tephra is often rapidly stripped from steep slopes and redeposited in depressions or basins (Malin et al., 1983). As a result of these redepositional processes, the thickness of *reworked* tephra deposits in even small basins may considerably exceed the original thickness of the primary airfall deposit. These redeposited or reworked deposits of ash are termed *secondary* deposits.

Characteristics of Silicic Tephras and Plinian Eruptions

Widely dispersed layers of pumice and ash (and their associated pyroclastic flows) derived from high eruption clouds are typical of Plinian style eruptive activity. The explosive eruption of large quantities of silicic magmas is often associated with the collapse of large calderas such as the one now holding Crater Lake. Plinian eruptions need not always be large volume, though. Relatively small-volume eruptions such as those that took place near the South Sister in the central Oregon Cascades are often associated with the extrusion of silicic lava domes.

During the eruption, gas-driven particles are ejected into the air, where they rapidly solidify and are carried leeward by the winds. The explosive decompression of the gas-charged magma creates a very vesicular ash that may rise to great heights before falling back to the surface as an airfall tephra blanket. The resultant tephra deposits are composed primarily of glassy particles created by the rapid quenching of the liquid magma, crystalline minerals that were present in the magma, and fragments of rocks that were torn from the vent wall or blown from the vent area. These three principal components of tephras are known, respectively, as their *vitric*, *crystalline*, and *lithic* components.

The relative proportions of the vitric, crystalline, and lithic fraction in a tephra unit are strongly dependent on its distance from the source vent. As the eruption cloud moves downwind from the vent, the denser and larger crystalline fraction is winnowed out through *aeolian fractionation*, relatively enriching the vitric component (Fisher and Schmincke, 1984:156-162; Felitsyn and Kir'yanov, 1990). Each of these three components is also chemically distinctive and these relative changes in the proportions of different fractions often result in differences in the *bulk composition* of samples collected at different distances from the source vent. As a result, bulk samples of tephra must be cautiously when chemical analysis of the samples is to be conducted. The chemical composition of the vitric fraction, however, is quite consistent over long distances, and it is this component that is often isolated for geochemical studies of silicic tephra. A variety of chemical and physical techniques can be used to separate and clean the vitric component for analysis (Borchardt, 1969:157-159; Steen-McIntyre, 1977:64-78).

Post-depositional weathering and alteration of the glassy silicic fraction must further be taken into account in the analysis of the tephra. The hydration and post-

depositional alteration of the glass over time (diagenesis) can result in changes in physical characteristics such as the index of refraction (Steen and Fryxell, 1965). Diagenetic changes can also influence the chemical composition of natural glasses. Elements such as Na, K, Ca, Li, Fl, and U may be relatively enriched or depleted as weathering progresses (Zielinski et al., 1977; Fisher and Schmincke, 1984:327-345).

The morphological characteristics of the high-silica tephras are related to the higher viscosities of the magmas from which they were derived. The resulting tephras consist mainly of varieties of pumice or their fragments. Nearly all these pumices are angular and highly vesicular (plate 22). They may be rather massive with few *vesicles* or may be highly vesicular. When viewed with a low-magnification microscope or hand lens, the vitric component of these high-silica tephras is often characterized by a frothy glassy texture and the presence of intact vesicles; fragmental pumice often retains a portion of the bubble-wall shape and may appear as curved, flat, or Y-shaped glass plates or *shards* (Heiken, 1972 and 1974; Heiken and Wohletz, 1985). This latter characteristic may be important in identifying fine-grained silicic tephra from deposits far removed from the primary vents (*distal facies*). Tephra shard morphology is related to chemical composition and eruptive style and may be sometimes used to characterize or distinguish individual tephra deposits.

Characteristics of Basaltic Tephras and Strombolian Eruptions

This eruptive style, named after the eruptive characteristics of Stromboli Volcano in the Mediterranean, typically produces a cinder cone at the vent. These cinder cones are composed of coarse scoria and ash that is ballistically deposited around the vent; finer ash is carried away by the wind, placing the highest point of the rim of most cinder cones on the leeward side of the vent (Heiken and Wohletz, 1985:34-45; Wood, 1980). The high point of the undisturbed cone rim may also be used to estimate the direction of the main axis of the tephra plume and the location of the thickest pyroclastic deposits.

Eruptive episodes of basaltic tephra are almost always short-lived. The tephra deposits that result from this type of volcanic activity, though they may be quite thick near the vent, typically represent a very short period of time. Wood (1980) notes that 50 percent of 42 observed cinder cone eruptions lasted less than 30 days and that 95 percent were over in less than one year. Cinder cones almost always have associated lava flows originating at their base. These flows are usually extruded after the eruption of tephra from the vent.

The tephra produced by Strombolian eruptions consists of a variety of pyroclasts, ranging from glassy *sideromelane* droplets to microcrystalline blocky black to dark brown pyroclasts (*tachylite*). The sideromelane pyroclasts are often smooth-skinned, vesicular droplets with an irregular and partly open framework of vesicle walls (see

plates 19-21). Angular tachylite pyroclasts range in shape from nonvesicular blocky grains to open-vesicle networks. The gradation from the microcrystalline tachylite grains to the glassy sideromelane droplets is a reflection of the degree of chilling and crystallization of the basaltic melt (Heiken and Wohletz, 1985:9-10).

The diagenesis of basaltic glasses over long periods of time leads to the formation of *palagonite* or hydrated basaltic glass. Palagonitized basaltic ash has been a subject of interest to geologists for many years - numerous studies have demonstrated that many major and trace elements are relatively depleted or enriched over time (Fisher and Schmincke, 1984:314). The degree and rate of palagonitization has been used in Hawaii and some other areas to estimate the age of basaltic glass artifacts though the method has never been used to date deposits of basaltic ash (Morganstein and Riley, 1975).

Unlike large-scale Plinian tephra eruptions, Strombolian eruptive activity typically distributes basaltic pyroclastic materials not more than a few kilometers to a few tens of kilometers from the vent. The deposit thickness and maximum grain size decreases very rapidly with its distance from the source. Because of the proximity of basaltic tephra deposits to their vents, the source of these pyroclastic materials is often easy to determine. The direction of the main axis (thickest part) of basaltic tephra ashfalls can be ascertained by the measurement of ash thickness or can be estimated by the summit morphology of the source cinder cone. The summits of most High Cascades cinder cones, for example, are somewhat irregular and highest in elevation on the northeast to east sides of the cone (the leeward side). The high point indicates the approximate direction of the axis of the resultant tephra blanket as well as the dominant wind direction during the eruption.

Sources of Information About Volcanic Tephra

The review of volcanic tephra that is presented in this overview is necessarily brief and limited to concepts that are particularly germane to Willamette National Forest research problems. The volume of available tephra-related literature, however, is considerable. Volcanic tephra has been described and discussed in many publications and a recent increase in the appearance of tephra-related literature suggests that interest in tephra research is on the rise. The three most important references for tephra researchers are *Pyroclastic Rocks* (Fisher and Schmincke, 1984), *A Manual for Tephrochronology* (Steen-McIntyre, 1977), and *Tephra Studies* (Self and Sparks, 1981). Excellent discussions or reviews about volcanic tephra are also found in Heiken (1972 and 1974), Kittleman (1979), and Heiken and Wohletz (1985). The 1980 eruptions of Mount St. Helens also stimulated considerable research into the geochemical and depositional characteristics of volcanic ash. Current geologically-related tephra literature is probably best tracked through the *Bibliography and Index of Geology* and *New Publications of the U.S. Geological Survey*.

Archaeological and geological literature related to Oregon tephra sources can best be examined with *Holocene Volcanic Tephra in Oregon: An Indexed Bibliography* (Skinner, 1990). This bibliography is currently available only as an on-disk document for IBM PC microcomputers (see Appendix 5 for details).

TEPHROCHRONOLOGIC AND TEPHROSTRATIGRAPHIC APPLICATIONS

Volcanic tephra is of considerable interest to archaeologists primarily because of its potential as a chronologic tool. In areas where volcanic ash is found, such as in the Willamette National Forest, the presence of volcanic tephra may provide a simple and cost-effective technique for establishing chronologies at archaeological sites.

Tephrochronology is a fairly recent field of research that is concerned with the use of volcanic tephra layers and deposits as dating tools. Tephrochronology is highly dependent on *tephrostratigraphic* techniques of the description of tephra layers and their age relationships. Tephrostratigraphy and tephrochronology are used synonymously by most researchers and will be used interchangeably in this report. Tephrostratigraphers and tephrochronologists attempt to provide limiting ages and dated stratigraphic/time horizons for tephra layers. This is accomplished through the use of independent chronologic methods such as radiocarbon dating and, more commonly, by the careful observation of *contact relationships* among different tephra units and their related volcanic rocks.

Under normal circumstances, a deposit or volcanic rock underlying a target tephra unit under consideration must be older than the target unit; overlying deposits must be younger than the target unit. If the target unit can be directly associated with a dated unit (as with the Mazama eruptions, for instance), then the *absolute age* of the tephra unit (within the limits of analytical uncertainty) can be established. Should the age of the underlying or overlying unit be known (say, through an associated radiocarbon date), then the maximum and/or minimum age limit of the tephra unit may be established. If the age of the underlying or overlying deposit is known only in relationship to other units, the *relative age* of the tephra unit can be ascertained. Through the interpretation of the contact relationships of overlying and underlying units with the target unit, a profile of regional tephra chronologies can eventually be constructed (see figure 16 for a Willamette National Forest example). These chronologies, while they may not always provide neat absolute ages for associated archaeological tephra deposits, can provide tephrochronologists with enough chronologic information to assign tephra units to varied ranges of time.

Principles of Tephrochronologic Analysis

Tephrochronologic and tephrostratigraphic studies are built on several basic postulates (Steen-McIntyre, 1977:3):

1. Volcanic eruptions of tephra from a single eruptive source occur at a specific point in time. Tephra eruptions tend to be short-lived and represent a fairly discrete point in time. Tephra deposits, unlike most stratigraphic units, accumulate over a rapid interval; the thickness of the deposit, then, has little bearing on the length of time it took to accumulate. A very thick tephra deposit can be formed in a very short period of time.

2. The fallout area for tephra dispersed by a single eruption may cover an area ranging from a few square kilometers (typical for eruptions of basaltic tephra) to thousands of square kilometers (not unusual for eruptions of silicic tephra). The geographic area covered is correlative with the chemical composition of the magmas from which the tephra was derived, allowing for the chemical *characterization* of many tephra units.

3. In most depositional environments, any given tephra layer will display one or more chemical, physical, or mineralogical characteristic(s) that allow it to be characterized or fingerprinted. A characterization attribute need only exhibit adequate intrasource homogeneity and intersource heterogeneity to allow it to be distinguished or discriminated from among all potential tephra layers that are likely to be encountered in a given region.

4. Remnants of the primary tephra blanket tend to be preserved within the fallout zone in areas of low potential energy. These include lake and pond sediments, low slope areas (such as saddles or hilltops in mountainous areas), and cave and rockshelter sediments.

5. Where remnants of a primary tephra fall are preserved, they mantle the topography that existed prior to the eruption (mantle bedding). This is quite unlike typical stratigraphic units which are deposited horizontally and which are interpreted with concepts like the *principle of original horizontality*.

6. Once a primary deposit of tephra has been dated (whether or not it is directly associated with a known source), deposits of tephra from the same source can be dated through the correlation of the dated with the undated unit.

7. With the exception of tephra that has been mixed with older sediments through human, bioturbaceous, cryoturbaceous, or other physical processes, the maximum age for deposits of primary or reworked tephra is determined by the age of the parent eruption.

These principles of tephra analysis form the basis for all tephrochronologic studies and provide useful general guidelines with which to approach virtually any tephra-related archaeological and geological problem.

Tephra Dating Methods

A variety of different chronologic techniques are available for determining the relative and absolute ages of tephra deposits (table 2). Only a few of these methods, however, are useful in dating the relatively recent eruptive products of Holocene tephragenic activity. In the Willamette National Forest, the radiocarbon dating of wood and charcoal from the base of tephra deposits, from lava tree-casts in tephra-associated lava flows, and from drowned forests in lava-dammed lakes has proven valuable. These radiocarbon dates, supplemented by studies of tephra stratigraphy, have allowed the construction of a fairly detailed chronology of tephragenic events in this region (see Section III and figure 16 for details).

DATING METHOD	BASALTIC (B) SILICIC (S)	REFERENCE
	ABSOLUTE METHODS	
Association with ^{14}Cdate	B S	Naeser et al., 1981
Association with Dated Tephra Deposit (Characterized and Correlated)	B S	Many references
Etching of Heavy-Mineral Phenocrysts	S	Steen-McIntyre, 1981
Fission-Track	B S	Naeser et al., 1981
Magnetostratigraphy	S	Verosub, 1981
Potassium-Argon (K-Ar)	B S	Naeser et al., 1981
Sedimentation Rate	B S	Scott, 1974
Soil Development	S	Scott, 1987
Tephra Hydration	S	Steen-McIntyre, 1981
Vegetation Cover or Tree Age	B S	Many references
	RELATIVE METHODS	
Association with Undated Tephra Deposit (Characterized and Correlated)	B S	Many references
Stratigraphic Placement/Contact Relationships	B S	Many references

Table 2. The major "absolute" and relative tephra dating methods. A number of different chronological techniques are available for dating tephra deposits and eruptions, though some of these are not applicable to Holocene deposits.

CHARACTERIZATION OF VOLCANIC TEPHRA

A principal tool of the archaeologist utilizing volcanic tephra as a dating method is that of the characterization or fingerprinting (*sourcing*) of volcanic ash deposits. Once the geologic source of a volcanic ash deposit at an archaeological site has been identified, it can often be associated with preexisting radiocarbon dates (or other absolute dates or relative sequences). In the absence of a known date, a characterized volcanic ash deposit can be used as a stratigraphic horizon with the ability to tie archaeological sites together chronologically on a regional scale.

Methods of Characterization

To be useful as a characterization attribute, some physical or chemical property of the tephra must display sufficient intersource heterogeneity so that different geologic sources can be identified and enough intrasource homogeneity so that individual sources may remain individually distinguishable. Kittleman (1979) refers to these characteristics as discrimination and persistence. He also points out that attributes chosen for their discrimination and persistence must also be relatively unaffected by weathering and contamination.

Fortunately, there are a wide variety of suitable attributes and characterization methods available, though their accuracy varies considerably (table 3). In general, the most powerful of the characterization techniques are the geochemical ones. *Trace element* abundances, and to a lesser degree, the *major element* composition of volcanic tephras, have been successfully used to characterize volcanic ash deposits and sources in many areas of the world. The most commonly-employed geochemical analytical methods for ascertaining tephra major and trace element abundances are x-ray fluorescence (XRF) analysis, instrumental neutron activation analysis (INAA), electron probe micro-analysis (EPMA), and atomic absorption spectrophotometry (AAS). The choice of a particular characterization method is governed by several considerations, including the particular suite of major or trace elements that is desired (for chemical analysis), whether the tephra is from a basaltic or a silicic source, the size of the available sample, the degree of alteration and weathering, the amount of sample contamination, the number of sources that must be distinguished in a region, degree of geologic expertise and stratigraphic or contextual data available for the sample, and, of course, the cost and availability of the methods. References in table 3, as well as in other books and review articles (Kittleman, 1979, Self and Sparks, 1981, and Harbottle, 1982, are recommended) may be consulted for more details concerning the different tephra characterization methods.

While these chemical characterization methods are powerful discriminators of tephra sources, other more basic methods can prove equally valuable. Properties that are easily observable in the field such as color, deposit thickness, maximum grain size, and mineralogical component may adequately characterize many, if not most, tephra

CHARACTERIZATION METHOD	BASALTIC (B) SILICIC (S)	REFERENCE
Age	B S	Many sources; see table 2
Alpha Emissions	S	Cormie et al, 1981; Cormie et al., 1982
Color	B S	Many references
Deposit Thickness	B S	Many references
Fission-Track Age	S	Westgate and Gorton, 1981
Grain Size	B S	Kittleman, 1973
Isotope Ratios (Oxygen)	S	Fisher and Schmincke, 1984:56
Major Element Composition (Magnetite Separates)	S	King et al., 1982; Beaudoin and King, 1986
Major Element Composition (Vitric Fraction):		
AA	B S	This study
EPMA	B	Larsen, 1981; Oviatt and Nash, 1989
EPMA	S	Smith and Westgate, 1969; Westgate and Gorton, 1981; Carrara, 1989, plus many other references
XRF	S	Czamanske and Porter, 1965
Magnetic Properties	S	Yoshida, 1979; Fisher and Schmincke, 1984:356
Mineral Abundances	S	Kittleman, 1973; Westgate and Gorton, 1981
Pore Volume	S	Borchardt et al., 1968; Doak, 1969
Proportions of vitric, lithic, crystalline components	S	Kittleman, 1973
Refractive Index	S	Powers and Wilcox, 1964; Wilcox, 1965; Kittleman, 1979; Westgate and Gorton, 1981
Relationship to Vent	B S	Many references
Shard Morphology	S	Tucker, 1977; Westgate and Gorton, 1981
Stratigraphic Position	B S	Many references
Trace Element Composition (Crystalline Fraction):		
INAA	S	Dudas et al., 1973
Trace Element Composition (Vitric Fraction):		
AA	B S	This study
INAA	S	Randle et al., 1971; Skinner and Radosevich, 1989, plus many other references
XRF	S	Cormie et al., 1981; Cormie and Nelson, 1983; Carrara, 1989

Table 3. Methods that have been used to characterize and correlate tephra deposits.

deposits. Chemical characterization techniques are most useful in deciphering tephra deposits in areas far removed from the source vent or in regions with complex eruptive histories. The most reliably identified tephra deposit is the one that has been characterized by as many different properties as possible.

Methods of Correlation

The geologic source of characterized volcanic tephra is determined through the correlation of characterized reference source samples and characterized samples whose geologic source provenance is not known. Samples that are geochemically characterized are most often correlated or clustered with either graphical or statistical methods.

Graphical or visual methods of correlation are most appropriate when the number of measured variables (chemical elements) are relatively few and the data sets are relatively small. In the current investigation, for example, we used visual methods as the primary correlation technique and relied on statistical methods only as ancillary techniques. Typical visual correlation methods include the use of bivariate scatterplots (see Section IV and V of this report for examples) and ternary diagrams. A variety of other multidimensional graphical methods for cluster recognition are also available, partially because of the increasing use of graphical methods of exploratory data analysis (EDA) in the analysis of data sets and partially because of their ease of use with microcomputers (Tukey, 1977; Chambers et al., 1983). (See the cover of Section V for an example of one of these multidimensional graphical methods, Chernoff faces). Graphical methods are surprisingly effective in the identification of clusters or groups from multidimensional chemical data sets; in the correlation of geochemically characterized samples, after all, we are merely attempting to find the known source cluster into which an unknown sample falls. The visual methods are, in fact, often superior to statistical methods in dealing with small- to medium-sized data sets ($n \leq 100$).

Multivariate statistical correlation methods are, however, sometimes required for large or complex data sets. These methods have become particularly popular since the advent of statistical packages and microcomputers. Statistical methods such as cluster analysis (Harbottle, 1983; Romesburg, 1984), discriminant function analysis (Borchardt et al., 1972; King et al., 1982, and Beaudoin and King, 1986; Stokes and Lowe, 1988), and the coefficient of similarity (Borchardt et al., 1972; Sarna-Wojcicki et al., 1979 and 1987) have all enjoyed some popularity as tephra correlation methods. While these statistical methods are useful in analyzing large data sets, they are also prone to considerable abuse when used as a "black-box" approach for dealing with geochemical data. These procedures will find clusters in any data set, even if no significant groups truly exist. We recommend only the careful and knowledgeable use of multivariate statistical techniques for correlation purposes and also suggest that they be used in conjunction with graphical methods, when possible.

III.
SOURCES OF HOLOCENE VOLCANIC TEPHRA IN THE WILLAMETTE NATIONAL FOREST

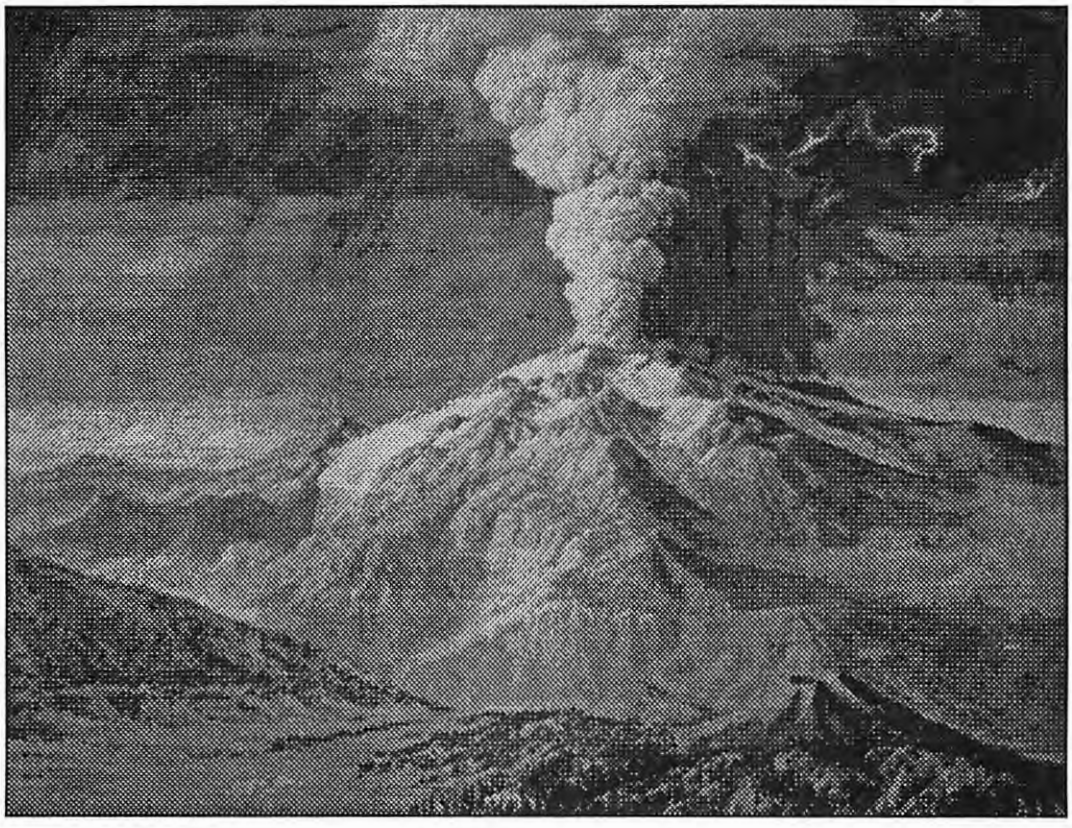

SOURCES OF HOLOCENE VOLCANIC TEPHRA IN THE WILLAMETTE NATIONAL FOREST

VOLCANIC TEPHRA IN OREGON

The most widespread deposits of volcanic *tephra* in Oregon have originated from eruptions of *silicic* volcanic ash. Several sources of silicic tephra have been identified in Oregon, all of them associated with vents in or near the High Cascades. In addition, small quantities of tephra from Mount St. Helens, Glacier Peak, and perhaps some Northern California sources have been found in Oregon (figure 4). The most extensive of the *Holocene tephragenic* eruptions in the western United States and the one most important to *tephrochronological* studies within the Willamette National Forest took place at Mount Mazama in the southern Oregon Cascade Range. Considerably less spectacular eruptions of silicic tephra also occurred on the highlands bordering the South Sister. Because of their potential importance in Willamette National Forest prehistory, these latter eruptions are described in some detail in the following section of the report.

SILICIC VOLCANIC TEPHRA IN THE WILLAMETTE NATIONAL FOREST

Mount Mazama

> *Day after day, night after night, the eruptions continued. There were brief intervals of comparative calm, but each was brought to a close by an outburst more violent than the one preceding. It was now increasingly difficult to see what was happening on the mountain. Fine dust and the smoke of forest fires permeated the air. The hot, acid fumes were suffocating. As the activity grew in strength, the winds veered toward the northeast, in the direction of what is now the town of Bend. The falling fragments, which at first had scarcely been larger than peas, were now as large as a man's fist. Over thousands of square miles the air was so charged with dust that the days were darker than the blackest night. Close to the mountain, it was impossible to see one's outstretched hand. Far off, on the plateau to the east, small bands of Indians gathered in dumb horror about their campfires, too bewildered to flee for safety. They had often seen the mountain burst into flame before, but this cataclysm, this ashy darkness, seemed to be the end of everything.*
>
> Dramatic description of the climactic eruptions of Mount Mazama by Howel Williams (1954:30)

By far, the most significant of all the tephra deposits found within the Willamette National Forest are those originating from Mount Mazama. The caldera resulting from the explosive climactic eruption of this High Cascades volcano about 6,850 *radiocarbon years* ago now holds Crater Lake, the deepest freshwater lake in North America. The tephra that originated during the eruptions of Mount Mazama has been identified throughout Oregon, Washington, California, Idaho, Montana, Utah, Nevada, British Columbia, Alberta, Saskatchewan, and the submarine sediments of the

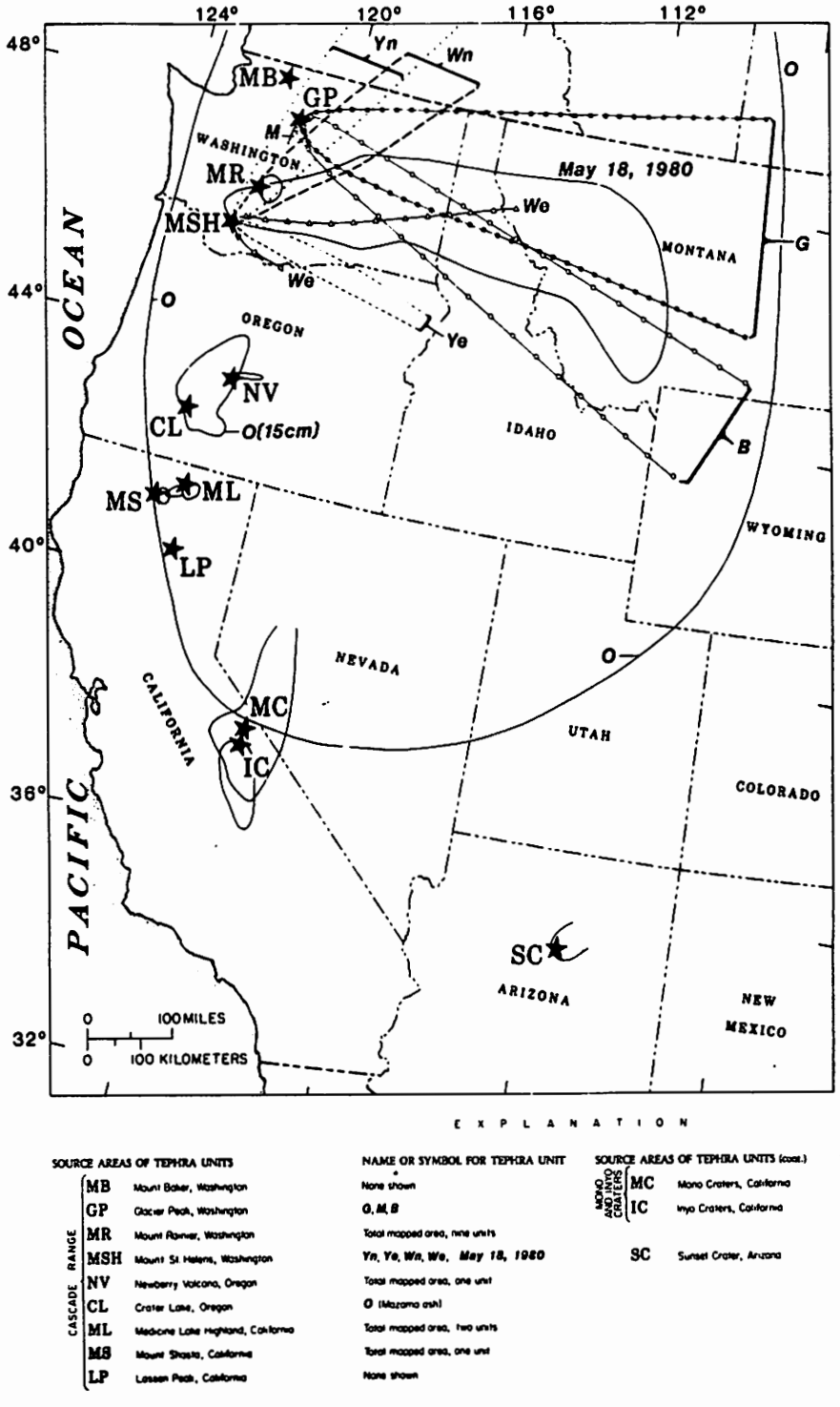

Figure 4. Areal distribution of Holocene tephra sources in the Far Western United States. The boundaries shown can be considered to be minimal ones and it is likely that tephra from the various vents can be found in favorable environments beyond the limits indicated. The distribution for the Mazama tephra is a composite of several different lobes. The map is from Sarna-Wojcicki et al., 1983:56.

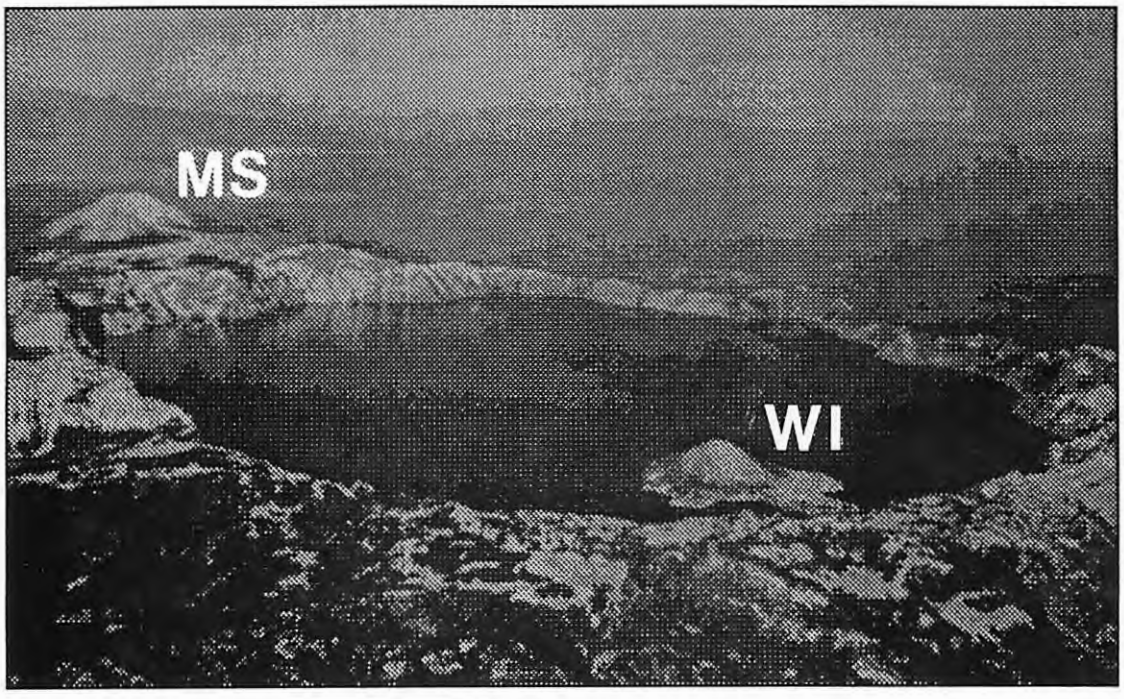

Plate 1. Crater Lake. The collapse and explosion crater left by the 6845 B.P. climactic eruptions of Mount Mazama now contains a 580 m-deep lake, the deepest in the United States. Wizard Island (WI), a cinder cone created not long after the formation of the caldera, is in the foreground near the caldera rim. Two other post-caldera cinder cones now lie under the waters of the lake. The peak on the left of the photograph is Mt. Scott (MS). Aerial photograph taken facing southeast.

Pacific Continental Shelf (figure 7). Mazama tephra has been found as a discrete bed as far away as Lec la Biche, Alberta, about 1550 km northeast of Crater Lake (Westgate and Briggs, 1980).

Mazama tephra deposits have been utilized extensively as a temporal horizon by archaeologists, geologists, geomorphologists, palynologists, and other researchers throughout the Far Western United States and Western Canada. (For detailed Mazama references, see the on-disk bibliography described in Appendix 5).

Mount Mazama has been known as a source of volcanic tephra since investigations in Crater Lake National Park began early in this century (Diller and Patton, 1902). In the 1930's, geologic interest in the tephra and its areal distribution was piqued during an early interdisciplinary archaeological research effort in the Fort Rock and Summer Lake basins of south-central Oregon. Joining Luther Cressman, a University of

Oregon archaeologist, were volcanologist Howel Williams from the University of California, and a geologist and palynologist from Oregon State University, Ira Allison, and Henry Hansen (Cressman et al., 1940). The discovery by Cressman of pre-Mazama human artifacts in the Northwest Great Basin of Oregon prompted a lively debate about the antiquity of occupation in the New World - at this time it was held by many professional archaeologists that North America had been occupied for only a few thousand years.

Williams soon moved on to the first detailed geologic description of Crater Lake and the Mazama eruptions, one in which the depth and distribution of the Mazama tephra was first ascertained for a large area (Williams, 1942). Research into the details of the eruptive history of the volcano has most recently been carried out by Charles Bacon of the U.S. Geological Survey (Bacon, 1983 and 1987; summaries in Cranson, 1982; Matz, 1987, and Nelson et al., 1987). Bacon's work forms the core of the geologic evidence summarized in the this section of this report.

THE CLIMACTIC ERUPTIONS OF MOUNT MAZAMA: HOLOCENE ERUPTIVE SEQUENCE AND CHRONOLOGY

During the early Holocene Epoch, Mount Mazama stood as a large glaciated volcano located towards the southern end of Oregon's Cascade Range. Williams (1942:66) estimated that the volcano probably stood at an elevation approaching 12,000 feet. Potassium-Argon dates indicate that the volcano was sporadically active throughout at least the last several hundred thousand years. Rocks from low in the exposed caldera walls above Crater Lake have been dated at about 400,000 *K-Ar* years B.P.

The Redcloud Eruption

In the early part of the post-glacial period, there was apparently little or no activity on the volcano. About 7,200 *paleomagnetic years* ago, however, this period of quiescence was broken by the eruption of the Redcloud rhyodacite flow near the rim of the present-day caldera (figure 5). The eruption of this flow was probably accompanied by discharges of tephra, though the distribution of the ash and pumice may have been fairly local in extent. This activity was probably the first of a series of precursors to the climactic eruption.

The Lower Pumice Fall and Llao Rock Eruption

About 7015 $\pm$ 45 radiocarbon years ago (USGS-870), not long after the emplacement of the Redcloud Flow, activity began at a vent now covered by the Llao Rock flow (figure 5). Several eruptions of tephra occurred at this vent; volcanic activity culminated with the extrusion of the flow now known as Llao Rock (plate 2). These tephra eruptions, collectively known as the Lower Pumice Fall, produced the only known voluminous tephra deposits associated with preclimactic eruptions at the

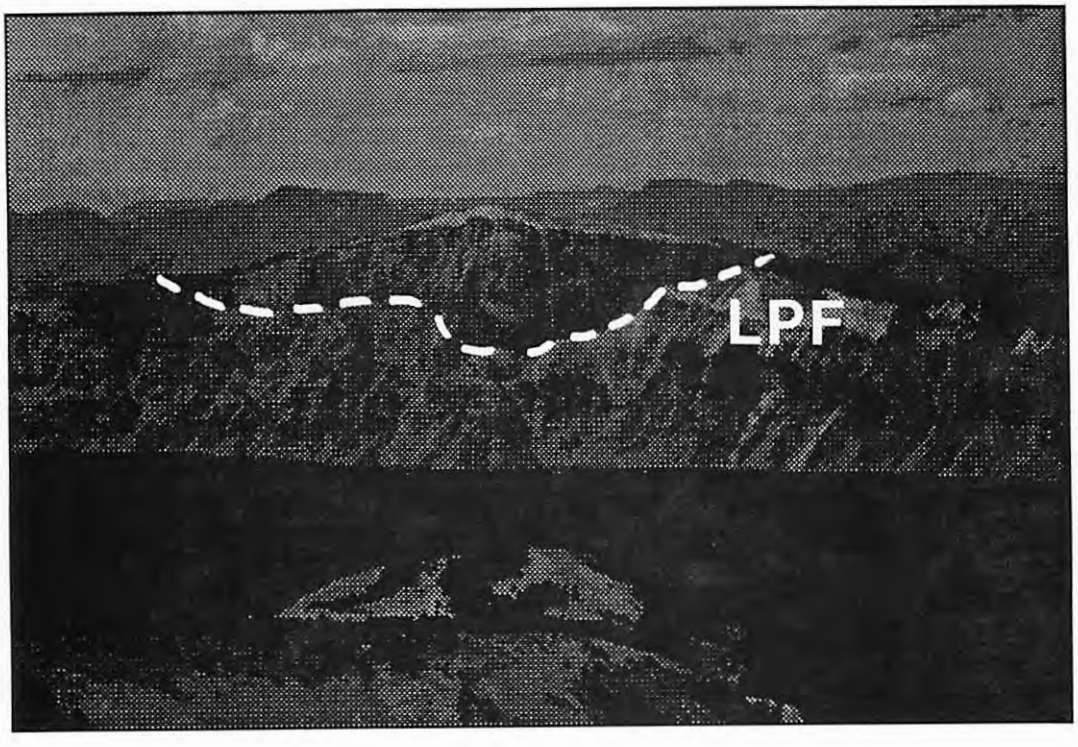

Plate 2. Llao Rock. This obsidian-*rhyolite* flow filled an explosion crater left by the 7015 B.P. eruption of the Lower Pumice Fall prior to the climactic eruptions of Mount Mazama. The later climactic eruptions and caldera collapse exposed a spectacular profile of the flow in the present-day caldera wall. The dashed line outlines the base of the Llao Rock flow and the crater left by the eruption of the tephra. The light-colored deposit to the right (east) of Llao Rock (LPF) is a thick unit of tephra from the Lower Pumice Fall eruption. Prior to recent geologic research at Crater Lake, it was thought that Llao Rock was a lava flow that had filled a glacial valley on the slopes of the ancestral Mount Mazama. Photograph taken facing northwest from the summit of Mt. Scott.

volcano. Bacon estimates that the volume of the Lower Pumice Fall deposits were probably equivalent to approximately 2-10 km^3 of magma or about two to ten times the volume of the 1980 eruptions of Mount St. Helens in Washington. The Lower Pumice Fall has been identified in many locations throughout the Western United States, including lake and bog sediments in Washington (Blinman et al., 1979; Mack et al., 1979), tephra outcrops in Nevada (J. Davis, 1978:102), Montana bogs (Lemke

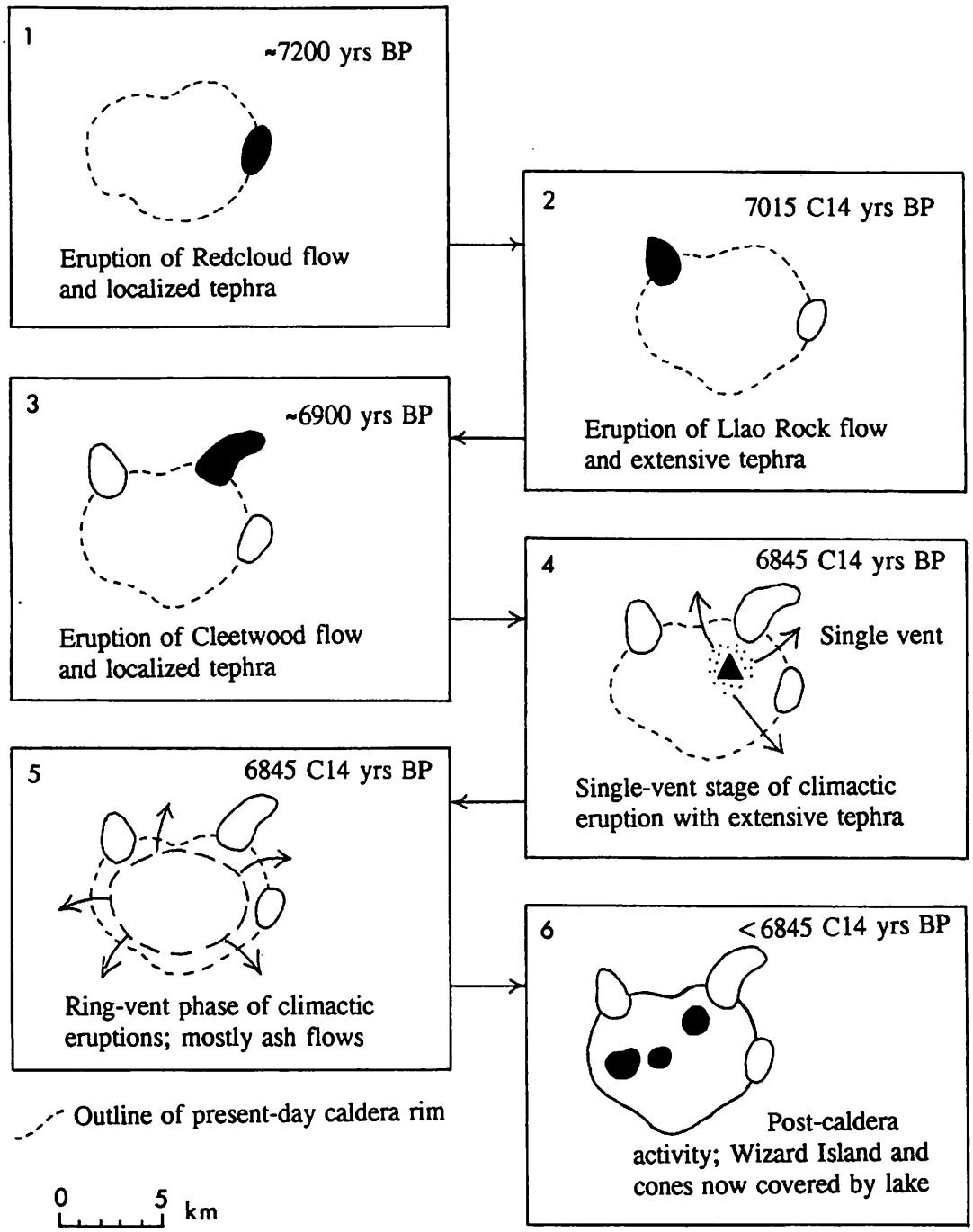

Figure 5. The eruptive sequence leading to and immediately following the climactic eruptions of Mount Mazama.

et al., 1975), and eastern Oregon soils and lakes (Rai, 1970; Blinman et al., 1979). Doak (1969:51) also independently deduced, based on the *vesicularity* characteristics of the ash, that the Mazama deposits in central Oregon must have resulted from more than one event. In Nevada, this tephra layer has also been called the Tsoyawata Bed (Davis, 1978:35-36; 1985). Bacon concluded that, in order for sufficient wind changes to occur to cause the wide dispersion of the tephra, the Lower Pumice Fall was deposited over a period of several days. Though tephra from the Lower Pumice Fall must have covered much of the Willamette National Forest, there are no reported occurrences of this tephra deposit to date.

The Cleetwood Eruption

The Cleetwood Flow eruption, accompanied by local tephra falls, was the last preclimactic eruptive event (figure 5). This eruption must have occurred immediately prior to the climactic eruption - the lava was still fluid enough to ooze down the caldera wall that was created during the climactic event.

The eruption of the Grouse Hill dome, located near the northern Caldera rim, was previously thought by Bacon to have occurred after the Llao Rock eruption and before the Cleetwood eruption (Bacon, 1983:87). This eruptive event is now believed to be late *Pleistocene* in age and is not considered to have been formed in the sequence of eruptions immediately preceding the climactic event (Bacon, 1987).

The Climactic Eruption

About 6850 radiocarbon years ago, the caldera-forming climactic eruptions of Mount Mazama began. The deposits that resulted from this massive explosive event consisted of airfall tephra distributed by a high *Plinian* column and *ash-flow* tuffs derived from the collapse of the eruptive column near the vent. The ash-flow tuffs flowed as clouds of suspended pumice particles and were carried as far as 60 km in all directions down the major drainages and topographic lows (figure 6). The *airfall tephra*, sometimes referred to as the Upper Pumice Fall, was carried primarily to the east and the northeast and has been identified in Canada over 1500 km from the vent (figures 4 and 7). Tephra from the eruption was spread over a minimum area of 1.7 million km^2 (Sarna-Wojcicki et al., 1983). The entire present-day Willamette National Forest was entirely blanketed with tephra that originated from this event.

Initially, the eruption was probably confined to a single event located somewhere within the present boundary of the caldera (figure 5). Following this phase, eruptions continued along multiple vents which likely formed a ring just inside the current caldera wall. Based on a study of the rate of pollen influx in a Montana bog, the climactic eruptions are estimated to have taken no longer than two or three years and probably began in the autumn of the year (Mehringer et al., 1977; Blinman 1978:45).

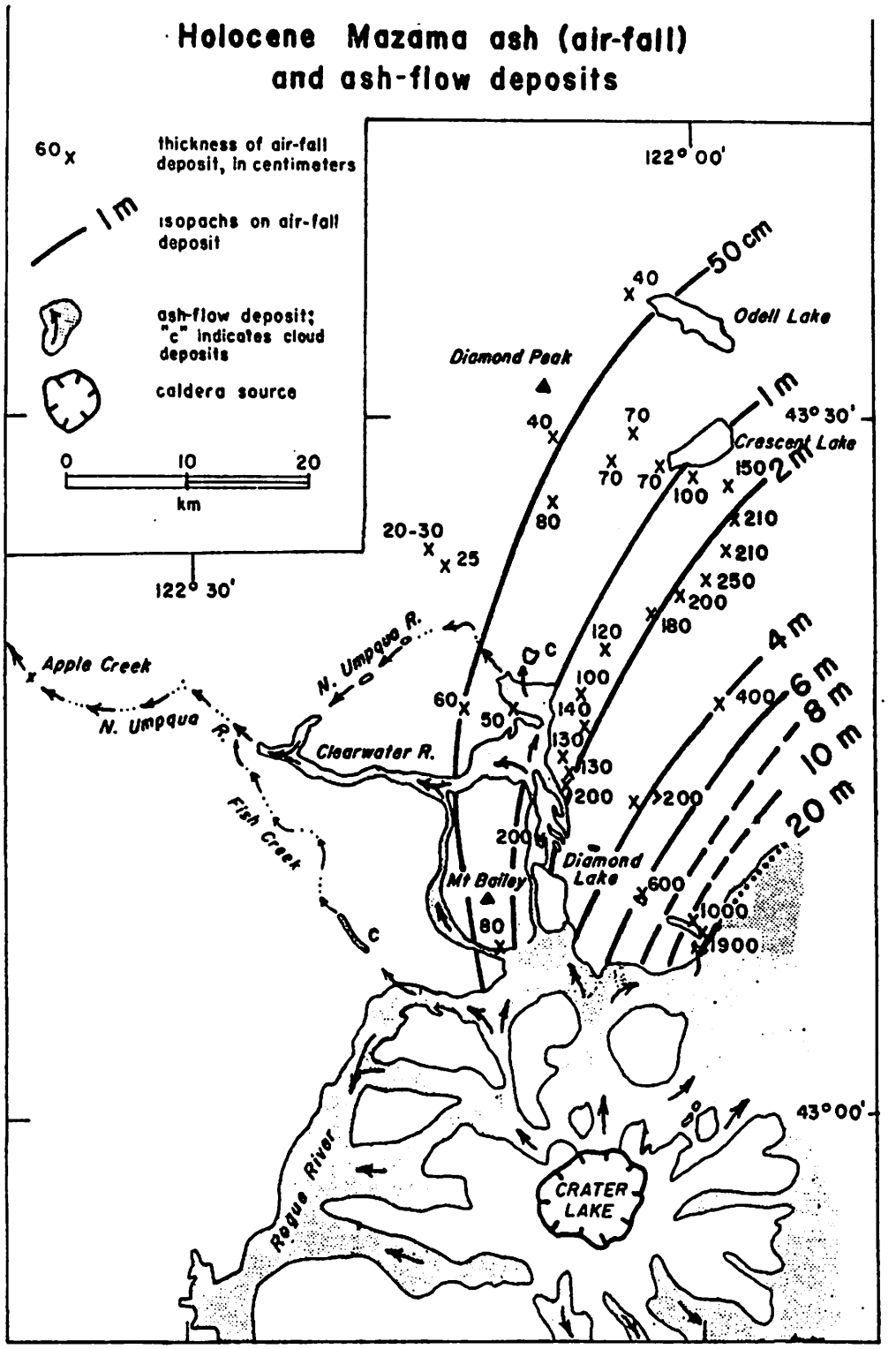

Figure 6. Distribution of Holocene Mazama air-fall and ash-flow deposits in the region surrounding Crater Lake. The map is from Sherrod, 1986:101.

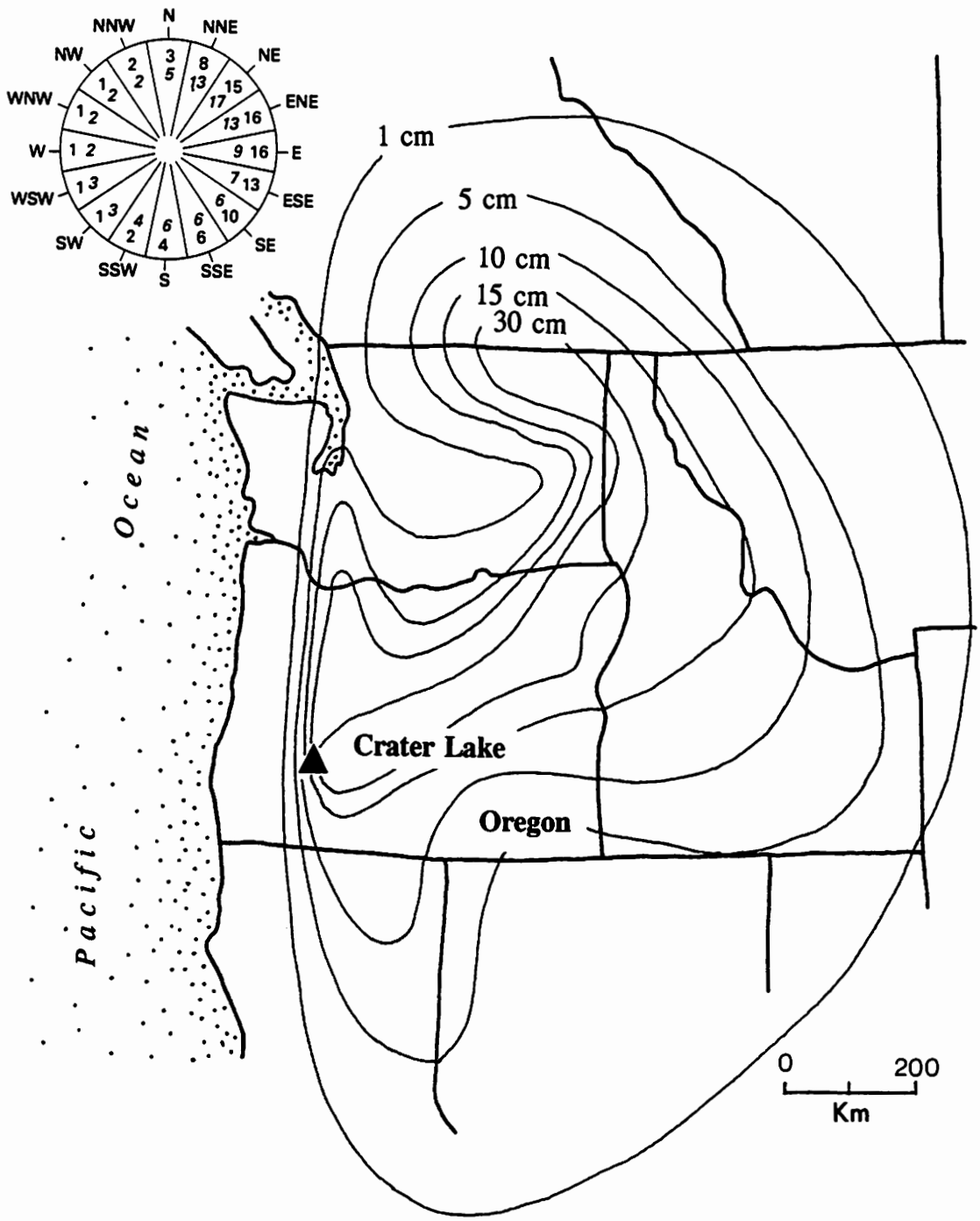

Figure 7. Distribution of Mazama tephra throughout the Far West (modified from Matz, 1987:95-96). Sampling locations are marked by dots. The rose diagram shows the approximate percentage of time that the wind blows toward various sectors at Salem, Oregon, at altitudes between 4,000 and 16,000 m. The percentages in italics are frequencies at an altitude of about 2,500 m. Rose diagram is from Crandell, 1980:62.

Though several estimates have been made, the volume of the material erupted may have exceeded 100 cubic kilometers, the equivalent of at least 34 cubic kilometers of *magma* (Williams, 1942; Williams and Goles, 1968; Lidstrom, 1972; Bacon, 1983). During and after the climactic eruptions, the remaining summit of Mount Mazama collapsed, creating the caldera that now holds Crater Lake. Limited volcanic activity not long after the formation of the caldera formed Wizard Island and two other cones now covered by the waters of the lake.

AGE OF ERUPTIONS

The ages of the climactic Mazama eruptions are very well known, adding to the importance of this event in tephrochronologic studies (table 4). Charcoal associated with the Mazama eruption was, in fact, one of the first samples to be dated with the then newly-developed radiocarbon dating technique (Arnold and Libby, 1951).

The considerable range of variation in the radiocarbon ages of the Mazama eruptions that is apparent in table 4 is due to at least four factors:

1. Analytical errors due to the statistical nature of the way in which radiocarbon ages are determined.

2. Sample contamination.

3. Problems of association of samples with the Mazama events. Many of the dates are derived from materials immediately overlying or underlying deposits of tephra and are not directly associated with the Mazama eruptions. Post-depositional stratigraphic time displacements of several hundred years have also been reported for tephra collected from lakes, the source of several of the radiocarbon dates (Anderson et al., 1984).

4. The dating of multiple eruptive events potentially spread out over several hundred years.

The weighted mean average of four carbon samples associated with the climactic eruptions is 6845 $\pm$ 50 ^{14}C years B.P. (Bacon, 1983), and it is this date that is most often quoted in the literature today as the age of the Mazama climactic eruptions. When *dendrochronologically corrected*, this figure yields an eruption date of a little over 7600 calendar years B.P. (see table 4).

SAMPLE LOCATION	^{14}C AGE (YRS B.P.)	DENDRO-DATE (A)	REFERENCE (NOTES)
Banff National Park, Canada	6,020 ± 90	6856-6886	1 (E)
Banff Area, Canada	6,170 ± 100	7090-7154	2
Mazama Ashflow, Oregon	6,453 ± 250	7331	3 (E)
Portland Borehole, Oregon	6,490 ± 100	7372-7421	4
Simpson Place Bog, Oregon	6,500 ± 130	7375-7423	5 C)
Mazama Ashflow, Oregon	6,500 ± 500	7375-7423	6,7 (E)
Arrow Lake, Washington	6,600 ± 400	7442	8 (C)
Arrow Lake, Washington	6,630 ± 400	7484	8 (B)
Mazama Ashflow, Oregon	6,640 ± 250	7490	8 (E)
Lost Trail Pass, Montana	6,700 ± 100	7532-7568	9,10 (C)
Lost Trail Pass, Montana	6,720 ± 120	7575	9,10 (B)
Wildcat Lake, Washington	6,750 ± 90	7584	10,11 (D)
Wildhorse Lake, Oregon	6,765 ± 70	7587	10,11 (D)
Mazama Ashflow, Oregon	6,780 ± 100	7590	12 (E)
Mineral Lake, Washington	6,800 ± 180	7594	13 (B)
Bonaparte Meadows, Washington	6,810 ± 190	7597	14 (C)
Labish Channel, Oregon	6,820 ± 200	7599	15 (C)
Mazama Ashflow, Oregon	6,830 ± 110	7606-7646	12 (E)
Umpqua River Valley, Oregon	6,840 ± 100	7614-7664	12 (F)
Mount Mazama Average Value	6,845 ± 50	7618-7667	12 (G)
Bonaparte Meadows, Washington	6,870 ± 110	7681	14 (D)
Labish Channel, Oregon	6,870 ± 190	7681	15 (B)
Mazama Ashflow, Oregon	6,880 ± 70	7684	12 (E)
Anthony Lakes, Oregon	6,910 ± 140	7693	5 (C)
Bonaparte Meadows, Washington	6,930 ± 110	7702	14 (D)
Lost Creek Damsite, Oregon	6,930 ± 115	7702	16 (F)
Wildcat lake, Washington	6,940 ± 100	7717	11 (C)
Wildcat Lake, Washington	6,940 ± 120	7717	10 (C)
Muir Creek, Oregon	6,940 ± 120	7717	6 (E)
Osgood Swamp, California	6,990 ± 300	7783	17 (C)
Mazama Ashflow, Oregon	7,000 ± 60	7789	12 (E)
Mazama Charcoal, Oregon	7,010 ± 120	7795-7900	6 (F)
Willamette Channel, Oregon	7,010 ± 220	7795-7900	15 (C)
Llao Rock, Oregon	7,015 ± 45	7797-7902	12 (C)
Mineral Lake, Washington	7,100 ± 120	7924	13 (C)
Labish Channel, Oregon	7,125 ± 160	7932	15 (C)
San Juan Area, Washington	7,140 ± 600	7937-7980	18 (F)
Paisley Cave Dung, Oregon	7,610 ± 120	8393	19 (F)

Table 4. Radiocarbon dates associated with Mazama eruptions; see the following page for details.

References:

1. Westgate and Dreimanis, 1967
2. Beaudoin and King, 1986
3. Arnold and Libby, 1951
4. Fairhall et al., 1976
5. Borchardt, 1969
6. Valastro et al., 1968
7. Crane, 1956
8. Rubin and Alexander, 1960
9. Mehringer et al., 1977
10. Blinman et al., 1979
11. Blinman, 1978
12. Bacon, 1983
13. Hibbert, 1979
14. Mack et al., 1979
15. Glenn, 1965
16. Buckley, 1973
17. Adam, 1967
18. Easterbrook, 1969
19. Preston et al., 1955

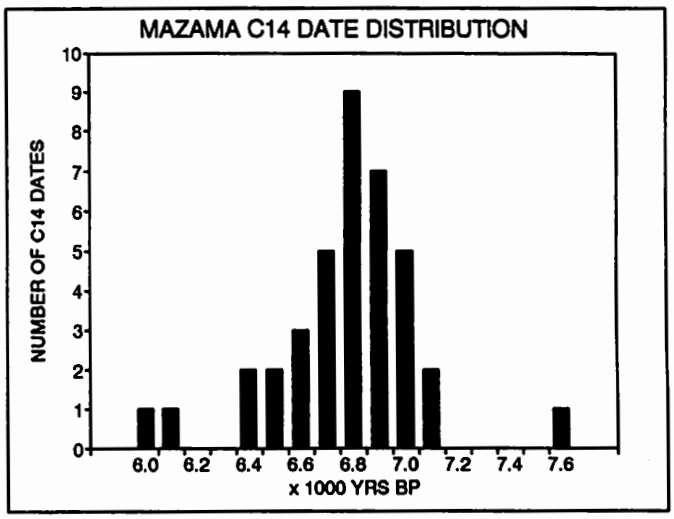

Notes:

(A) Dendrochronologically-corrected date (reported in calendar years B.P.); results based on a bi-decadal atmospheric record.
(B) Peat or organic materials from directly above Mazama tephra layer
(C) Peat or organic materials from directly below Mazama tephra layer
(D) Peat or organic materials from between the Upper and Lower Pumice Fall tephra layers
(E) Charcoal in direct association with ashflow or pumice deposit
(F) Charcoal or organic material underlying airfall tephra deposit
(G) Weighted mean age of four samples; this date is currently used by most researchers to fix the age of the Mazama climactic eruption

Table 4 (Continued). Radiocarbon dates associated with the Holocene eruptions of Mount Mazama. Dendrochronologically-corrected radiocarbon dates were calculated using the CALIB 2.0 software of Stuiver and Reimer(1986).

AREAL DISTRIBUTION OF AIRBORNE MAZAMA TEPHRA

Just how many different eruptive events are recorded in the airfall deposits of Mazama ash is still not well-known. Nearer to Crater Lake, at least six separate layers of tephra have been identified by Mullineaux and Wilcox (1980). Grain size analysis of the tephra by Fisher (1964) indicates the presence of at least three major lobes of air fall ash - one to the north, one to the northeast, and one to the southeast. The northeast and southeast lobes are readily identifiable in figure 7 by the shape of the isopachs. Whether these lobes were attributable to separate eruptive events or to changes in wind direction during the course of the eruptions is not known. Fisher (1964:344) does caution, though: "It must be noted that the top of the pumice-fall layer is of different ages in different places; therefore, a single contour map represents more than one volcanic outburst at varying intensity in a field of changing wind direction." Recent studies of Mount St. Helens tephra have demonstrated, though, that multiple layers of morphologically differentiated tephra can be deposited near the vent during a single eruptive event and it is unclear how many eruptive events might be responsible for the multiple Mazama layers (Waitt and Dzurisin, 1981). Four major Mazama lobes have also been reported in more distal areas, though details of their origin in the eruptive sequence of Mount Mazama are lacking (Sarna-Wojcicki et al., 1983). Because of the difficulties in interpreting tephra stratigraphy, the thickness and distribution of the Mazama tephra unit (even though it resulted from several different eruptions spanning a period of perhaps 150 years) is usually mapped as a single unit. Due to the widespread use of the Mazama tephra as a stratigraphic marker, the areal distribution and thickness of the airfall tephra are quite well-known (figures 4,6, and 7).

Distribution of Mazama Tephra in the Willamette National Forest

Mazama tephra has been reported from many locations within the Willamette National Forest. It is a certainty that the entire region was originally covered by airfall ash from the Mazama eruptions, though the thickness of the tephra decreased very rapidly to the west of the Cascade Divide. Hansen (1942), for example, reports only about 2 cm of reworked Mazama tephra from shallow lake deposits in the central Willamette Valley.

On the upper southern slopes of Mount Jefferson in the Forked Butte and South Cinder Peak region (figure 13), reworked Mazama tephra up to 40 cm thick along meadows and lake margins is reported by Gannon (1981:84) and Scott (1974:54). Thicknesses of about 15 cm are reported, though, as more common in this area, a figure that agrees with the expected fallout thickness (Williams and Goles, 1968). Individual *lapilli* size rarely exceeds 1 mm in this area and is commonly sand-sized. The weathered tephra is a distinctive yellowish-orange and is discontinuously distributed in this area. Field reconnaissance along the Cascade Crest in this area illustrates that

the distinctive Mazama ash is often exposed in trail cuts and is commonly directly overlain by more recent *basaltic tephra* deposits from local vents. At the sampling location for sample CARLL-1, 2 km southwest of Forked Butte, 20 cm of basaltic tephra from Forked Butte directly overlays Mazama tephra; at site SCINP-1 immediately east of South Cinder Peak, 16 cm of basaltic ash overlay Mazama tephra.

Rollins (1976:58) describes a thin layer of light-colored Mazama ash present in several locations in the northwestern portion of the Willamette National Forest in the Triangulation Peak area. The tephra was most commonly found in soil horizons that had been dissected by small streams.

Swanson and James (1975), in a study of the geomorphic history of the Lower Blue River - Lookout Creek area located about 85 km east of Eugene, used Mazama tephra as a *chronostratigraphic* marker. Layers of Mazama ash were used to establish maximum and minimum ages of fluvial terraces, alluvial fans, and of strata overlying or underlying the tephra.

A distinctive layer of Mazama tephra was encountered at a depth of 51 cm in a test pit dug in a McKenzie Pass area *kipuka* surrounded by basalt flows from Little Belknap Crater (see figure 35). This Mazama *paleosol* was directly overlain by more recent basaltic tephras from Belknap Volcano.

Near the intersection of Highways 20 and 162 just east of the town of McKenzie Bridge, deposits of glacial till capped with Mazama tephra can be seen in local roadcuts. Similar deposits of till blanketed with *mantle* deposits of Mazama ash can also be seen in many other locales throughout the higher elevation Cascades, including roadcuts near the intersection of Highways 126 and 20 (also see plate 12).

Woller and Black (1983) mention that Mazama tephra occurs widely in the Waldo Lake-Willamette Pass area of the Western and High Cascades. The Mazama layer of ash and small lapilli are best exposed near the Willamette Pass in roadcuts; elsewhere in the area, the tephra makes up most of the surficial deposits.

Even though the entire Willamette National Forest was originally covered by tephra from the Mazama eruptions, tephra distribution is somewhat discontinuous today (though very widespread, as demonstrated by the preceding discussion), particularly in areas farther west of the Cascade Crest. Volcanic ash is very susceptible to aeolian and fluvial erosional processes and the Mazama ash depth *isopachs* shown in figures 6 and 7 must be considered only as averages or approximations. Published accounts of the amount of Mazama tephra found at different locations must also be considered not only as estimations of the original ashfall blanket thickness, but as the probable result of two, and possibly more, separate eruptive events spread out over a period of up to 200 years. As indicated by the previously discussed Mount Jefferson area tephra, ash thicknesses may also vary considerably in the same locale. In natural

basins the tephra accumulates to thicknesses considerably exceeding the depth of the original ashfall, while on steep slopes tephra may be entirely absent. Soils developed on Mazama tephra are light-colored yellowish-tan, loamy and rich in volcanic ash and small *pumice lapilli*. These small lapilli and ash *pyroclasts* can often be seen with a 10x - 20x hand lens (see plates 22 and 23) and identify the associated soils throughout the Willamette National Forest as post-Mazama in age.

DISTANCE-RELATED CHARACTERISTICS OF MAZAMA TEPHRA

Several important characteristics of Mazama tephra are related to the distance of the tephra from the vent. An understanding of some of these characteristics is important because of their value in identifying Mazama tephra in the Willamette National Forest and in sampling the tephra for geochemical analysis. Largely because of prevailing wind directions at the time of the eruptions, volcanic tephra from Mount Mazama was not symmetrically spread around the vent - the depth isopachs in figures 6 and 7 clearly show the asymmetrical geographic distribution of the ash. The three attributes of Mazama tephra discussed here are a function, then, not only of their distance from the vent, but also of their location in relationship to the main axis of the ashfall. Any analysis or interpretation of distance-dependent tephra characteristics must take geographic location into account.

One of the most apparent tephra characteristics related to distance from Crater Lake is the thickness of the resultant deposits (figures 6 and 8). Because of the potential of tephra for *reworking* and redeposition, though, the use of the thickness of deposits to infer geologic sources should always be used cautiously. Tephra isopachs that are shown on isopach maps should always be considered as average thicknesses of primary ash deposits. The actual thickness of deposits of Mazama tephra may be quite locally variable.

Grain size, particularly maximum grain size, is highly dependent on the distance from the source and has proven a valuable indicator of the proximity of the source of a tephra deposit (figure 8). Within the Willamette National Forest, the maximum size of pumice lapilli ranges from several centimeters at the southern boundaries to 1-2 mm at the northern boundaries (observed along a High Cascades north-south transect). Lapilli size also decreases rapidly to the west of the Cascade Divide away from the north to northeast-trending axes of the ashfall. During this investigation, we found maximum grain size to be one of the simplest attributes for identifying deposits of Mazama tephra in areas where Mazama and South Sister tephras co-occurred. As an example, in an earlier geochemical study of silicic tephras by Randle et al. (1971), pumice samples from the Sparks Lake area (only a few kilometers from the Rock Mesa and Devils Hill vents) were mistakenly collected as Mazama tephra. Lapilli at the collection site were up to 4 cm in diameter and the deposit thickness was at least 1 m, two distance-dependent characteristics quite inconsistent for Mazama tephra at this distance from the vent. It was only after the geochemical analysis of the tephra was

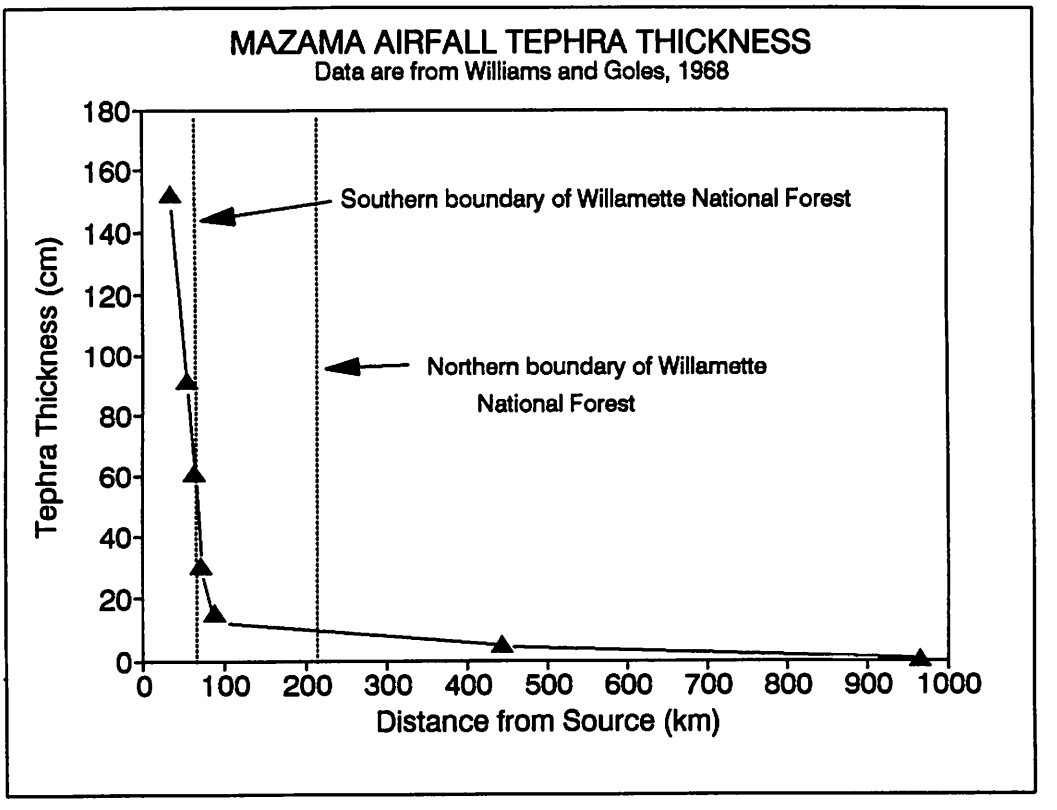

Figure 8. Relationship of the thickness of Mazama tephra deposits and the distance from the source. Thickness data are from Williams and Goles, 1968.

completed that the researchers realized the non-Mazama origin of the samples and their contradictory geologic context.

The mineralogical components of Mazama tephra are also strongly influenced by their distance from the vent. Juvigne and Porter (1985) found that both the heavy mineral fraction and other mineral components decrease downwind from the volcano (it should be noted that their results differ from those obtained earlier by Kittleman, 1973). An important implication is that the geochemical characterization of ***bulk samples*** of Mazama ash should be approached with caution; the changing mineralogical fraction of the tephra will result in bulk analyses that will vary in relationship to their distance from the source. Differences in the chemical composition of samples between sources could easily be obscured by the intrasource compositional variation introduced by mineralogical variation.

The *vitric* component of Mazama tephra, on the other hand, is quite chemically consistent and is not influenced by its distance from the vent. The use of *glass separates* (the vitric fraction of the tephra) for geochemical characterization has proven to be a reliable technique for chemically characterizing Mazama tephra (Borchardt, 1969; Borchardt et al, 1971). Our own experience in the geochemical characterization of tephra samples indicates that minimal sample preparation (removal of magnetite, obvious *phenocrysts*, and apparent contaminants) is adequate for pumice lapilli collected from *near-source* and *intermediate-source facies*.

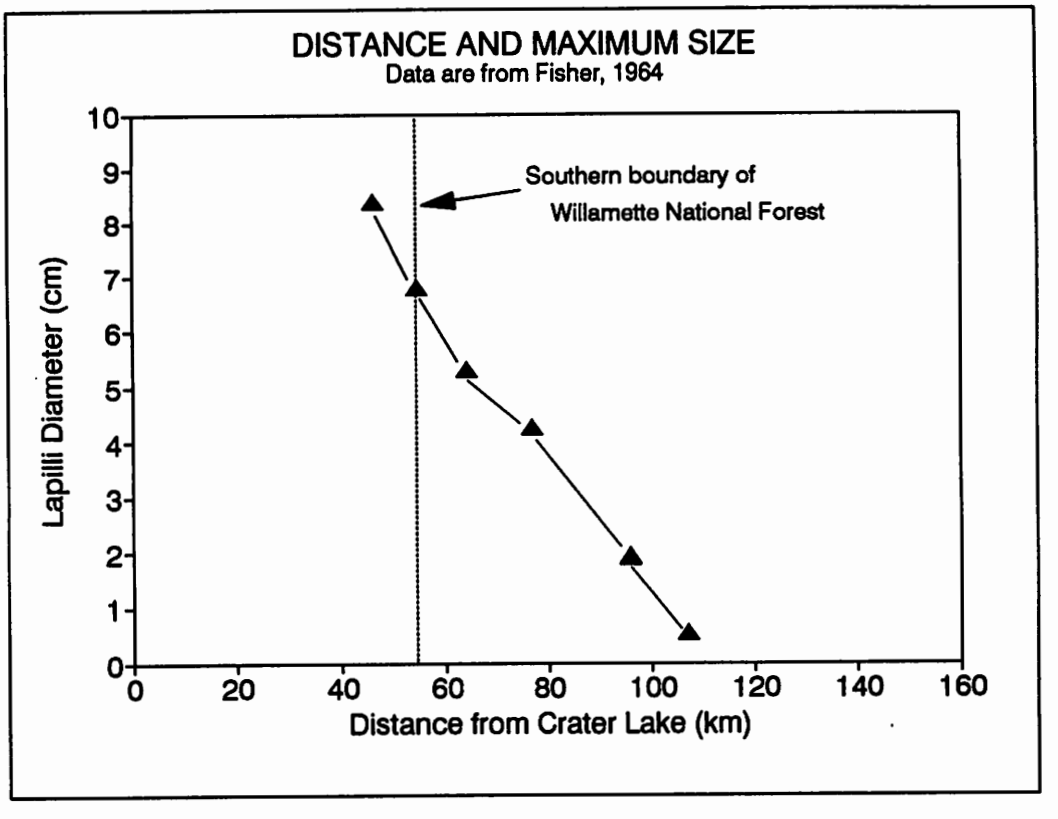

Figure 9. Relationship of the grain (lapilli)-size of Mazama tephra and the distance from the source. The maximum lapilli size data in this figure are from the mean diameter of the five largest fragments measured at a sample location. Samples are from the main northeast lobe of the ashfall. After Fisher, 1964:343.

Tephra Eruptions at South Sister Volcano

Eruptions from vents on the southwest, southeast, and northwest flanks of the South Sister during two brief volcanic episodes between about 2,000 and 2,300 radiocarbon years ago produced relatively modest volumes of silicic volcanic tephra (figure 10).

During the first, or Rock Mesa, episode, eruptions took place from a vent now covered by the Rock Mesa obsidian flow and from a short vent system 1 km east-northeast of Rock Mesa, the Rock Mesa-ENE vent. The second, or Devils Hill, episode occurred along an alignment of vents that stretches from near the shores of Sparks Lake to the upper southeastern slopes of the South Sister. The northernmost and largest of the domes that were extruded after the eruption of tephra at Devils Hill chain of vents is known as the Newberry flow. At about the same time as the activity along the Devils Hill chain of vents, another short alignment of vents on the northeastern flanks of the South Sister were also active, erupting a small quantity of silicic tephra (Scott, 1987).

The eruptions of silicic tephra at the South Sister were first described in some detail in an early work by Hodge (1925a) and later, in more detail, by Williams (1944). Recent research by Taylor (1978), Wozniak (1982), Clark (1983), and especially Scott (1987; also see Scott et al., 1989; Scott, 1990; and Scott and Gardner, 1990) provides the most up-to-date description and interpretation of tephragenic volcanic activity in this area. Their work forms the basis for the following descriptions of tephra eruptions at the South Sister.

ROCK MESA

The first of the late Holocene *pyroclastic* episodes at the South Sister took place at the Rock Mesa vent (figure 10). Initial eruptions of tephra at this event were accompanied by small *pyroclastic flows* and the emplacement of several lava flows and domes, most notably the Rock Mesa obsidian flow (plate 3). The main vent for these tephra eruptions now lies under the Rock Mesa flow. Another vent, the Rock Mesa-ENE vent, consists of a small graben that contains several domes (most of them buried by pyroclastic materials). This vent is marked by a prominent 200 m-high dome that is clearly visible in the frontispiece to this report.

Tephra from the Rock Mesa episode was distributed in two lobes, one to the south and the other to the east of the vents (figure 11). The tephra is coarse-grained near the vents and large fragments of *porphyritic* gray to black obsidian and rhyolite can be found in the pumice fields directly east of the vent. At Moraine lake, about 2 km east of the vents, fragments of dense pyroclastic materials several centimeters in diameter are common. Rock Mesa tephra is found as far as 20 km east of the vents where 1 to 3 cm-thick layers of fine ash and lapilli are reported by Scott (1987). Tephra from the vents is also found several kilometers west of the Cascade Crest in the Willamette National Forest, though the westward limits of the areal extent of the airfall tephra are still poorly-known (figure 11). Rock Mesa tephra most often overlies Mazama ash soils or late Pleistocene glacial till deposits.

Radiocarbon dates of materials associated with the Rock Mesa eruptions (table 5) along with limited paleomagnetic data indicate that the eruption of the tephra probably took place between 2,000 and 2,300 radiocarbon years ago.

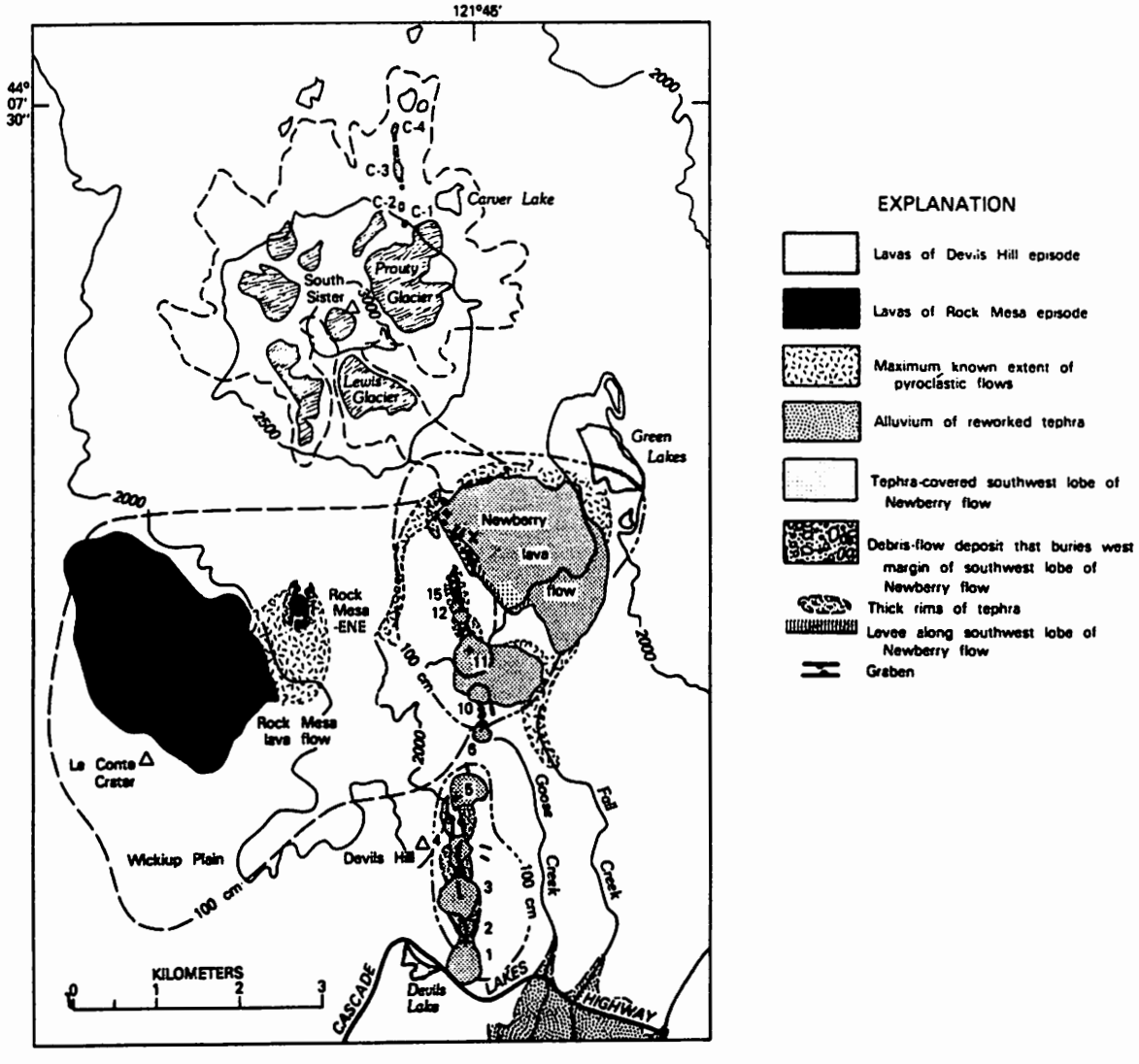

Figure 10. Geologic sketch map of Holocene rhyolite flows and pyroclastic deposits on the flanks of the South Sister volcano. The long-dashed line marks the 100 cm isopach for the Rock Mesa tephra; the dashed and dotted line is the 100 cm isopach for the Devils Hill chain of vents ash. Positions numbered 1 through 15 are major vents for the Devils Hill dome chain. The locations numbered C-1 through C-4 mark the location of the Carver Lake tephra vents. The eastern boundary of the Willamette National Forest runs down the center of the Rock Mesa flow. Map is from Scott, 1987:36.

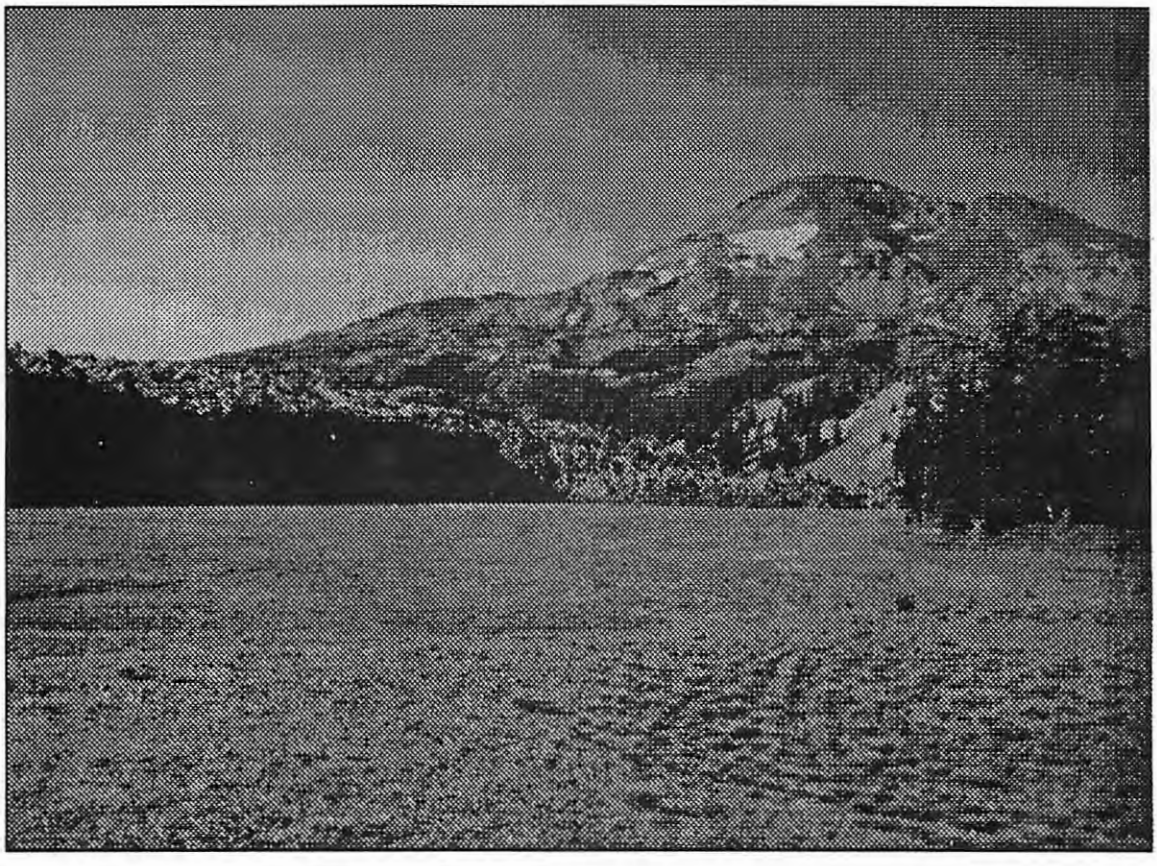

Plate 3. Rock Mesa obsidian flow. Prior to the extrusion of this obsidian flow (left center of picture) a little over 2,000 years ago, about 0.1 km^3 of silicic volcanic tephra was explosively erupted from the Rock Mesa vents. The plain adjacent to the flow consists of a blanket at least 10 m-thick of pyroclastic debris erupted from the vents. The South Sister volcano is in the background. Photograph taken facing north.

DEVILS HILL (SOUTH SISTER) CHAIN OF VENTS

A chain of more than a dozen rhyolite domes and flows runs for about 5 km from Century Drive (the Cascade Lakes Highway) to an elevation of about 8,000 feet on the southeast slopes of the South Sister (plates 4 and 5). Activity at this alignment of vents began with the near contemporaneous eruption of silicic tephra from numerous events and ended with the extrusion of about 16 flows or domes along the chain. The eruption of tephra from these vents is well-described by Williams (1944:58):

Eruptions of pumice also preceded the opening of the Newberry obsidian flow and the recent domes near by, and once more the winds were blowing south and east. Where the trail to Moraine Lake crosses Fall Creek, waterworn lumps of pumice up to a yard across are plentiful on the riverbanks. On the moraines south of broken Top, the mantle of pumice is fairly continuous and includes fragments up to three inches across. On Talapus Butte, pieces up to eight inches across are accompanied by fragments of obsidian three inches in diameter. On Tumalo Mountain, few fragments measure more than an inch. Though mineralogically similar to the pumice from Mount Mazama, most of this local pumice is easy to recognize by its coarseness and admixture with chips of obsidian and lithoidal dacite.

The Devils Hill eruptive episode began not long after the Rock Mesa eruptions had ceased (table 5). Tephra from the Devils Hill vents overlies much of the east lobe of the Rock Mesa airfall tephra and the northeast part of south lobe (Scott, 1987).

The eruption of silicic tephra from the Devils Hill chain of vents spread primarily to the east and south of the vents (figure 11). It is unlikely that any significant amount of tephra from the Devils Hill eruptive episode is found today west of the Cascade Divide in the Willamette National Forest, though the tephra could prove to be a valuable local stratigraphic marker on the east slope of the Cascades.

ERUPTIVE UNIT	^{14}C AGE (YRS BP)	LAB. NO.	DENDRO-DATE (A)	REFERENCE
Devils Hill Tephra	1970 ± 200	W-4013	1928	1
Rock Mesa Tephra	2150 ± 150	W-5556	2141	1
Rock Mesa Tephra	2300 ± 200	W-3402	2341	1,2
Devils Hill Tephra	2410 ± 80	W-5208	2359	1
Devils Hill Tephra	2480 ± 100	W-5016	2499-2709	1
Rock Mesa Tephra	2560 ± 200	W-4016	2742	1
Rock Mesa Tephra	2740 ± 70	W-5021	2850	1

References:

1. Scott, 1987
2. Taylor, 1978

Notes:

(A) Dendrochronologically-corrected date (reported in calendar years B.P.); based on a bi-decadal atmospheric record.

Table 5. Radiocarbon dates associated with late Holocene eruptions of silicic tephra in the South Sister area. Dendrochronologically-corrected radiocarbon dates were calculated using the CALIB 2.0 software of Stuiver and Reimer (1986).

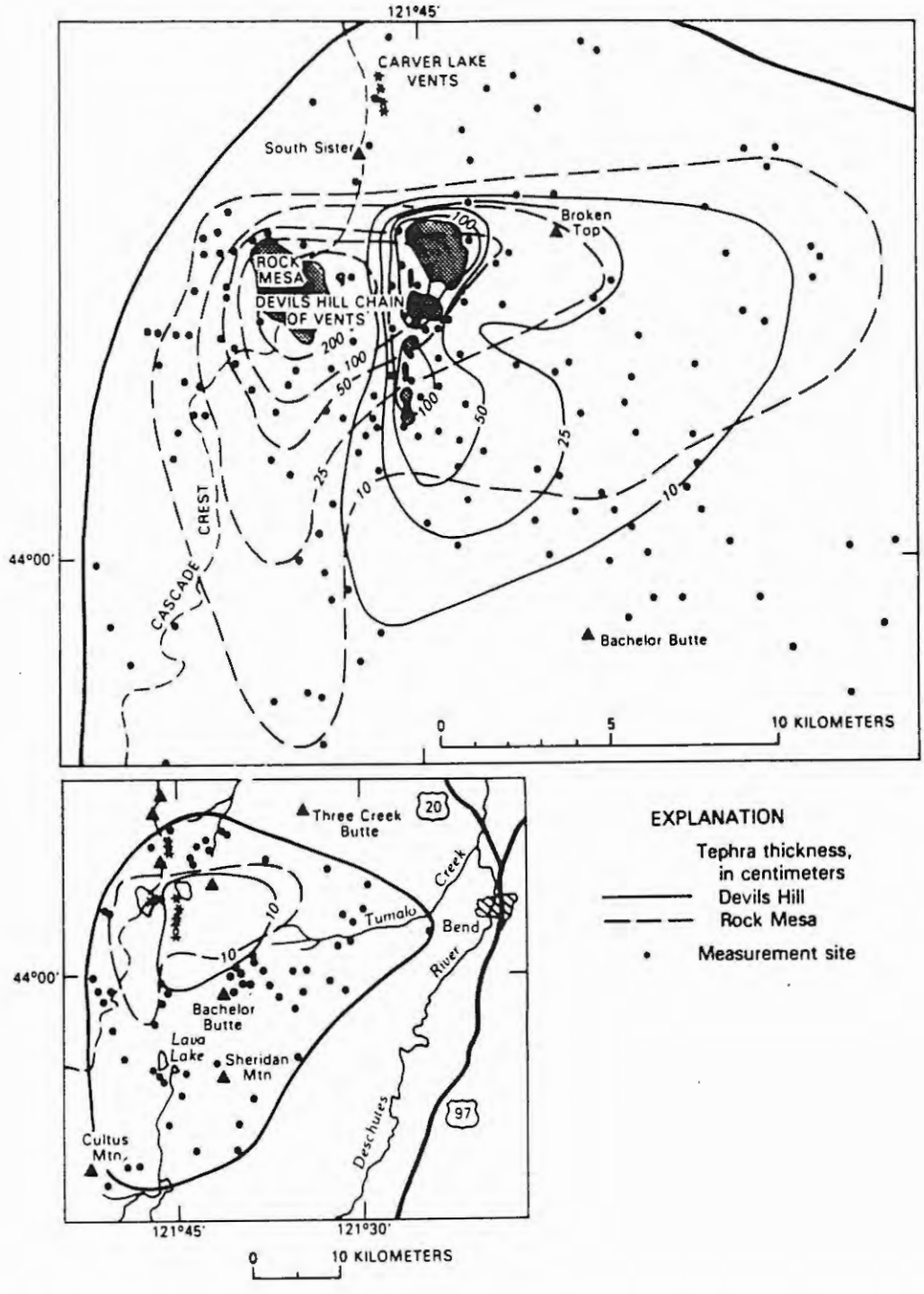

Figure 11. Isopachs of tephra from the Rock Mesa and Devils Hill vents. Asterisks represent flows and domes too small to be outlined on the map. The heavy line marks the approximate outer limit of tephra from both episodes (except in the west and southwest where only Rock Mesa ash is found). The eastern limits of the Willamette National Forest are bounded by the Cascade Crest. Maps are from Scott, 1987:41.

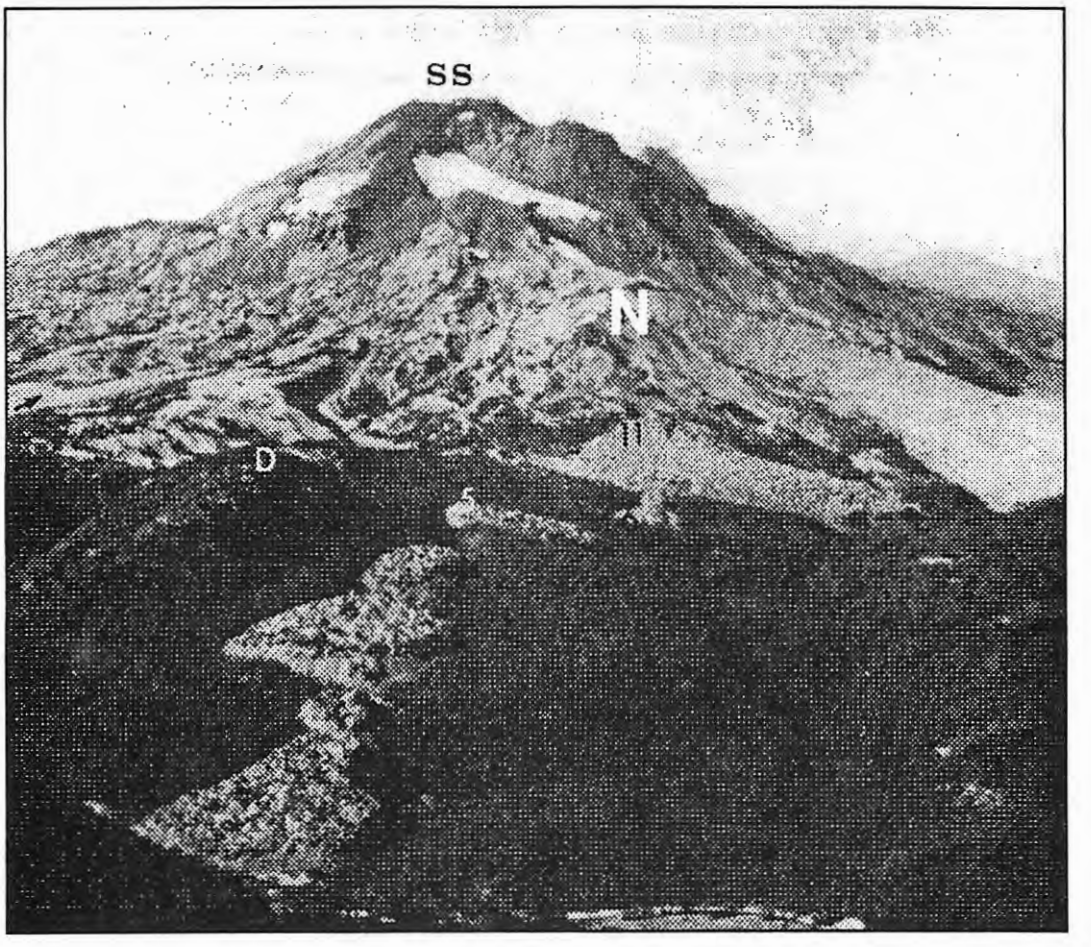

Plate 4. Aerial photograph of the south flank of the South Sister volcano (SS). The Devils Hill chain of domes runs from the shores of Sparks Lake at the lower left edge of the photograph to the Newberry flow (N) on the upper slopes of the South Sister. Devils Hill (D) lies just to the west (left) of the dome chain. The faint numbers (1, 5, 6, and 11) refer to the vent number; vent 11 is also locally known as the Miller flow. The arrow on the center left points to the Rock Mesa-ENE dome; the Rock Mesa flow is located just to the west of this vent. The Carver Lake vents (not visible) lie over the east (right) shoulder of the volcano. The photograph is from Scott, 1977:37.

Radiocarbon dates associated with the Devils Hill activity range from 1970 $\pm$ 200 ^{14}C years to 2480 $\pm$ 100 years ^{14}C B.P. (table 5). Limited paleomagnetic data suggests that both the Devils Hill and Rock Mesa eruptions probably took place between about 2,000 and 2,300 radiocarbon years B.P. (Scott, 1987). The period of time that separated the two events can be estimated by the amount of soil development and peat accumulation on the Rock Mesa tephra. Rock Mesa buried soils are very poorly-

developed, pointing to a relatively short interval before they were covered by the more recent Devils Hill pyroclastic deposits. Several centimeters of peat have accumulated between deposits from the two events in some locations and Scott (1987) speculates that the length of time between the two eruptive episodes was probably no more than a few hundred years but probably at least 100 years.

The chemical composition of the tephras is also virtually identical, pointing to a common source of magmas for both series of eruptions (Scott, 1987).

CARVER LAKE CHAIN OF VENTS

At about the same time as the eruptions along the Devils Hill chain of vents, eruptions of silicic tephra also took place from several aligned vents high on the northern slopes of the South Sister. These vents (C-1 through C-4 in figure 10) were the source of a much thinner and less extensive tephra blanket than the one from the Devils Hill vents. Several rhyolite domes were extruded after the tephra eruptions.

The small quantity of ash from the Carver Lake vents was carried primarily to the east and forms a thinner, more discontinuous, and much less extensive cover than tephra from the Devils Hill chain of vents. The pyroclastic activity that preceded the emplacement of the domes was relatively brief and small when compared with other tephragenic volcanic activity in the South Sister area. Ash from the Carver Lake eruptions overlies Rock Mesa tephra and is overlain by and perhaps interbedded with Devils Hill ash. The Carver Lake and Devils Hill eruptions appear to be, in any interpretation, virtually coeval. Ash from the Carver Lake vents, because of its poor exposure and limited extent, was not mapped by Scott (figure 11). Though the vents lie less than 1 km east of the Willamette National Forest boundary, it is unlikely that significant deposits of the Carver Lake tephra are found there today.

The chemical composition of the Carver Lakes tephra is also indistinguishable from the Devils Hill and Rock Mesa tephra. It is probable that the magmas erupted at the Carver Lake vents, as well as those at Rock Mesa and Devils Hill, originated from a radial dike fed by a single magma chamber located under the south flank of the South Sister volcano (Scott, 1987). This would account for the compositional similarities and contemporaneity of the eruptions of tephra in this region.

Some Unusual Deposits of Silicic Tephra

In addition to the Holocene sources of silicic volcanic tephra previously described, two additional deposits resembling Holocene tephra units were encountered that could easily be confused with Holocene airfall or ashflow deposits.

Upper Salt Creek Near-Vent Tephra and Obsidian

Outcrops of tephra-like deposits are exposed in several roadcuts along Highway 58 as the road passes the southern flank of Mt. David Douglas about 30 km east of Oakridge. The deposits consist of light-colored ash with a large percentage of gray to black glassy to microcrystalline obsidian and devitrified glass nodules. The glassy (obsidian) zone of a *rhyolite* flow is intersected by one of the roadcuts and the presence of Oligocene-Miocene rhyolite and obsidian flows are mentioned in the area by Woller and Black (1983). While the Salt Creek unit could be mistaken for a Holocene airfall or ashflow deposit, it is interpreted here to be a pre-Holocene near-vent deposit associated with the flows of rhyolite and obsidian erupted at this location.

Carver Obsidian Flow Pumice Zones

The Carver Obsidian flow is located on the middle northeastern flank of the South Sister volcano about 1.5 km east of the Cascade Crest. This large glaciated flow of microcrystalline gray obsidian and rhyolite is approximately 3 km long and over 100 m thick in many locations. Williams (1944:49) mentions that "...some of it consists of massive, unbanded lava so frothy as to resemble pumice."

A field check of the western margin of the flow revealed areas covered with silicic lapilli-like clasts of pumice >10 cm in diameter that could be easily confused with airfall pumice lapilli from a nearby vent, particularly one of the Carver Lake chain of vents. The pumice outcrops are all found at about the same elevation at scattered localities around the western margin of the flow. The large size of the clasts, the discontinuous exposures, and the lack of a suitably proximate vent argue against an airfall origin, however. The pumice outcrops are interpreted here to represent exposures of the pumice zone formed during the emplacement of the rhyolite flow. Vertical and horizontal zoned textural variations in rhyolite flows are well-documented and it is likely that the Carver Flow pumice clasts are simply surface exposures of these pumiceous zones (Fink and Manley, 1987).

HOLOCENE BASALTIC TEPHRA IN THE WILLAMETTE NATIONAL FOREST

Basaltic to *basaltic andesite* volcanic activity took place in numerous locations in the present-day Willamette National Forest during the Holocene. These Holocene volcanic vents, particularly those associated with deposits of basaltic tephra are described in the following section. A summary of all published radiocarbon dates associated with basaltic volcanic activity in this region appears in table 6.

Southern Flank of Mt. Jefferson to Santiam Pass

The upper southern flank of Mount Jefferson was the site of several episodes of tephragenic volcanic activity during the post-glacial period. These tephra sources,

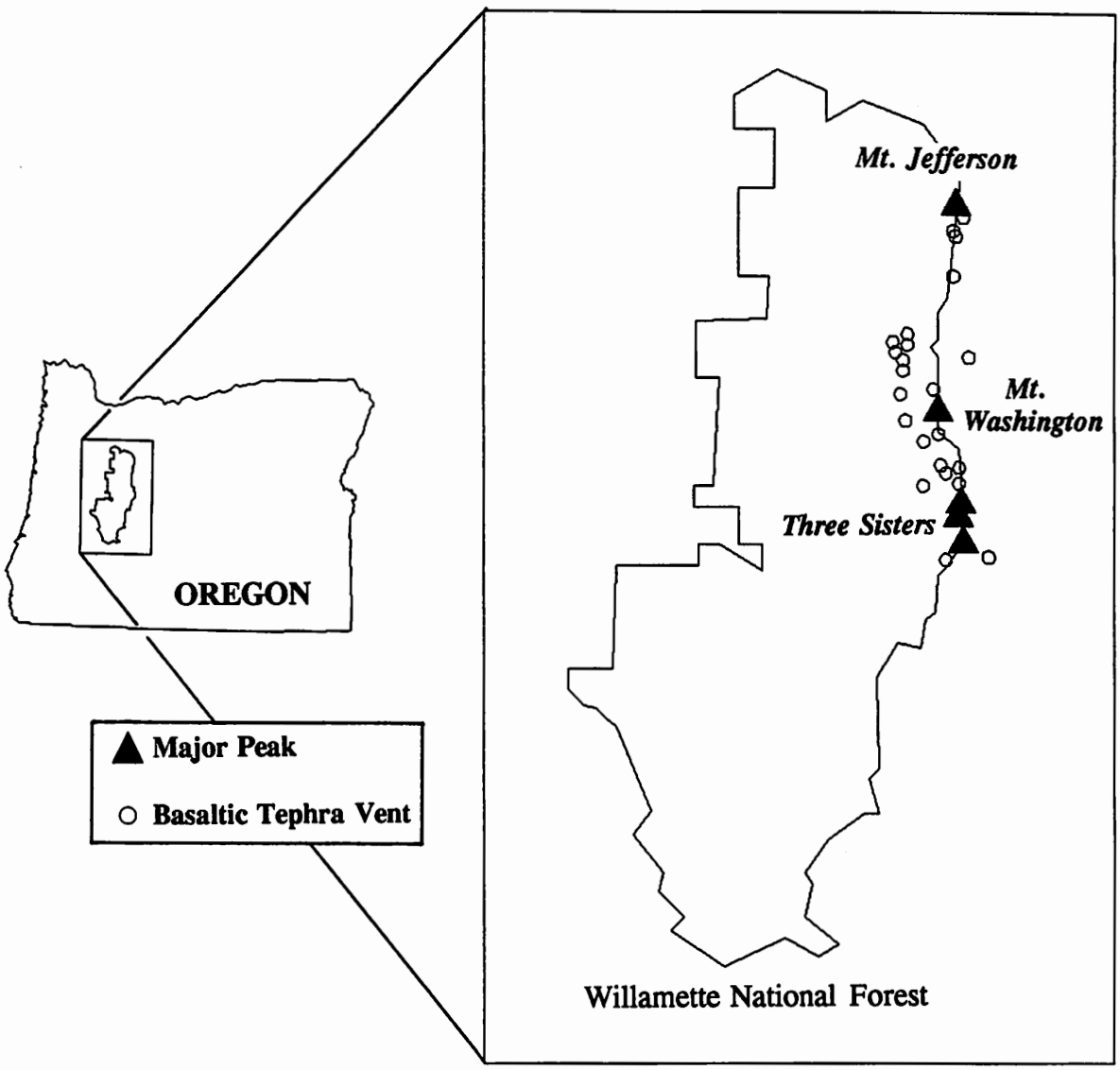

Figure 12. Distribution of Willamette National Forest Holocene basaltic tephra vents and potential sources of basaltic tephra deposits.

more isolated than most within and adjacent to the Willamette National Forest, also include some of the youngest potential ash deposits in the High Cascades of Oregon. The location and tephra distribution of Holocene volcanic vents is shown on the geologic sketch map of the Mount Jefferson area (figure 13).

ERUPTIVE UNIT	^{14}C AGE (YRS BP)	LAB. NO.	DENDRO-DATE (A)	REFERENCE (NOTES)
Belknap Summit Cone, North Vent Lavas	1400 ± 100	WSU-270	1303	1,2
Belknap Summit Cone, North Vent Lavas	1590 ± 160	WSU-292	1515	1,2
Lost Lake Group South Cone Cinders	1950 ± 150	WSU-371	1892	1,2
Four-In-One Cone Cinders	2550 ± 165	WSU-365	2740	1,2
Clear Lake Drowned Forest	2705 ± 200	-	2789	3
Little Belknap Lava	2883 ± 175	WSU-364	2996	1,2
Clear Lake Drowned Forest	3200 ± 220	-	3414-3455	3
Blue Lake Cinders	3440 ± 250	WSU-291	3695	1,2
Lava Flow Southeast of Fish Lake	3850 ± 215	WSU-327	4283	1,2
Cayuse Crater Scoria	9520 ± 100	W-5209	-	4 (B)

References:

1. Taylor, 1967:40
2. Chatters, 1968
3. Benson, 1965
4. Scott, 1987

Notes:

(A) Dendrochronologically-corrected date (reported in calendar years B.P.); based on a bi-decadal atmospheric record

(B) Date should regarded as a minimum

Table 6. Radiocarbon dates associated with Holocene volcanic activity in the Willamette National Forest. Dendrochronologically-corrected radiocarbon dates were calculated using the CALIB 2.0 software of Stuiver and Reimer (1986).

RED CINDER CONE

Red Cinder Cone, a Holocene tephra source located at an elevation of 2130 m asl on the south shoulder of Mount Jefferson, was first named and briefly described by Hodge (1925b:49):

> *On the south side just east of Cathedral Rocks is "Red Cinder Cone" rising to an elevation of 7750 feet. The ridge which is decorated by the Cathedral rocks is buried on its east side for over a mile by a thick mantle of black cinders. The cinder field descends from 7900 to 6200 feet ...*

This *cinder cone*, standing about 180 m high and covering an area of about 0.5 km^2, is located 1 km northeast of Goat Peak (plate 5). The cone is mantled by red and black scoriaceous lapilli, *bombs*, and ash, and is breached on the southwestern side by flows of basaltic andesite lavas that moved to the east. The cone was mentioned by Sutton (1974:29) and most recently was described and mapped by Gannon (1981:80-82)

The blanket of tephra that originated from Red Cinder Cone covers much of the north-south ridge leading from The Table past Goat Peak to the upper southern flank of Mount Jefferson (plate 5). The thickness of the tephra drops off rapidly at the southern edge of the ridge and finally disappears from surficial deposits at the southern border of The Table, about 3.5 km south of the vent. The areal extent of the Red Cinder Cone tephra was estimated by field checks of the southern part of the deposit, by color changes visible from viewpoints at Forked Butte and the Pacific Crest Trail (plate 6), and from aerial photograph interpretation.

HODGE CONE

This small cinder cone, located at the base of the southernmost dome of The Table (figure 13), was named and described by Gannon (1981:91-92), though it was earlier mapped as a Holocene cone by Scott (1974, Plate I). The cone rises 84 m above the surrounding glaciated landscape and is topped by a well-preserved crater with an ice-fed lake. No lava flows are associated with Hodge Cone and any eruptions of tephra from the vent appear to have been very localized.

Hodge Cone is post-Mazama in age and Gannon (1981:92) suggests that the cone may be no more than a few thousand years old.

FORKED BUTTE

Originally named Twin Volcano and Twin Cinder Peak by Hodge (1925), Forked Butte is a large cinder cone situated about 1 km east of the Cascade Crest (plate 7). Two remnant craters occur at the summit of the cone and at least six lava flows erupted from vents at the cone.

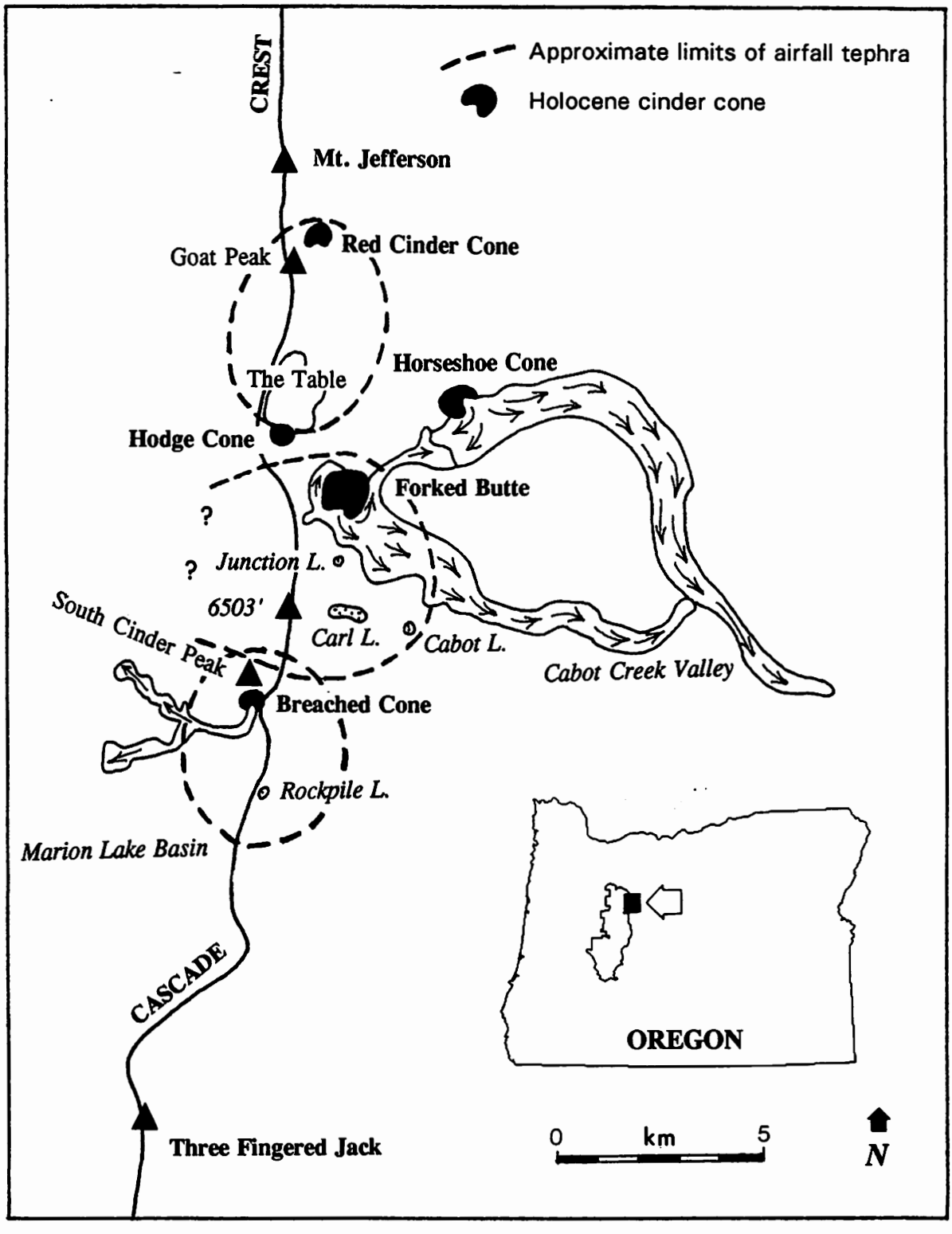

Figure 13. Geologic sketch map of the south flanks of Mount Jefferson. Map is adapted from Scott, 1977.

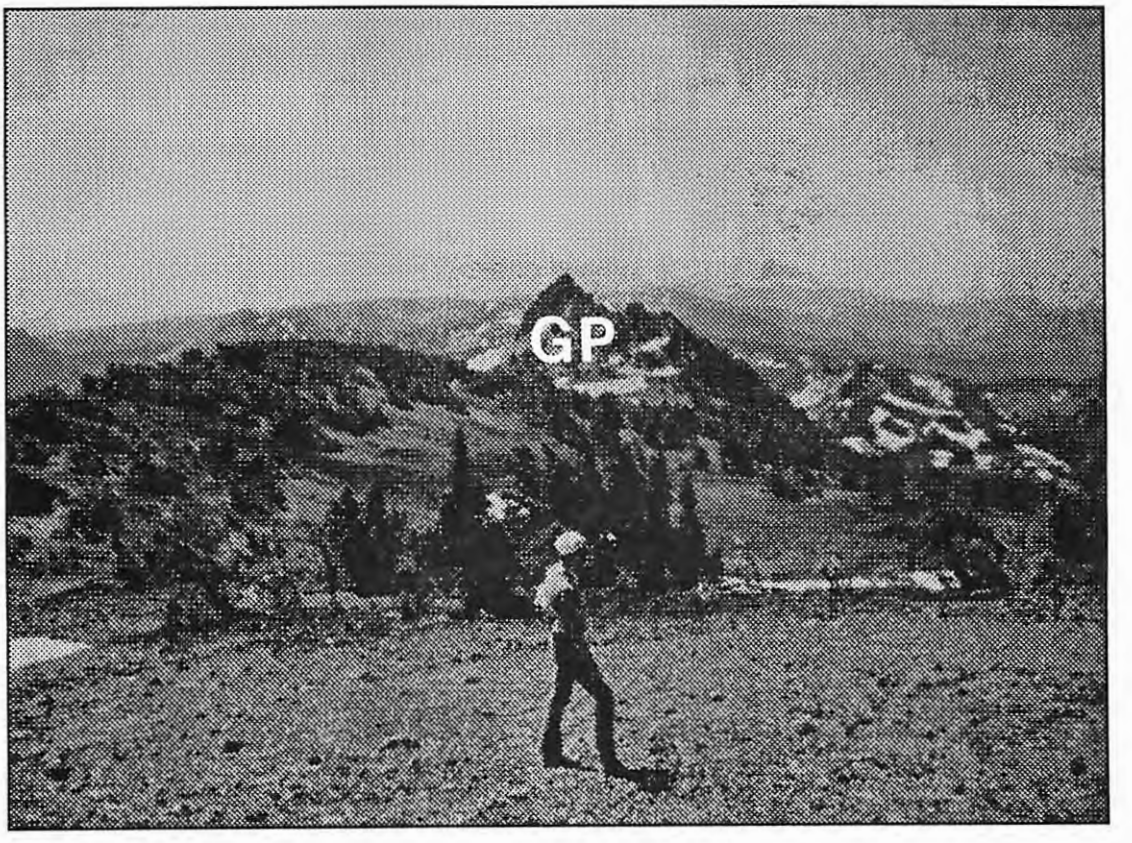

Plate 5. Cinder and ash fields immediately west and southwest of Red Cinder Cone. Basaltic tephra from the Red Cinder Cone vent covered the ridge to the south of the vent with a thick blanket of pyroclastic debris. The thickness of the tephra decreases rapidly about 0.5 km south of Goat Peak (GP).

Tephragenic volcanic activity at Forked Butte took place not long after the eruption of Mount Mazama and the deposition of Mazama tephra in the region. Exposures in trail cuts about 1 km northwest of Carl Lake show approximately 14 cm of tan to orange Mazama tephra overlain by about 20 cm of ash from Forked Butte. The Mazama tephra shows no sign of soil development, suggesting a relatively short period of time between the deposition of the two tephra units. Numerous other additional exposures along the Pacific Crest north of South Cinder Peak show 10-20 cm-thick layers of Mazama tephra mantled by dark basaltic ash from Forked Butte.

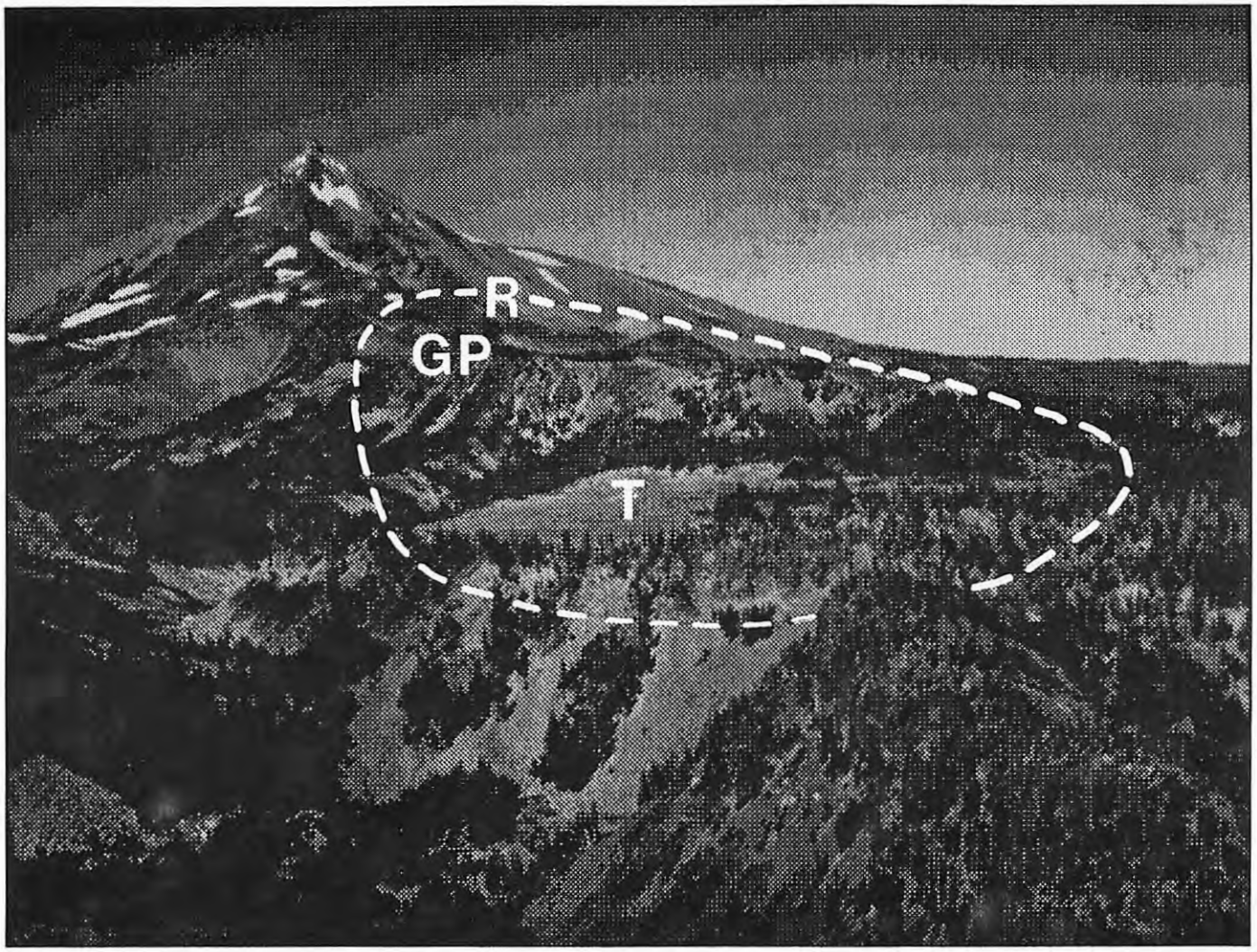

Plate 6. The southern flank of Mount Jefferson. Basaltic tephra from Red Cinder Cone (R), located upslope from Goat Peak (GP), was strewn as far as 3 km west-southwest of the vent. The dashed line indicates the approximate boundaries of the airfall ash. A thin dusting of the tephra reaches as far as the southern edge of the Table (T), a complex of three distinctive coalescing flat-topped domes of glaciated andesite. Photograph taken facing northeast.

The Forked Butte tephra was erupted in several nearly contemporaneous episodes prior to the extrusion of lava flows from vents around the base of the cone. At least two different eruptive sequences are suggested by a repetition in the stratigraphic profile visible in a test pit described by Gannon (1981:87) and in one dug about 1 km southwest of the cone during the current investigation.

The main axis of the Forked Butte tephra fall, unlike those from most High Cascades vents, lies almost due west of the vent. Well-stratified *cinders* and ash from the eruptions form prominent cinder fields to the west and southwest of the cone and blanket the area to the west and southwest for at least 3 km (plate 8). The tephra blanket thins very rapidly to the north and is not visible in trail cuts on the north side of the Patsy Lake Basin, only about 1 km from the source. The volume of *scoria* deposits from Forked Butte has been estimated to be 25 to 30 million cubic yards (Walker et al., 1966:28-29).

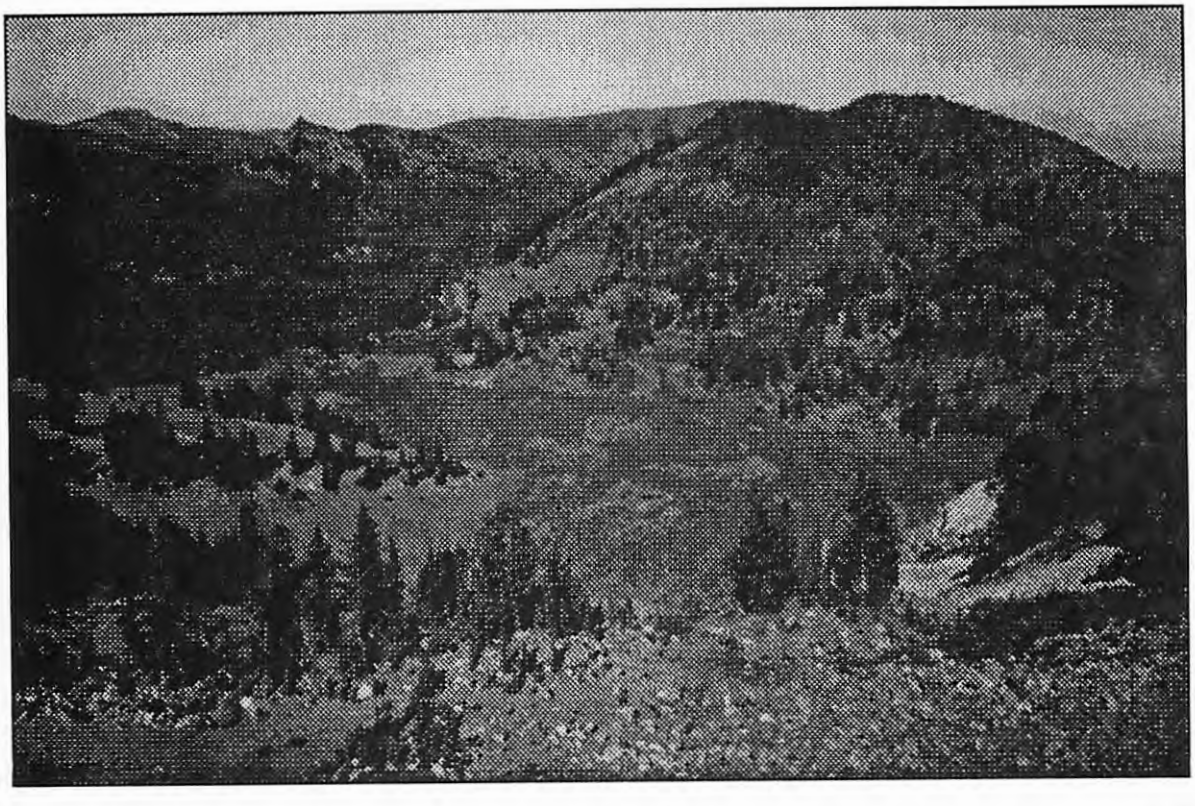

Plate 7. Forked Butte. Basaltic cinders and ash from this vent, unlike most of the High Cascades cinder cones, were carried almost directly west. The post-Mazama cone was active perhaps only a few hundred years after airfall Mazama tephra covered the entire region. Photograph facing northeast from an overlook of the Pacific Crest Trail along the Cascade Crest.

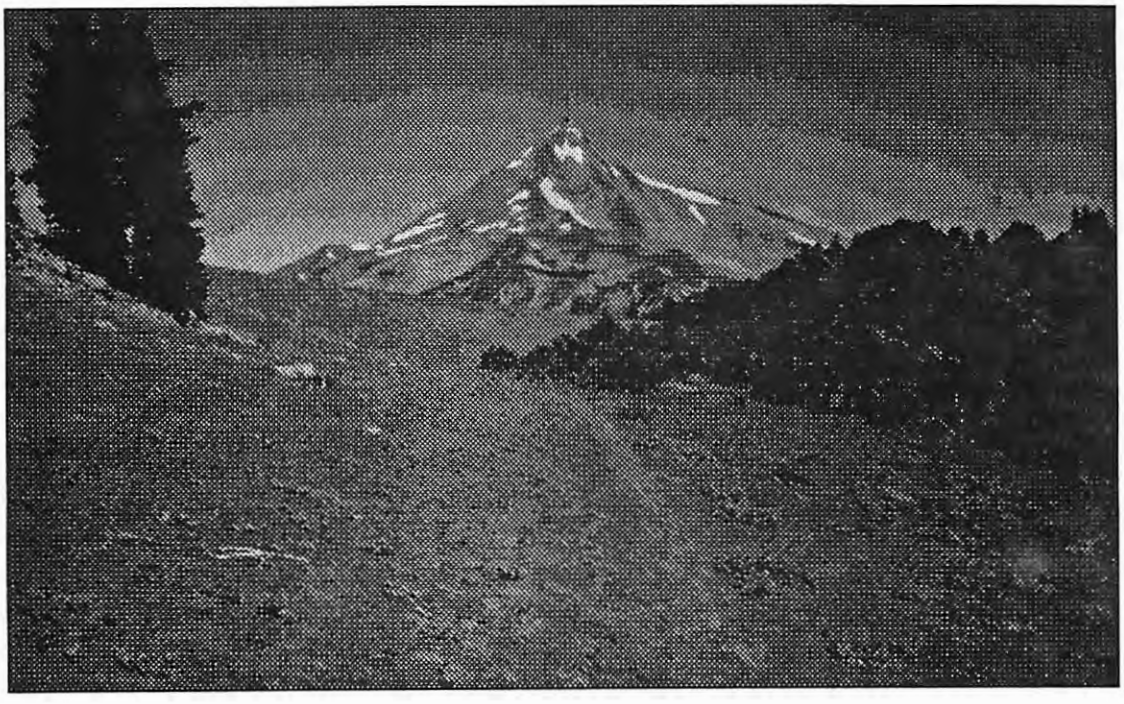

Plate 8. Fields of cinders and ash located less than 1 km west of the Forked Butte vent. The lava flows at the left were extruded from a vent at the base of Forked Butte, probably only a very short time after the deposition of the pyroclastic materials that make up the cinder field. Photograph taken facing north; Mount Jefferson is in the background.

A core from Cabot Lake, located 3 km southeast of Forked Butte, contained a 20 cm-thick layer of coarse, black Forked Butte tephra separated from 15 cm of Mazama ash by 9 cm of lake sediments. Scott (1974:54 and 1977), using a calculated average sedimentation rate of 0.07 cm/^{14}C yr, estimated that the eruptions of tephra at Forked Butte took place about 6400-6500 C14 years ago.

An unnamed peak (elevation 6503 ft) adjacent to the Pacific Crest Trail about 1.5 km north of South Cinder Peak was identified in aerial photographs as a possible Holocene tephra source. Field reconnaissance indicated that the peak was a probable Pleistocene vent mantled by volcanic ash originating at Forked Butte, 2.5 km to the northeast.

HORSESHOE (BEAR BUTTE) CONE

Shortly after the first Forked Butte eruptions, Horseshoe Cone (an unofficial name used by Scott, 1974:55), erupted lavas that flowed 13 km to the east down the Jefferson Creek and Candle Creek valleys. Located 2.5 km northeast of Forked Butte on the south side of Bear, this cone appears to have produced little volcanic tephra. Eruptions at Forked Butte and Horseshoe are considered nearly contemporaneous, and occurred very shortly after the deposition of Mazama tephra in the region (Gannon, 1981:89). No tephra from this source was found in a reconnaissance of the Cascade Crest area about 3 km west of Horseshoe Cone.

BREACHED CONE (SOUTH CINDER PEAK)

The youngest dated tephragenic volcanic activity along the south flank of Mount Jefferson took place at Breached Cone, the unofficial name for a 120 m-high cinder cone situated on the southern flank of South Cinder Peak along the Cascade Crest

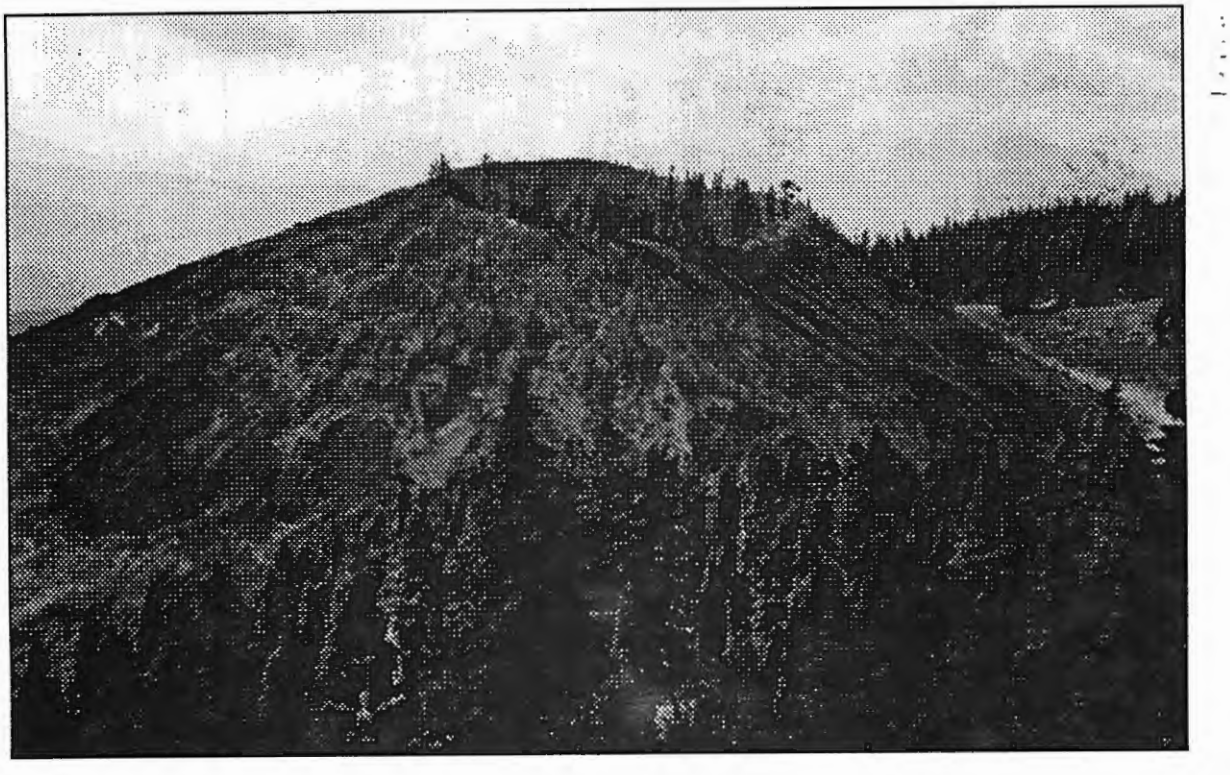

Plate 9. Breached Cone, one of the youngest cinder cones in the Willamette National Forest. Located on the south side of South Cinder Peak, basaltic tephra from this vent was erupted only about 1,000 ^{14}C years ago.

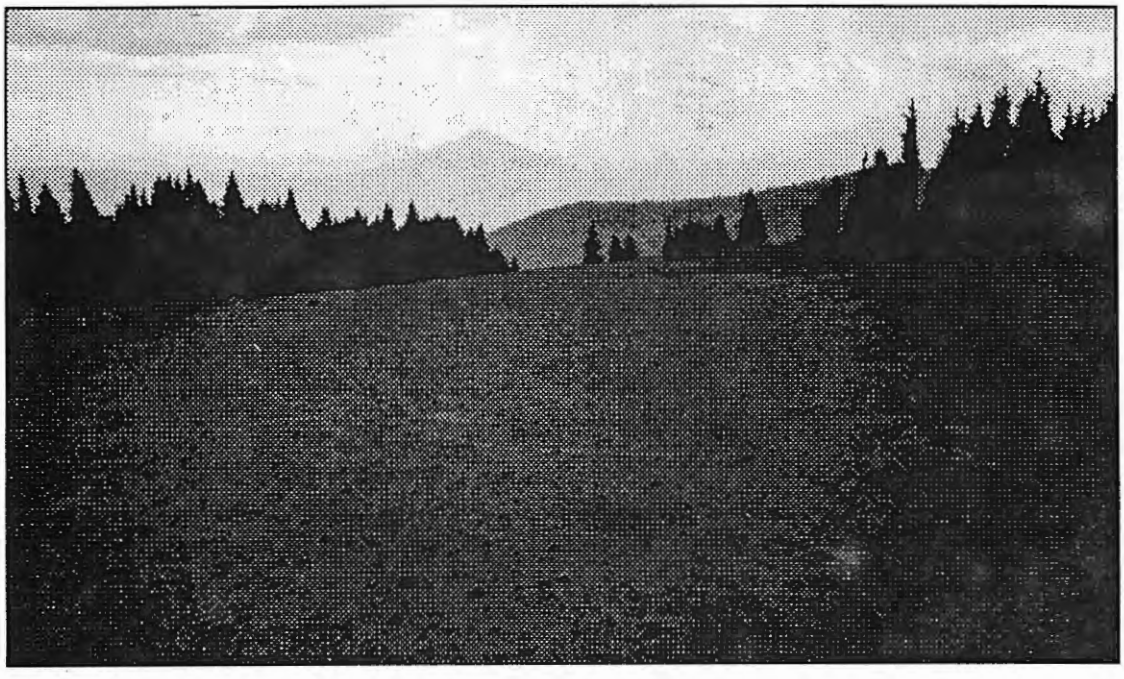

Plate 10. Cinder and ash fields located immediately east of Breached Cone on the Cascade Divide. The pyroclastic materials from Breached Cone directly overlie the considerably earlier tephra from Mount Mazama at this location.

(Walker et al., 1966:26-27,30-31)(plate 9). Lava flows of basalt were extruded from a vent at the southern base of Breached Cone and reached several kilometers west into the Marion Lake Basin.

Tephra from the eruption of Breached Cone covers the vicinity around South Cinder Peak and the head of the Cabot Creek Valley immediately to the east. Field reconnaissance and aerial photograph interpretation indicate that cinder fields of reddish-brown pyroclasts extend east and southeast of the cone for 1-2 km (plate 10). The volume of the cinders and ash from Breached Cone has been estimated at about 11 to 14 million cubic yards (Walker et al., 1966:26). The tephra thins very rapidly to the north and northeast of South Cinder Peak, suggesting that the main eruption plume was probably directed on an east to southeast axis. At sampling location SCINP-1, 16 cm of cinders from the eruption directly overlay Mazama tephra. Cinders are also reported at the bottom of Rockpile Lake 1.5 km south of the cone (Scott, 1974:55). Several centimeters of Breached Cone ash were found by Scott (1974:55) at a depth of 75 cm in Cabot Lake. Using the Carl Lake sedimentation rate

that was calibrated by Mazama tephra, Scott estimated that the eruption of the Breached Cone tephra occurred only about 1000 ^{14}C years ago. This age would place it as one of the most recent volcanic events in Oregon. The age determination of the Breached Cone eruption was erroneously attributed to radiocarbon dating methods by Davie (1980:36).

Though tephra from Breached Cone has not been reported from any archaeological sites, it has been used to establish the relative age of recent glacial advances in the area (Scott, 1977:118).

Sand Mountain Alignment

The Sand Mountain alignment is a north-south linear alignment of 22 cinder cones and 41 distinct vents that stretches about 9 km from the Lost Lake area to a group of vents about 2 km south of South Sand Mountain. The major landforms of the Sand Mountain Alignment are, from north to south: Little Nash Crater and the Lost Lake Group on the north; Nash Crater and the Central Group farther south; the Sand Mountain cones, and the South Group (figure 14). Throughout the Holocene , these closely spaced vents discharged over 4 km^3 of lavas and a considerable, though still unknown, volume of tephra of basaltic to basaltic andesite composition (Taylor, 1965; Taylor, 1967:4-6). Volcanic tephra is known to be associated with several of the vents of the Sand Mountain chain: Little Nash Crater, the Lost lake Group, Nash Crater, and Sand Mountain. Much of the recent geologic information concerning the geology and tephra of the Sand Mountain originates from the work of Edward Taylor of Oregon State University (Taylor, 1965, 1967, 1968, 1981; Taylor et al., 1987). The geology of the Sand Mountain area has also been discussed by Brown (1941), Jan (1967), Davie (1980:36), Goles (1980), and Scott (1974:55). The limits of airfall tephra from the major Sand Mountain vents were conservatively estimated and the tephra boundaries shown in figure 14 should be considered as absolute minimums.

It should be noted that the coarse reddish volcanic cinders that are common in many roadcuts in the Santiam Junction to Santiam Pass area were often not deposited by volcanic eruptions in the Sand Mountain alignment area, but by snowplows.

LOST LAKE GROUP

A short alignment of four Holocene cinder cones forms a prominent ridge across the glaciated valley of Lost Lake Creek 3 km east of Santiam Junction. The lava-dammed Lost Lake provides the name for this chain of cinder cones, the Lost Lake Group. The smallest cones lies above the north valley wall above Lost Lake, while the remaining three cones are spaced around the northwestern and western shores of the lake. The southernmost cone of the Lost Lake Group rises about 100 m above the Santiam Highway and is intersected by the road not far west of Lost Lake. Lava flows from the Lost Lake vents are largely obscured by a cover of basaltic tephra from these vents and from Little Nash Crater to the west (Taylor, 1965; 1967:8-9).

To the west of the vents, tephra is restricted to the immediate area in the vicinity of the cones. The greatest volume of pyroclastic materials is found to the east of the Lost Lake cones, where they were carried by prevailing winds at the time of the eruptions. Bogs on the summit of Hogg Rock, 3 km to the east of the vents, contains fine ash that can be traced to the Lost Lake Group (Taylor, 1967:8). Fine ash is also exposed in Santiam Highway roadcuts just east of Lost Lake where it is overlain by tephra from Little Nash Crater.

Fragments of charred limbs recovered at the base of coarse cinders traced to the south cone of the Lost Lake Group have been dated at 1950 ± 150 radiocarbon years B.P. (WSU-371)(Taylor, 1967:8-9; see table 6).

LITTLE NASH CRATER

The youngest eruptions along the Sand Mountain Alignment occurred at Little Nash Crater, a 140 m-high cinder cone located at the junction of the North and South Santiam highways (22 and 20). The cone has been extensively quarried for cinders for many years and is slowly vanishing. After the eruption of pyroclastic materials early in development of the cone, lavas were extruded from a vent at the western base of the volcano.

Road cuts immediately north of Little Nash Crater (plate 11) display an 8 cm-thick layer of fine ash from Nash Crater overlain by 1-2 m of Little Nash Crater pyroclastic deposits. Both of these tephra deposits are underlain by 6,845 year-old Mazama tephra which rests directly upon glacial moraine deposits.

Tephra from Little Nash Crater thins rapidly to the north, west, and south of the vent, and cannot be found 0.4 km (.25 mi) from the cone in these directions. East of the vent, however, the tephra blankets an area of more that 250 km^2. A thick deposit of coarse cinders is spread eastward from the vent, rapidly grading to a fine ash that covers the entire Santiam Junction area. This fine ash from Little Nash Crater is well-exposed in Santiam Highway roadcuts immediately east of Lost Lake where it overlies tephra from the Lost Lake Group (Taylor, 1965; 1967:6-7).

No radiocarbon dates are associated with Little Nash Crater, though tephra from the cone overlies the ash and lavas of the Lost Lake Group eruptions that are dated at about 1950 radiocarbon years. The presence of 300-400 year-old living trees on the cone places the age of eruptions at Little Nash Crater at no earlier than 1950 radiocarbon years and no later than the age of the trees (Taylor, 1967:40-41).

NASH CRATER

Nash Crater, a 150 m-high cinder cone found 2 km south of Little Nash Crater, was the source of several late Holocene lava flows and eruptions of tephra. Lavas from

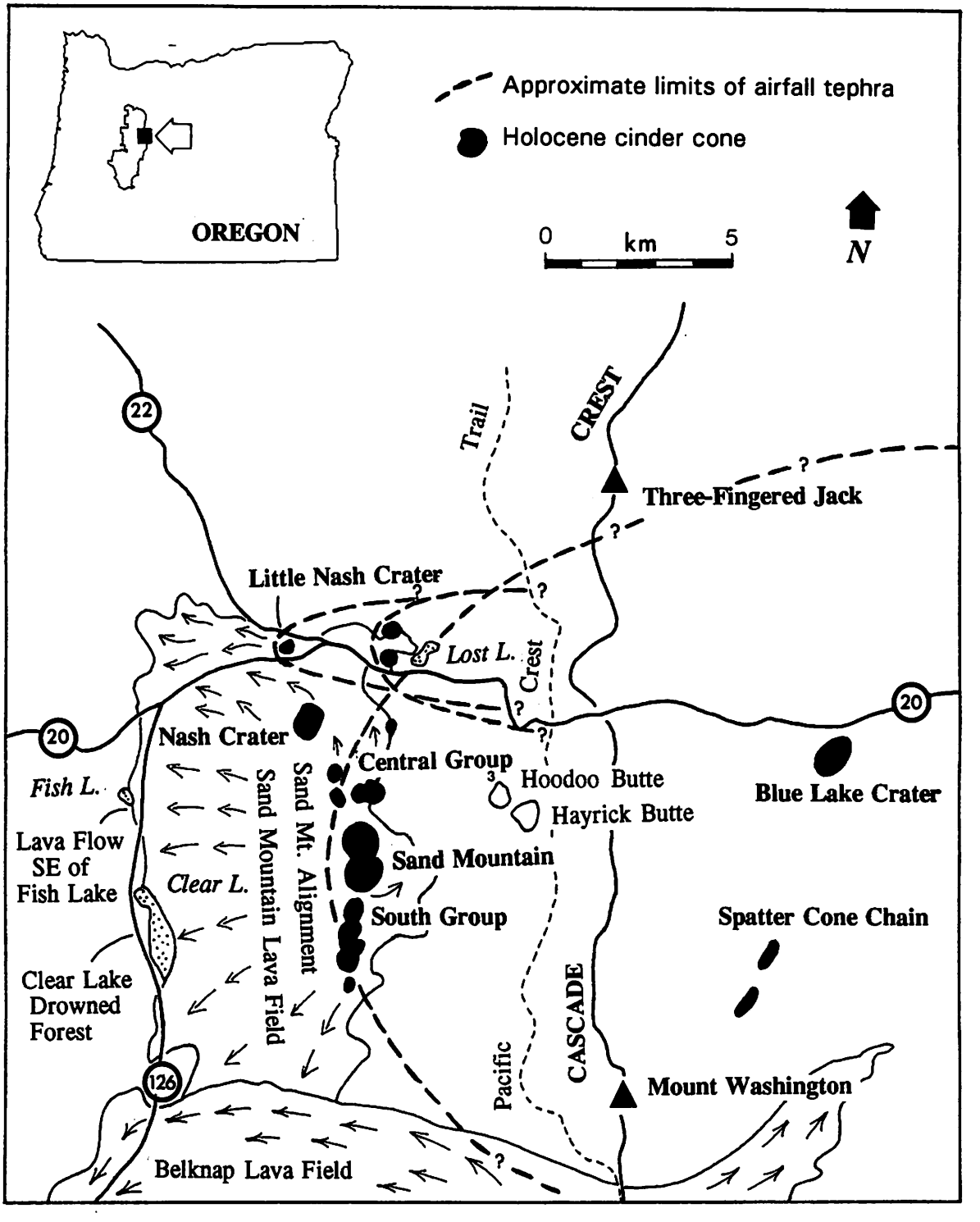

Figure 14. Geologic sketch map of the Sand Mountain Alignment and Santiam Pass region. Base map is adapted from Taylor, 1965:2.

Plate 11. Roadcut in Highway 22 immediately north of Little Nash Crater. Tephra from Little Nash Crater and Nash Crater overlie Mazama (M) ash in the exposure. The Mazama tephra directly overlie glacial deposits (G). The dashed line marks the contact of these glacial deposits and the Mazama ash. The identity of the Mazama tephra was confirmed by electron microprobe characterization of a sample from this location (LNASH-6). The presence of glacial deposits capped by Mazama tephra is common in roadcuts in this area. Scientist for scale.

vents on the northwest and south flank of the cone flowed several kilometers west to the Fish Lake area.

The distribution of tephra from Nash Crater is poorly known. A thin layer of ash is exposed just north of Little Nash Crater in a previously-described roadcut. Taylor (1967:9 and 1968) also reports that fine ash from the summit crater of the cone can be found near the vent in interstices of lavas from the northwest vent. Like most of the High Cascades vents, much of the pyroclastic material associated with Nash Crater eruptions probably lies to the east of the vent where it is now buried under the more recent tephra deposits from Sand Mountain.

The age of tephragenic activity at Nash Crater can be only broadly established. Lava flows originating from a vent at the northern base of Nash Crater flowed to the east where they overlie an older flow unit that was probably associated with early eruptions at the volcano. These north vent flows, also known as the Fish Lake Flows, overlie ash from several other Sand Mountain alignment vents as well as lavas from the west vent of North Sand Mountain. Fish Lake, a lava-dammed lake located 5 km west of Nash Crater, was created by a lava flow (known as the flow southeast of Fish Lake) that is overlain by the Fish Lake Flows from Nash Crater. The flow southeast of Fish Lake contains tree molds from which charcoal was recovered and dated at 3850 $\pm$ 214 ^{14}C years B.P. This date, then, sets the maximum age for the Fish Lake Flows. Assuming contemporaneity between basaltic pyroclastic eruptions and the extrusion of lava flows, this date also fixes the possible earliest age of tephra deposits from Nash Crater. The minimum age of the Nash Crater tephra can also be only broadly placed. The Nash Crater scoria and ash are overlain by Little Nash Crater tephra, establishing the minimum age of the Nash Crater pyroclastic deposits as pre-Little Nash Crater, or somewhere beteen 1950 ^{14}C years ago and a few hundred years ago (Taylor, 1965; 1967:40-41).

SAND MOUNTAIN

The Sand Mountain cones are the two largest volcanoes in the Sand Mountain Alignment and stand about 230 m above the surrounding lava flows and ash fields. The most areally widespread and voluminous deposits of basaltic tephra in the Sand Mountain Alignment area originated from these two cones. These two large coalescing cinder cones, found 6.5 km west of the Cascade Divide, are the source of an extensive deposit of basaltic tephra that covers an area of more than 250 km^2 (100 mi^2). Much of the Sand Mountain tephra has been reworked by surface water and it is difficult to reconstruct the original thickness of the primary deposits (Taylor, 1967:11-13.).

Sometime before 3850 radiocarbon years ago, eruptions from the cones spread up to 90 cm of black ash over the Suttle Lake area. Ash from the Sand Mountain eruptions was deposited largely to the east and northeast of the vents and can be traced for many

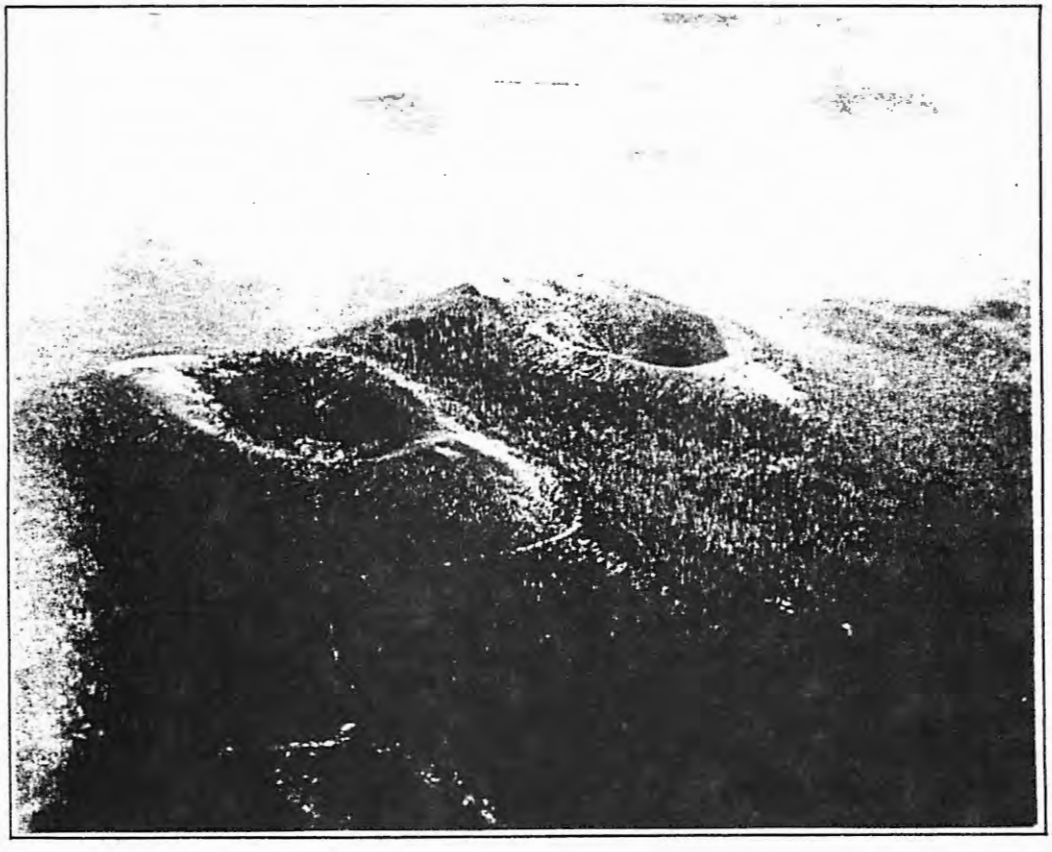

Plate 12. Aerial view of the North and South Sand Mountain cones (facing southeast). These two coalescing cinder cones, the largest in the Sand Mountain Alignment, were the sources of basaltic tephra that covered an area of area of over 350 km^2 to the east of the vents. Photograph is from Taylor, 1968:9.

kilometers along the roadcuts of the Santiam Highway. About 20 cm of basaltic tephra is reported from the Canyon Creek cirque to the northeast; farther north in Cabot Lake, only about 1 cm is found (Scott, 1974:55). The main axis of the airfall deposits from the Sand Mountain cones lies from east to east-northeast of the vents.

The age of this locally widespread and chronologically significant basaltic deposit has, unfortunately, not been firmly established. Cinders from the Blue Lake Crater eruption, an event placed at 3440 $\pm$ 250 radiocarbon years ago (table 6), overlie the Sand Mountain tephra in exposures 12 km east of Sand Mountain at Blue Lake. The Sand Mountain ash is also overlain by the lava flow southeast of Fish Lake (discussed previously in association with Nash Crater), a flow dated at 3850 $\pm$ 214 radiocarbon

years. The previous contact relationship establishes the minimum age of the Sand Mountain tephra at 3850 ^{14}C years ago (Taylor, 1965:23-24,41; see table 6). These data contraindieate the circa 3,000 B.P. age for the Sand Mountain eruptions that is suggested by radiocarbon dates from the Clear Lake drowned forest (table 6). Sand Mountain ash overlies the lava flows that created Clear Lake and it was initially assumed that the age of the Clear Lake drowned forest was closely associated with the age of the emplacement of the flow (Benson, 1965). It appears, however, that the Clear Lake radiocarbon dates do not reflect the actual age of the Sand Mountain eruptions (Taylor, 1967:24).

The age of other eruptive events along the Sand Mountain alignment suggests that the maximum age of the Sand Mountain tephra probably lies near the minimum contact age of 3850 ^{14}C years B.P. At this point, however, the maximum age of the Sand Mountain events simply has not been clearly established. The refinement of the Sand Mountain eruptive chronology remains a significant problem to be resolved.

Santiam Pass to McKenzie Pass

Several Holocene vents are found along the Cascade Crest between Santiam Pass and McKenzie Pass, though only one of them, Belknap Volcano, was a source of volcanic tephra deposits located within the Willamette National Forest.

Hoodoo Butte, a prominent unglaciated cinder cone located at the Santiam Pass, is assigned a late Pleistocene rather than Holocene age. Taylor (1981) speculates that the cone was shielded from Pleistocene glaciation by Hayrick Butte, a large andesite dome located immediately to the east of Hoodoo Butte.

The Holocene volcanic history of the area from Santiam Pass has been described by a number of researchers, most notably by Brown (1941) and Taylor (1965, 1967, 1968, and 1981).

BLUE LAKE

Blue Lake Crater was created by explosive eruptions that began about 3440 ^{14}C years ago (Taylor, 1965 and 1967). The large crater left by the eruptions is now filled by Blue Lake. A coarse layer of scoria is well-exposed in road cuts to the east of the crater; 50 cm of Blue Lake scoria overlies 70 cm of Sand Mountain tephra on the Suttle Lake Moraine. The tephra from Blue Lake Crater rapidly thins to the north; in Cabot Lake it may be present as a thin, fine-grained black ash (Scott, 1974:55). No tephra from the Blue Lake eruption was located within the boundaries of the Willamette National Forest.

MOUNT WASHINGTON SPATTER CONE CHAIN

This alignment of post-Mazama spatter cones and small craters runs for about 1.5 km between Blue Lake and Mount Washington. Pyroclastic deposits (mainly bombs and scoria) associated with this chain of spatter cones are very localized and restricted to the immediate vicinity of the vents (Taylor, 1965 and 1967:24). No pyroclastic deposits from these vents are found in the Willamette National Forest.

BELKNAP CRATER

Located along the eastern border of the Willamette National Forest, the Belknap Crater shield volcano complex was the source of the most extensive Holocene lava flows in the central High Cascades of Oregon. Flows from the many vents on the Belknap Crater shield covered an area of nearly 100 km^2 (Taylor, 1968). The Belknap shield was also the source of some of the most extensive Holocene eruptions of basaltic tephra recorded in this region (plate 13).

The main portion of ash from Belknap Volcano was ejected from the southern crater of the cone and is described by Taylor (1967:18):

> *The distribution of ash and cinders on the rim of Belknap Crater ... was caused by strong and prevailing wind transport to the east. Thin deposits of scoria are found on lava immediately west of the cone, but as the eastern slopes are approached the lavas become mantled in black ash and fine cinders. A wide area from Dry Creek on the north to Black Crater on the south was heavily blanketed and a continuous ash deposit can be traced eight miles to the east.*

Ash deposits from Belknap Crater have been traced over an area greater than 250 km^2, though only a very small percentage is found in the Willamette National Forest (Taylor, 1981). Exposures of the ash are common along the McKenzie Highway for several kilometers east of the McKenzie Pass. The Belknap ash thins rapidly to the north of the McKenzie Pass along the Pacific Crest Trail - within a few kilometers, Belknap tephra has disappeared completely from trail cuts and the ubiquitous Mazama-derived soil with its characteristic small pumice lapilli and pyroclasts (less than a few mm in diameter in this area) is exposed as the uppermost deposit.

A test pit dug in the southernmost kipuka on the lower southern slopes of Belknap Volcano revealed evidence of at least one major post-Mazama airfall tephra deposit (figure 35). Thirty-one centimeters of basaltic tephra that appeared to represent a single eruptive sequence overlay a Mazama paleosol.

No volcanic ash is associated with Little Nash Crater, a small cone located on the southeastern flank of Belknap Volcano. This vent was the source of extensive basalt flows on the eastern slopes of Belknap Volcano and is dated at 2883 $\pm$ 175

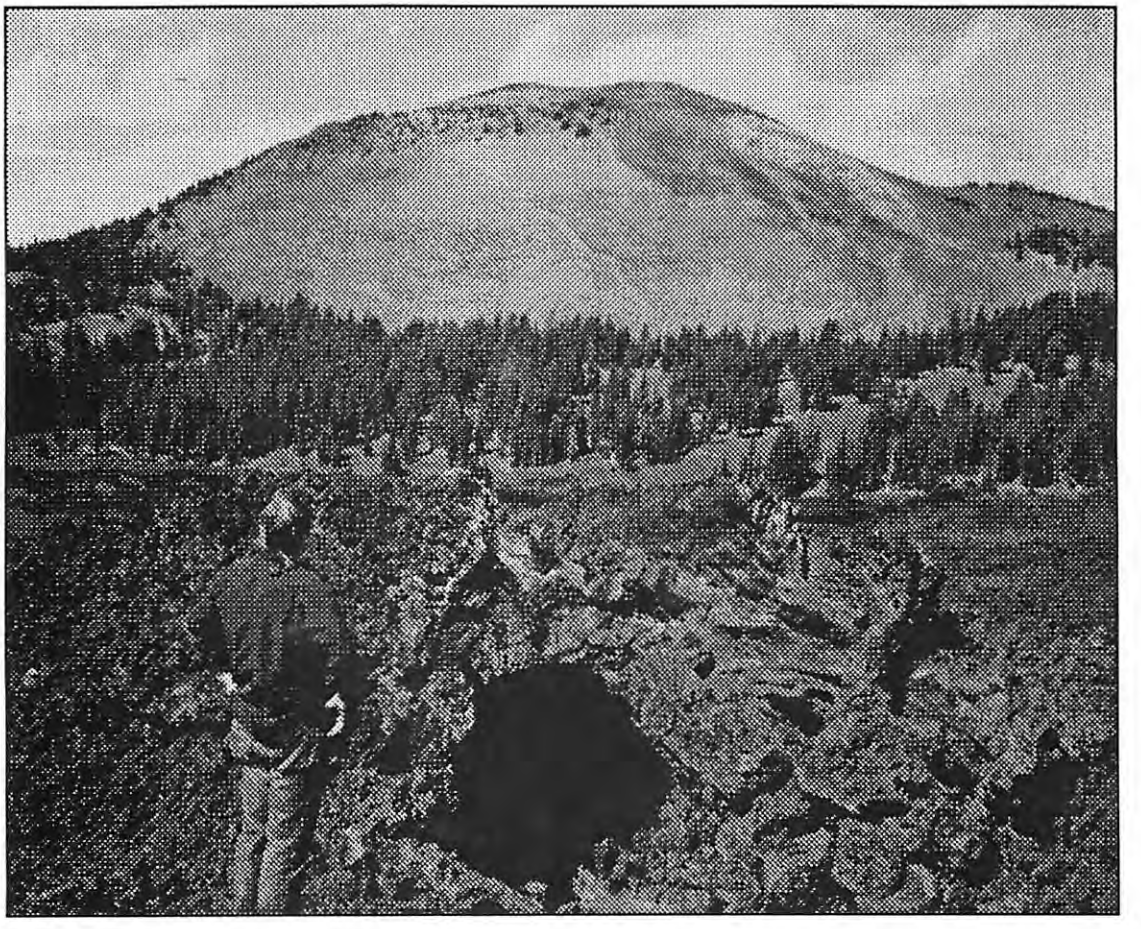

Plate 13. Belknap Crater. This cone, located on the Cascade Crest, was a major source of basaltic tephra in this region, though little of the ash drifted west into the Willamette National Forest. Photograph taken facing west from Little Belknap. Lavas from Little Belknap were erupted about 2900 ^{14}C years ago and covered the earlier Belknap Crater tephra deposits.

radiocarbon years (WSU-364)(Chatters, 1968; Taylor, 1967:40; see table 6). The lavas from Little Belknap Crater overlie all the Belknap tephra deposits that were examined in this area.

Volcanic activity at Belknap Crater appears to span well over 1000 years, with radiocarbon dates ranging from 1400 to 2883 ^{14}C yrs B.P. associated with lava flows from vents in the area (table 6). Deposits of basaltic tephra in the Belknap Crater are overlain by lavas from Little Belknap Crater and must have been deposited no sooner than 2883 ^{14}C years ago. The maximum date of the tephra eruptions has not been well-established. Pyroclastic deposits from Belknap Crater directly overlie well-

developed paleosols derived from Mazama tephra (see figure 35), suggesting that a considerable period of time elapsed between the Mazama ashfall and the ensuing Belknap tephra-falls. It is likely that the age the Belknap tephra lies nearer its minimum age of 2883 ^{14}C years than the 6850 ^{14}C-year-old age of the underlying Mazama tephra deposits.

McKenzie Pass to North Sister

Several tephragenic vents are found in the region between the McKenzie Pass and the base of the North Sister. The geology of this region has been most extensively described by Taylor (1965, 1967, 1968, 1981) and Taylor et al. (1987), with other contributions by Hodge (1925), Williams (1944), and Peterson and Groh (1965). The location of tephragenic vents and the areal distribution of volcanic ash deposits in the region are illustrated in figure 15, a geologic sketch map of the region.

YAPOAH CRATER

Rising 150 m above its surroundings, Yapoah Crater is the largest of a 2 km-long alignment consisting of several cones and vents. The southern side of the cone abuts against a glaciated ridge covered with ash and cinders from Yapoah Crater and the more recent Collier Cone (plate 14). Several flows of basaltic lava originated at the base of Yapoah Cone and spread northward as far as the McKenzie Highway area (Taylor, 1965; 1967:26-31). In the vicinity of Yapoah Crater, these flows are lightly mantled by a cover of basaltic tephra.

In the field, we found it difficult to distinguish tephra originating from Yapoah Crater from pyroclastic deposits from the younger and more widespread Collier Cone eruptions. Samples that were collected from tephra units thought to have originated from Yapoah Crater and Collier Cone are mineralogically and chemically similar (see Section V). We suspect that the tephra collected from deposits overlying and bordering Yapoah Crater lava flows did not originate from Yapoah Crater, as we thought, but from Collier Cone.

Basaltic tephra begins to appear adjacent to the Pacific Crest Trail about 2 km north of Yapoah Crater in the South Matthieu Lake vicinity. Though we originally thought that the ash originated from Yapoah Crater, in the light of our reinterpretation, we consider it likely that these deposits represent the distal margin of the Collier Cone ash deposits.

Lavas from Yapoah Crater, apparently coeval with the eruption of tephra, overlie Little Belknap Crater flows and are overlain by cinders from Four-In-One-Cone. This establishes the maximum age of Yapoah lavas and tephra at 2883 $\pm$ 175 ^{14}C years and the minimum age at 2550 $\pm$ 165 ^{14}C years (Taylor, 1965:40-42; Chatters, 1968; see table 6).

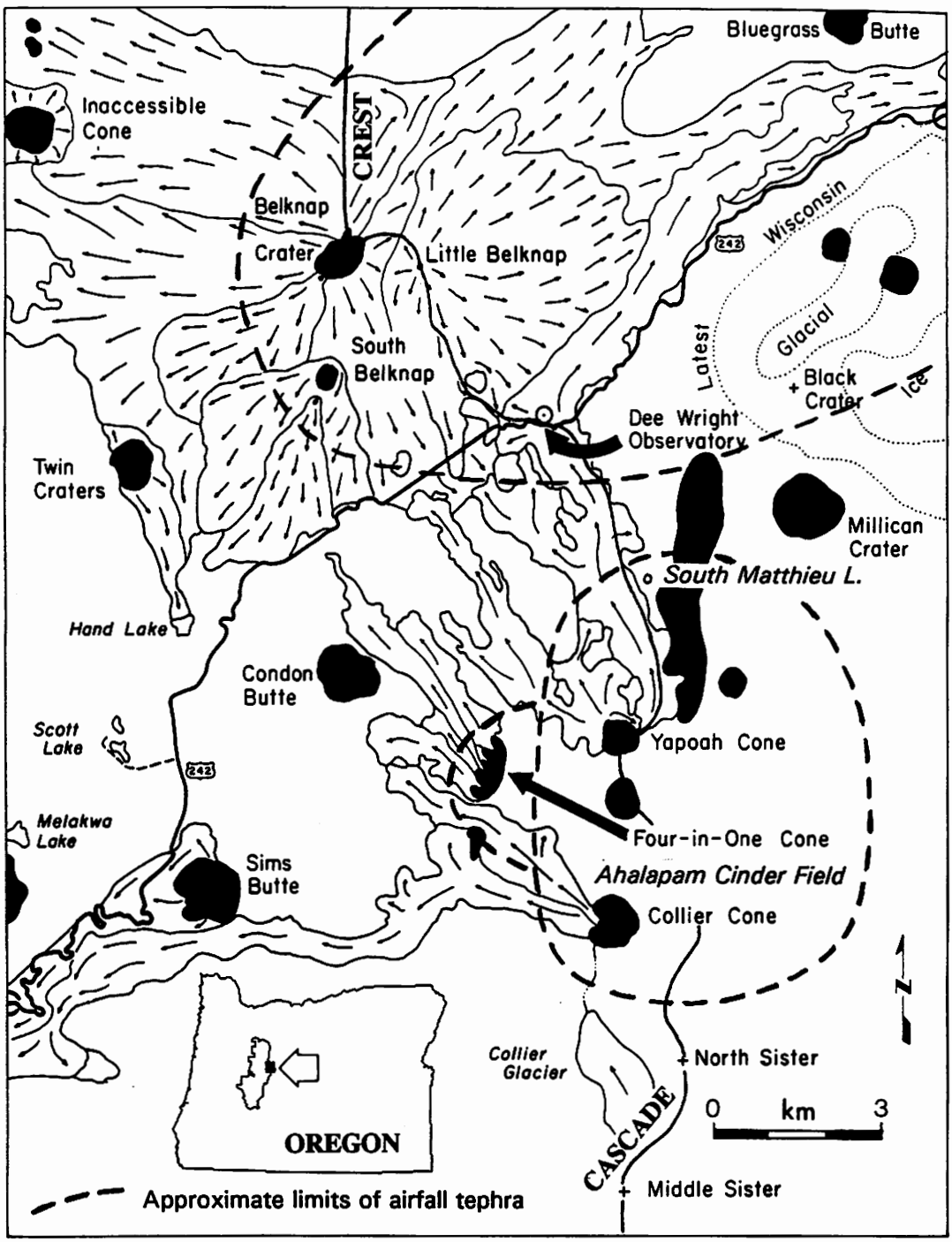

Figure 15. Geologic sketch map of the McKenzie Pass to North Sister region. Base map is from Taylor, 1968:17.

Plate 14. Aerial photograph of Yapoah Crater. The flows of basalt in the foreground have been dusted with basaltic volcanic tephra, probably from the nearby Collier Cone. South is to the upper right corner of the picture. The ridge on the south (right) side of the cone is the northern end of the Ahalapam Cinder Field. Original photograph is from Peterson and Groh, 1965:37.

COLLIER CONE

Collier Cone stands 175 m above its surrounding fields of lava and pyroclastic deposits near the north-northwestern base of the North Sister (plate 15). Flows of lava from the base of the dome flowed west for over 13 km and northwest for about 5 km. Basaltic tephra from this large cinder cone covers an area of several km^2 to the east and northeast of the vent. Ash from Collier Cone mantles Yapoah Crater lavas to the north and is found at least 5 km north in the South Matthieu Lake area.

Lying to the east and northeast of Collier Cone is the extensive Ahalapam Cinder Field (plate 16). First named and described by Hodge (1925a:53), this treeless area was

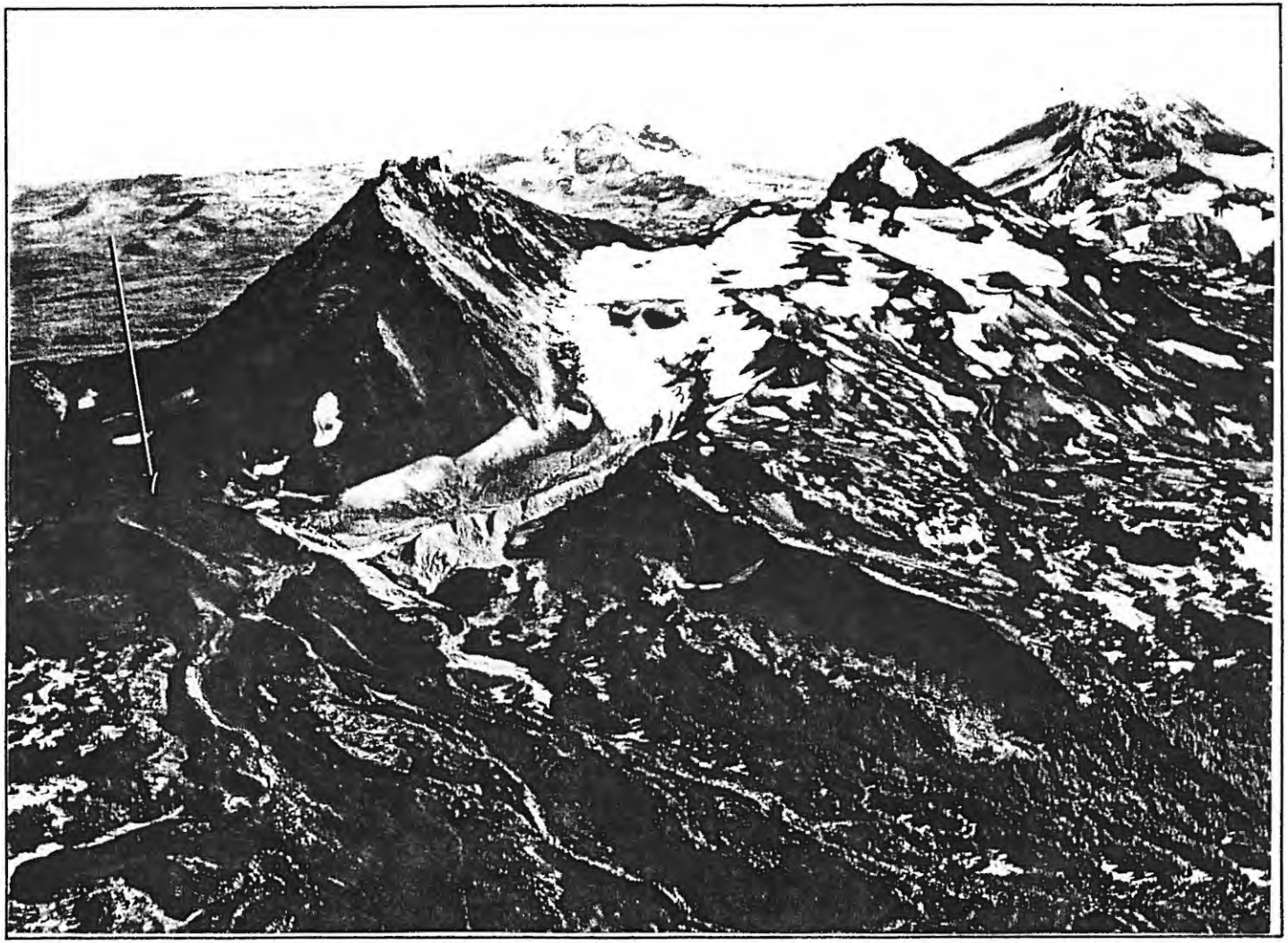

Plate 15. Collier Cone is located in the center left side of the plate. A little less than 2500 ^{14}C years ago, flows of basalt and basaltic andesite erupted from this vent and flowed many kilometers to the west. The lighter-colored deposits immediately south of Collier Cone on the northern flank of the North Sister volcano are lateral moraines left by the retreat of Collier Glacier. Original photograph is from Peterson and Groh, 1965:37.

originally thought by Williams (1944) to have been an accumulation of pyroclastic debris from Yapoah Crater and Collier Cone. More recently, Taylor (1967:28) interprets the cinder field to be a mantle of scoria and ash that can be directly traced to Collier Cone. Our observations corroborate this and leave little doubt that the deposits of the Ahalapam Cinder Field originated at Collier Cone. The distinctive cinder field, almost devoid of vegetation, covers an area of several square kilometers.

Tephragenic activity at Collier Cone is among the more recent in the central High Cascades. Collier Cone lavas overlie cinders from Four-In-One Cone, establishing the maximum age of the Collier Cone tephra at 2550 $\pm$ 165 ^{14}C years B.P. (Taylor, 1967:40,43; Chatters, 1968; see table 6). The minimum age of the Collier Cone activity is less certain. The presence of living trees several hundred years old on Collier Cone lavas sets the minimum limiting age of the tephra from this vent to at least a few centuries.

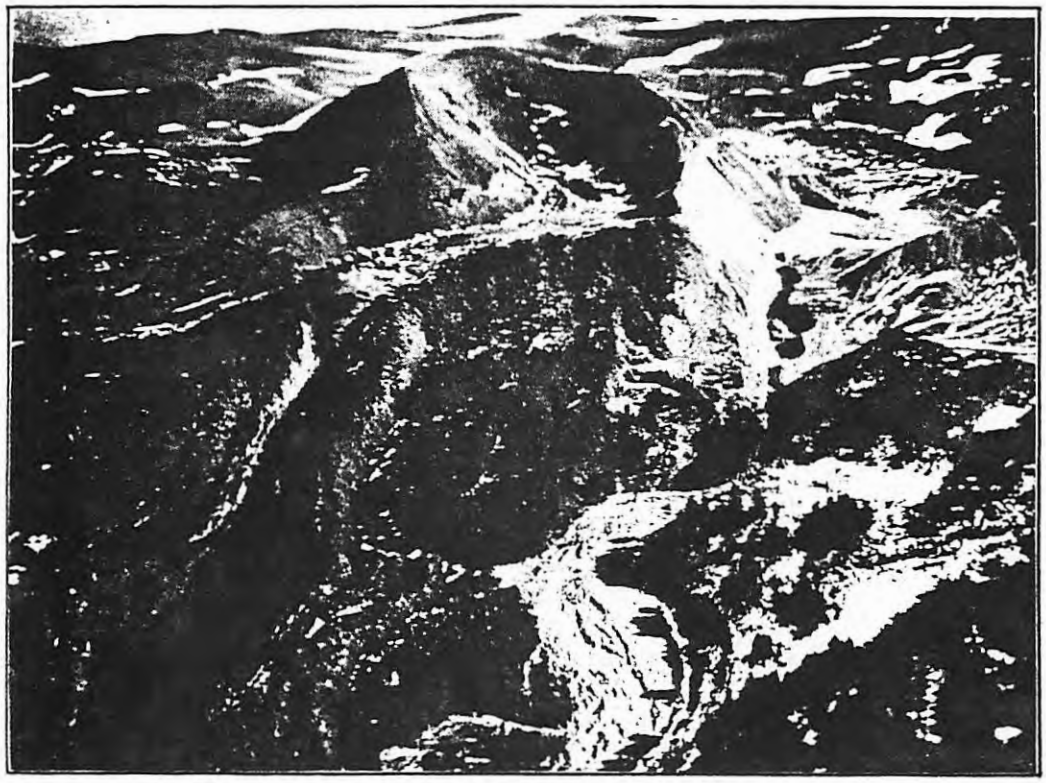

Plate 16. Aerial view of Collier Cone. The Ahalapam Cinder Field, consisting of tephra erupted from Collier Cone, is located immediately behind the cone. This large field of ash and cinders stretches several kilometers downwind (north to northeast) from Collier Cone. Original photograph is from Taylor, 1968:19.

FOUR-IN-ONE CONE

The northern end of a short volcanic alignment located about 2.5 km southwest of Yapoah Crater is marked by a series of four overlapping cinder cones (plate 17). These cones give this chain of 19 vents its name of Four-In-One Cone. The eruption of bombs and cinders that built the cones also created a field of pyroclastic debris in the vicinity of the vents. East of the cones, the tephra deposits are more than 15 m thick and form a prominent cinder field. To the west, the tephra rapidly thins out.

Tephra from Four-In-One Cone is overlain to the south by the more recent Collier Cone lavas; to the north, it lies on lavas from Yapoah Crater (Taylor, 1965; 1967:31-33). Charcoal from the base of a Four-In-One cinder deposit has been dated at 2550 $\pm$ 165 radiocarbon years B.P. (Taylor, 1967:40; Chatters, 1968; see table 6), fixing the age of the eruptions at that date.

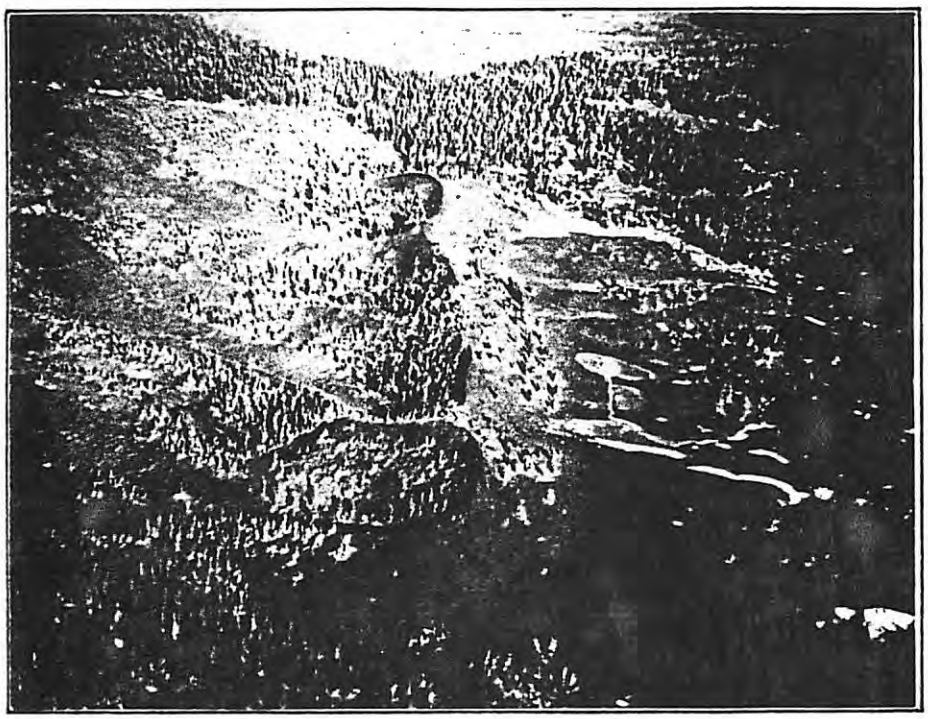

Plate 17. Four-In-One Cone. Basaltic cinders and ash ejected from this alignment of cones about 2600 ^{14}C years ago were followed by flows of lava from vents on the north (left) side of the cones. Photograph is from Taylor, 1968:19.

SIMS BUTTE

The presence of coarse yellow cinders from Sims Butte in road cuts to the west of the 250 m-high cinder cone is noted by Taylor (1968:16). Pyroclastic deposits from the Sims Butte vent are coarse and are largely confined to a radius of about 1.5 km from the vent. Thin lava flows from Sims Butte flowed many kilometers to the west down the glaciated canyon that intersects the McKenzie River (Taylor, 1965 and 1967:24-26). The lavas from the unglaciated cone of Sims Butte are overlain by Mazama tephra, placing the age of the eruptions as pre-Mazama but post-glacial.

CONDON BUTTE

Condon Butte is located 7.5 km northeast of Sims Butte and is about the same size as Sims Butte. Basaltic tephra from Condon Butte appears to be restricted to the immediate vicinity of the cone. Like Sims Butte, Condon Butte is unglaciated and covered with Mazama tephra, placing the age of the eruptions there at between about 6850 radiocarbon years ago and about 10,000 years ago (Taylor, 1965 and 1967:26).

OTHER MINOR VENTS

Several other minor Holocene eruptive centers or vents with limited or dubious tephragenic potential have been described by Taylor (1965 and 1967) in the region between Broken Top volcano and the North Sister (figures 14 and 15). They include:

1. The Inaccessible Alignment, a short north-south chain of cinder cones southwest of Mount Washington that was bordered by Belknap Crater Flows.

2. Twin Craters, a cinder cone located at the southern margin of the Belknap lava fields about 5 km southwest of Belknap Crater.

3. Several small vents north and south of Yapoah Crater that have been assigned Holocene, pre-Yapoah ages.

These areas, as well as other vents of questionable Holocene age such as those at Maxwell Butte, Scott Mountain, and Two Butte were not included in the scope of this current investigation.

South Sister Region

Only two potential Holocene basaltic vents were located in the South Sister region near the Willamette National Forest boundaries, LeConte Cone and Cayuse Crater. These two cones are located, respectively, on the Willamette National Forest boundary at the Cascade Divide and 7 km east of the Divide on the southern slopes of Broken Top.

Several early Holocene basaltic vents and their associated tephra deposits have also been recently described from the Mount Bachelor area (Scott and Gardner, 1990). Located southeast of the South Sister about 10 km, this pre-Mazama alignment of cinder cones and volcanoes was not considered a likely source for potential Willamette National Forest volcanic tephra deposits.

LE CONTE CONE

First named and described by Edwin Hodge (1925a), LeConte Cone rises 60 m above the Wickiup Plain, an area of open meadows covered by tephra from the Rock Mesa eruptions. The obsidian flow that was extruded after the eruption of tephra from the Rock Mesa vent banked up against the northern flank of the cone (see figure 10).

Except for a few exposures of red scoria on the upper flank of the cone, LeConte Cone is almost entirely covered by pumice lapilli and angular fragments of obsidian, rhyolite, and other ejecta from the nearby Rock Mesa vent. Test units dug on the middle southern flank of the cone revealed the mantle of Rock Mesa ejecta to be about 0.5 - 0.7 m thick. The age of the LeConte Cone eruptions can be placed as early Holocene to very late Pleistocene - the Rock Mesa pyroclastic materials directly overlie a poorly-developed soil of mixed Mazama ash and LeConte basaltic tephra. The cone and lava flows from the cone exposed in the Cascade Lakes Highway a few miles to the southeast are covered with tephra from the Mazama eruptions, placing the age of the LeConte eruptions as pre-Mazama. Scott (1990) speculates that the LeConte vent may have been active at the same time as nearby vents in the Mount Bachelor area and estimates the age of the cone as somewhere between 6845 and about 18,000 radiocarbon years B.P.

The original basaltic tephra blanket that was left by LeConte Cone eruptive activity has been entirely covered by thick deposits of pyroclastic debris from the adjacent Rock Mesa vent, as well as less extensive tephra units from the Devils Hill Dome Chain and Mount Mazama. Like most of the High Cascades cinder cones that were examined in this study, basaltic tephra from LeConte Cone was probably limited to the immediate locale of the vent. Considering this and the presence of prevailing winds from the west, it is highly unlikely that LeConte tephra would have penetrated more than a few kilometers to the west in the present-day Willamette National Forest.

CAYUSE CRATER

Cayuse Crater is a prominent cinder cone located on the southern flank of Broken Top volcano (Williams, 1944:54). Basaltic tephra from the Cayuse Crater eruptions has been almost completely covered by later deposits of airfall ash and pumice lapilli from Rock Mesa, the South Sister Dome Chain, and Mount Mazama. The reddish to black

basaltic scoria lapilli of the original eruptions can be seen only on the upper slopes of the cone and in a spring channel exposure located a few hundred meters to the southeast of the vent. Organic-rich mud from this location yielded a radiocarbon date of 9520 ± 100 radiocarbon years B.P. (W-5209), considered by Scott (1987:39) to represent a minimum date for the Cayuse Crater eruptions. Two other small aligned cinder cones located immediately west-northwest of Cayuse Crater are probably contemporaneous with volcanic activity at the Cayuse Crater vent. Considering the direction of prevailing winds and the location of Cayuse Crater 7 km east of the Cascade Divide, we consider it highly unlikely that basaltic tephra from any of these vents will be found within the Willamette National Forest boundaries.

ERUPTIVE CHRONOLOGY OF TEPHRA VENTS IN THE WILLAMETTE NATIONAL FOREST: A SUMMARY

The absolute and relative chronologies of basaltic eruptive activity in the Willamette National Forest is relatively well-known, though there are still many large gaps in our chronologic knowledge of volcanic activity in the region.

Radiocarbon dates associated with Holocene volcanic activity have been determined for several eruptive events (tables 4,5, and 6). These dates provide benchmarks for the sometimes complex contact relationships that still make up the bulk of our knowledge of recent volcanic chronologies in the Oregon central High Cascades.

The ages of silicic tephra deposits within and immediately adjacent to the Willamette National Forest are very well-known, with numerous available radiocarbon dates available, particularly for the Mazama eruptions (tables 4 and 5).

Basaltic volcanic activity in the study area, while common along the Cascade Crest between Three-Fingered Jack and the South Sister, is not as chronologically well-known as the silicic tephras. Much of our knowledge of basaltic eruptive sequences comes from contact relationship among the different tephra and flow units. While some of these are associated with or can be bracketed by radiocarbon dates, there are still several significant tephra-fall whose ages can only be broadly ascertained.

A summary of chronologic evidence for Holocene volcanic in the Willamette National Forest and bordering areas is presented in figures 16 and 17. The reader is also referred to discussions of eruptive chronologies for individual vents in this report, as well as to tables 4,5, and 6 for a summary of radiocarbon dating evidence. For more detailed descriptions of basaltic eruptive activity in the region from Three-Fingered Jack to the North Sister, we recommend the work of Edward Taylor (1965, 1967) and Taylor et al., 1987. Charles Bacon (1983) provides the primary reference for the Mazama eruptions, while William Scott's research at the South Sister supplies much more detail than we were able to relate here.

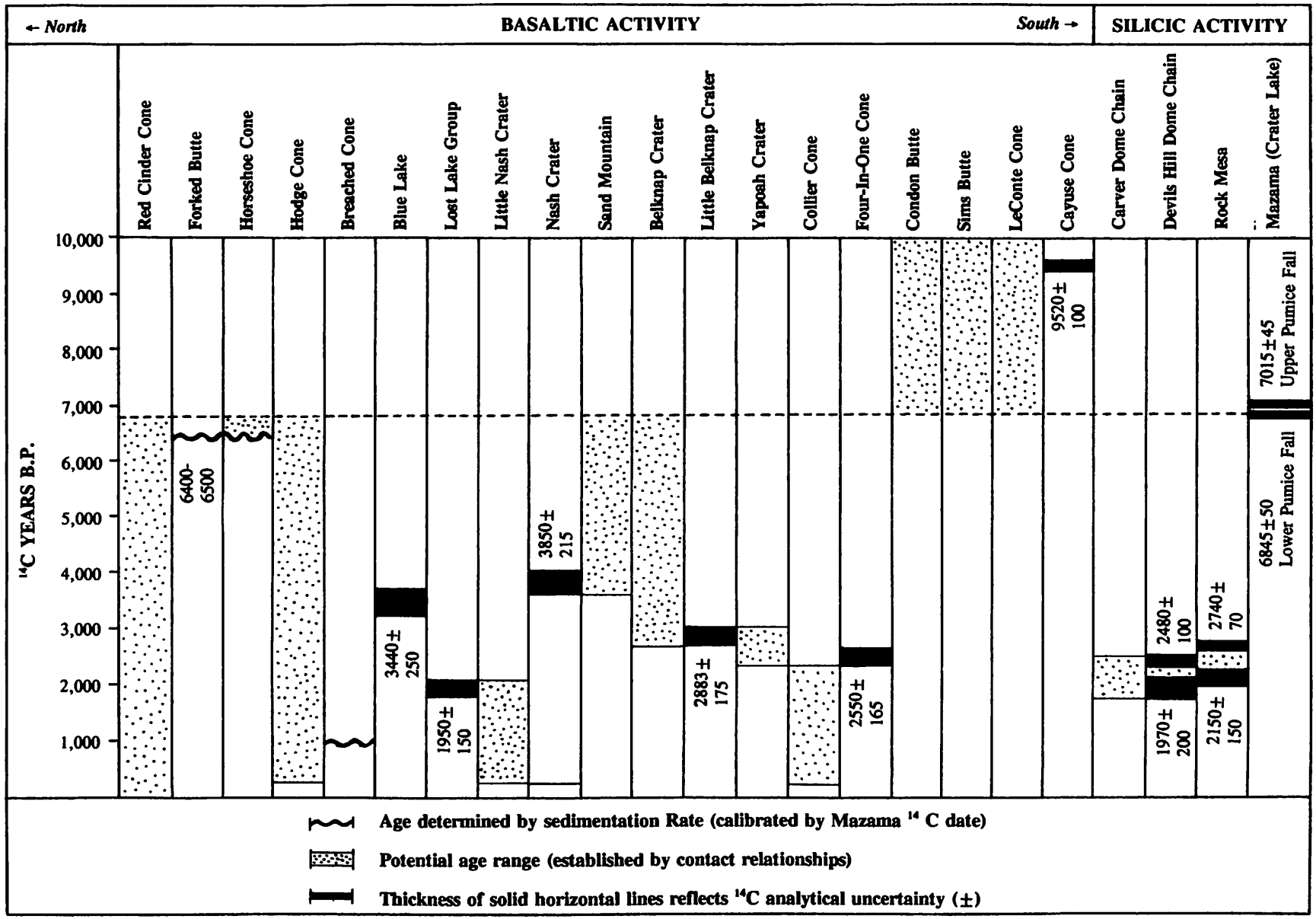

Figure 16. Summary chronology of Holocene volcanic activity associated with tephra deposits found in the Willamette National Forest. Some of the minimum constraining ages are set by the presence of living trees on ash deposits. See tables 4, 5, and 6 for additional radiocarbon date information.

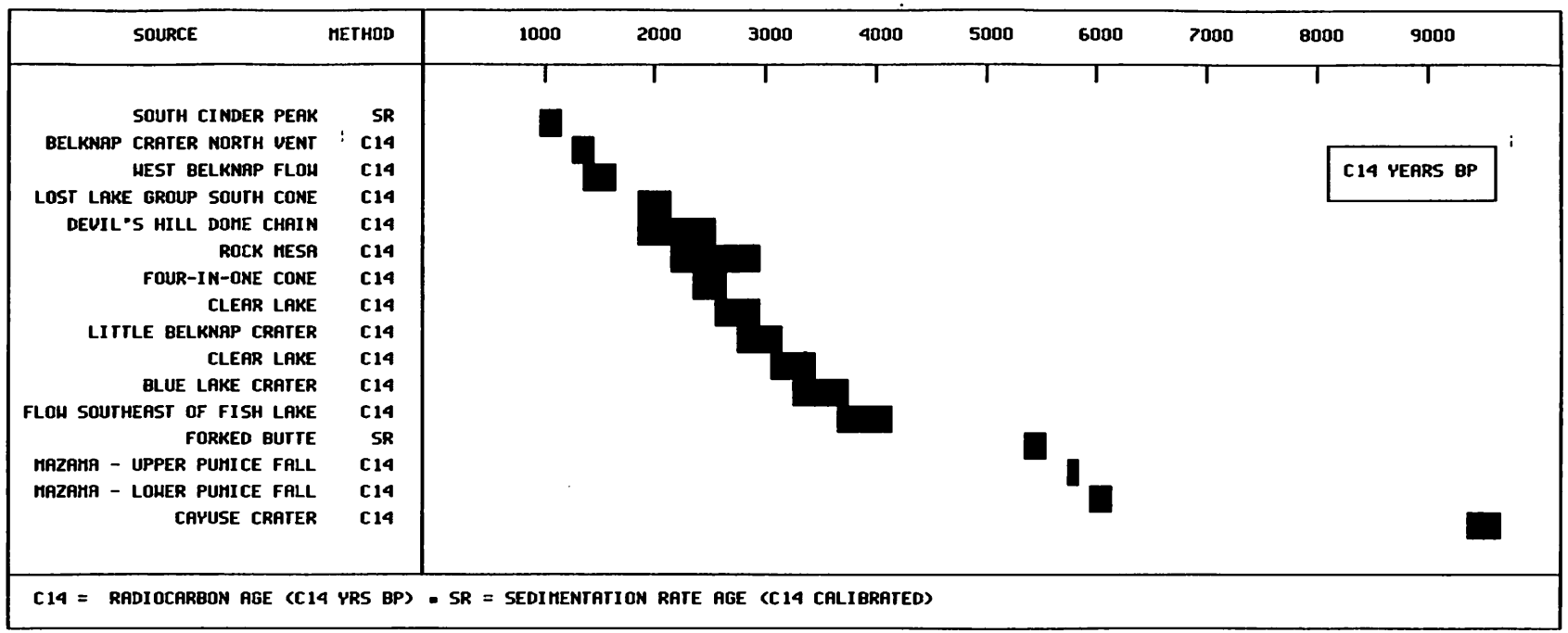

Figure 17. Radiocarbon date coverage for Holocene volcanic activity within the Willamette National Forest. Some of the dates are directly associated with tephragenic activity, while others can be only tentatively linked to deposits of volcanic ash. These dates provide the benchmark chronologic data for relative sequences of deposits constructed through contact relationships.

IV.
VOLCANIC TEPHRA AND WILLAMETTE NATIONAL FOREST PREHISTORY

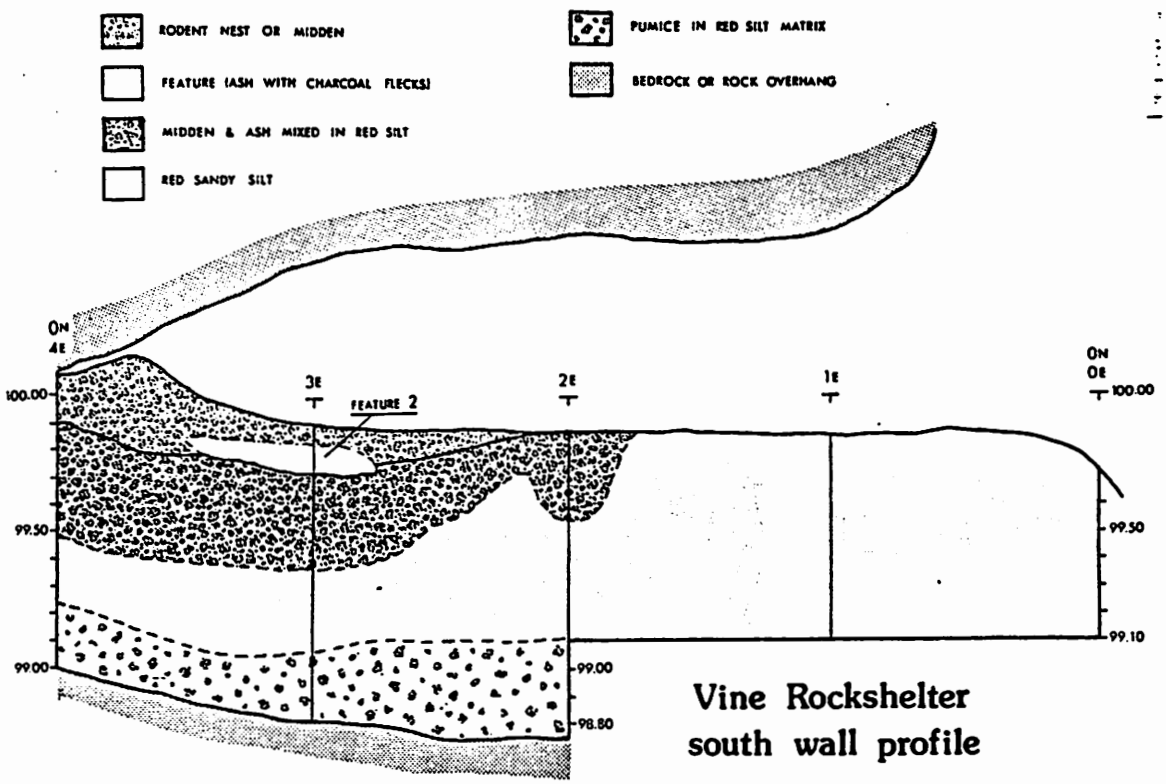

Vine Rockshelter
south wall profile

VOLCANIC TEPHRA AND WILLAMETTE NATIONAL FOREST PREHISTORY AND ARCHAEOLOGY

The Nespelim chief told me that about 1770, when his grandmother was a very young girl, a shower of dry dust fell over the country. It covered the land to a depth of 3 to 4 inches and was like a white dust. It is said that this shower of volcanic ash fell over a large area, including part of the Wallawalla country. The people were much alarmed at this phenomenon and were afraid it prognosticated evil. They beat drums and sang, and for a time held the ***praying*** *dance almost every day and night. They prayed to the* ***dry snow****, called it* ***Chief*** *and* ***Mystery****, and asked it to explain itself and tell why it came. The people danced a great deal all summer, and in large measure neglected their usual work. They put up only small stores of berries, roots, salmon, and dried meat; and consequently the following winter, which happened to be rather long and severe, they ran out of supplies. A few of the old people died of starvation and others became so weak that they could not hunt.*

Account of the effects of a Mount St. Helens ashfall on the Okanagan of eastern Washington (Teit, 1930)

INTRODUCTION

Archaeological research in the Western and High Cascades of the Willamette National Forest has conclusively demonstrated the presence of long-term prehistoric human occupation and utilization of this region throughout much of the *Holocene*. The extensive use of the Western and High Cascades by prehistoric inhabitants of central and western Oregon in areas where volcanic *tephra* has been found is supported by several lines of evidence, including:

1. The presence of pre-Mazama components in Western and High Cascades archaeological sites (Olsen, 1975; Snyder, 1981; Flenniken et al., 1989a:74)).

2. The existence of numerous trans-Cascade trails in the ethnographic period (Minto, 1903; Rarick, 1962:32-36; Minor and Pecor, 1977:154-157).

3. Ethnographic accounts of Western Cascades food procurement by central Oregon Indians (Rarick, 1962:32; Henn, 1975; Murdock, 1980; Minor, 1987:23-24; Silvermoon, 1988:18).

4. The presence of characterized artifactual obsidian from central Oregon obsidian sources in Western Cascades archaeological sites, particularly at sites in the southern half of the Willamette National Forest (Baxter, 1986b:137-144; Jenkins, 1988:57-64; Churchill, 1989:89-97; Churchill and Jenkins, 1989b:91-96;

Flenniken et al., 1989a: 166-172; Flenniken et al., 1990a:193-206; Flenniken et al., 1990b:107-114; Nilsson, 1989:131-141; Spencer, 1989a:181-183).

5. The presence of extensive prehistoric obsidian quarrying activity at the Obsidian Cliffs obsidian source in the High Cascades near the Middle Sister (Silvermoon and Farque, 1986; Skinner, unpublished research).

6. Radiocarbon dates associated with Willamette National Forest archaeological materials that span the period of about the last 8,000 years (Newman, 1966:23; Minor, 1987:42).

7. The presence of hydration rim measurements ranging from less than one micron to 6.1 microns for characterized obsidian artifacts (Obsidian Cliffs source) from Willamette National Forest sites (Baxter, 1986b:134-136; Minor, 1987:52-53; Flenniken and Ozbun, 1988:83-86; Lindberg-Muir, 1988:234-239; Jenkins, 1988: 65-67; Spencer, 1988:227-230; Churchill, 1989:98-102 ; Churchill and Jenkins, 1989a:165-169; Churchill and Jenkins, 1989b:97-99; Flenniken et al., 1989a: 114-118;173-178; Flenniken et al., 1989b:91-94; Nilsson, 1989:124-130; Spencer, 1989a:185-188; Spencer, 1989b:103-106; Flenniken et al., 1990a:207-214; Flenniken et al., 1990b:173-178; Flenniken et al., 1990c:89-92). While it is still not possible to convert hydration rim measurements to calendar dates, the range in measurements suggests an potential occupation span of several thousand years.

8. The widespread distribution of archaeological sites in higher elevation areas where volcanic tephra has been found or would be expected (Newman, 1966; Henn, 1975; Olsen, 1975; Minor and Pecor, 1977; Toepel and Minor, 1980; Baxter, 1986a; Silvermoon, 1986; Minor, 1987; Flenniken and Ozbun, 1988; Jenkins, 1988; Silvermoon, 1988; Spencer, 1988; Nilsson, 1989; Churchill, 1989; Churchill and Jenkins, 1989a; Churchill and Jenkins, 1989b; Flenniken et al., 1989a; Flenniken et al., 1989b; Spencer, 1989a; Spencer, 1989b; Flenniken et al., 1990a; Flenniken et al., 1990b; Flenniken et al., 1990c - these references apply to excavated sites only).

Given the well-documented use of the Western and High Cascades in the prehistoric period, it is likely that aboriginal groups witnessed at least some of the volcanic tephragenic eruptions that took place. This would have been particularly true during the mid- to late-Holocene when widespread prehistoric use of the Western and High Cascades is most clearly documented.

Archaeological Implications of Volcanic Eruptions

There is no doubt that volcanic activity can affect prehistoric groups and that these effects can affect the archaeological record. Examples of this are not uncommon in the archaeological literature - the 1500 B.P. eruption of Thera (Santorini) in the

Mediterranean (Renfrew, 1979); the catastrophic *ashfalls* and mudflows of Vesuvius in A.D. 79 (Jashemski, 1979); the eruption of El Salvador's Ilopango Volcano in the third century A.D. (Sheets, 1983); the volcanic activity of Sunset Crater, Arizona, early in the present millenia (Pilles, 1979), and the prehistoric eruptions of volcanic tephra in the subarctic regions of northwest North America (Workman, 1979). All of these have indelibly left their mark in the archaeological record and in their disastrous effects on the populations that were affected by these volcanic events.

How might the volcanic ashfalls of the Western and High Cascades have affected the groups that used this region? Despite the multiple eruptions of volcanic tephra that occurred in the Willamette National Forest, the effects of these ashfalls on the prehistoric inhabitants were probably relatively minimal and short-lived. Blong (1984:79) points out: "The most important thing about tephra falls is that they kill relatively few people, being responsible for only about 4.6% of recorded volcano-related deaths since AD 1600." Fatalities directly resulting from ashfalls are rare except in instances, such as at Pompeii, where great quantities of ash have fallen in a very short period of time. Deleterious effects of ashfalls to human populations are most likely to result from damage to the environment and to the subsistence base. As research following the 1980 eruptions of Mount St. Helens showed, even severe damage to vegetation and faunal resources is likely to be quite short-term (Matz, 1987:31-49).

Ethnographic accounts of the effects of recent ashfalls on populations in the Western United States are, understandably, uncommon and are limited to the nineteenth century eruptions of Mount St. Helens in Washington (Teit, 1930; Ray, 1932; Holmes, 1955). These brief descriptions (the one at the beginning of this chapter is typical) suggest, however, that the primary impact of ashfalls on aboriginal groups is related not to environmental damage, but to the disruption of annual subsistence activities.

Eruptions of *basaltic tephra* from vents near the Cascade Crest were geographically limited and probably had little or no effect on the groups that passed through the area during the summer and fall months.

The explosive eruptions of *silicic* tephra at Rock Mesa and the Devils Hill Dome Chain were also fairly areally restricted, though they may yet eventually prove to be significant local stratigraphic horizons for archaeologists. Significant adverse effects of these eruptions were probably confined to an area only a few kilometers from the vents. The Mazama ashfall, though unquestionably the most significant of the Oregon Cascades tephra eruptions, also probably had only a limited impact on human groups in the Cascades. While the environmental effects of the eruptions were undoubtedly significant in the High Cascades, the thickness of the *primary tephra deposits* decreased very rapidly to the west of the Cascade Crest. Given that the most heavily affected areas of the Cascades were only seasonally utilized for non-essential food and lithic resources, it is likely that only a few years were required for compaction or

erosion of ash and recovery of animal and vegetation populations. It seems unlikely that any significant disruption to critical subsistence scheduling occurred as a result of the eruptions.

The *pyroclastic flows* of pumice and ash that swept down the valleys that led into Western Oregon claimed at least one known human victim. In 1940, skeletal remains were found under six feet of *pumice* by a road construction crew working on the Medford-Crater Lake Highway west of Crater Lake. The find was reported to Luther Cressman who confirmed that the skeleton was a casualty of the climactic eruptions of Mount Mazama (Cressman, 1939-40).

Though the direct environmental effects of volcanic ashfalls on the prehistoric groups using the Cascades were probably limited, the potential importance of the resultant tephra deposits to archaeologists is still considerable. Not only do these volcanic ash layers provide a potential means of dating archaeological sites, but the rapid burial of sites provides one of the few archaeological environments in which the *pompeii effect* may be demonstrated (Binford, 1981). The very rapid deposition of volcanic ash has the ability to literally capture and preserve a moment in time at an occupation site. The many cultural and natural post-depositional processes that typically modify and obscure the archaeological record may be largely obviated by a thick cover of volcanic tephra. It is perhaps unfortunate that the archaeological sites of the Western and High Cascades that are most amenable to preservation through rapid tephra burial are probably relatively minor ones related primarily to seasonal subsistence and procurement activities. It is a virtual certainty, though, that many of these sites remain undiscovered and preserved today by their protective cover of volcanic ash. Serendipity may play an important role in the future discovery of these particular sites. It is important to remember, however, that many site locations are periodically reoccupied for long periods of time because of favorable environmental settings. The discovery of a culturally sterile stratum of volcanic ash, no matter how thick, during the excavation of a site should not be taken as an indication that the earliest site occupation level has been reached. It should be approached instead as an atypical stratigraphic unit representing a very rapid depositional event that has taken place over a short period of time.

PREVIOUS TEPHRA-RELATED ARCHAEOLOGICAL RESEARCH

Despite the presence of Mazama tephra throughout the entire Willamette National Forest and the existence of many other more areally-restricted basaltic and silicic tephra deposits, archaeological use of volcanic tephra as a stratigraphic marker has been minimal (figure 18). An interest in the explicit use of tephra deposits in archaeological studies, though, has recently begun to surface in regional archaeological studies. Davis (1987:25) noted that volcanic deposits could be important temporal horizons, though he admitted that "... little systematic research toward using these deposits as time markers at lithic scatter sites within the western

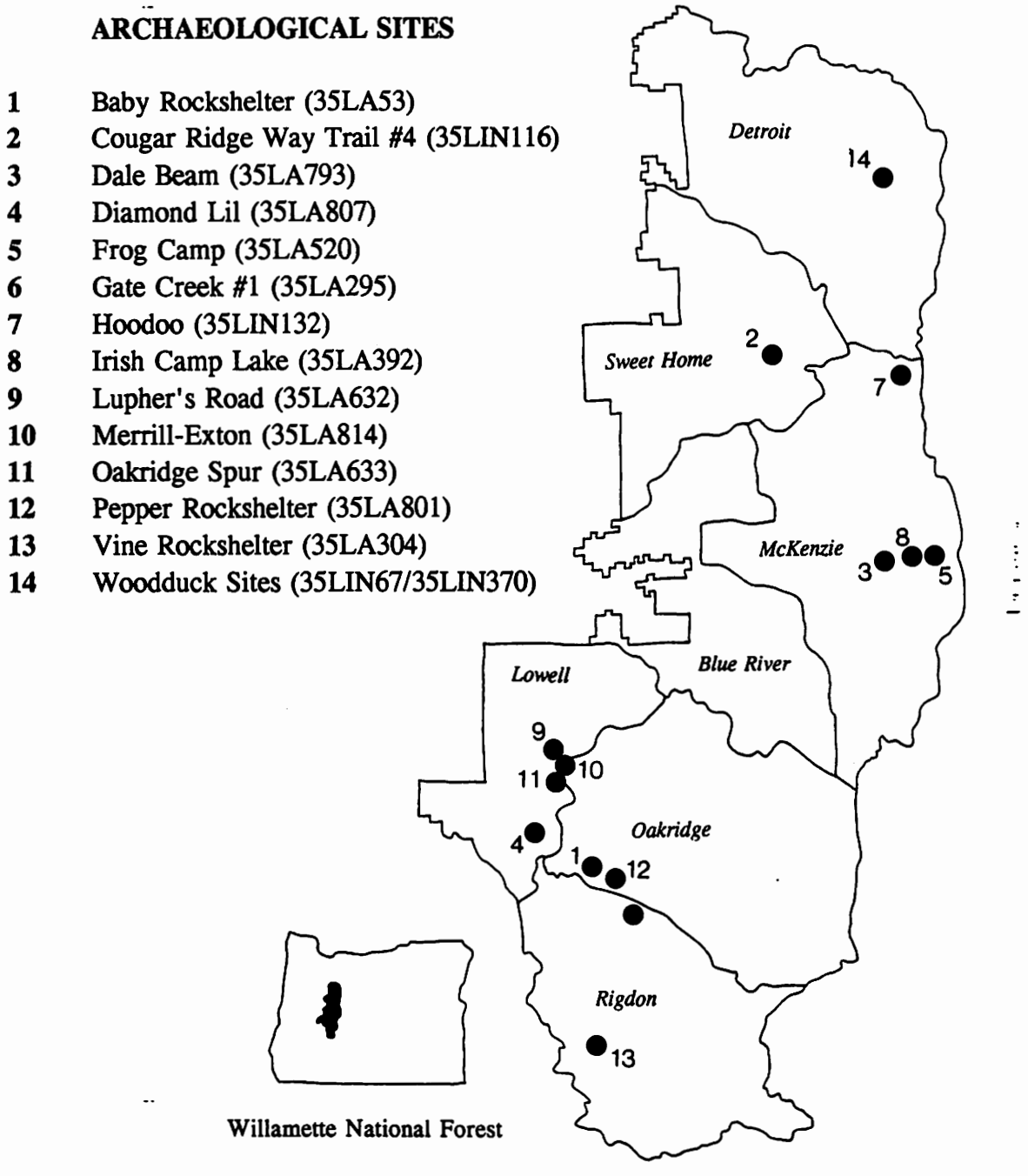

Figure 18. Distribution of archaeological sites in the Willamette National Forest where volcanic tephra has been explicitly identified.

Cascades" had been carried out. In a preliminary research design study of the Scott Mountain Plateau Study Unit in the McKenzie Ranger District, Silvermoon (1988:20) directly addressed the need for tephra studies in this region:

> *An important and basic component of future research conducted at Scott Mountain Plateau Study Unit sites will be the detailed identification and analysis of the soil matrix at each site and the identification, trace element analysis, and description of tephra deposits which may be present.*

The use of volcanic tephra in previous Willamette National Forest archaeological research is summarized and evaluated in the remainder of this section of the overview.

Baby Rockshelter Site (35LA53)

The first archaeological site within the Willamette National Forest in which volcanic tephra was explicitly used as a *tephrochronologic* marker was at Baby Rockshelter, a small overhang found not far east of Oakridge in the Western Cascades. This probable

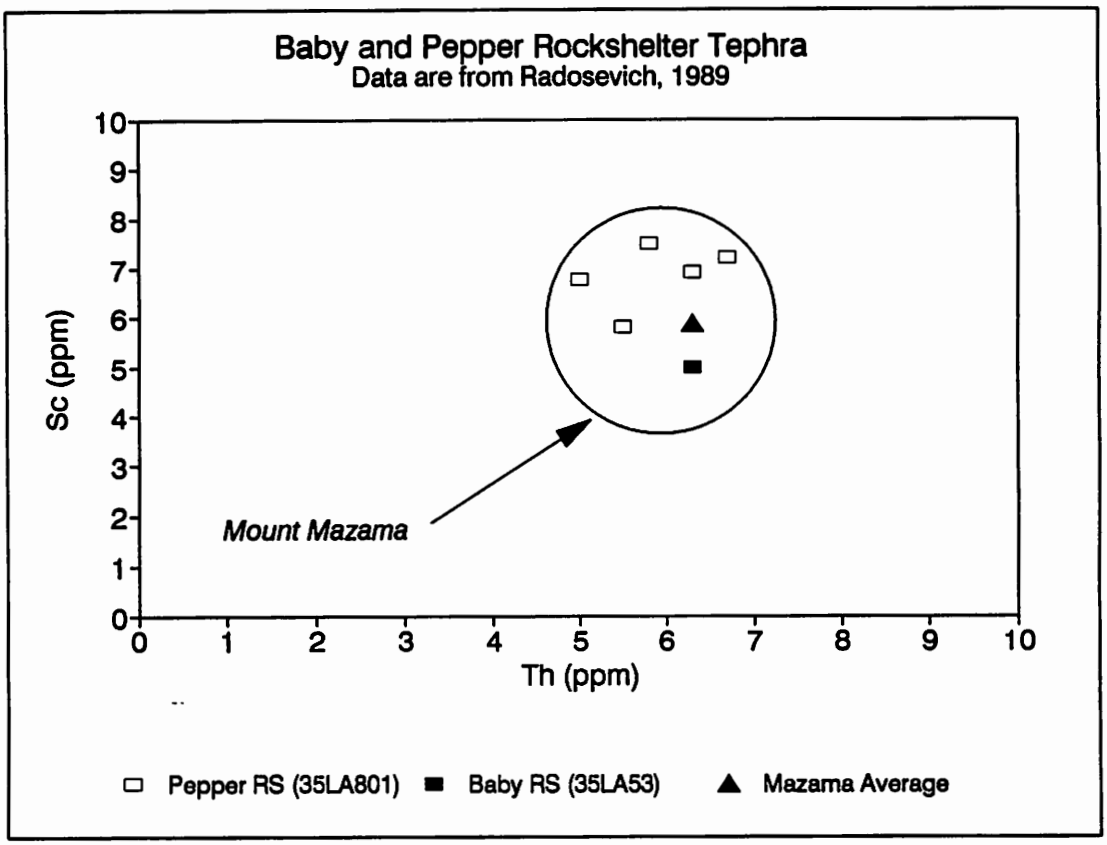

Figure 19. Scatterplot of selected trace element data for tephra from the Baby Rockshelter and Pepper Rockshelter archaeological sites. Graphical correlation of the tephra with published values of Mazama tephra suggest that Mount Mazama, as expected, was the source of the volcanic ash.

hunting camp had been extensively disturbed by relic collectors prior to excavation. Bands of Mazama tephra were identified (no method indicated) in Stratum C which directly overlay the earliest occupation level at the site (Olsen, 1975). The existence of a pre-Mazama occupation layer was also corroborated by obsidian hydration analysis of artifacts from the site. Hydration rim measurements indicated that the pre-Mazama component lay in undisturbed sediments; hydration rim thicknesses of up to 5.1 microns were also consistent with artifacts of considerable antiquity (Fagan, 1975).

Recently, the tephra from Baby Rockshelter and Pepper Rockshelter was characterized using neutron activation analysis and correlated with known sources of silicic volcanic ash (Radosevich, 1989). Not surprisingly, the most likely source of the Baby Rockshelter tephra was found to be Mount Mazama (figure 19).

Cougar Ridge Way Trail #4 Site (35LIN116)

During excavation of the Cougar Ridge Way Trail #4 Site, a probable prehistoric temporary campsite in the Western Cascades, a few small lenses of homogeneous, fine-grained and well-sorted pure gray to white volcanic ash were found (Flenniken and Ozbun, 1988:30). In an attempt to identify the geologic source of the ash, samples of this tephra were subjected to electron microprobe analysis. Though the location of the site and the intact lenses of tephra would suggest Mount Mazama as the source of the ash, the results of the microprobe analysis proved to be surprising and somewhat enigmatic (figure 20). Out of 18 *shards* analyzed, 12 correlated well with the Mazama eruption, as expected. The remaining six shards, though, presented a surprise - two were chemically similar to Glacier Peak Layers B and M (dated at about 11,000-12,000 years B.P.), sample 31 was correlated with Mount St. Helens *Set* S (dated at about 13,000 years ago), and three remained unidentified (Cochran, 1988).

These findings are particularly enigmatic considering the previously described distribution of the tephra sets B and M from Glacier Peak and Set S from Mount St. Helens. Mount St. Helens Set S consists of several tephra layers, the products of multiple eruptive events that have been described from deposits primarily east of the volcano; a few eruptions also deposited ash to the north of the vent (Sarna-Wojcicki et al., 1983; Mullineaux, 1986). While tephra associated with the S Set has been identified several hundred kilometers downwind to the east and the northeast of Mount St. Helens, none has been recognized in Oregon (Mullineaux et al., 1978). Similarly, tephra deposits associated with sets B and M from Glacier Peak have been found several hundred kilometers east and southeast of the volcano and perhaps in the northeastern corner of Oregon (Rai, 1970; Porter, 1978). It seems unlikely, however, that tephra from the sets identified from either of these volcanoes, particularly those from Glacier Peak, would have made its way into central western Oregon.

We suggest that the presence of Glacier Peak and Mount St. Helens tephra at the Cougar Ridge Trail #4 Site be accepted only very tentatively. The data are presented in percentages and, as such, are not directly comparable to published chemical data relating to these two sources. Before the acceptance of the existence of tephra from these two sources, a reanalysis of the ash should be carried out.

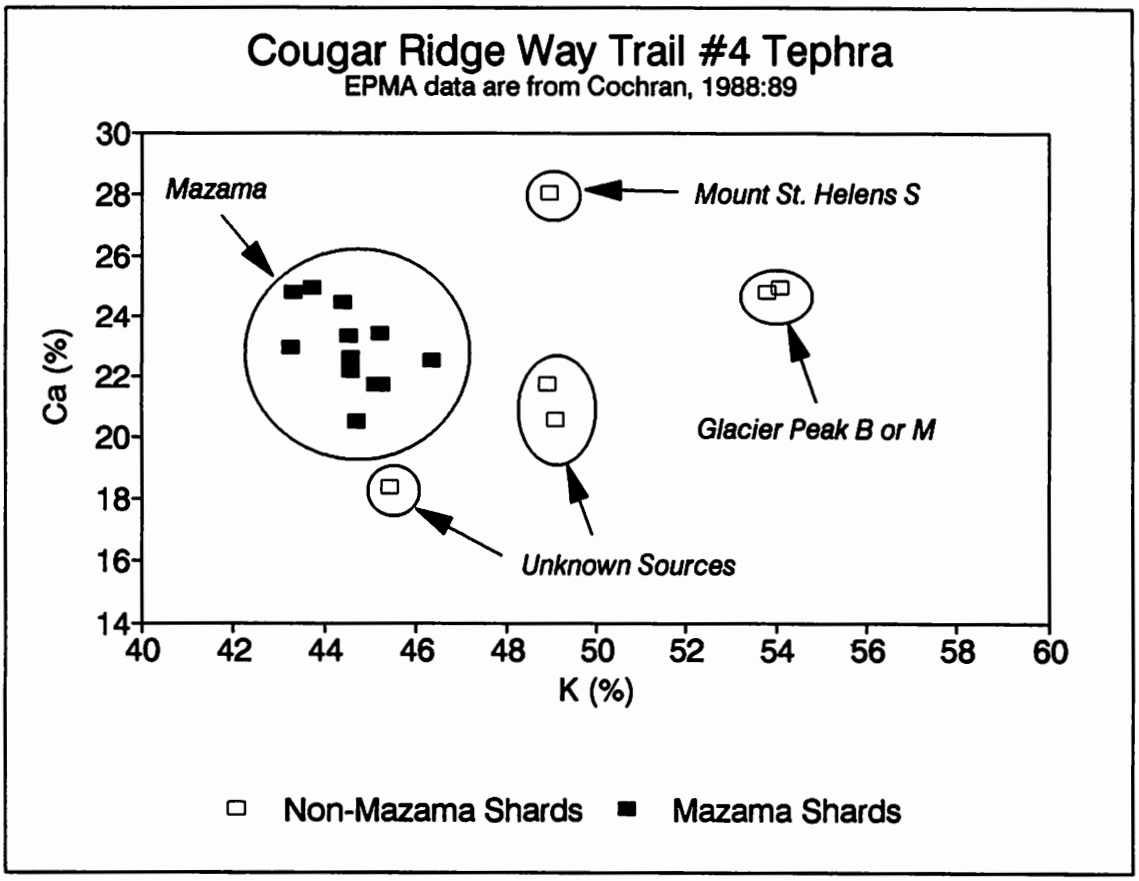

Figure 20. Scatterplot of electron microprobe analysis major element data from volcanic tephra recovered at the Cougar Ridge Way Trail #4 archaeological site. Individual shards of tephra from this site were initially correlated with eruptions at Mount Mazama, Mount St. Helens, Glacier Peak, and two unknown sources. Data were normalized to 100 percent.

Dale Beam Site (35LA793)

"Tephra-like" material was found in many test units at the Dale Beam Site, a prehistoric campsite located about 17 km east of the McKenzie Pass. This "tephra-like" material was found at an average depth of 28 cm below the surface and was reported in 15 test units at the site (Spencer, 1989a:45). The tephra occurred as small

(1-2 mm diameter) cream-yellow to pink-colored *pyroclasts* in a soil matrix. McDowell (1989), in an analysis of the tephra, confirmed that the soil from the site was a poorly sorted pebbly loam containing a proportion of redeposited volcanic ash.

No attempt was made to identify the geologic source of the volcanic tephra from the site.

The *lapilli* size and color of the pyroclasts are both consistent with a Mazama origin and it is almost certain that the tephra at the Dale Beam site came from Crater Lake. The description of the sediments at the site suggests that the tephra was incorporated into soils that developed after the primary deposition of the ash. Post-Mazama soils containing a significant proportion of small *pumice lapilli* and volcanic ash are found throughout the High and Western Cascades within the Willamette National Forest. These soils are particularly noticeable in higher altitude areas such as those at the Dale Beam Site (994 m asl) where soil development is slow and vegetational cover is limited. A radiocarbon date of 3100 $\pm$ 90 (Beta-25882) from carbon recovered at a depth of 22-27 cm below the surface provides some limited temporal control for the tephra. Rock Mesa and the Devils Hill Dome Chain, local sources of silicic tephra that erupted about 2,000 years B.P., are located about 23 km southeast of the site, but are considered unlikely sources of the tephra at the Dale Beam Site. The radiocarbon date and known distribution of ash from the Rock Mesa and Devils Hill vents (Scott, 1987) further support the Mazama origin to tephra incorporated into soils at the Dale Beam Site.

Diamond Lil Site (35LA807)

Volcanic ash from an undetermined source was identified in sediment samples collected at the Diamond Lil Deer Kill Site located in the lower elevation Western Cascades (Flenniken et al., 1990a:58). Hassan (1990:180) reported that volcanic glass shards were found in the upper two samples of a sediment column collected in Test Unit 5 of the site. Volcanic tephra was not found in the lower six sediment samples. The volcanic glass was thought to be mixed (redeposited) and no attempt was made to characterize the glass. Obsidian hydration measurements of artifacts from the site, virtually the only chronologic information available, indicated a very late prehistoric age of the site and this, along with the geographic location of the site, suggest that the ash almost certainly originated from Mount Mazama.

Frog Camp Site (35LA520)

Located about 1 km north of Sims Butte, the Frog Camp Site was tested and evaluated in 1985 prior to construction activity in the area (Silvermoon, 1986). The site is located at a major trailhead into the Three Sisters Wilderness Area about 8 km west of the Cascade Divide. Though it is apparent that much of the site deposits consist of basaltic *cinders* and ash, details of the tephra and its association with cultural materials

are not well-documented. The location of the site suggests that a nearby vent or vents, possibly Sims Butte, was the source of the parent material. The presence of obsidian debitage throughout the basaltic tephra deposits at the site further suggests that the deposits are *secondary*, *reworked* materials that gradually accumulated during the occupation of the site. No stratum resembling Mazama tephra was described. Based on the presence of two projectile points found on the surface, the occupation span at the site was estimated to range from the Ethnohistoric period to as early as the Late Archaic (Silvermoon, 1986:38,41). The presence of reworked basaltic tephra in the site deposits does little to add to these chronologic speculations. If the tephra did originate at nearby Sims Butte, the age of the deposits must be younger than the eruption of the tephra at some time between about 7,000 and 10,000 years ago.

Gate Creek #1 Site (35LA295)

The Gate Creek site is located in the Western Cascades in the Hills Creek drainage southwest of Oakridge. This site is a probable temporary campsite, is situated on a ridge saddle about 80 km north of Crater Lake and 5 km southeast of McCredie Hot Springs. Excavations at the site revealed aeolian sediments containing *pyroclastic* materials that resemble Mazama tephra. These sediments overlie near-surface glacial deposits. Tephra "gravels" (small pumice lapilli) averaging about 4 mm in diameter and 20-30% by volume were identified in the A horizon; the tephra in the B horizon was estimated at about 30-40% volume (Flenniken et al., 1990b:31,34). The geographic location of the site, the lapilli size, and the volume of tephra in the sediments confirms Mount Mazama as the original source of the ash. No attempt was made to use the tephra for chronological purposes at the site and obsidian hydration analysis of materials from the Gate Creek site was considered the only means of chronological association available (Flenniken et al., 1990b:71).

Hoodoo Site (35LIN132)

One of the few archaeological tephrochronologic applications within the Willamette National Forest involving basaltic tephra occurred at a small obsidian scatter positioned about 4 km east of Sand Mountain. This minor site, located about 1 km south of Hoodoo Butte in the area burned by a 1967 fire, was found directly on top of a basaltic tephra deposit that originated from the Sand Mountain vents to the west (Toepel and Minor, 1980). Volcanic sand (e.g. basaltic tephra) removed from a 30 cm-deep test pit "...yielded no flakes, strongly suggesting that most of the cultural material is confined to the surface of the site." The deposit was identified as Sand Mountain volcanic sands, and the site was dated at younger than 3,000 years because the flakes overlay the tephra deposits.

Several meters of basaltic tephra from the Sand Mountain vents were deposited during a relatively short interval at some point prior to the occupation the site, easily explaining the lack of cultural subsurface materials in the deposit under the surface

artifacts. This rapid deposition is one of the chief characteristics of volcanic ash that makes it particularly useful in tephrochronologic applications at archaeological sites.

The age of eruption of the important and widespread Sand Mountain basaltic tephra deposit has still not been firmly placed (see Section III for a discussion). The 3,000 year old date used as the age of the tephra at this site utilization appears to have originated from the radiocarbon dates of Benson (1965 and table 6). Benson dated trees drowned by a lake created when Sand Mountain lava flows dammed a creek to the west of the cones. A more accurate estimate of the minimum age of the Sand Mountain tephra deposits (and the earliest maximum age of the Hoodoo Butte Site) would be about 3,850 years B.P.

Irish Camp Lake Site (35LA392)

The Irish Camp Lake Site is located in the High Cascades about 11 km west of the Cascade Crest and 4 km west of Sims Butte (R. Davis, 1978). Limited test excavations and a soil analysis at the site identified silicic volcanic tephra as the parent material for soils found at the site (Radosevich, no date). Yellowish pumice lapilli up to 2 mm in diameter were reported. The location of the site and lapilli diameter leave little doubt that the parent tephra originated from Mount Mazama and that any archaeological materials found in association with the Mazama soils must be less than 7,000 radiocarbon years in age.

Lupher's Road Site (35LA632)

The Lupher's Road Site is situated on a ridge immediately southeast of Saddleblanket Mountain in the southwestern quadrant of the Willamette National Forest. This site is located only a few kilometers from two other sites described here, the Merrill-Exton and Oakridge Spur sites. A single stratum consisting of silty to sandy sediments with poorly-sorted granule to cobble-sized gravels (lapilli) of "pumice or tuffacious rock" was described from test units in a highly disturbed area of the site (Flenniken et al., 1989a:104). The yellowish color of the pumice (10YR7/6) and the location of the site only about 110 km WNW of Crater Lake suggests that the tephra in the sediments almost certainly originated from the Mazama eruptions. No attempt was made to characterize the tephra or to use it for tephrochronologic purposes.

Merrill-Exton Site (35LA814)

Located along a saddle in the southwestern part of the Willamette National Forest, the Merrill-Exton Site is another in which volcanic tephra has been identified. A primary deposit of tephra up to 5 cm in thickness is reported from the southeastern portion of the site within the upper twenty to thirty centimeters of the deposit (Flenniken et al., 1989a:74). The ash appears to overlie sediments containing artifacts in this part of the site. Some additional artifacts were also recovered from redeposited ash

sediments. The location of this site, approximately 110 km WNW of Crater Lake, points to Mount Mazama as the original source of tephra at the site. The possible presence of artifacts below the well-dated Mazama tephra also suggests a considerable potential age of occupation of the Merrill-Exton Site. Hydration rim measurements of obsidian artifacts from the Obsidian Cliffs source ranged in thickness from only 2.0 to 2.8 microns, though, and do not directly support a pre-Mazama antiquity to the artifacts (see the Baby Rockshelter discussion)(Flenniken et al., 1989:173-178). The tephra at the Merrill-Exton Site was neither characterized nor used for tephrochronologic purposes.

Oakridge Spur Site (35LA633)

Situated less than 2 km south of the Merrill-Exton Site on a level bench of a eastward-sloping ridge system, volcanic tephra is also reported from the Oakridge Spur Site (Flenniken, 1989a:89). Yellow granule-sized gravels within Stratum II of the site were thought to be redeposited tephras. This description, along with the proximity of Crater Lake about 100 km to the south, again suggests Mount Mazama as the source of any silicic tephra found at this location.

Pepper Rockshelter Site (35LA801)

Excavations in 1988 at Pepper Rockshelter revealed the presence of pumice deposits associated with cultural materials. Redeposited pea-sized and smaller pumice lapilli were found mixed with silty sands and basaltic clasts from a depth of 20-30 cm to about 70 cm below the surface of the site (Churchill and Jenkins, 1989b:23-27). This secondary deposit of pumice was used to separate the assemblage at the rockshelter into two separate components representing multiple site occupations (Churchill and Jenkins, 1989b:45). The *trace element* composition of the tephra was determined with neutron activation analysis and the geologic source of the ash was identified as Mount Mazama (Radosevich, 1989)(figure 19).

Vine Rockshelter Site (35LA304) and the Mazama Mimic Problem

Vine Rockshelter is located in the central Western Cascades of Oregon immediately south of the Middle Fork of the Willamette River and about 20 km west of the Cascade Crest. During excavations in 1983, a thick primary deposit of silicic volcanic ash and pumice lapilli was found near the bottom of the deposits in front of the rockshelter. Pumice lapilli were also found scattered throughout the rockshelter deposits. Though the tephra was initially thought to have originated from nearby Mount Mazama, neutron activation analysis of the ash suggested that the 6,845 year-old eruption was not the source (figure 21). The Vine Rockshelter tephra was very similar in color, lapilli-size, and mineralogical characteristics to Mazama ash, however, and became known as the Mazama Mimic tephra. Tephra from another archaeological site located 30 mi NNE of Vine Rockshelter, 35LA51, was

characterized at the same time and was also found to have originated from the same source. Limited archaeological evidence also suggested that the Mazama Mimic tephra might be considerably younger than the Mazama tephra (Baxter and Connolly, 1985:19-21; Baxter, 1986a:67-69).

A new tephra horizon in the central Cascades would provide an important tephrochronological tool for archaeologists and geologists working in the region. Additionally, a new source of volcanic tephra would also call into question all previous archaeological conclusions that had been based on the unquestioned assumption of the presence of Mount Mazama as the source of any silicic volcanic ash that was found. Any former archaeological studies that had assumed that silicic ash originated from Mount Mazama would have to be reevaluated. The resolution of this

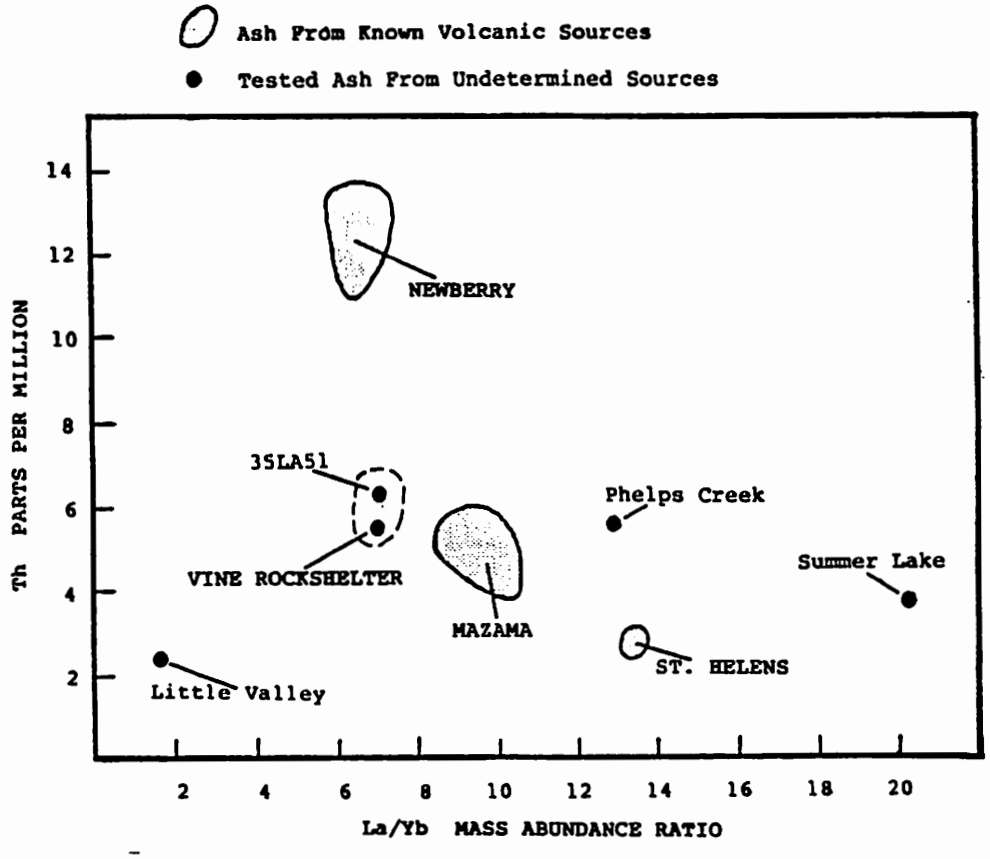

Figure 21. Scatterplot illustrating the Lanthanum/Ytterbium ratio versus the Thorium content for small pumice lapilli from Vine Rockshelter, 35LA51, and several other Oregon tephra sources. The lack of correlation between the archaeological tephra and the published values for other sources led to speculation about the existence of a new Mazama Mimic tephra source somewhere in the Cascades. The diagram is from Baxter and Connolly, 1986:21.

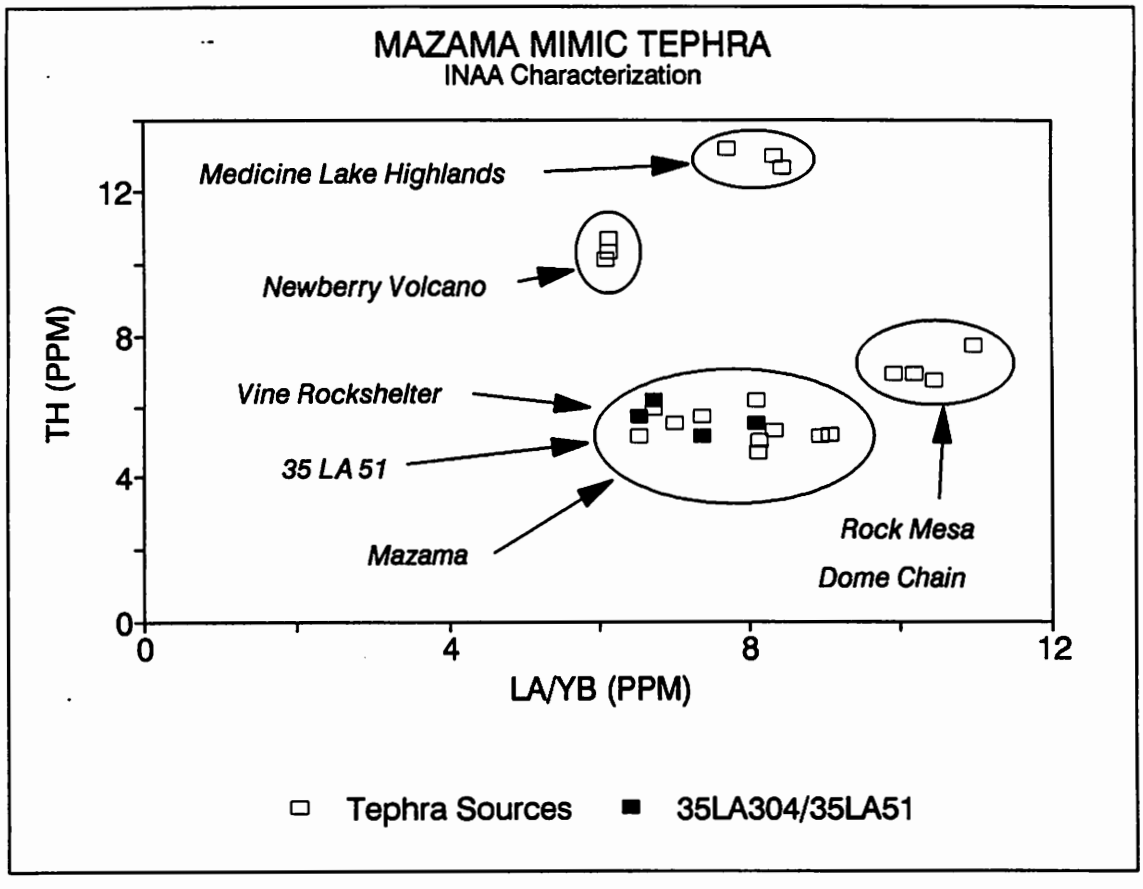

Figure 22. Scatterplot of the same elements and archaeological tephra samples that were illustrated in figure 20. The data are from a reanalysis of the Vine Rockshelter and 35LA51 tephra that was instigated to clear up the Mazama Mimic tephra problem. In the reanalysis, tephra samples from the archaeological sites were found to correlate with Mazama tephra, effectively solving the mimic problem.

problem, as pointed out by Baxter and Connolly (1985:20), was essential to Western Cascades archaeological chronologies.

The presence of a new source of volcanic ash in the geologically well-studied and mapped central Cascades, however, would be rather unexpected. Was the Mazama Mimic tephra from a new and previously unidentified source or was it a from an already known source, most likely Mount Mazama? Was the problem a real or an analytical one? Only a reinvestigation of the tephra could provide evidence that would answer these questions.

In an attempt to solve these nagging questions, a new study of the Mazama Mimic tephra was initiated in 1989 (Skinner and Radosevich, 1989). Volcanic ash was collected from several different Holocene vents in the Vine Rockshelter region for comparison to the archaeological tephra: Mount Mazama (Crater Lake), Newberry Volcano, Rock Mesa, and the Devils Hill Dome Chain. Tephra samples from several late Holocene eruptions in the Medicine Lake Highlands of Northern California were also included for additional comparison.

Neutron activation analysis and correlation of tephra from Vine Rockshelter, 35LA51, and the Oregon and Northern California tephra sources indicated that Mount Mazama was clearly the source of the so-called Mazama Mimic tephra (figure 22). The initial misidentification of the source of the archaeological tephra was attributed to unexpected analytical geochemical variation encountered during the correlation of the original archaeological samples with previously published geochemical source data.

The identification of Mount Mazama as the source of the Vine Rockshelter and 35LA51 tephra effectively solved the mystery of the Mazama Mimic tephra - it simply did not exist. The correct identification of the source of the tephra, however, does suggest that the initial occupation of Vine Rockshelter may have begun at an earlier date than was previously thought.

Woodduck Sites (35LIN67/35LIN370)

A soil deposit containing volcanic ash was also found at the Woodduck Site Complex during limited test excavations at the site. These sites, lithic scatters consisting primarily of obsidian debitage and occasional cores, are located about 8 km east of Mount Jefferson. Well-consolidated soils containing tephra were reported from a depth of about 30 to 70 cm below the surface (Beardsley, 1989, and personal communication).

Examination of a soil sample from the Woodduck sites confirmed the presence of small pyroclasts of pumice with a maximum diameter of about 2 mm. The small lapilli are easily recognizable when examined with a 10x-30x hand lens or microscope (plate 23). The location of the sites and the size of the pyroclasts are consistent with soils developed on deposits of parent Mazama tephra. Electron microprobe characterization of glass tephra shards from a soil sample collected at this location confirmed Mount Mazama as the source of the ash (see Section V).

EVALUATION OF PREVIOUS ARCHAEOLOGICAL RESEARCH

There is little doubt that volcanic tephra deposits, particularly those that originated from Mount Mazama, are present in many Willamette National Forest archaeological sites. There is also no question as to the contemporaneity of prehistoric human utilization of the Western and High Cascades and the eruption of volcanic ash in the

region. Despite this, volcanic tephra has rarely been used for tephrochronological purposes in archaeological contexts, even when it has been recognized within sites. When volcanic ash has been found at a site, the relationship of tephra deposits and artifactual materials has often been poorly-described. It is also likely that the presence of tephra at sites is commonly overlooked during excavations and that volcanic tephra is much more widespread in archaeological contexts than the literature would indicate. Potential high-probability occupation areas such as ridges, basins, saddles, and rockshelters are often areas in which tephra is also well-preserved.

A literature review of Willamette National Forest sites in which volcanic tephra was identified demonstrates that silicic tephra, almost certainly originating during the climactic eruptions of Mount Mazama, is widely distributed, particularly in the High Cascades and the eastern part of the Western Cascades. Silicic tephra from the Rock Mesa and Devils Hill vents, on the other hand, has not been identified at any known archaeological sites in western Oregon. Tephra from basaltic eruptions, so far found in only a few Western Oregon archaeological sites, still holds some tephrochronologic potential, though only in relatively limited areas within the Willamette National Forest.

It appears that a major problem of tephrochronological research lies in the simple identification of tephra at sites, a topic discussed in the previous section. The presence of Mazama tephra, in particular, should be anticipated in Cascades archaeological sites. When sites are found in the vicinity of known basaltic tephra vents, site deposits should be carefully evaluated for the presence of datable pyroclastic materials. It is also important in future archaeological studies that the relationship of analyzed artifactual materials, intrasite stratigraphy, and tephra deposits or soils be clearly documented. The well-described provenance of all datable artifactual and ecofactual materials is significant not only for the construction of site chronologies, but in their ability to provide internal cross-checks among different chronologic techniques. Chronologic information from obsidian hydration measurements, volcanic tephra deposits, radiocarbon dates, and temporally-diagnostic artifacts can be used to these ends, though, only when their intrasite stratigraphic relationships are thoroughly recorded.

Future archaeological research in the Willamette National Forest has much to gain from the adoption of more rigorous tephrochronologic evaluation methods.

MAJOR ISSUES IN WILLAMETTE NATIONAL FOREST ARCHAEOLOGICAL TEPHRA STUDIES

During the course of this investigation, four interrelated key issues germane to archaeological tephra studies in the Willamette National Forest were identified. For archaeological and tephrochronologic studies to be successfully carried out in the study region, these issues must be explicitly and sequentially addressed (table 7).

Is It Volcanic Tephra?
↓
How Can the Deposit Boundaries Be Distinguished?
↓
What is the Geologic Source of the Tephra Deposit?
Where are the Potential Sources?
↓
How Old Is It?

Table 7. Major issues in Willamette National Forest tephrochronologic studies.

Is It Volcanic Tephra?

The initial problem facing an archaeologist using tephrochronologic methods is the simple recognition of tephra at an archaeological site. A variety of different natural deposits resemble volcanic ash, though, and it is not always obvious whether a deposit in an archaeological context is volcanic ash or a soil that merely resembles volcanic ash. This can be a significant problem if archaeologists have not previously worked with volcanic tephra or if the tephra layer is thin or stained with iron or organic matter.

IDENTIFICATION OF SILICIC TEPHRA

Light-colored layers or deposits of silicic tephra often stand in contrast to darker soils or deposits of basaltic ash. The identification of silicic ash, though more straightforward than for basaltic ash, is not always a simple matter.

In arid environments, light-colored layers of well-consolidated caliche are sometimes mistaken for volcanic ash. Caliche layers contain significant quantities of calcium salts and will fizz and dissolve away in dilute hydrochloric acid (10% HCl). If a light-colored layer dissolves in water, it is probably a mineral salt. If the sample is inert in acid but feels slippery to the touch, it may be gypsum. Silicic tephra feels gritty between the fingers or teeth, though this characteristic may also indicate the presence of diatomite, silt, or opal phytoliths. A small sample examined with a microscope at about 100x magnification will clearly distinguish among these materials, though volcanic ash will consist of irregularly shaped glass shards and fragments of mineral crystals (Steen-McIntyre, 1985).

Within the Willamette National Forest, primary deposits of *airfall* silicic tephra occur as loosely-consolidated units ranging in color from light gray to yellowish-tan to

orange. Near vents, the presence of easily-identifiable pumice lapilli up to several centimeters in diameter characterizes these deposits. The surface and internal texture of the larger pumice lapilli is quite distinctive and can be discerned with the naked eye or with a low-magnification hand lens (plate 21). As the distance from the vent increases, the grain size of the lapilli rapidly decreases. In the northern part of the Willamette National Forest, primary Mazama deposits and Mazama-derived soils contain pyroclasts of pumice no larger that 1-2 mm in diameter. These pumice pyroclasts are rounded to subrounded, yellowish-tan to orange in color, and are relatively easy to identify with a low-magnification hand lens (plate 22). When the pumice grains are examined under higher magnification (>30x), the distinctive glassy texture that is evident in plate 21 is usually quite easy to see. Soils developed on Mazama tephra can be identified by their yellowish-tan color and loamy texture. They usually contain a large percentage of pumice grains, though they may be thoroughly mixed with a matrix of organic debris, basaltic tephra, and various erosional products. The pyroclasts in these soils can often be identified with a 10x-20x hand lens, though slightly higher magnification (<100x) may be useful when the pyroclasts are very small (plate 23).

Other sources of evidence for the presence of silicic Holocene tephra deposits include:

1. Co-occurrence of obsidian fragments. Small angular to subangular fragments of *porphyritic* gray obsidian are found in association with pyroclastic products erupted from the Rock Mesa and Devils Hill chain of domes vents. These are discussed in more detail later in this section.

2. Stratigraphic Position. Is the suspected tephra deposit in a reasonable stratigraphic position? The previously-described Upper Salt Creek tephra (see Section III), for example, could be confused for a Holocene tephra deposit except that it is locally overlain by Miocene basalt flows.

3. Grain size. Is the grain size of pyroclasts in the suspected tephra deposit consistent with the distance of the unit from known sources?

4. Deposit thickness. Does the thickness of the suspected ash unit agree with what would be expected in relation to the distance from potential sources?

5. Geographic location. Is the potential ash deposit found in a geographically feasible area? Are known sources of volcanic tephra close enough to reasonably account for the deposit?

One source of misunderstanding among archaeologists in the identification of volcanic tephra appears to be the confusion of soil structures such as *peds* for lapilli. Peds are non-slaking soil aggregates formed in soils that are moderately to well-developed (Retallack, 1988). Peds are usually recognizable by an encasing clay layer on the ped

Plates 18-23 (Overleaf). Low-magnification photomicrographs of basaltic and silicic tephra samples from some important Willamette National Forest sources. These photographs approximate what would be seen if a sample was examined with a hand lens, although a little of the fine detail has been lost in the reproduction. The scale bars in the upper left corners of the pictures are 1 mm long.

Plate 18 (1): Basaltic tephra from the Sand Mountain. Tephra from these eruptions is characteristically fine-grained and consists almost exclusively of small droplets of sideromelane and tachylite. The scoriaceous texture of many of the pyroclasts is typical of those from basaltic tephra deposits. Sample SANDM-3; 10x.

Plate 19 (2): Fine-grained basaltic tephra from Belknap Crater. Sample BELKC-9; 15x.

Plate 20 (3): Fine-grained ash from Collier Cone. Tephra from this source is distinguished from many (but not all) basaltic ash sources in this region by the presence of a significant free crystalline component - the arrow points to a single crystal of quartz. Sample COLLC-2; 15x.

Plate 21 (4): Close-up of the surface of a small pumice lapillus of silicic tephra from Mount Mazama. The frothy, glassy texture of a typical silicic pyroclast is illustrated in this photograph. The same general texture can clearly be seen in many silicic pyroclasts, even very small ones. Sample MAZA-2; 10x.

Plate 22 (5): Buried Mazama soil. This paleosol was overlain by about 0.5 m of basaltic tephra from nearby Belknap Crater. The yellowish-tan color of the deposit and the presence of small pumiceous pyroclasts (such as the largest granule in the image) mark this as silicic tephra unit. The rounded grains (pyroclasts) are not a reflection of the depositional environment (e.g. fluvial), but of their volcanic origin. The geographic location of the soil, the maximum grain size (1-2 mm), and the thickness of the deposit (several centimeters) were used to identify the geologic source of the tephra as Mount Mazama (later confirmed by electron microprobe analysis). Sample BELKC-7; 15x.

Plate 23 (6): Soil from the Woodduck Site Complex (35LA67 and 35LA370). The circle surrounds a single pyroclast of silicic tephra enclosed in a darker soil matrix; the arrow points to a larger pyroclast about 1 mm in diameter. The fine frothy, glassy texture of the granules that identifies them as silicic tephra pyroclasts is not clear in the photographs, though it is readily apparent with a hand lens. The geographic location of the sample pointed to a Mazama origin and this was later confirmed by electron microprobe analysis. The presence of Mazama tephra in the soil dates the soil and any associated archaeological materials as post-Mazama in age. Sample WDUCK-1; 30x.


1

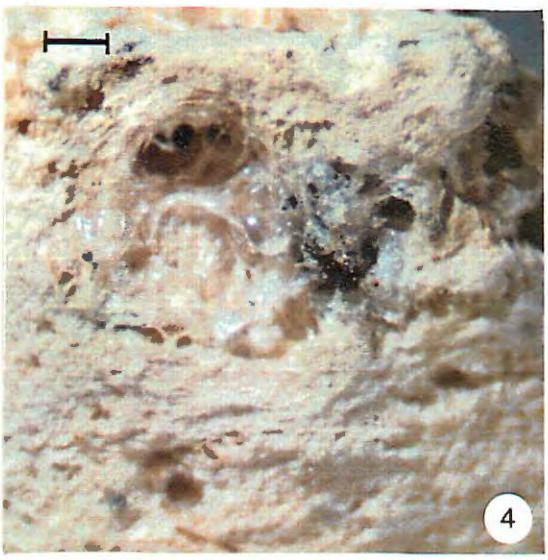
4

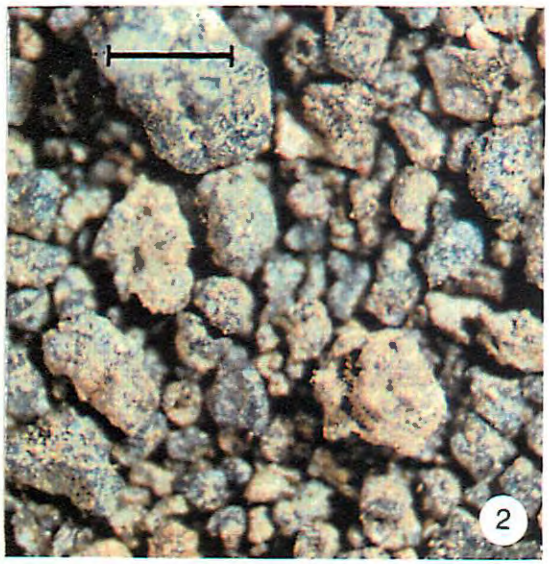
2

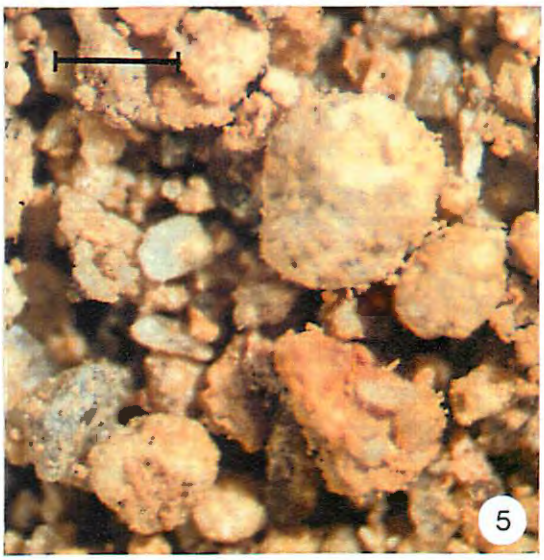
5

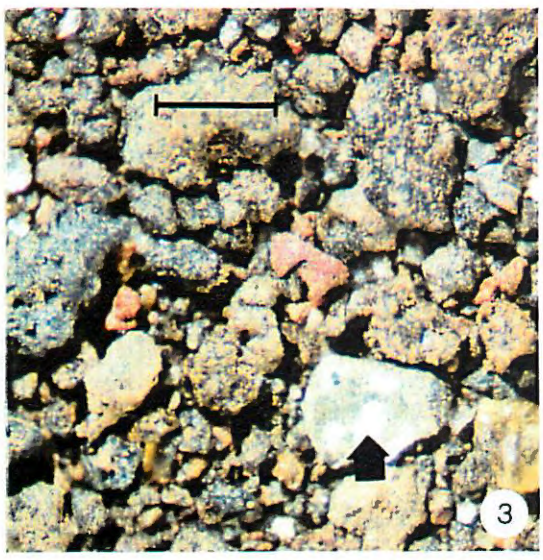
3

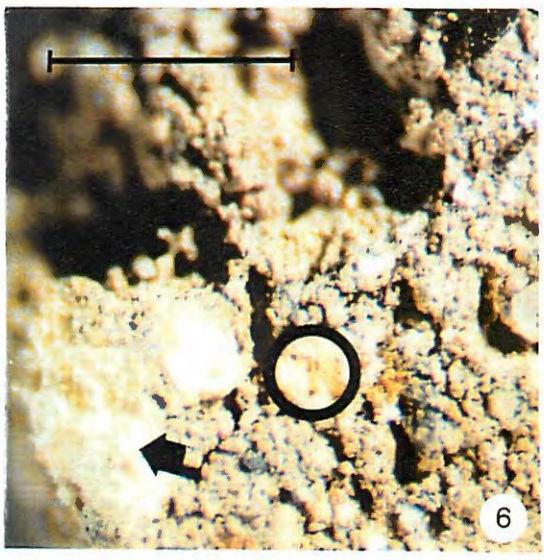
6

face, but in this project region where little clay has formed in most areas, the peds must be distinguished by their structural form and texture. In the slow-forming soils of much of the Willamette National Forest, peds do occur, but not commonly. The typical peds in this area are medium-sized granular to subangular-blocky, typical of an A and Bw horizon or, if clay has been formed, Bt horizons (Birkeland, 1984). Typical sizes for these moderately friable peds are from 5-10 mm (Soil Survey Staff, 1975; Buol et al., 1981). Peds typical of lower C horizons, such as prismatic or platy ones, generally are not found because of the attenuated development processes, the sandy soils, and the episodic nature of volcanic events over the last 10,000 years which have not allowed time for such below-B horizon development.

Mazama tephra and Mazama-derived soils are extensively distributed throughout the Willamette National Forest. In the higher elevations, many if not most of the surficial deposits are Mazama in origin, though organic debris and more recent airfall deposits of basaltic tephra cover them in some locations. Once the origin and characteristics of these tephra-based soils are recognized, however, they are quite easy to identify with only minimal equipment (a hand lens is mandatory) in the field.

IDENTIFICATION OF BASALTIC TEPHRA

The identity of basaltic tephra deposits can be verified through many of the same contextual means as silicic ash - geographic location, thickness, stratigraphic position, and grain size. The physical characteristics of basaltic ash are quite different than those of silicic tephra and require different criteria for identication. We find that deposits of basaltic tephra are relatively easy to distinguish in the field if adequate contextual information is available, particularly the location of known vents. We also note that it may be quite difficult to identify the presence of small amounts of basaltic tephra that have been incorporated into redeposited units.

Basaltic tephra deposits usually range in color from brown to reddish-brown to near black and are easily distinguished from silicic deposits on the basis of this one trait. When examined with a hand lens or low-magnification microscope, basaltic pyroclasts display a number of morphological characteristics which can be used to distinguish them from other materials. The tephra can sometimes be identified by its "sandy" feel. Under low magnification, the typical scoriaceous texture of individual small pyroclasts can often be seen (plates 18-20). The pyroclasts are usually rounded to subrounded and their unbroken surfaces are often smooth or slightly glassy, a reflection of their rapid cooling during eruption. Numerous scanning electron microscope (SEM) images of basaltic pyroclasts are available in Heiken (1974) and Heiken and Wohletz (1985) and may prove some help in the identification of basaltic pyroclasts.

How Can Deposit Boundaries Be Distinguished?

In tephra-rich area such as the Western and High Cascades of the Willamette National Forest, tephra deposits may be stacked one upon the other with few indications as to where one deposit ends and another begins. The volcanic ash may have originated from sources that are temporally or geographically widely dispersed or they may come from separate eruptive episodes at the same vent or volcano. Once deposits have been identified as volcanic ash, the boundaries between different units may be difficult to ascertain. The identification of these discrete tephra units, however, is important both for tephrochronological purposes and for the interpretation of site stratigraphy.

Individual beds of airfall tephra commonly have few or no internal structures, bedding or laminations. They can, however, be differentiated from each other by color differences (caused by differences in chemical composition or in varying percentages of *vitric-lithic-crystalline* components), by post-depositional diagenetic changes (like soil formation), and by grain size or grading differences (Fisher and Schmincke, 1984:142).

Changes in color offer one of the best indications of a tephra unit boundary. This is particularly true when a dark-colored basaltic unit is bounded by a light-colored silicic deposit. In thicker tephra deposits, the boundary between two units is often sharp and clearly distinguishable, the result of the rapid deposition of ash.

The products of a single eruptive event or brief eruptive eruptive cycle tend to show some grading from coarse material at the bottom of a deposit to finer material above (Williams and McBirney, 1979:135). Sudden vertical changes in grain size may indicate the boundary between two different eruptive events, though the period of time separating them may be difficult to determine. In a test pit near Belknap Crater (figure 35), we interpreted the two uppermost stratigraphic units (differentiated by grain size) to represent early and late phases of the same eruptive event. The distinct grain size and color boundary between the lower of the two units and an underlying tephra deposit were interpreted to result from a boundary between two different tephra units. Later geochemical studies (see Section V) bore out this conclusion.

If enough time passes between the deposition of successive tephra units, surficial deposits will begin to show signs of soil development. When covered by later airfall pyroclastic deposits, these now-buried soils (*paleosols*) will retain relict features that characterize them as former surface deposits. The boundaries between deposits can be identified on the basis of the presence or absence of these distinguishing characteristics. Palesols can be distinguished in the field by the presence of root traces, soil horizons, and soil structures such as peds (Retallack, 1988).

Chemical data provides some of the best evidence for the existence of borders between units. Rapid vertical stratigraphic changes in the *major* and trace element composition

of tephra units indicate the presence of a boundary between two compositionally-distinguishable tephra units. In a stratigraphic section near Belknap Crater (figure 46), we encountered what we thought was post-Mazama basaltic ash paleosol (BELKC-6) covered by more recent ash and cinders from Belknap Volcano. Chemical analysis of the soil revealed that the paleosols were A and B horizons that had developed on the Mazama tephra. The unit that we had initially identified as the uppermost Mazama tephra proved to be the C horizon of the Mazama airfall ash at this location. The chemical data also confirmed that the two upper units of the test pit were probably deposited during a single volcanic event.

Where is the Geologic Source of the Tephra?

Once the deposit in question has been confirmed as silicic or basaltic volcanic ash and the deposit boundaries have been established, the geologic source may be identified. While a variety of sophisticated tephra source identification or characterization techniques are available for the archaeologist and tephrochronologist, we find that in the study region these are often unnecessary. In a restricted area such as the Willamette National Forest, the problem of source identification is further simplified by the geographic constraints of potential sources.

BASALTIC SOURCES OF TEPHRA IN THE WILLAMETTE NATIONAL FOREST

The geologic sources of Holocene primary basaltic tephra deposits in the Willamette National Forest can usually be determined if several of six parameters are known: the geographic location of potential sources, the eruptive chronology of local basaltic ash eruptions, the geographic distribution of tephra sheets from potential vents, the prevailing wind direction at the time of eruption, the thickness of the deposit at the sampling location or archaeological site, and the grain size characteristics of different local basaltic tephra blankets. Basaltic tephra rarely travels farther than a few tens of kilometers from the vent. If the distribution of the tephra from local sources is known, the location of the sampling site should point to a probable upwind source or limited group of sources. If the tephra distribution is not known, any local tephragenic source can be considered a possibility, with those located to the west the most likely candidates. When multiple tephra units have been found at a site, a knowledge of the local eruptive chronology may be necessary to determine the stratigraphic sequence of tephra deposition. Deposit thickness (a function of vent distance and wind direction) and deposit grain size (dependent on grain size and eruptive style) may be further used to distinguish among different possible sources.

SILICIC SOURCES OF TEPHRA IN THE WILLAMETTE NATIONAL FOREST

The identification of silicic tephra within the boundaries of the Willamette National Forest immediately limits the potential sources to only three - Mazama, Rock Mesa, and the Devils Hill Dome Chain. Additionally, the Rock Mesa and Devils Hill Dome

Chain tephra are visually, mineralogically, and compositionally indistinguishable. (Tephra from the Carver Lake vents, though not examined in this current investigation, is also reported by Scott, 1987, as indistinguishable from the other South Sister silicic ashes.). Only where stratigraphic relationships are visible in the field is it possible to confidently distinguish between these two source areas. Since the two South Sister sources of tephra (along with the Carver Lake tephra) are geographically and chronologically proximate, the need to distinguish between them is something of a non-problem.

Distinguishing Mazama from Rock Mesa/Devils Hill Tephra

Though the geographic distribution of the South Sister tephra deposits is quite limited in the Willamette National Forest, there are locations in which Mazama tephra and that from the South Sister vents are found together. Along the Cascade Lakes Highway south of the Devils Hill Dome Chain, the stratigraphic relationships of the Mazama, Rock Mesa, and Devils Hill Dome Chain tephra is clearly exposed in road cuts.

In this limited geographic area, there are several different ways in which tephra from Mount Mazama may be easily distinguished from the Rock Mesa-Dome Chain:

1. **Color.** Mazama tends toward very pale brown (10YR 8/1-2) while Rock Mesa-Dome Chain tends to light gray (10YR 7/1-2). There are typically noticeable color differences when moving from Mazama to Rock Mesa-Dome Chain tephra.

2. **Co-occurrence of obsidian with Rock Mesa-Dome Chain tephra.** Angular to subangular fragments of porphyritic gray-black and occasionally black obsidian co-occur with both the Rock Mesa and Dome Chain tephra for an undetermined distance from the source vents. Obsidian is found in association with Mazama tephra only in the immediate vicinity of the Crater Lake caldera far to the south.

3. **Lapilli size in relation to geographic locality (distance from source vent).** The maximum lapilli size is closely related, in most cases, to the distance of the tephra deposit from its source. Pumice lapilli from the South Sister vents will be found, except near the limits of the airfall blanket, to be larger in diameter than those from Mount Mazama.

4. **Chemical composition.** The chemical composition of tephra from the Mount Mazama and the South Sister vents, as demonstrated by this and other investigations, are clearly distinguishable.

What is the Age of the Tephra?

Once the source of the tephra has been identified, it may be possible to assign an *absolute* or *relative age* to the unit in question. While this is the primary objective of

most archaeological studies of volcanic tephra, it must be emphasized that this step must be preceded by the three stages previously discussed.

The potential silicic and basaltic tephragenic sources for Willamette National Forest deposits are relatively well-known. Fortunately, there are a substantial collection of radiocarbon dates associated with Holocene volcanic activity within the Willamette National Forest (tables 4, 5, and 6). Even lacking associated radiocarbon dates, the ages of many of the tephra units may be bracketed stratigraphically through their contact relationships with underlying and overlying deposits or through their relationships to deposits of known ages (figures 16 and 17).

V.
GEOCHEMICAL CHARACTERIZATION OF TEPHRA FROM WILLAMETTE NATIONAL FOREST SOURCES

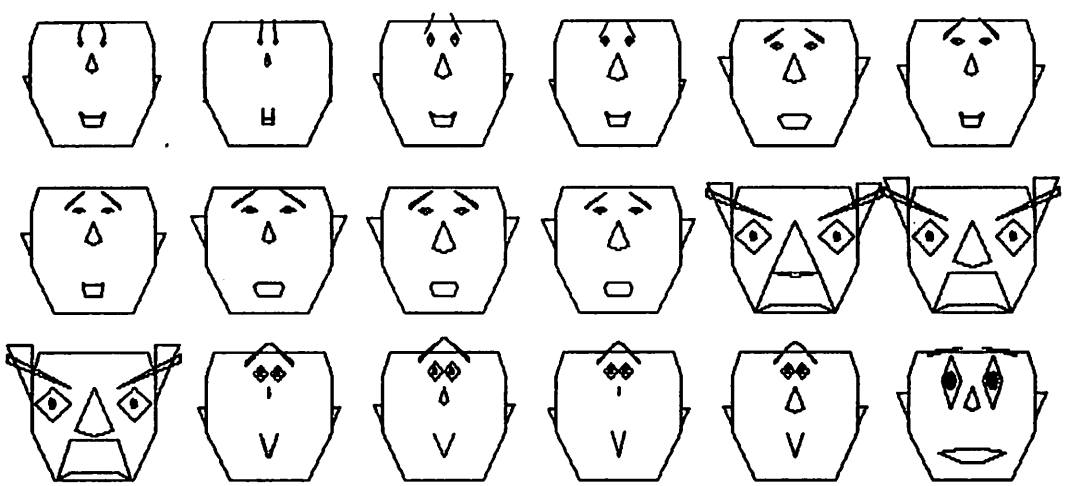

GEOCHEMICAL CHARACTERIZATION OF VOLCANIC TEPHRA FROM GEOLOGIC SOURCES AND ARCHAEOLOGICAL CONTEXTS

INTRODUCTION

A major objective of this investigation was to ascertain whether the different *basaltic* and *silicic* sources of volcanic *tephra* found in the Willamette National Forest could be characterized and differentiated on the basis of their major and trace element composition. A secondary objective was to verify the viability of atomic absorption analysis as an analytical technique for the geochemical *characterization* of the tephra.

In this chapter, we report the results of *major* and *trace element* analyses of 51 samples of silicic and basaltic tephra from numerous locations throughout the Willamette National Forest (Appendix 4). Samples were collected and analyzed from nine basaltic ash sources and three silicic tephra sources. Two complementary analytical techniques, atomic absorption spectrophotometry (AAS), and electron probe microanalysis (EPMA), were used.

Although we had originally proposed that EPMA be used as the primary tephra characterization analytical method, after examining the literature and consulting with other geologists and analysts we decided that AAS might prove more useful for future geoarchaeological tephra studies. AAS was chosen as the primary characterization technique because of the relatively low cost of the method, easy sample preparation, rapid turnaround time, local availability (Atomic Absorption Laboratory, Center for Volcanology, University of Oregon), and overall availability (many more AAS than EPMA facilities are available in general). Most important, though, were the lower trace element detection limits of AAS relative to EPMA - we could simply determine the trace element composition of more trace elements with greater analytical precision by switching to AAS. We anticipated that trace elements would be more useful than major element abundances in distinguishing among the different tephra sources, particularly those sources of basaltic composition.

The electron microprobe was used to analyze a subset of 10 samples of silicic ash from *primary* and *secondary* contexts. This subset included a single archaeological sample from the Woodduck Site Complex, a Willamette National Forest site in which tephra has been recently identified. EPMA was selected because of its ability to analyze very small samples and tephra *shards* that would be difficult to separate from a soil matrix or highly contaminated sample. This latter characteristic allows the technique to be used to characterize tephra-derived soils found at archaeological sites, even when only small quantities of volcanic ash are found in the soils. The instrumentation necessary for the EPMA phase of the research is locally available at the Electron Microprobe Laboratory, Department of Earth Sciences, University of Oregon.

METHODS USED

Field Methods and Procedures

Potential *Holocene tephragenic* vents were identified prior to field investigations through literature research and examination of aerial stereo photographs. All vents that were considered as possible significant sources of Willamette National Forest tephra deposits were visited and sampled. Field studies were conducted from the period of July, 1990, through September, 1990. A total of 42 person-days were spent in the field phase of the research. Samples of Mazama tephra used in a previous study (Skinner and Radosevich, 1989) were collected along a north-south transect reaching from Crater Lake to the La Pine area of central Oregon and were used to characterize the Mazama source.

As recommended by Steen-McIntyre (1977:13), samples of medium-grained (2-64 mm) tephra *pyroclasts* were chosen for characterization whenever possible. The primary objective was the preliminary characterization of volcanic tephra units in the Willamette National Forest. As such, our sampling strategy was to collect a minimum number of samples from as many of the major tephra sources as possible. A comprehensive investigation of intraunit chemical variability was explicitly recognized as beyond the scope of this initial investigation. A minimum of 100 gm of tephra was collected from at least four dispersed locations at most tephra units. A total of 50 samples from 12 tephra sources and one specimen from a single archaeological site were included in the analyses.

Observations of tephra stratigraphy and contact relationships between airfall units came primarily from road and trail cuts. When these were not available, shallow test pits (< 1 m) were dug.

Geochemical Analytical Methods

ATOMIC ABSORPTION SPECTROPHOTOMETRY (AAS)

Atomic absorption occurs when light energy of a specific wavelength is absorbed into a ground state atom, causing that atom to be excited. The amount of light absorbed is directly proportional to the number of atoms in the light path, thus allowing quantitative determination of the amount of analyte by measuring the absorbed light (Johnson and Maxwell, 1982).

There are several advantages to this method. AAS is good at detecting a number of major and trace elements at or below 0.001 mg/L, detection limits not available for EPMA. A small amount of sample is required for the actual analysis (about 250 mg), though to ensure sample comparability, it is preferable that this sample be removed from a larger homogenized reservoir. Sample preparation is minimal - the specimen

need only be cleaned of contaminants and crushed to a fine powder. Unlike more exotic analytical methods such as instrumental neutron activation analysis (INAA), AAS also has a short turn around time and is relatively inexpensive.

There are also several disadvantages to AAS. The sample is completely destroyed in the process of analysis; if questions arise about the analytical procedures, the original sample cannot be reanalyzed. Also, if only small quantities of sample material are available for analysis (as is sometimes the case with archaeological materials), the destructive qualities of AAS may be seen as a major liability. This is likely to not prove a liability for tephra from archaeological sites, however, where adequate quantities of volcanic ash are usually available.

While AAS is an excellent technique for analyzing bulk samples of volcanic tephra, in some cases it may be difficult to obtain these fractions from the original specimen. This is particularly true when the sample must be separated from a soil matrix, contains a significant *lithic* or *crystalline* component, is heavily contaminated, is severely weathered, or when only small amounts are available. During the course of the current investigation it became clear that several secondary samples (Mazama *paleosols*) were not yielding data consistent with their Mazama origin. This was apparently due to the contamination or weathering of the *airfall tephra* samples after deposition. Airfall *lapilli* associated with the primary sources, on the other hand, returned excellent data when analyzed. Methods of tephra pretreatment to remove contaminants and to isolate the *vitric* fractions of the ash are discussed by Borchardt (1969:157-159), Steen-McIntyre (1977:64-78), and Carrara (1989:60).

A review of the literature indicated that AAS had not been previously used to characterize volcanic tephra, though it appeared to be well suited for this type of analytical work. Bulk analyses of the ash are used, as they have been for many other characterization studies, and many of the major and trace elements used by other methods are also determinable by AAS.

ELECTRON PROBE MICROANALYSIS (EPMA)

Electron microprobe analysis allows the determination of elements with an atomic number greater than Be by focusing an electron beam on the surface of a sample. The beam may be focused in an area ranging from about one to 100 microns in diameter, permitting the analysis of very small or very specific samples. As an electron is knocked out of one shell by an impinging electron, it is replaced by another from an outer shell. This replacement results in the emission of an X-ray, the energy level of which is characteristic of each element. Based on the assumption that the intensity of a typical X-ray line generated per unit of time is directly proportional to the concentration of the target element, peaks of the X-ray spectrum can also be quantified (Johnson and Maxwell, 1982).

Plates 24 and 25. Top (24): SEM of elongate tephra shard from a lapillus originating from Crater Lake (MAZA-9); 2500x. The circular feature on the smooth flat surface of the shard in the left-hand side of the image is the damage scar left by the electron beam after the glass was analyzed with the electron microprobe. The dark oval structure above the scar is a small vesicle. Bottom (25): SEM of a platy tephra shard from the Rock Mesa eruptions (ROCKM-4); 1500x.

EPMA is semi-destructive. Thin sections must be prepared from the sample but are preserved for later reanalysis or examination. See the following section on sample preparation for details concerning EPMA sample preparation.

A major benefit of EPMA analysis is that very small areas (1-100 μm in diameter) may be precisely sampled for analysis. This is of particular advantage in volcanic tephra studies if it is difficult to separate the vitric component from a soil or heavily contaminated matrix or if only very small scattered shards of glass are available for analysis. Individual shards of glass or very small pyroclasts and lapilli may be identified and analyzed, even when very little ash is present. In the present study, we used a 5 μm diameter 15 kV electron beam to sample the surfaces of vitric shards of silicic tephra (plates 24 and 25). Each sample was analyzed in several locations to account for compositional variability and analytical variation. The average values of these combined analyses (table 10) were used for the later visual and statistical analyses of the data. EPMA is also relatively inexpensive once sample preparation is complete. It is possible to analyze several samples per hour at multiple loci, provided that glass shards are abundant and are not too severely weathered. It is also possible to obtain SEM images of the individual shards and sampling locations (plates 24 and 25). In this way, it is also feasible to combine morphological studies of tephra shards while performing EPMA analyses.

There are some drawbacks in EPMA analysis of tephra, however. The method is reliable for determining the major element composition of samples, but has relatively high detection limits and high uncertainties for most trace elements. While the major element composition of volcanic glass may often be adequate to characterize samples and identify tephra sources, the trace element composition of the glass is usually a more sensitive discriminator of the geologic origin of the sample. In the Willamette National Forest, only two geochemically-distinguishable Holocene sources of silicic tephra are present. In this case, the use of major element abundances to characterize the samples was expected to prove adequate. After reviewing the results of the already completed AAS major element analyses of the tephra samples, we decided that the major element composition, as expected, would be almost certainly adequate to characterize silicic tephra samples with EPMA. In areas with more complex tephrostratigraphic problems, the use of trace element abundances to characterize the glass shards may prove a more appropriate choice.

Another significant disadvantage of EPMA analysis is the relatively involved and time-consuming sample preparation that is required. See the next section for details.

EPMA has been used to chemically characterize silicic tephra for many years, and is a widely-used and reliable characterization method (Smith and Westgate, 1969; Self and Sparks, 1981). EPMA techniques have also been used to characterize basaltic tephra deposits in Iceland (Larsen, 1981) and Utah (Oviatt and Nash, 1989), though analytical details are very sparse. Because of the lack of information concerning

sample preparation and analytical techniques about EPMA and basaltic tephra characterization, we decided to limit our current EPMA investigation to silicic tephra. We anticipate, though, that EPMA analyses of sideromelane basaltic glass would yield the most reliable results if basaltic samples of basaltic tephra were to be analyzed for characterization purposes.

Sample Preparation Methods

AAS SAMPLE PREPARATION

The preparation of the tephra samples for AAS was purposefully kept to a minimum. Our strategy throughout the project was to attempt the simplest and least time-consuming method of analysis, whenever possible. Though the distance from source is a known variable affecting the bulk composition of silicic tephra (Hinkley et al., 1987; Kir'yanov et al., 1990), we reasoned that the relatively limited geographic area that made up the study area would not significantly affect the analytical results.

Our previous experience with INAA studies of the Mazama and the South Sister tephra sources had demonstrated that minimal sample preparation methods using single pumice lapillus were adequate for tephra trace element characterization studies in the Willamette National Forest region (Skinner and Radosevich, 1989). A previous major element study of tephra by Czamanske and Porter (1965) had also successfully characterized volcanic ash without extensive pretreatment.

Each tephra sample to be analyzed was carefully examined with a 15x stereoscopic microscope for contaminants. All organic debris and obvious accidental inclusions were removed by hand with fine tweezers. Single lapillus from each source of silicic tephra, when available, were selected for preparation. Each lapillus was gently crushed and obvious lithic or crystalline components (such as large hornblende crystals) were removed by hand. Samples from secondary silicic tephra deposits with pumice lapilli too small for bulk sample preparation were cleaned of any obvious contaminants from overlying or underlying units (primarily basaltic tephra deposits and organic debris). After cleaning, approximately 10 gm of all samples were crushed to a fine powder in a mullite mortar and pestle for final AAS sample preparation.

EPMA SAMPLE PREPARATION

Sample preparation for EPMA study was considerably different than for AAS analysis. A subset of silicic samples from known geologic sources (Mazama, Rock Mesa, and Devils Hill Dome Chain) was drawn from the sample population used for AAS analysis. In addition, three samples of secondary silicic tephra from deposits underlying more recent basaltic tephra units were selected. A single archaeological sample from the Woodduck Site Complex (a soil containing small pumice pyroclasts) was also included. All of the silicic tephra samples from secondary contexts were strongly suspected to have originated from Mount Mazama.

The samples were prepared as standard petrographic slides. Individual lapillus were impregnated with epoxy, sectioned, and glued to a petrographic slide. The Mazama paleosol samples from secondary deposits were first impregnated on a slide with epoxy. The top of each slide sample was then trimmed and ground to a flat surface and a new slide was attached to this freshly exposed surface. In this manner, a cross section of the small lapilli was exposed for the EPMA studies. After initial preparation, each sample was trimmed and ground to a thickness of approximately 30μm and polished to a smooth surface. The finished slides were then coated with a thin layer of carbon before analysis with the electron microprobe.

Correlation, Clustering and Statistical Methods

Prior to examining the analytical results for clusters, all major element data sets were normalized to 100 percent water-free. This aided in the comparison of AAS and EPMA data and in the comparison of samples with organic contaminants and different degrees of hydration of the vitric fraction.

The *coefficient of variation* (CV%) was used to quantitatively ascertain the extent of intraunit compositional variability for each of the analyzed sources (table 9). This statistic is used as a way of expressing the variation for a set of data relative to its mean and is defined as:

$$CV\% = \frac{S}{X} \times 100 \qquad (1)$$

where CV% is the coefficient of variation, S = 1 standard deviation of the data set, and X = the average of the data set (Anderson and Sclove, 1986:136). The coefficient of variation is particularly useful for assessing the relative homogeneity of groups independent of their respective means. A small CV% indicates a small degree of intrasource variation. A CV% of less than approximately 20 for a selected element suggests that the element may prove useful in characterizing the source, i.e. its dispersion within the source is relatively small (Borchardt et al., 1973). The ideal element for characterizing a tephra source is one which exhibits a small intrasource CV% but which also maintains a degree of interunit variability.

In this study, elements with a CV% of less than about 20 were chosen for inclusion in the visual and statistical clustering analyses (though we recognize that the small number of samples for each tephra source limits the validity of this statistic). Elements which showed little variation among the different sources were eliminated from the sample group analysis. The basaltic and silicic tephra data sets were treated separately and these criteria were applied to each data matrix. The major and trace elements which were selected for further visual and statistical analyses include:

Basaltic Tephra	Silicic Tephra
SiO_2	SiO_2
TiO_2	TiO_2
Al_2O3	Al_2O_3
MgO	MnO
CaO	CaO
Na_2O	K_2O
Co	Ba
Cr	Cu
Cu	Rb
Rb	Sr
Sr	Zn
Zn	

Visual correlational and clustering methods were primarily limited to graphical techniques drawn from EDA concepts (Tukey, 1977; Chambers et al., 1983; also see Section II of this report). Bivariate scatterplots, ternary plots, and other multidimensional methods were used to examine the data for geochemical groupings. The microcomputer software used to plot these graphs is described in Appendix 5.

During graphical analysis of the data, different pairs of elements were plotted visually as bivariate scatterplots and were examined for clustering tendencies. When visual clusters were found, the particular pair of elements were considered as potentially useful for the statistical correlation with known sources and between known sources and secondary samples of unknown origin. By examining many bivariate pairs it is possible to identify element pairs which can be most effectively used to identify differences between specific geochemical source groups. The more geochemically dissimilar a single cluster group identified by examination of bivariate plots is from the remaining cluster groups, the more useful the bivariate element components become in distinguishing one geochemical source from another. Ternary plots, as well as spider plots, of selected elements were also occasionally used in the exploratory analysis of the data, though scatterplots generally proved most useful in distinguishing among the often compositionally similar sources of basaltic tephra.

After examination of the geochemical data set with visual techniques, the data were examined for groups or clusters using *cluster analysis* classification methods. Only major and trace elements exhibiting intraunit homogeneity (low CV%) and observable interunit heterogeneity were used in the data matrices to be analyzed.

All cluster analyses were performed with the MVSP 2.0 multivariate statistical package (see Appendix 5). A dissimilarity matrix for each analyzed data set was constructed

using the Euclidean distance coefficient while the cluster analyses were carried out with the unweighted pair-group method (see Romesburg, 1984:10-28, for details). Additional analyses of the data using different clustering algorithms yielded almost identical results. The results of the cluster analyses are presented here as dendrograms.

Cluster analyses were used both to verify visually identified groups and to heuristically examine the data sets for clusters relating to tephra sources. Parametric statistical methods such as cluster analysis assume that geochemical sample concentrations are normally distributed, an assumption that may sometimes be without merit. This presupposition can lead to the misclassification of chemically-characterized samples and it has been recommended that parametric and non-parametric clustering techniques be used in tandem for the reliable classification of specimens (Leach et al., 1986). For exploratory purposes, however, cluster analyses provide a useful method for quickly examining multi-element arrays of geochemical data.

Analytical Results

The results of the AAS and EPMA analyses are presented in tables 8 and 10. Summary AAS statistics for each source are presented in table 9. All AAS major element data were normalized to 100 percent water-free. EPMA data for each sample are presented in table 8 and is an average of at least five shard analyses for each sample. Analyses for each sample point are reported in Appendix 3 (table 11) Only the normalized AAS data and average EPMA data were used for visual and statistical analyses. Original AAS and EPMA data for the tephra samples and analytical standards can be found in Appendices 2 and 3 (tables 11 and 12). AAS and EPMA data are also available in Lotus-compatible worksheets for the IBM-PC (see Appendix 5).

Discussion

AAS

AAS proved a successful analytical method to varying degrees for characterizing the basaltic and silicic deposits of volcanic tephra. The method was very productive for characterizing silicic sources of ash, moderately useful for characterizing basaltic tephra sources, and surprisingly unsuccessful for characterizing the Mazama paleosols.

Predictably, the two major compositional suites of tephra samples, basaltic and silicic, were clearly distinguishable from one another. When plotted as scatterplots, virtually any major or trace element pair could be used to separate basaltic and silicic tephra samples. The scatterplot presented in figure 23 was typical of most of the major and trace elements, particularly the high CV% elements selected.

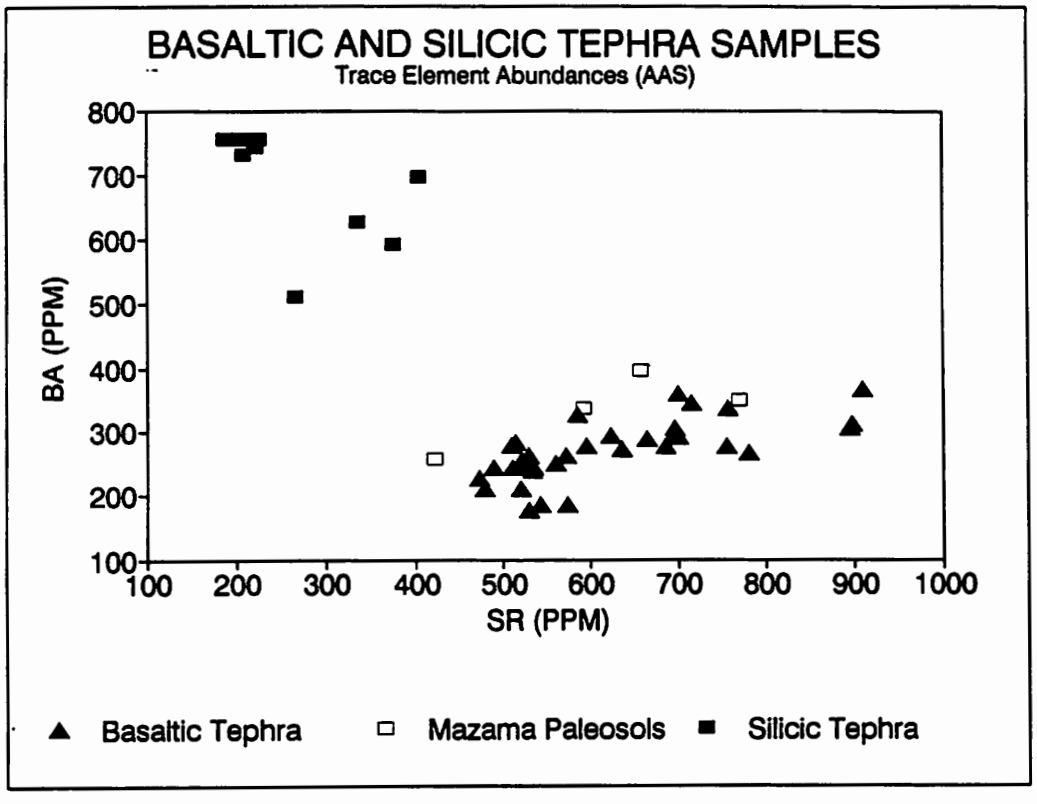

Figure 23. Ba plotted versus Sr for all tephra samples analyzed in the current project. The clear visual differentiation of basaltic and silicic tephra sources was expected and was typical of many major and trace element pairs. The poor visual discrimination of the Mazama paleosols is discussed further in the text.

The secondary Mazama paleosols, however, did not plot with the Mazama source samples, though the paleosols are distinguishable as a somewhat scattered cluster. The problem of the secondary Mazama samples is discussed shortly.

Basaltic Tephra Clusters

Graphical analysis of major and trace element data for the basaltic tephra samples indicates that source clusters are distinguishable, but that only some of the sources form compositionally unique clusters. In the scatterplots presented here, the Nash Crater source has been omitted. This source of basaltic ash showed the greatest compositional variation of the basaltic samples and preliminary graphical analysis suggested that very little identifiable clustering is present. We also considered the Nash Crater source the least significant of those sampled for investigation - the distribution of ash and chronology of tephragenic eruptive activity at this vent are not

	BELKC-4	BELKC-5	BELKC-6	BELKC-7	BELKC-9	BNASH-1	BNASH-2	BNASH-3	CARLL-1	COLLC-1
SIO2	49.97	51.21	52.27	52.97	52.41	52.73	54.82	51.84	57.00	55.00
TIO2	1.62	1.45	1.41	1.44	1.32	1.23	1.19	1.36	0.92	1.05
AL203	19.54	17.34	17.26	21.41	18.74	17.95	17.98	18.43	20.44	17.39
FE203	3.78	3.57	3.65	6.30	3.64	3.30	5.31	3.70	2.89	4.10
FEO	5.63	5.85	5.57	4.11	4.99	5.39	3.68	5.41	4.04	3.96
MNO	0.17	0.15	0.15	0.15	0.15	0.14	0.12	0.15	0.12	0.14
MGO	6.15	7.83	6.46	3.61	5.97	6.27	4.57	6.37	2.93	5.53
CAO	8.62	8.16	8.51	5.11	8.20	8.18	7.82	8.06	5.69	7.93
NA20	3.37	3.35	3.35	3.62	3.54	3.66	3.36	3.56	4.63	3.89
K20	0.71	0.73	1.01	0.86	0.81	0.77	0.74	0.73	0.91	0.82
P205	0.42	0.35	0.35	0.41	0.23	0.37	0.41	0.39	0.43	0.19
BA	211	210	396	337	326	277	277	305	349	244
CO	39	36	32	19	28	38	26	36	18	33
CR	117	138	157	55	91	105	108	107	35	74
CU	56	64	54	62	56	53	47	63	33	54
NI	94	160	87	29	46	172	85	140	20	110
RB	11	12	15	18	13	11	11	11	18	13
SR	479	520	658	593	585	755	686	697	771	521
ZN	80	77	83	91	78	97	81	94	80	79

MAJOR ELEMENT ABUNDANCES REPORTED AS WEIGHT PERCENT OXIDES
TRACE ELEMENT ABUNDANCES REPORTED IN PARTS PER MILLION

Table 8. Atomic absorption spectrophotometry (AAS) data. All major element data have been normalized to 100 percent water-free. TR = trace present. See Appendix 2 for original data and standards.

	COLLC-2	COLLC-3	COLLC-4	FORKB-1	FORKB-2	FORKB-3	FORKB-4	LNASH-1	LNASH-2	LNASH-3
SIO2	56.24	54.77	56.25	50.82	49.70	51.00	49.49	50.55	51.79	52.06
TIO2	0.89	0.70	0.89	1.22	1.25	1.10	1.25	1.25	1.38	1.19
AL203	19.37	18.26	19.60	20.03	22.03	20.90	20.89	19.28	18.34	18.14
FE203	2.89	2.37	2.66	3.76	5.39	3.39	4.52	4.66	7.25	6.79
FEO	3.56	4.44	4.37	5.41	4.70	4.97	4.90	4.83	1.58	2.05
MNO	0.11	0.12	0.13	0.16	0.15	0.15	0.17	0.16	0.15	0.14
MGO	4.43	6.40	4.45	6.96	5.82	6.27	7.30	6.76	5.73	5.90
CAO	7.61	8.42	6.67	7.35	6.92	7.82	7.46	7.93	8.19	8.33
NA2O	3.90	3.57	3.88	3.20	3.05	3.38	3.07	3.42	4.34	4.11
K2O	0.89	0.79	0.94	0.67	0.64	0.66	0.53	0.71	0.87	0.88
P2O5	0.12	0.17	0.16	0.42	0.36	0.36	0.41	0.45	0.39	0.40
BA	238	244	227	186	177	250	186	294	360	344
CO	28	32	29	37	38	38	43	41	38	36
CR	61	60	55	226	141	170	207	108	109	105
CU	47	49	52	47	51	45	57	61	66	78
NI	85	160	101	159	112	127	164	134	134	125
RB	17	18	18	10	11	11	9	11	12	12
SR	533	489	473	543	530	561	574	695	700	716
ZN	65	69	67	72	79	74	71	96	95	92

MAJOR ELEMENT ABUNDANCES REPORTED AS WEIGHT PERCENT OXIDES
TRACE ELEMENT ABUNDANCES REPORTED IN PARTS PER MILLION

Table 8 (Continued). AAS tephra data.

	LNASH-5	LNASH-6	LOSTL-2	LOSTL-3	LOSTL-4	LOSTL-5	MAZA-2	MAZA-5	MAZA-8	MAZA-9
SIO2	51.39	53.02	48.04	49.88	49.91	50.15	63.99	69.00	67.18	67.63
TIO2	1.34	1.24	1.60	1.32	1.50	1.19	0.61	0.55	0.54	0.59
AL203	17.73	21.57	18.42	16.15	17.29	16.41	22.33	15.78	18.26	18.38
FE203	4.15	5.19	4.24	2.97	3.60	3.35	1.45	2.30	2.04	2.02
FEO	5.22	4.33	6.05	6.39	6.00	6.22	2.07	1.17	1.33	1.23
MNO	0.14	0.15	0.17	0.16	0.16	0.15	0.07	0.06	0.08	0.06
MGO	7.44	5.22	9.67	10.17	8.95	9.62	0.62	0.89	0.90	0.69
CAO	7.87	5.11	8.05	8.63	8.44	8.56	2.16	2.49	2.60	2.51
NA2O	3.56	3.02	2.82	3.22	3.13	3.22	4.28	5.09	4.63	4.43
K2O	0.76	0.73	0.58	0.77	0.65	0.79	2.01	2.46	2.18	2.14
P2O5	0.39	0.41	0.36	0.34	0.35	0.34	0.41	0.20	0.28	0.31
BA	337	256	294	288	272	291	512	698	629	593
CO	36	32	48	48	46	39	8	4	3	7
CR	116	100	164	165	175	162	15	15	15	19
CU	58	48	70	65	61	64	15	21	19	18
NI	171	85	222	238	202	181	4	7	6	7
RB	11	12	9	12	10	11	33	47	36	38
SR	757	422	624	665	637	701	266	404	335	376
ZN	87	93	83	82	83	77	46	50	51	48

MAJOR ELEMENT ABUNDANCES REPORTED AS WEIGHT PERCENT OXIDES
TRACE ELEMENT ABUNDANCES REPORTED IN PARTS PER MILLION

Table 8 (Continued). AAS tephra data.

	NEWBE-1	ROCKM-1	ROCKM-2	ROCKM-3	ROCKM-4	SANDM-18	SANDM-2	SANDM-3	SANDM-5	SCINP-1
SIO2	72.46	73.25	73.09	72.57	72.15	50.90	52.74	50.42	51.18	50.19
TIO2	0.38	0.34	0.38	0.31	0.36	1.04	1.23	1.59	1.28	1.55
AL203	14.49	14.12	14.27	14.50	14.77	18.74	18.72	17.43	18.25	20.41
FE203	0.67	0.77	0.80	0.84	0.69	3.82	3.49	3.59	3.54	5.08
FEO	1.66	1.39	1.40	1.40	1.51	5.09	4.62	5.44	5.15	5.15
MNO	0.06	0.05	0.05	0.05	0.06	0.16	0.14	0.16	0.15	0.17
MGO	0.58	0.50	0.52	0.62	0.55	7.22	5.65	7.63	6.90	6.30
CAO	2.03	1.86	1.82	1.98	2.14	8.61	8.63	9.39	9.05	7.07
NA2O	4.47	4.33	4.28	4.38	4.57	3.37	3.66	3.22	3.32	3.03
K2O	3.04	3.23	3.26	3.21	3.03	0.69	0.77	0.76	0.80	0.66
P2O5	0.15	0.16	0.13	0.13	0.16	0.36	0.35	0.37	0.37	0.39
BA	756	756	756	756	745	305	366	266	311	244
CO	1	1	1	1	1	41	35	41	38	36
CR	18	15	16	15	16	134	97	148	127	139
CU	8	8	8	9	9	54	55	65	57	57
NI	4	92	4	4	6	130	83	134	108	122
RB	66	70	76	75	71	10	11	11	11	11
SR	211	187	202	205	222	895	909	781	897	511
ZN	42	40	42	38	42	83	115	79	81	76

MAJOR ELEMENT ABUNDANCES REPORTED AS WEIGHT PERCENT OXIDES
TRACE ELEMENT ABUNDANCES REPORTED IN PARTS PER MILLION

Table 8 (Continued). AAS tephra data.

	SCINP-2	SCINP-3	SCINP-4	SSDCH-1	SSDCH-3	SSDCH-6	YAPOA-1	YAPOA-3	YAPOA-4	YAPOA-6
SIO2	49.82	49.84	48.63	72.47	72.34	72.06	55.54	55.82	55.50	54.96
TIO2	1.56	1.60	1.66	0.36	0.35	0.36	1.08	0.13	0.92	1.00
AL203	19.97	19.72	21.13	14.49	14.74	14.70	18.64	18.27	19.21	18.72
FE203	4.87	4.63	4.95	0.87	0.80	0.93	2.54	3.15	2.41	3.34
FEO	5.11	5.29	5.10	1.45	1.43	1.44	4.57	4.81	4.29	4.35
MNO	0.18	0.18	0.17	0.06	0.06	0.06	0.13	0.15	0.12	0.13
MGO	6.77	6.83	6.59	0.62	0.54	0.65	5.26	4.99	5.15	5.35
CAO	7.56	7.49	7.53	1.99	2.05	2.11	7.22	7.52	7.63	7.23
NA20	3.08	3.30	3.13	4.62	4.58	4.53	3.88	3.91	3.78	3.72
K20	0.69	0.69	0.66	2.96	2.96	3.03	0.94	0.95	0.86	0.93
P205	0.39	0.43	0.44	0.11	0.14	0.13	0.20	0.28	0.14	0.26
BA	244	261	277	756	756	733	283	279	255	261
CO	37	38	42	TR	TR	TR	31	30	31	30
CR	128	126	140	14	15	14	55	78	57	68
CU	59	54	60	10	9	8	53	64	53	57
NI	144	130	150	0	2	2	105	41	110	75
RB	11	11	12	67	63	71	18	16	17	19
SR	535	573	596	225	214	207	514	510	521	530
ZN	79	103	91	40	42	37	69	72	68	73

MAJOR ELEMENT ABUNDANCES REPORTED AS WEIGHT PERCENT OXIDES
TRACE ELEMENT ABUNDANCES REPORTED IN PARTS PER MILLION

Table 8 (Continued). AAS tephra data.

	SIO2	TIO2	AL203	FE203	FEO	MNO	MGO	CAO	NA2O	K2O	P2O5	BA	CO	CR	CU	NI	RB	SR	ZN
BELKNAP VOLCANO (N=3):																			
AVERAGE	51.19	1.46	18.54	3.66	5.49	0.16	6.65	8.33	3.42	0.75	0.33	249.0	34.3	115.3	58.7	100.0	12.0	528.0	78.3
S.D.	1.00	0.12	0.91	0.09	0.37	0.01	0.84	0.21	0.09	0.04	0.08	54.4	4.6	19.2	3.8	46.7	0.8	43.6	1.2
CVZ	1.9	8.3	4.9	2.5	6.7	5.7	12.6	2.5	2.5	5.3	23.5	21.9	13.5	16.7	6.4	46.7	6.8	8.3	1.6
HIGH	52.41	1.62	19.54	3.78	5.85	0.17	7.83	8.62	3.54	0.81	0.42	326	39	138	64	160	13	585	80
LOW	49.97	1.32	17.34	3.57	4.99	0.15	5.97	8.16	3.35	0.71	0.23	210	28	91	56	46	11	479	77
RANGE	2.44	0.30	2.21	0.22	0.87	0.02	1.86	0.46	0.19	0.09	0.19	116	11	47	8	114	2	106	3
COLLIER CONE (N=4):																			
AVERAGE	55.56	0.88	18.65	3.00	4.08	0.13	5.20	7.66	3.81	0.86	0.16	238.3	30.5	62.5	50.5	114.0	16.5	504.0	70.0
S.D.	0.69	0.13	0.89	0.66	0.35	0.01	0.82	0.64	0.14	0.06	0.02	6.9	2.1	7.0	2.7	28.0	2.1	24.1	5.4
CVZ	1.2	14.4	4.8	21.9	8.7	8.3	15.8	8.3	3.6	6.9	15.7	2.9	6.8	11.2	5.3	24.6	12.5	4.8	7.7
HIGH	56.25	1.05	19.60	4.10	4.44	0.14	6.40	8.42	3.90	0.94	0.19	244	33	74	54	160	18	533	79
LOW	54.77	0.70	17.39	2.37	3.56	0.11	4.43	6.67	3.57	0.79	0.12	227	28	55	47	85	13	473	65
RANGE	1.49	0.36	2.21	1.73	0.88	0.03	1.98	1.74	0.33	0.15	0.07	17	5	19	7	75	5	60	14
DEVILS HILL DOME CHAIN (N=4):																			
AVERAGE	72.33	0.36	14.61	0.82	1.50	0.06	0.60	2.04	4.55	3.00	0.13	750.3	-	15.3	8.8	1.9	66.8	214.3	40.3
S.D.	0.17	0.01	0.12	0.10	0.10	.00	0.04	0.04	0.06	0.04	0.01	10.0	-	1.6	0.8	1.4	2.9	6.7	2.0
CVZ	0.2	3.4	0.8	11.8	6.4	0.8	7.1	2.0	1.2	1.2	10.9	1.3	-	10.7	9.5	74.6	4.3	3.1	5.1
HIGH	72.47	0.38	14.74	0.93	1.66	0.06	0.65	2.11	4.62	3.04	0.15	756	-	18	10	4	71	225	42
LOW	72.06	0.35	14.49	0.67	1.43	0.06	0.54	1.99	4.47	2.96	0.11	733	-	14	8	0	63	207	37
RANGE	0.41	0.03	0.26	0.26	0.23	.00	0.11	0.11	0.15	0.08	0.04	23	-	4	2	4	8	18	5
FORKED BUTTE (N=4):																			
AVERAGE	50.25	1.21	20.96	4.27	4.99	0.16	6.59	7.39	3.17	0.63	0.39	199.8	39.0	186.0	50.0	140.5	10.3	552.0	74.0
S.D.	0.66	0.06	0.71	0.77	0.26	0.01	0.58	0.32	0.13	0.06	0.03	29.2	2.3	32.9	4.6	21.7	0.8	16.8	3.1
CVZ	1.3	5.1	3.4	17.9	5.2	5.2	8.8	4.4	4.2	9.3	7.6	14.6	6.0	17.7	9.2	15.5	8.1	3.0	4.2
HIGH	51.00	1.25	22.03	5.39	5.41	0.17	7.30	7.82	3.38	0.67	0.42	250	43	226	57	164	11	574	79
LOW	49.49	1.10	20.03	3.39	4.70	0.15	5.82	6.92	3.05	0.53	0.36	177	37	141	45	112	9	530	71
RANGE	1.51	0.15	1.99	2.00	0.71	0.02	1.48	0.90	0.33	0.15	0.06	73	6	85	12	52	2	44	8
LITTLE NASH CRATER (N=4):																			
AVERAGE	51.45	1.29	18.37	5.71	3.42	0.15	6.46	8.08	3.86	0.81	0.41	333.8	37.8	109.5	65.8	141.0	11.5	717.0	92.5
S.D.	0.57	0.08	0.57	1.33	1.62	0.01	0.69	0.19	0.38	0.07	0.02	24.4	2.0	4.0	7.6	17.7	0.5	24.4	3.5
CVZ	1.1	5.8	3.1	23.3	47.4	5.9	10.7	2.3	9.8	8.7	6.1	7.3	5.4	3.7	11.6	12.6	4.3	3.4	3.8
HIGH	52.06	1.38	19.28	7.25	5.22	0.16	7.44	8.33	4.34	0.88	0.45	360	41	116	78	171	12	757	96
LOW	50.55	1.19	17.73	4.15	1.58	0.14	5.73	7.87	3.42	0.71	0.39	294	36	105	58	125	11	695	87
RANGE	1.51	0.19	1.55	3.10	3.64	0.02	1.71	0.46	0.92	0.17	0.06	66	5	11	20	46	1	62	9
LOST LAKE GROUP (N=4):																			
AVERAGE	49.50	1.40	17.07	3.54	6.17	0.16	9.60	8.42	3.10	0.70	0.35	286.3	45.3	166.5	65.0	210.8	10.5	656.8	81.3
S.D.	0.85	0.16	0.89	0.46	0.15	0.01	0.43	0.22	0.16	0.08	0.01	8.5	3.7	5.0	3.2	21.4	1.1	29.5	2.5
CVZ	1.7	11.3	5.2	13.0	2.5	4.1	4.5	2.7	5.3	12.1	2.2	3.0	8.2	3.0	5.0	10.2	10.6	4.5	3.1
HIGH	50.15	1.60	18.42	4.24	6.39	0.17	10.17	8.63	3.22	0.79	0.36	294	48	175	70	238	12	701	83
LOW	48.04	1.19	16.15	2.97	6.00	0.15	8.95	8.05	2.82	0.58	0.34	272	39	162	61	181	9	624	77
RANGE	2.11	0.41	2.28	1.26	0.39	0.02	1.22	0.58	0.40	0.20	0.02	22	9	13	9	57	3	77	6
MAZAMA (N=4):																			
AVERAGE	66.95	0.57	18.69	1.95	1.45	0.07	0.78	2.44	4.61	2.19	0.30	608.0	5.2	16.0	18.3	6.1	38.5	345.3	48.8
S.D.	1.83	0.03	2.34	0.31	0.36	0.01	0.12	0.17	0.30	0.17	0.07	67.0	2.0	1.7	2.2	1.5	5.2	51.9	1.9
CVZ	2.7	5.1	12.5	15.9	25.1	7.5	15.9	6.8	6.6	7.5	24.0	11.0	38.7	10.8	11.9	25.2	13.6	15.0	3.9
HIGH	69.00	0.61	22.33	2.30	2.07	0.08	0.90	2.60	5.09	2.46	0.41	698	8	19	21	7	47	404	51
LOW	63.99	0.54	15.78	1.45	1.17	0.06	0.62	2.16	4.28	2.01	0.20	512	3	15	15	4	33	266	46
RANGE	5.00	0.07	6.55	0.85	0.91	0.01	0.28	0.44	0.81	0.45	0.20	186	5	4	6	4	14	138	5
NASH CRATER (N=3):																			
AVERAGE	53.13	1.26	18.12	4.10	4.83	0.14	5.74	8.02	3.53	0.75	0.39	286.3	33.3	106.7	54.3	132.3	11.0	712.7	90.7
S.D.	1.25	0.08	0.22	0.87	0.81	0.01	0.83	0.15	0.13	0.02	0.02	13.2	5.2	1.2	6.6	35.9	0.0	30.3	6.9
CVZ	2.4	6.1	1.2	21.2	16.8	8.6	14.4	1.9	3.6	2.4	4.2	4.6	15.7	1.2	12.1	27.2	0.0	4.2	7.7
HIGH	54.82	1.36	18.43	5.31	5.41	0.15	6.37	8.18	3.66	0.77	0.41	305	38	108	63	172	11	755	97
LOW	51.84	1.19	17.95	3.30	3.68	0.12	4.57	7.82	3.36	0.73	0.37	277	26	105	47	85	11	686	81
RANGE	2.98	0.18	0.47	2.01	1.72	0.03	1.81	0.37	0.30	0.04	0.04	28	12	3	16	87	0	69	16
ROCK MESA (N=4):																			
AVERAGE	72.77	0.35	14.41	0.77	1.42	0.05	0.55	1.95	4.39	3.18	0.15	753.3	1.2	15.5	8.5	3.7	73.0	204.0	40.5
S.D.	0.43	0.03	0.25	0.05	0.05	.00	0.05	0.13	0.11	0.09	0.01	4.8	0.1	0.5	0.5	1.3	2.5	12.4	1.7
CVZ	0.6	7.5	1.7	6.8	3.5	8.2	8.5	6.4	2.5	2.8	9.2	0.6	10.6	3.2	5.9	35.6	3.5	6.1	4.1
HIGH	73.25	0.38	14.77	0.84	1.51	0.06	0.62	2.14	4.57	3.26	0.16	756	1	16	9	6	76	222	42
LOW	72.15	0.31	14.12	0.69	1.39	0.05	0.50	1.82	4.28	3.03	0.13	745	1	15	8	2	70	187	38
RANGE	1.10	0.07	0.65	0.14	0.12	0.01	0.12	0.32	0.29	0.23	0.03	11	0	1	1	4	6	35	4
SAND MOUNTAIN (N=4):																			
AVERAGE	51.31	1.29	18.29	3.61	5.07	0.15	6.85	8.92	3.39	0.75	0.36	312.0	38.8	126.5	57.8	113.8	10.8	870.5	89.5
S.D.	0.87	0.20	0.53	0.12	0.30	0.01	0.74	0.32	0.16	0.04	0.01	35.6	2.5	18.6	4.3	20.3	0.4	51.9	14.8
CVZ	1.7	15.4	2.9	3.5	5.8	5.0	10.8	3.6	4.8	5.4	2.0	11.4	6.4	14.7	7.5	17.9	4.0	6.0	16.5
HIGH	52.74	1.59	18.74	3.82	5.44	0.16	7.63	9.39	3.66	0.80	0.37	366	41	148	65	134	11	909	115
LOW	50.42	1.04	17.43	3.49	4.62	0.14	5.65	8.61	3.22	0.69	0.35	266	35	97	54	83	10	781	79
RANGE	2.32	0.55	1.31	0.32	0.82	0.02	1.98	0.78	0.44	0.11	0.02	100	6	51	11	51	1	128	36
SOUTH CINDER PEAK (N=4):																			
AVERAGE	49.62	1.59	20.31	4.88	5.16	0.18	6.62	7.41	3.14	0.67	0.41	256.5	38.3	133.3	57.5	136.5	11.3	553.8	87.3
S.D.	0.56	0.04	0.61	0.14	0.09	0.01	0.10	0.03	0.09	0.01	0.02	13.5	2.2	6.2	2.6	8.4	0.5	25.2	9.8
CVZ	1.1	2.5	-3.0	2.8	1.7	3.4	1.5	0.4	3.0	1.7	5.1	5.3	5.6	4.6	4.6	6.1	4.2	4.5	11.2
HIGH	50.19	1.66	21.13	5.08	5.29	0.18	6.83	7.56	3.30	0.69	0.44	277	42	140	60	150	12	596	103
LOW	48.63	1.55	19.72	4.63	5.10	0.17	6.30	7.07	3.03	0.66	0.39	244	36	126	54	122	11	511	76
RANGE	1.56	0.11	1.40	0.46	0.19	0.01	0.53	0.50	0.26	0.03	0.05	33	6	14	6	28	1	85	27
YAPOAH CRATER (N=4):																			
AVERAGE	55.34	1.00	18.67	2.85	4.50	0.14	5.18	7.39	3.81	0.92	0.22	269.5	30.5	64.5	56.8	82.8	17.5	518.8	70.5
S.D.	0.23	0.06	0.39	0.39	0.19	0.01	0.15	0.17	0.07	0.04	0.05	11.8	0.5	9.2	4.5	27.6	1.1	7.6	2.1
CVZ	0.4	5.7	2.1	13.6	4.2	8.0	2.9	2.3	1.8	4.2	24.8	4.4	1.6	14.3	7.9	33.3	6.4	1.5	2.9
HIGH	55.54	1.08	19.21	3.34	4.77	0.15	5.35	7.63	3.88	0.95	0.28	283	31	78	64	110	19	530	73
LOW	54.96	0.92	18.11	2.41	4.29	0.12	4.95	7.22	3.72	0.86	0.14	255	30	55	53	41	16	510	68
RANGE	0.58	0.16	1.10	0.93	0.48	0.03	0.40	0.40	0.16	0.10	0.14	28	1	23	11	69	3	20	5

Table 9. Summary statistics for AAS data.

well documented. The Forked Butte and South Cinder Peak samples often formed discrete combined clusters and were united for the graphical analysis. The Collier Cone and Yapoah Crater samples were analyzed as a single unit for much the same reason. We also suspected, after analysis of aerial photographs and microscopic examination of the tephra, that the samples identified in the field as Yapoah Crater samples actually originated from the later eruptions of Collier Cone.

Scatterplots illustrating different pairs of major elements are presented in figure 24. These scatterplots were the most effective at distinguishing the different groups, though several other major element pairs were also useful. The Forked Butte/South Cinder Peak, Collier Cone/Yapoah Crater, and Lost Lake Group sources consistently fall into discrete clusters. The Sand Mountain, Little Nash Crater, and Belknap Crater sources, though they show obvious tendencies for intrasource clustering, typically form overlapping clusters when considered together. Some geographic patterning to the clusters is also evident. Sources from the northern part of the Willamette National Forest (Forked Butte and South Cinder Peak) form one group, sources (or, more likely, a single source) from the North Sister area (Collier Cone and Yapoah Crater) form a second group, and several of the sources from the Santiam Pass to Belknap Crater area (Little Nash Crater, Sand Mountain, Belknap Crater) constitute a third, somewhat more variable and complex group. The Lost Lake Group stands apart as the fourth geochemically separable cluster.

Cluster analysis of the sources (using only major element data) confirms the conclusions drawn from the graphical analysis (figure 26). The cluster analysis dendrogram correctly identifies the same four chemically-discrete source groups as does the graphical analysis.

The trace element composition of the basaltic tephra samples was also useful in visually discriminating several source groups (figure 25). The Collier Cone/Yapoah Crater group was clearly distinguishable from other sources. Tephra from the remaining sources also demonstrated compositional clustering, though the samples from Sand Mountain, the Lost Lake Group, and Little Nash Crater showed the most graphically identifiable clusters. The tendency towards geographical patterning of similar clusters is also evident, though not as pronounced as for clusters identified through their major element composition.

Cluster analysis results of the trace element composition of the basaltic ash sources once again mirrors the conclusions drawn from the graphical analysis of the source data (figure 26). The Collier Cone/Yapoah group is readily identifiable while the other sources show a tendency to form less sharply delineated clusters.

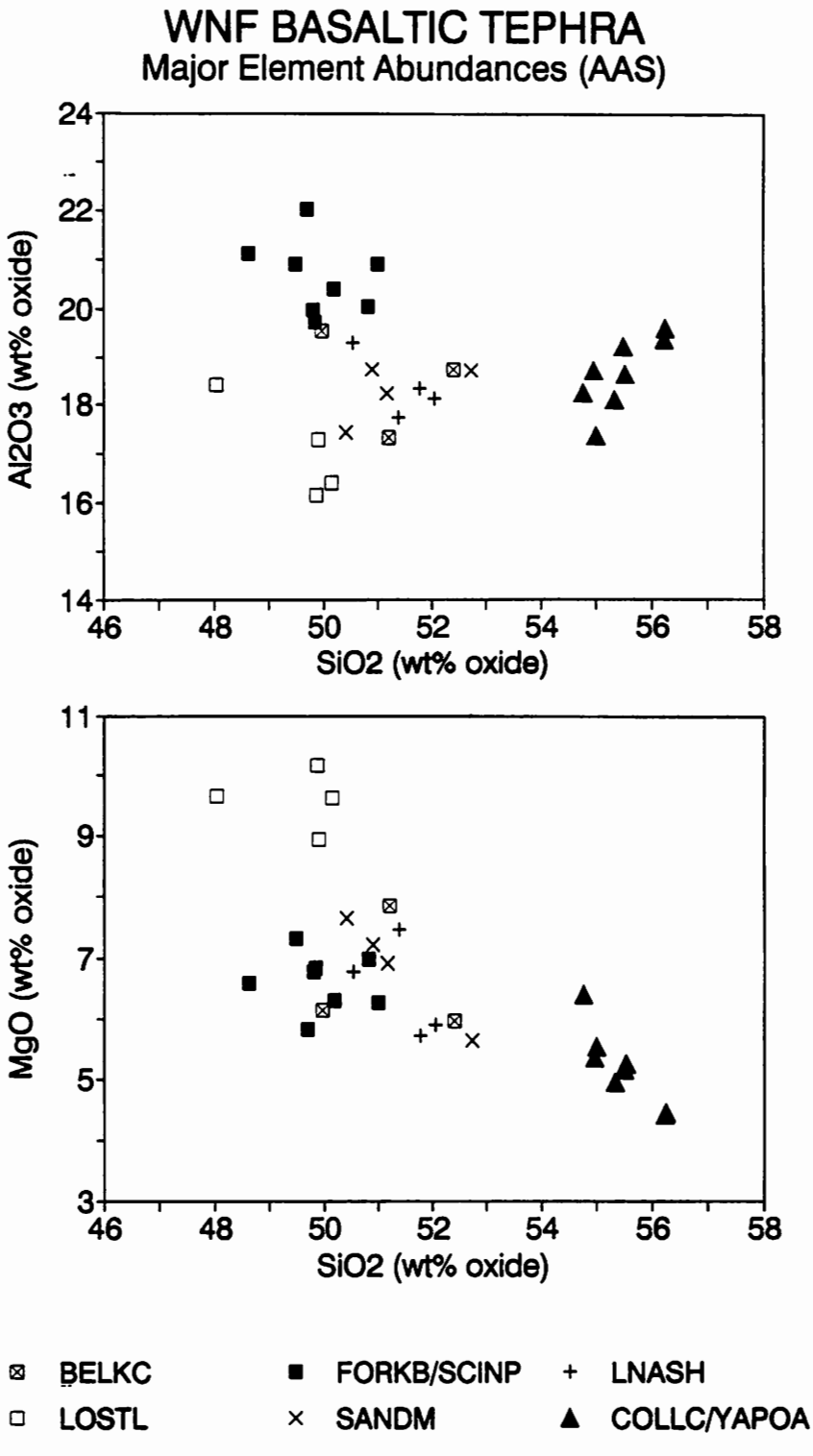

Figure 24. Al_2O_3 and MgO plotted versus SiO_2 for all basaltic tephra samples (AAS). Discrete clusters are identifiable for the Collier Cone/Yapoah Crater (COLLC/YAPOA), Forked Butte/South Cinder Peak (FORKB/SCINP), and Lost Lake Group (LOSTL) samples. Overlapping clusters are plotted for the remaining Belknap Crater (BELKC), Sand Mountain (SANDM), and Little Nash Crater (LNASH) sources.

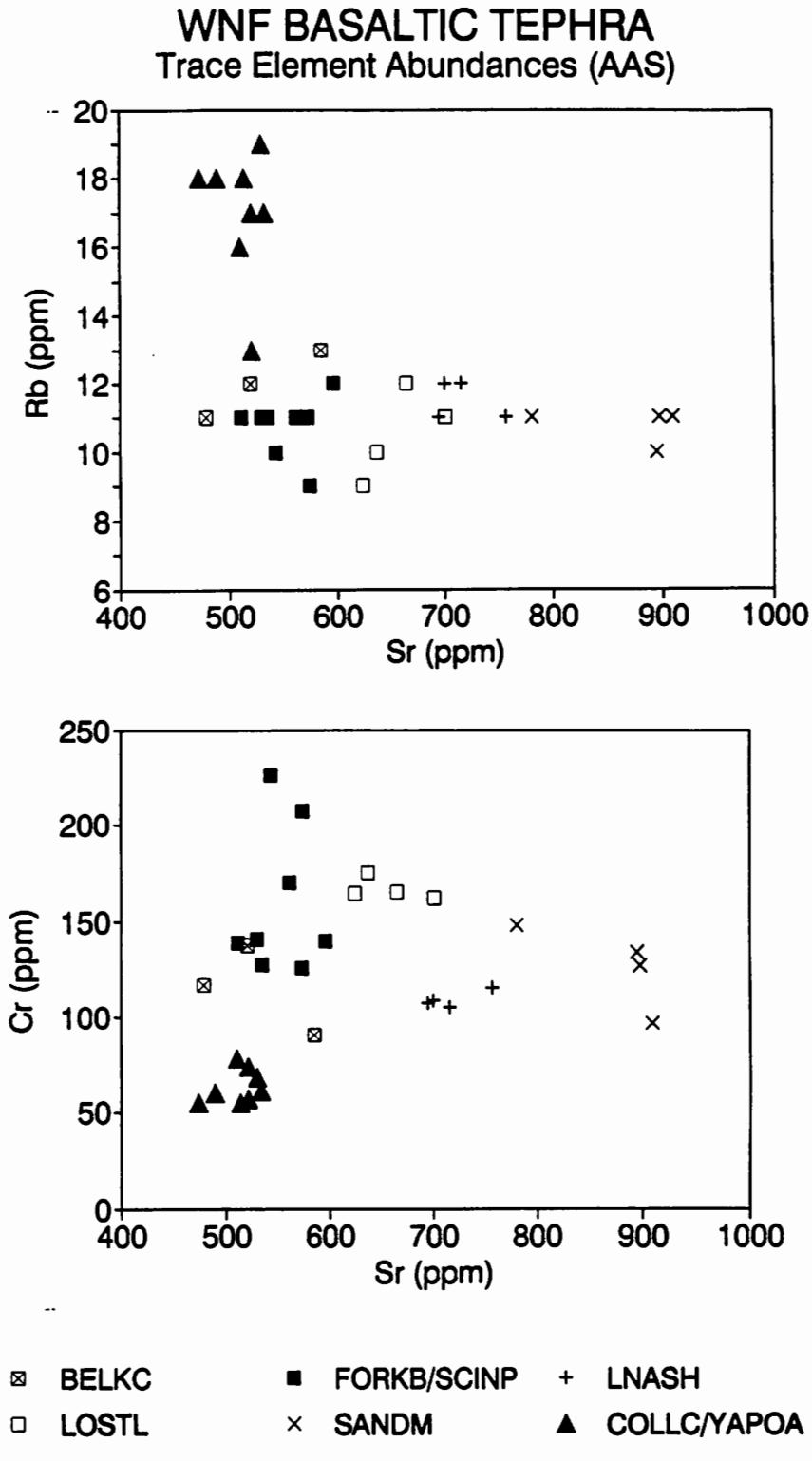

Figure 25. Rb and Cr plotted versus Sr for basaltic tephra samples (AAS). The Yapoah Crater/Collier Cone and Sand Mountain samples are fairly clearly distinguished with these trace elements pairs.

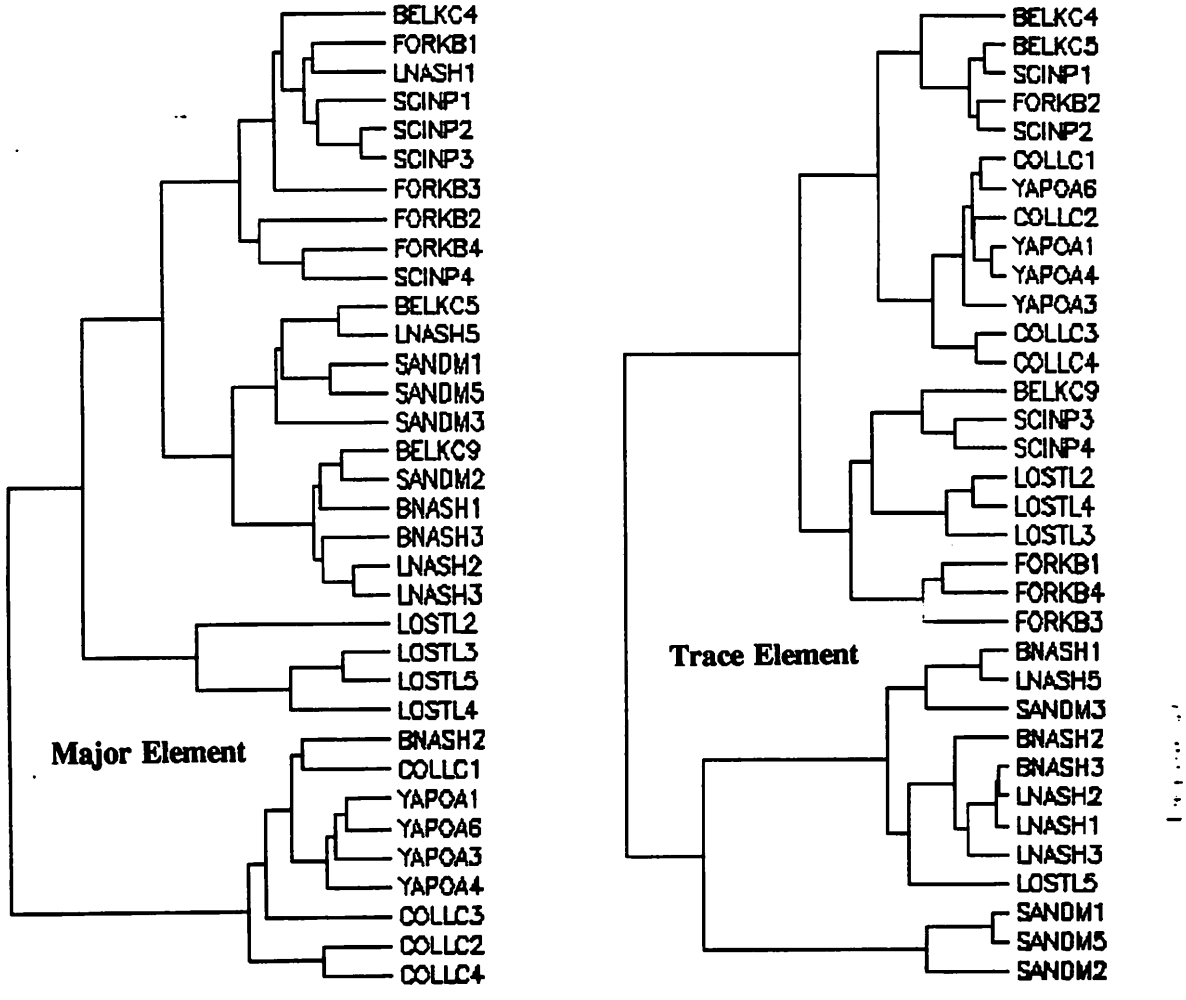

Figure 26. Dendrograms showing results of cluster analysis of basaltic tephra classified with major and trace elements. Major elements used for cluster analysis were SiO_2, TiO_2, Al_2O_3, MgO, CaO, Na_2O); trace elements used were Co, Cr, Cu, Rb, Sr, Zn. Groups identified on the basis of their major and trace element composition are very similar to those identified with scatterplots.

Silicic Tephra Clusters

AAS characterization of the major sources of silicic tephra found in the Willamette National Forest was quite productive. Both the major and trace element composition of pumice lapilli from Mount Mazama, Rock Mesa, and the Devils Hill chain of domes can be used to distinguish between the two major source areas (figures 27 and 28). AAS characterization of the *bulk samples* of the Mazama paleosols, however, was quite unsuccessful. These samples, though they originated from Mount Mazama, fell completely outside the range of variation of the analyzed Mazama lapilli (figures 27 and 28).

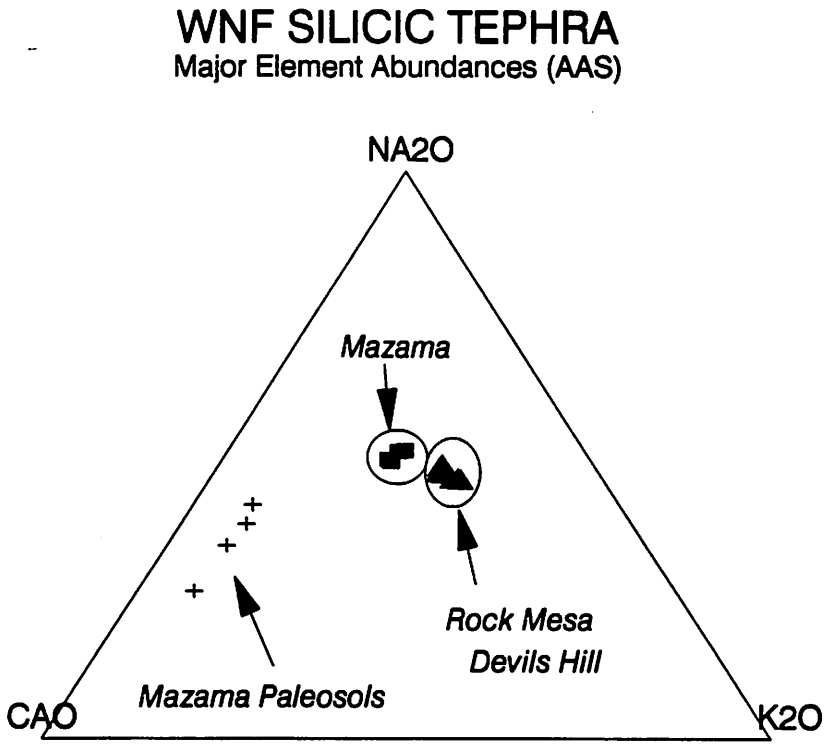

Figure 27. Ternary plot of Na_2O, CaO, and K_2O for all silicic tephra samples (AAS). The Mazama paleosols clearly do not visually correlate with the Mazama source samples, although they all share a common source.

Major element abundances were quite effective in distinguishing the Mazama and South Sister tephra sources. The ternary plots pictured in figures 27 and 28 are typical of the different scatterplots and ternary diagrams examined during the graphical analysis of the tephra. The two South Sister sources, while easily separable from the Mazama source, are not distinguishable from each. This was expected, as the compositional similarities of pumice from the two vents has been previously documented (Scott, 1987). The Mazama paleosols are apparent in figure 27 as a third, distinct cluster.

The results of the graphical analysis of the major element groupings of the silicic tephra are corroborated by cluster analysis of the major element data. The three groups are clearly identified in the dendrogram in figure 29.

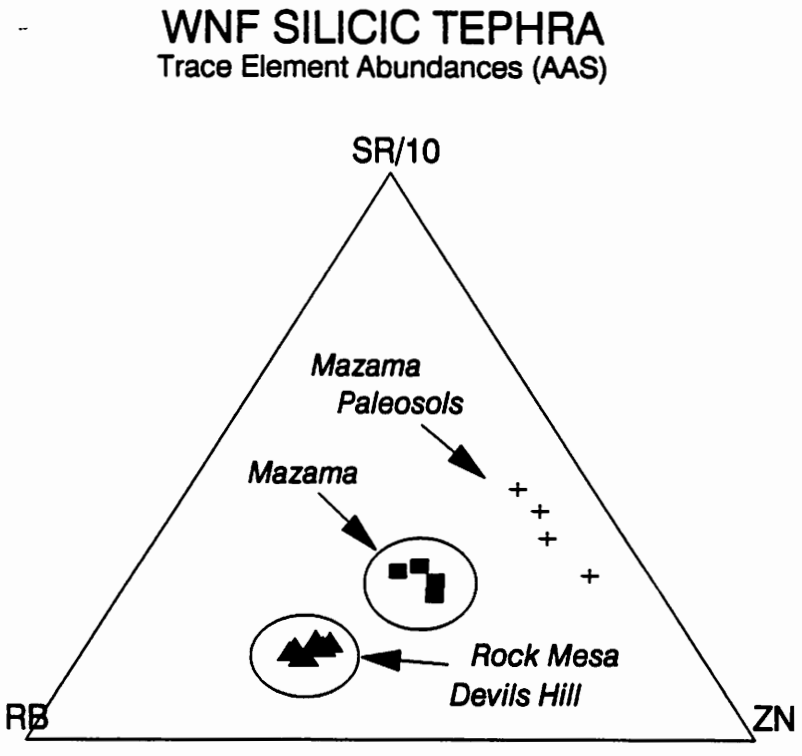

Figure 28. Ternary plot of Sr, Rb, and Zn for silicic tephra samples (AAS). The results of trace element analysis of the ash yielded similar results as major element analysis.

The trace element composition of the silicic tephra samples yielded clusters similar to those produced by the major element analysis of the tephra (figure 28). The Mazama and South Sister sources are easily distinguished from one another, although the two South Sister sources cannot be distinguished from one another. Once again, the trace element values of the Mazama paleosols fall well out of the range of the Mazama source samples. The composition of the paleosols form a relatively distinct cluster, however, suggesting that similar processes might be responsible for the failure of AAS data to chemically identify the Mazama origin of the secondary samples.

Cluster analysis of the trace element values of the silicic tephra samples again verified the graphical analysis of the data (figure 29). Mazama and South Sister sources are classified as two separate clusters while the Mazama paleosols are classified as a third group.

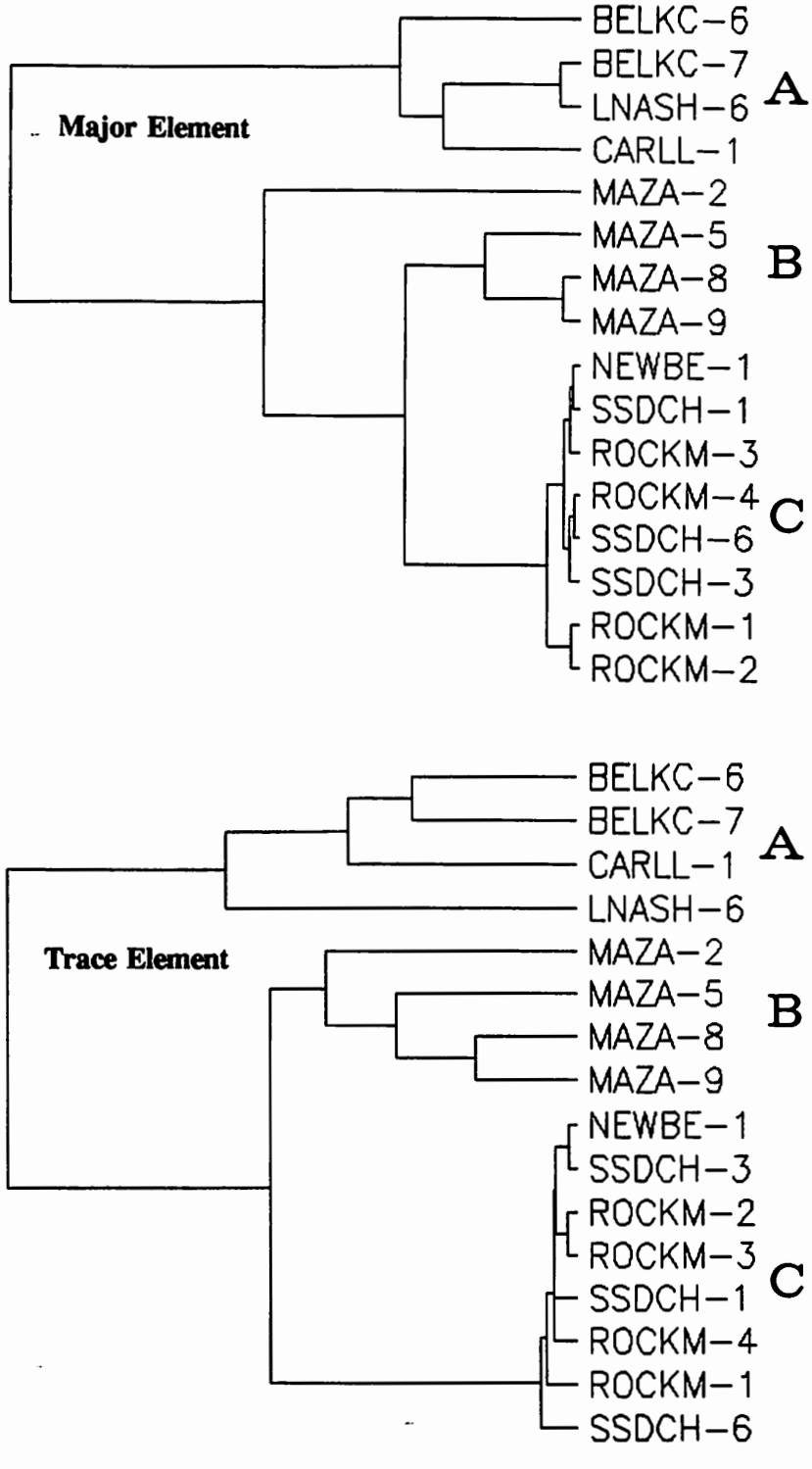

Figure 29. Dendrogram results of cluster analysis of silicic tephra classified by major and trace element abundances. Major elements used for cluster analysis were SiO_2, TiO_2, Al_2O_3, MnO, CaO, K_2O); trace elements used were Ba, Cu, Rb, Sr, Zn. The two major source areas are correctly classified and are distinguished from the Mazama paleosols.

We suspect that the failure of AAS analysis of the bulk samples of the Mazama paleosols is due either to contamination of the samples or to post-depositional diagenetic alteration of the tephra. The clustering of the four Mazama paleosols that is evident in the preceding ternary diagrams and dendrograms suggests that a similar process is affecting the samples at all four sampling locations. Possible major sources of contamination that could affect the chemical composition of the paleosols include contributions from organic matter and from overlying or underlying stratigraphic units (including basaltic tephra). Weathering of the tephra after deposition could also be responsible for chemical changes in the bulk composition of the tephra. The small pyroclast size of the ash at the four sample locations would leave the paleosols much more susceptible to the effects of weathering than the larger pumice lapilli used to characterize the Mazama eruptions. Studies of obsidian-perlite pairs indicate that post-depositional chemical changes due to the weathering and hydration of silicic volcanic glasses often lead to a loss of Na, an increase of K, and variable depletion or enrichment of Sr and Ba (Zielinski et al., 1977; Fisher and Schmincke, 1984:327-345).

When the major and trace element composition of the Mazama paleosols and the Mazama pumice lapilli are compared (figure 30), several patterns of enrichment and depletion are evident. The paleosols are high in MnO, Cao, Cu, Rb, and Zn relative to the unweathered Mazama lapilli and low in SiO_2, Na_2O, K_2O, Ba, and Rb. The regularities in compositional variation between the relatively unweathered large lapilli and the weathered Mazama soils lead us to believe post-depositional diagenetic alteration is responsible, at least in part, for the differences in chemical composition between the primary and secondary Mazama samples. We suggest that further AAS studies of Mazama paleosols should include more detailed pretreatment than we used in this investigation. Possible pretreatment methods are discussed by Borchardt (1969:157-159) and Steen-McIntyre (1977:64-78).

EPMA

Silicic tephra samples selected for electron microprobe analysis included three samples of Mazama paleosols from known geologic contexts at scattered locations within the Willamette National Forest (BELKC-7, CARLL-1, LNASH-6), three pumice lapilli from the Mazama climactic eruptions (MAZA-5, MAZA-8, MAZA-9), two pumice lapilli from the Rock Mesa eruptions (ROCKM-1 and ROCKM-4), one pumice lapillus from the Devils Hill chain of domes, and a pumice soil from the Woodduck Site Complex (WDUCK-1). Because of the small number of samples used for the EPMA studies, any conclusions drawn here must be considered as tentative.

The results of these preliminary EPMA studies indicate that the major element data collected during the analysis of individual silicic glass shards in the samples is very adequate for discriminating, characterizing and correlating the Mazama source, both of the South Sister sources, the Mazama Paleosols, and the archaeological pumice soil.

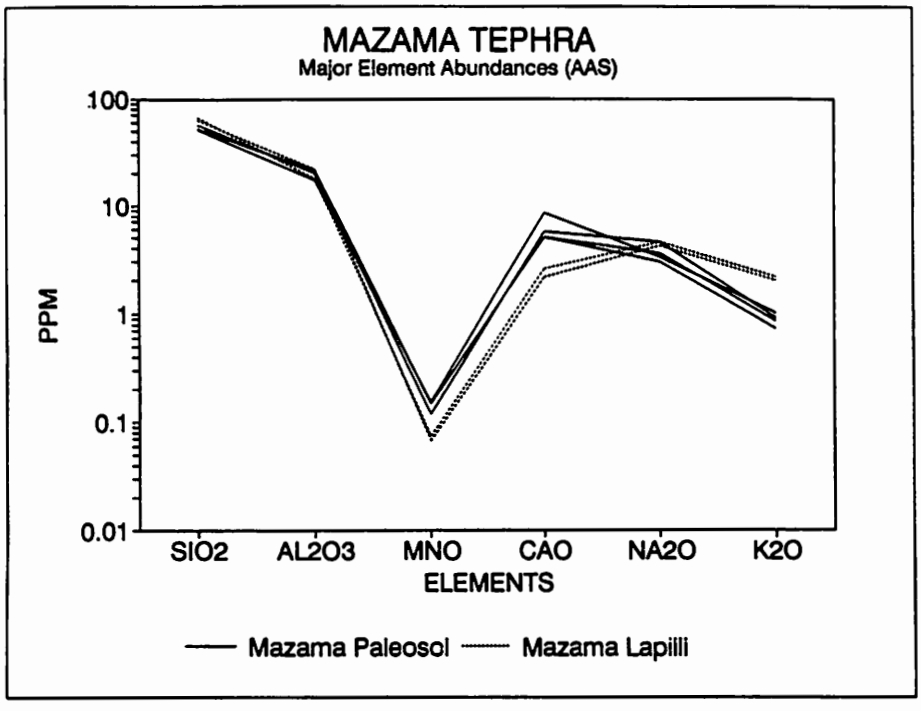

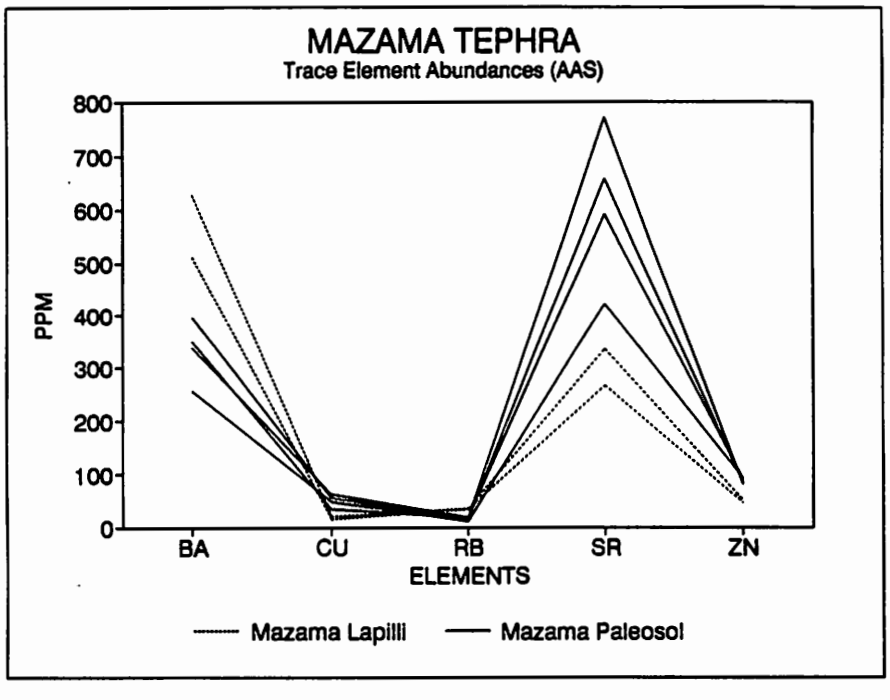

Figure 30. Spider plots of major and trace element abundances for primary and secondary Mazama tephra samples (AAS). These plots indicate that some elements in the Mazama paleosols are systematically enriched and depleted relative to the Mazama source samples.

Sample #	BELKC-7	CARLL-1	LNASH-6	MAZA-5	MAZA-8	MAZA-9	NEWBE-1	ROCKM-1	ROCKM-4	WDUCK-1
SiO2	74.16	73.33	73.87	74.27	74.08	74.66	71.05	77.40	77.05	73.87
TiO2	0.41	0.45	0.41	0.40	0.38	0.41	0.15	0.18	0.26	0.42
Al2O3	14.63	14.98	14.81	14.47	14.72	14.76	16.96	12.83	13.05	14.82
MgO	0.45	0.58	0.50	0.45	0.47	0.45	0.15	0.17	0.19	0.47
CaO	1.54	1.79	1.73	1.53	1.59	1.63	2.65	0.93	0.91	1.61
MnO	0.07	0.07	0.06	0.06	0.05	0.06	0.04	0.03	0.04	0.06
FeO	1.90	2.17	1.94	1.90	1.97	1.90	1.07	1.19	1.32	2.05
Na2O	3.87	3.92	3.37	4.09	3.92	3.26	5.43	3.38	3.40	3.87
K2O	2.97	2.71	3.30	2.83	2.83	2.87	2.50	3.89	3.78	2.82
Total	100.00	100.00	100.00	100.00	100.00	100.00	100.00	100.00	100.00	100.00

Major element abundances reported as weight percent oxides
Each sample value represents the average of 6 analysis points normalized to 100 percent

Table 10. Results of electron probe analysis. See Appendix 3 for complete data.

When all three primary sources of silicic tephra are compared (figure 31), each is found to exhibit a distinctive major element profile. The spider plot not only points out compositional dissimilarities among the samples, but allows for easy visual identification of elements that may prove useful in distinguishing among the sources. Cao, for example, appears to be useful in the separation of all three groups. Because of the y-axis log scale, however, this technique is most useful for examining elements with abundances of less than about 10 percent.

When the major element abundances of the Mazama source lapilli and the Mazama paleosols are compared in the spider diagrams of figure 32, their composition can be seen to be almost identical. Unlike the results of the previously described AAS characterization of Mazama paleosols, electron microprobe analysis of the tephra shards appears to be an excellent technique with which to characterize secondary silicic tephra deposits within the Willamette National Forest.

The differences between the two South Sister silicic tephra sources was not anticipated. Previous chemical studies had indicated that their chemical composition was very similar. Whether the major element differences between the two sources indicated in this study are real or are due to the very small sample size is not known. When the results of the analysis of the Woodduck Site Complex pumice are examined in scatterplots and compared with the Mazama and South Sister sources (figure 33), the Mazama origin of the small pumice pyroclasts found in the archaeological soil is readily apparent. This soil unit and any associated artifacts, if they shows no signs of mixing, must postdate the eruption of Mount Mazama.

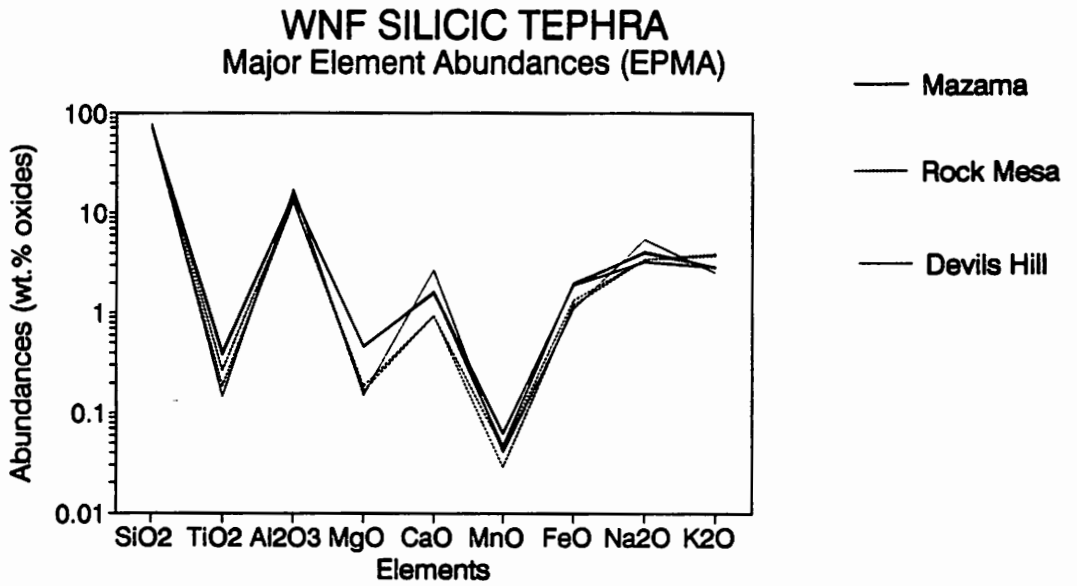

Figure 31. Spider plot comparing the major element composition of pumice lapilli from the Mazama, Rock Mesa, and Devils Hill sources of silicic tephra.

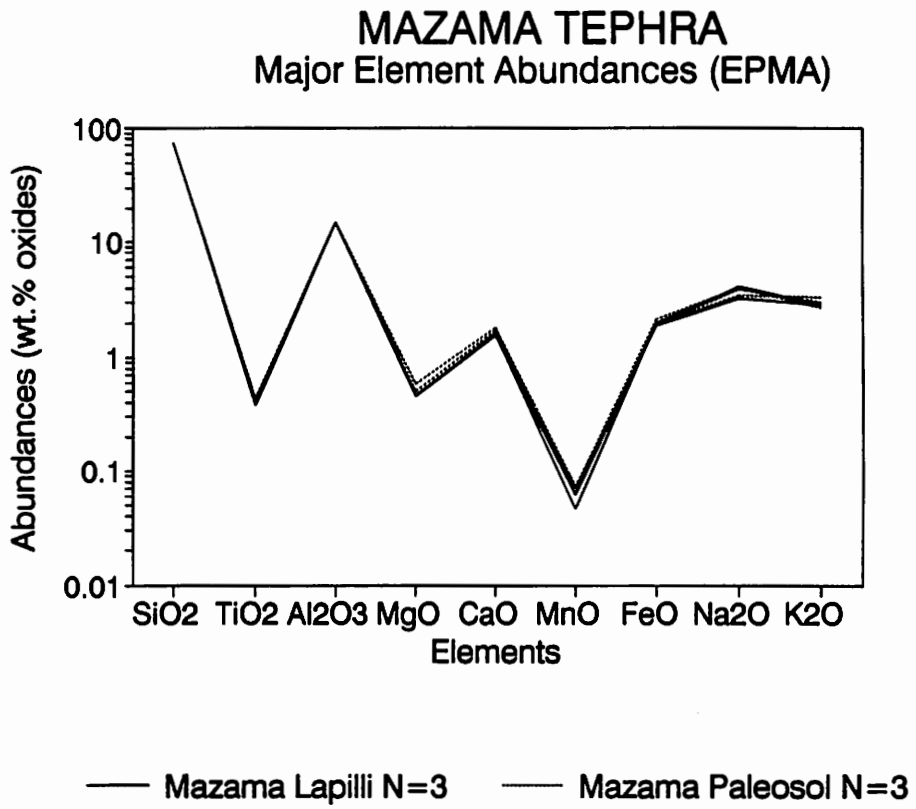

Figure 32. Spider plot comparing the major element composition (EPMA) of three pumice lapilli from Mount Mazama and three paleosols (BELKC-7, CARLL-1, LNASH-6) identified in the field as originating from the Mazama eruptions. The similarity in profiles visually illustrates the nearly identical composition of all six samples, confirming the Mazama climactic eruptions as the source of the paleosols.

The cluster analysis results, like the graphical analyses, easily discriminate among the different sources (figure 34). The secondary geologic and archaeological paleosols are classified with the Mazama source cluster, while the Rock Mesa and Devils Hill tephra sources each occupy their own distinct cluster.

The results of EPMA analyses of potential silicic tephra sources for Willamette National Forest pyroclastic deposits indicate the overall viability of the EPMA characterization method. The ability of the technique to sample individual glass tephra

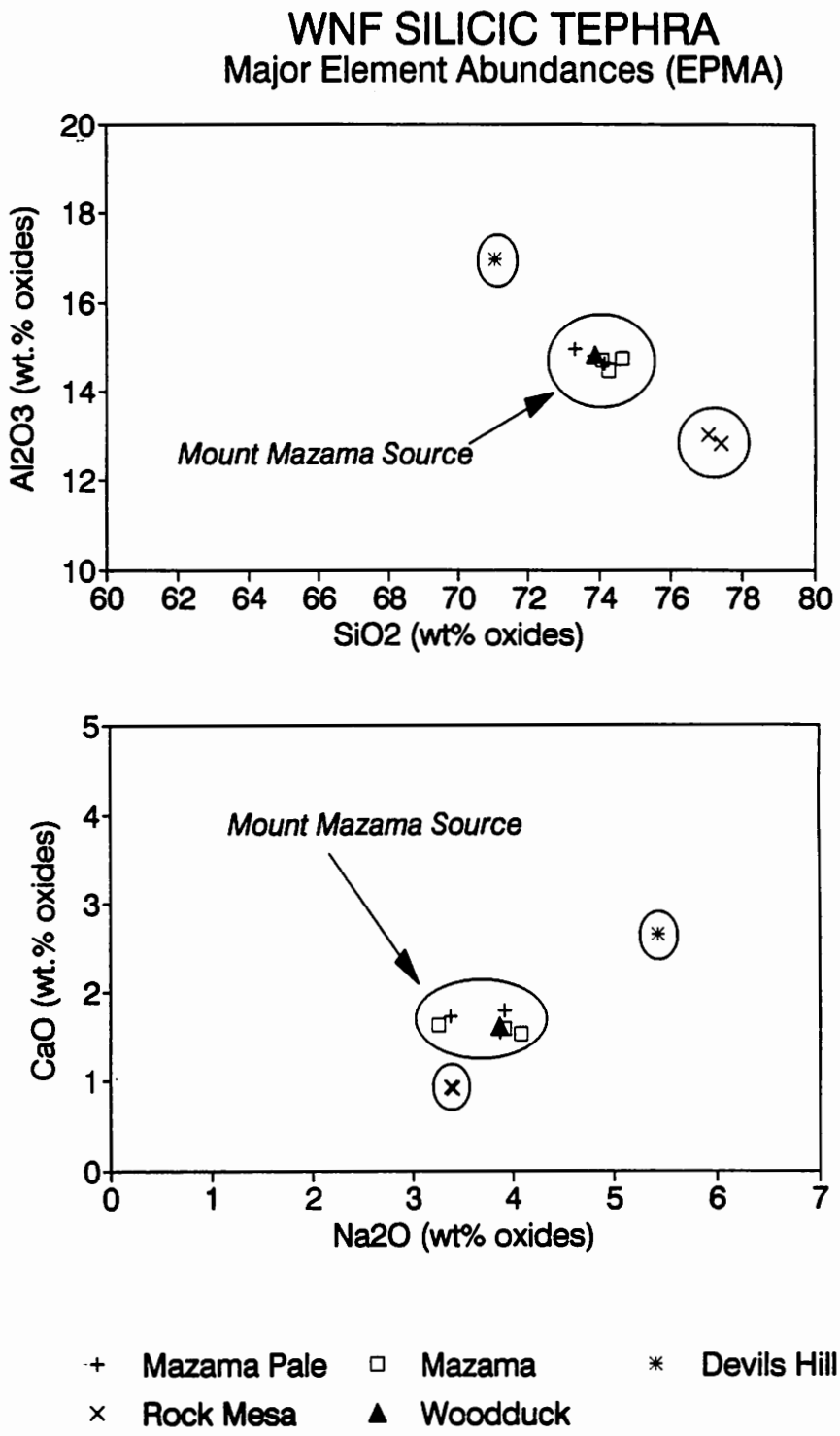

Figure 33. Scatterplots of EPMA major element pairs. The three sources of silicic tephra in the study area characterized with the electron microprobe are clearly distinguished in the scatterplot. The three Mazama paleosol samples (Mazama Pale in the scatterplot above) all fall within the range of the Mazama source samples as does the Woodduck Site Complex archaeological sample.

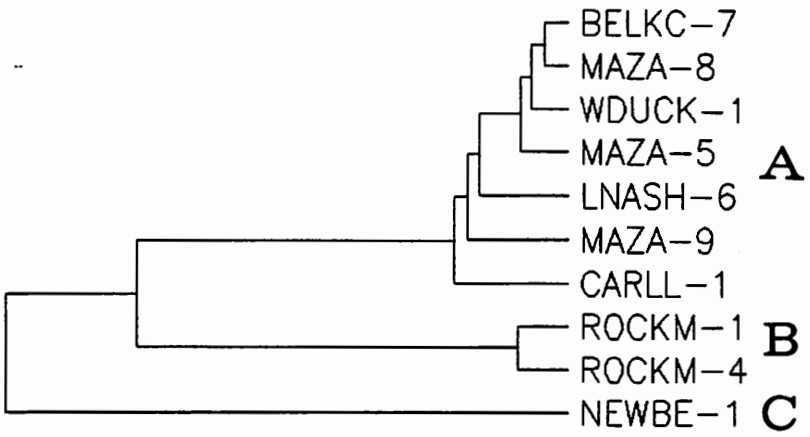

Figure 34. Dendrogram results of cluster analysis results of silicic tephra samples with EPMA data. Cluster analysis easily distinguished the three major silicic tephra sources and correctly identified the Mazama origin of the Mazama paleosols and the Woodduck Site soil. All nine major elements were included in the cluster analysis matrix. Cluster analysis methods of classification proved effective in the correlation of known sources and samples of unknown provenience and should prove useful in future EPMA studies in the study region.

shards in a soil matrix convincingly obviates the problems presented by bulk analyses of secondary tephra samples. The presence of only three probable sources of silicic tephra in the study region presents a relatively simple characterization problem that is effectively solved using the major element composition of the glass shards. Electron microprobe analysis of Mazama soils, while entailing more involved sample preparation techniques, is recommended as the technique of choice when dealing with either small fractions of silicic tephra in a soil matrix (such as the Woodduck Site sample) or samples with small pyroclast size (the remaining paleosols).

Conclusions: Geochemical Characterization

Results of AAS characterization of basaltic and silicic tephra showed varied degrees of success in delineating geochemically identifiable clusters. AAS was successful as a characterization technique when applied to individual samples of silicic pumice lapilli but was unsatisfactory when used with secondary deposits of paleosols composed of small pyroclastic materials. We suspect that the problems observed with bulk samples from these secondary deposits (those that might be found in many archaeological

contexts) stem from chemical changes related to weathering and to contamination. AAS analysis of basaltic tephra sources indicates that some geochemical clustering can be identified but that the clusters often overlap among sources. The Collier Cone/Yapoah Crater, Lost Lake Group, and Forked Butte/South Cinder Peak sources showed the most clearly delineated clustering. The other sources also demonstrated some chemical clustering, though they often tended to fall into overlapping groups. The range of chemical variation for the bulk sample analyses is simply too great to allow for the simple identification of basaltic tephra source clusters for all the analyzed sources. Identifiable clusters, though, appear to be somewhat related to geographic locality. It is likely that the limited areal distribution of ash from basaltic sources combined with the known chemical clustering can be used together to identify the sources of many deposits of basaltic pyroclastic materials. Even when the geochemical signature of the basaltic tephra may not prove definitive, the chemical data plus the geographic provenience may prove adequate. We suspect that further pretreatment of bulk samples of basaltic ash prior to analysis (e.g. separation of glassy pyroclasts from crystalline and organic components) would reduce the range of intraunit chemical variation and add to the utility of the method as a characterization tool.

The electron microprobe characterization of silicic tephra from the primary and secondary geological and archaeological deposits proved quite successful. The major element composition of individual glass tephra shards from primary and secondary location of Mazama ash correlated very well. The Rock Mesa and Devils Hill tephra sources could also be clearly differentiated from the Mazama tephra as well from each other. EPMA techniques were not used to characterize basaltic tephra sources in this preliminary study, though we suspect that microprobe analysis of glassy sideromelane and *tachylite* pyroclasts would yield the most usable geochemical data.

Cluster analysis methods proved quite adequate in classifying samples and should be a valuable correlational technique in future geochemical studies of volcanic tephra in the study area. The results of the cluster analyses were consistent with the conclusions drawn from graphical analyses of the major and trace element geochemical data and provided a rapid way to examine multidimensional arrays of geochemical data for groupings. When both known source data and data from unknown tephra sources are included in the same data set, cluster analysis techniques can be used to classify the samples, and by doing so, can be used to identify the geologic sources of secondary samples of volcanic ash. We recommend that cluster analysis of geochemical tephra data be used in conjunction with graphical analysis of the same data. It is also important that geochemical data used for cluster analysis be screened for elements that show high intersource variation and low intrasource variability. The coefficient of variation was used in this investigation for this purpose. By selecting elements which exhibit these two characteristics, multivariate statistical analyses of the data should prove much more reliable. These same elements will also prove most effective for graphical analysis for clustering.

So, which analytical method (AAS or EPMA) is the most effective for use by archaeologists concerned with tephrochronologic research at Willamette National Forest sites? The answer to this question depends on two factors, the pyroclast size and the chemical composition (silicic or basaltic) of the samples to be analyzed. Both analytical methods have clear strengths and weaknesses with regards to sample preparation complexity, turnaround time, cost, and analytical limits. AAS characterization of bulk silicic tephra samples should prove adequate for the characterization of clean pumice lapilli that can be easily isolated from archaeological deposits. In the field, this characterization method would prove most useful in the southern part of the Willamette National Forest where larger pumice lapilli are found. Pretreatment of bulk silicic tephra samples would probably extend the usefulness of the technique to secondary tephra units within Willamette National Forest boundaries. This added step, however, would negate a major advantage of using AAS as a characterization method, the ease of sample preparation. AAS characterization of bulk samples of basaltic ash can also be used, though the resolution of the method is somewhat limited.

EPMA characterization of silicic tephra should prove especially useful at sites where pyroclast size is small or where pyroclasts are found mixed in a matrix of volcanic glass, organic debris, and other material (such as at the Woodduck Site Complex). The low number of silicic tephra sources to be considered coupled with the ability of the method to analyze single isolated shards makes EPMA analysis the characterization technique of choice at many locations.

In practice, though, the chemical characterization of silicic and basaltic tephra should not be required for many, if not most, areas of the Willamette National Forest. The chemical methods of characterization described in this report, while they are compelling to the archaeologist in search of scientific site data, are unnecessary in most cases. These methods, while they offer powerful analytical tools for approaching tephrochronological problems, can easily create as many problems as they may solve (see Section IV for some examples). Once volcanic ash has been positively identified in a deposit in the Willamette National Forest, the geologic source of the ash is often determinable with straightforward geological field methods. The use of grain size parameters, for example, combined with a thorough knowledge of the distribution and chronology of tephragenic volcanic events, is often all that is needed to identify the geologic source of an archaeological tephra deposit. Geochemical characterization methods like those investigated here should only be used when less technical approaches have failed.

VI.
CONCLUSIONS AND RECOMMENDATIONS

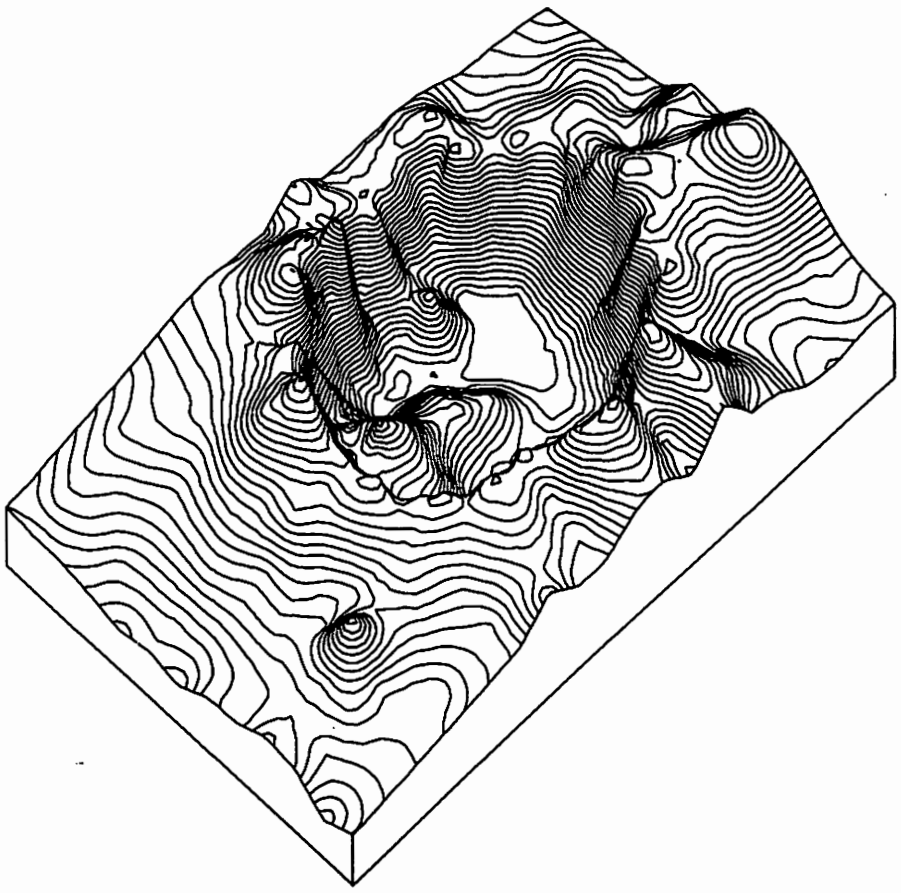

CONCLUSIONS AND RECOMMENDATIONS

CONCLUSIONS

Volcanic Tephra in the Willamette National Forest

1. Many deposits of *Holocene* volcanic *tephra* have been identified within and immediately adjacent to the Willamette National Forest in western Oregon. The ages of these *pyroclastic* deposits range throughout much of the last 10,000 years, from as recent as about 1,000 years ago to the beginning of the Holocene Epoch.

2. The most widespread and voluminous of the tephra deposits originated from Mount Mazama during a series of explosive eruptions about 6,845 to 7,010 *radiocarbon years* ago. Ash from the Mazama eruptions covered the entire present-day Willamette National Forest and is found today in many geologic and archaeological contexts throughout the region.

3. Explosive eruptions of *silicic* tephra also occurred about 2,000 ^{14}C years ago near South Sister volcano at Rock Mesa and the Devils Hill chain of domes. Small amounts of tephra from these eruptions are found today in the eastern central periphery of the Willamette National Forest, though none has been identified in any archaeological sites to date.

4. Mazama tephra has been identified in several central western Cascades archaeological sites, though the presence of the ash has undoubtedly gone unrecognized in numerous other archaeological investigations. The Mazama eruption was unquestionably the most archaeologically significant *tephragenic* event to affect the Willamette National Forest.

5. *Basaltic* tephra blankets are found associated with several Holocene *cinder cones* located within a few kilometers of the Cascade Crest. These deposits of basaltic ash are quite areally-restricted in comparison to the more widespread silicic ashes, though they have been identified in a few High Cascades archaeological sites.

6. The silicic ashfalls probably had only a limited impact on the human groups using the Cascades. Observations of ashfalls suggest that environmental damage caused by tephra falls is quite short-lived. Given that the most heavily affected, higher elevation areas of the Cascades were only seasonally utilized for non-essential food and lithic resources, it is likely that only a few years were required for compaction or erosion of ash and recovery of animal and vegetation populations. It seems unlikely that any significant disruption to critical subsistence scheduling occurred as a result of the eruptions. The major archaeological significance of the airfall deposits of silicic and basaltic ash appears to lie in their potential importance as chronologic tools.

7. It is a virtual certainty that many Willamette National Forest archaeological sites remain undiscovered and preserved today by their protective cover of volcanic ash. Serendipity may play an important role in the future discovery of these particular sites.

8. Many site locations are periodically reoccupied for long periods of time because of favorable environmental settings. The discovery of a culturally sterile stratum of volcanic ash, no matter how thick, during the excavation of a site should not be taken as an indication that the earliest site occupation level has been reached.

9. Volcanic ash from Mount Mazama and basaltic tephra sources have almost certainly gone unrecognized in excavations in many parts of the Willamette National Forest. When volcanic tephra has been identified in archaeological sites, it has often not been used as a temporal marker and the relationship of the tephra to artifactual remains is often only sketchily-described. We attribute these problems to a lack of familiarity by archaeologists with *tephrochronologic* methods and with the geographic distribution of potential Holocene sources of volcanic ash in the Willamette National Forest.

Characterization Studies

1. Atomic absorption spectrophotometry (AAS) studies of 50 basaltic and silicic tephra samples from 12 geologic sources resulted in varied degrees of success. Low cost, ease of sample preparation, and rapid turnaround time were important criteria in selecting AAS as the primary *characterization* method for this study.

2. *Major* and *trace* element abundances determined by AAS easily distinguished between silicic and basaltic tephra sources, as expected, as well as between the two major silicic source areas. AAS characterization studies of Mazama *paleosols* from several locations were less successful - these paleosols could not be clearly correlated with the Mazama eruptions, even though their geologic context verified Crater Lake as the source of the ash.

3. In locations where individual pumice lapillus are available for analysis, AAS analysis should prove to be an effective characterization technique. The chemical characterization of paleosols or fine-grained ash deposits should be reserved for other analytical methods.

4. AAS characterization of basaltic tephra deposits showed some promise, although the chemical clustering of different sources was not as marked as for the silicic tephra sources. The chemical characterization of basaltic tephra deposits, when combined with a knowledge of the distribution of basaltic tephra sources, may be useful in identifying the geologic source of basaltic tephra in most locations.

5. Electron probe microanalysis (EPMA) of a subset of 10 silicic tephra samples was used to evaluate the effectiveness of this method for Willamette National Forest tephra studies. EPMA, while being more expensive, requiring more elaborate sample preparation, and lacking in analytical precision for the trace elements, was of interest because of the small sample size required for analysis.

6. Major element abundances determined by EPMA were used to characterize pumice lapilli from three geologic sources, paleosols from three secondary geologic contexts, and a paleosol from the Woodduck Site near Mount Jefferson. Visual and statistical analysis of the major element data from this small sample showed that all three sources can be easily distinguished from one another. Additionally, the suspected Mazama paleosols from the geologic and archaeological contexts were clearly correlated with the Mazama source.

7. EPMA characterization of silicic tephra should prove especially useful at sites where pyroclast size is small or where small pyroclasts are found mixed with other materials (such as at the Woodduck Site Complex). The low number of silicic sources to be considered combined with the ability of the method to analyze single isolated shards makes EPMA analysis the characterization technique of choice at many locations.

8. Graphical comparison of major and trace element abundances indicates that considerable variation is found in literature values for volcanic tephra originating from Mount Mazama. Because of this variation in analytical results, interlaboratory or intermethod comparison of geochemical data should be attempted only after systematic comparisons of results produced by participating laboratories.

■

We conclude that the geoarchaeological study and geochemical characterization of basaltic and silicic volcanic tephra deposits in the Willamette National Forest is likely to be of further use in archaeological studies in this region. The chronologic value of these ash deposits simply must not be ignored in future archaeological research projects.

We also conclude that these geochemical studies, however compelling they might be to the archaeological researcher, may be needed only on rare occasions. Because of the highly technical nature of these powerful characterization techniques and the special problems inherent in correlation studies, it is distressingly easy to misidentify sources of tephra. A familiarity with the Holocene volcanic history of the region, with basic geological field techniques, and with tephra identification methods may be all that are needed to identify the geologic sources of most Willamette National Forest tephra deposits. Geochemical characterization methods like those investigated here should generally be used only when less technical approaches have failed.

RECOMMENDATIONS FOR FURTHER RESEARCH

1. *Geologic and geoarchaeological mapping and interpretation of Holocene tephragenic sources and deposits within the Willamette National Forest.*

We believe that most, if not all, sources of Holocene basaltic and silicic volcanic tephra deposits in the Willamette National Forest have been identified. What is now needed is additional geoarchaeological and geological study of these known tephra units.

Within the boundaries of the Willamette National Forest, the identification of the sources of Holocene tephra deposits can often be reliably made without the use of sophisticated chemical characterization methods. A knowledge of the location of tephra sources, the areal distribution and physical characteristics of tephra deposits from these sources, the chronology of the tephragenic eruptive events, and basic stratigraphic interpretative methods are, in most cases, all one needs to identify the source vent. We recommend that further studies of volcanic tephra in this region be directed towards these ends.

Detailed field studies of the areal distribution, thickness, and grain size characteristics of tephra deposits from major Willamette National Forest sources are needed. Additional chronologic work directed specifically towards tephragenic volcanic activity is also required. Without detailed tephrochronologic information, specifically that provided by radiocarbon dates, the archaeological value of many of the tephra deposits will remain limited.

The investigation of cores from Western and High Cascades shallow lakes and bogs has the potential to provide considerable information about the eruptive sequences and chronologies of tephragenic events. Tephra deposits found at these lakes could be characterized, correlated, and dated to provide a detailed record of regional ashfalls. Radiocarbon dating of organic sediments bracketing tephra layers and the calibration and computation of sedimentation rates could add considerable chronologic information that would be of interest to archaeologists. We suggest that a lake core study could be a very productive adjunct to the field research described above.

The results of additional studies of volcanic tephra in the Willamette National Forest should be made available to archaeologists as research reports, supplements to the current Tephra Project report, and as geologic maps with an archaeological emphasis.

2. *Tephrochronologic Methods and Willamette National Forest Archaeological Research.*

We recommend that tephrochronologic studies be incorporated into future Willamette National Forest archaeological research as an explicit design component.

This does not mean that detailed studies of volcanic tephra are always required or that geochemical studies of ash are necessary but only that the potential value of tephra should be specifically recognized. This is particularly true of volcanic tephra from the widespread and well-dated Mazama eruptions. In areas that include known or expected deposits of basaltic or silicic tephra, a study of these materials should definitely be included in the research design. When volcanic tephra is found, it is important that descriptions of intrasite stratigraphy include the thickness and distribution of tephra-bearing units, a brief physical description of the ash (color, grain size, bedding characteristics, etc.), and the relationship of the unit to other stratigraphic deposits and major archaeological features. The provenience of tephra-bearing stratigraphic units and their relationship to artifacts (particularly temporally-sensitive artifact types), materials collected for radiocarbon dating, obsidian sampled for hydration measurements, and any other items that may provide independent chronological data, should be explicitly recorded.

3. Geochemical Characterization studies of Willamette National Forest tephra.

We recommend that further geochemical tephra characterization studies be pursued in the Willamette National Forest. Basic research concerning these geochemical techniques, should they be pursued in future Willamette National Forest archaeological studies, would most productively be undertaken after the more fundamental tephra-related problems described in recommendation 1 have been thoroughly investigated.

We recommend additional EPMA studies of silicic volcanic using a considerably larger source sample. Tephragenic sources included in the sample should include Mount Mazama, Rock Mesa, the Devils Hill chain of domes, the Carver Lake chain, and a scattering of other samples for comparison from Mount St. Helens, Glacier Peak, and the Medicine Lake Highlands of Northern California. This EPMA study could readily be carried out in conjunction with an EPMA study of silicic tephra from multiple Willamette National Forest archaeological sites or geologic contexts.

We also recommend the further exploration of basaltic tephra characterization methods. Preliminary EPMA studies of basaltic pyroclasts could be easily integrated into a more comprehensive study of silicic tephra such as the one outlined above. AAS analyses of pretreated basaltic *bulk tephra samples* are also likely to prove useful in basaltic tephra characterization research problems.

BIBLIOGRAPHY

REFERENCES CITED

Adam, David P.
1967 Late Pleistocene Palynology in the Central Sierra Nevada, California, in *Quaternary Paleoecology*, ed. by C.J. Cushing and H.W. Wright, Jr. Yale University Press: New Haven Connecticut, pp.175-200.

Anderson, Roger Y.; Edward B. Nuhfer, and Walter E. Dean
1984 Sinking of Volcanic Ash in Uncompacted Sediments in Williams Lake, Washington. *Science*, 225:505-508.

Anderson, T.W. and Stanley Sclove
1986 *The Statistical Analysis of Data*. The Scientific Press: Palo Alto, California, 628p.

Arnold, J.R. and F.W. Libby
1951 Radiocarbon Dates. *Science*, 113:111-120.

Bacon, Charles R.
1983 Eruptive History of Mount Mazama and Crater Lake Caldera, Cascade Range, U.S.A. *J. Volcanology and Geothermal Research*, 18(1-4):57-114.

Bacon, Charles R.
1987 Mount Mazama and Crater Lake Caldera, Oregon, in *Centennial Field Guide, Volume 1*, ed. by M.L. Hill. Geological Society of America Centennial Field Guide - Cordilleran Section, pp.301-306.

Bates, Robert L. and Julia A. Jackson, eds.
1987 *Glossary of Geology (Third Edition)*. American Geological Institute: Alexandria, Virginia, 788p.

Baxter, Paul W.
1986a *Archaic Upland Adaptations in the Central Oregon Cascades*. Unpublished Ph.D. Dissertation, Department of Anthropology, University of Oregon: Eugene, Oregon, 213p.

Baxter, Paul W.
1986b *The Colt and Saddle Sites: Excavations on Dead Horse Creek*. Report prepared for the Willamette National Forest, Eugene, Oregon, by the Department of Anthropology, University of Oregon: Eugene, Oregon, 180p.

Baxter, Paul W. and Thomas J. Connolly
1985 *Vine Rockshelter: A Report of Excavations at An Intermittent Hunting Camp in the Western Cascades*. Baxter & Connolly Archaeological Data Consultants, BC/AD Report No.6: Eugene, Oregon, 91p.

Beardsley, Felicia R.
1989 *Archaeological Site Testing Summary Sheet: Woodpecker Site Complex*. Report on file at Detroit District Office, Mill City, Oregon.

Beaudoin, A.B. and R.H. King
1986 Using Discriminant Function Analysis to Identify Holocene Tephras Based on Magnetite Composition: A Case Study from the Sunwapta Pass Area, Jasper National Park. *Canadian J. Earth Sciences*, 23:804-812.

Benson, G.T.
1965 The Age of Clear Lake. *Ore Bin*, 27:37-40.

Binford, Lewis R.
1981 Behavioral Archaeology and the "Pompeii Premise". *J. Anthropological Research*, 37(3):195-208.

Birkeland, P.W.
1984 *Soils and Geomorphology*. Oxford and New York Oxford University Press: New York, New York.

Blinman, Eric
1978 *Pollen Analysis of Glacier Peak and Mount Mazama Volcanic Ashes*. Unpublished Master's Thesis, Washington State University: Pullman, Washington, 49p.

Blinman, Eric; Peter J. Mehringer, Jr., and John C. Sheppard
1979 Pollen Influx and the Deposition of Mazama and Glacier Peak Tephra, in *Volcanic Activity and Human Ecology*, ed. by P. Sheets and D. Grayson. Academic Press: New York, New York, pp.393-426.

Blong, R.J.
1984 *Volcanic Hazards: A Sourcebook on the Effects of Eruptions*. Academic Press: Orlando, Florida, 424p.

Borchardt, Glenn A.
1969 *Neutron Activation Analysis for Correlating Volcanic Ash Soils*. Unpublished Ph.D. Dissertation, Oregon State University: Corvallis, Oregon, 219p.

Borchardt, Glenn A.; P.J. Aruscavage, and H.T. Millard, Jr.
1972 Correlation of the Bishop Ash, A Pleistocene Marker Bed, Using Instrumental Neutron Activation Analysis. *J. Sedimentary Petrology*, 42(2):301-306.

Borchardt, Glenn A.; M.E. Harward, and R.A. Schmitt
1971 Correlation of Volcanic Ash Deposits by Activation Analysis of Glass Separates. *Quaternary Research*, 1:247-260.

Borchardt, Glenn A.; Joel A. Norgren, and Moyle E. Harward
1973 Correlation of Ash Layers in Peat Bogs of Eastern Oregon. *Geological Society of America Bulletin*, 84:3101-3108.

Borchardt, Glenn A.; A.A. Theisen, and M.E. Harward
1968 Vesicular Pores of Pumice by Mercury Intrusion. *Soil Science of America Proceedings*, 32:735-737.

Brenner, Isaac B.; L. Gleit, and A. Harel
1976 Interlaboratory and Intrainstrumental Spectrochemical Precision: Comparison of dc Carbon Arc Optical Emission Spectrographic, Atomic Absorption, and X-Ray Fluorescence Spectrometric Procedures. *Applied Spectroscopy*, 39:335-343.

Brown, Randall E.
1941 *The Geology and Petrography of the Mount Washington Area, Oregon*. Unpublished Master's Thesis, Yale University: New Haven, Connecticut, 48p.

Bruggman, P.E.; C.R. Bacon; P.J. Aruscavage; R.W. Lerner; L.J. Schwarz, and K.C. Stewart
1987 *Chemical Analyses of Rocks and Glass Separates from Crater Lake National Park and Vicinity, Oregon*. U.S. Geological Survey Open-File Report 87-57, 36p.

Buckley, James
1973 Isotopes' Radiocarbon Measurements VI. *Radiocarbon*, 12:53-105.

Buol, S.W.; F.O. Hole, and R.J. McCracken
1981 *Soil Genesis and Classification*. Iowa State Press: Ames, Iowa.

Byrne, John V.
1962 Bathymetry of Crater Lake, Oregon. *Ore Bin*, 24(10):161-164.

Carrara, Paul E.
1989 *Late Quaternary Glacial and Vegetative History of the Glacier Peak National Park Region, Montana*. U.S. Geological Survey Bulletin 1902, 64p.

Chambers, John M.; William S. Cleveland; Beat Kleiner, and Paul A. Tukey
1983 *Graphical Methods for Data Analysis*. Duxbury Press: Boston, Massachusetts, 395p.

Chatters, Roy M.
1968 Washington State University Natural Radiocarbon Dates I. *Radiocarbon*, 10: 479-498.

Chernoff, H.
1973 Using Faces to Represent Points in K-Dimensional Space Graphically. *J. American Statistical Association*, 68:361-368.

Churchill, Thomas E.
1989 *Archaeological Investigations at Olsen 1 (35LA190), Olsen 2 (35LA191), and Deadhorse (35LA656) Rockshelters, Lane County, Oregon*. Report prepared for the Willamette National Forest, Eugene, Oregon. Coastal Magnetic Search and Survey Report No.40, 179p.

Churchill, Thomas E. and Paul C. Jenkins
1989a *Archaeological Investigations of Five Prehistoric Sites in the Scott Mountain Plateau, McKenzie Ranger District, Willamette National Forest.* Report prepared for the Willamette National Forest, Eugene, Oregon. Coastal Magnetic Search and Survey Report No.43, 222p.

Churchill, Thomas E. and Paul C. Jenkins
1989b *Archaeological Investigations of Pepper Rockshelter (35LA801) and Katz Rockshelter (35LA802).* Report prepared for the Oakridge and Lowell Ranger Districts of the Willamette National Forest, Eugene, Oregon. Coastal Magnetic Search and Survey Report No.38, 185p.

Clark, James G.
1983 *Geology and Petrology of South Sister Volcano, High Cascade Range, Oregon.* Unpublished Ph.D. Dissertation, Department of Geology, University of Oregon: Eugene, Oregon, 235p.

Cochran, Bruce
1988 Appendix C: Tephra Analysis, in *Archaeological Data Recovery from the Cougar Ridge Way Trail #4 Site, 35LIN116, Willamette National Forest, Oregon*, by J.J. Flenniken and T. Ozbun. Report prepared for the Willamette National Forest, Eugene, Oregon, by Lithic Analysts: Pullman, Washington, pp.87-89.

Cormie, Allison B. and D.E. Nelson
1983 Energy-Dispersive X-Ray Fluorescence as a Rapid Method for Identifying Tephras. *Quaternary Research*, 19(2):102-211.

Cormie, Allison B.; D.J. Huntley, and D.E. Nelson
1982 Identifying Tephra by Alpha Counting. *Canadian J. Earth Sciences*, 19(4):662-665.

Cormie, Allison B.; D.E. Nelson, and D.J. Huntley
1981 X-Ray Fluorescence as a Rapid Method Identifying Tephras Discovered in Archaeological Sites, in *Tephra Studies*, ed. by S. Self and R.S.J. Sparks. D. Reidel Publishing Co.: Boston, Massachusetts, pp.103-107.

Crandell, Dwight R.
1980 Recent Eruptive History of Mount Hood, Oregon, and Potential Hazards from Future Eruptions. *U.S. Geological Survey Bulletin 1492*, 81p.

Crane, H.R.
1956 University of Michigan Radiocarbon Dates I. *Science*, 124:664-672.

Cranson, K.R.
1982 *Crater Lake: Gem of the Cascades.* KRC Press: Lansing, Michigan, 111p.

Cressman, Luther S.
1939-40 Studies on Early Man in South Central Oregon. *Carnegie Institute of Washington Yearbook*, 39:300-309.

Cressman, Luther S.; Howel Williams, and Alex Krieger
1940 *Early Man in Oregon: Archaeological Studies in the Northern Great Basin.* University of Oregon Monographs, Studies in Anthropology 3: Eugene, Oregon, 78p.

Czamanske, Gerald K. and Stephen C. Porter
1965 Titanium Dioxide in Pyroclastic Layers from Volcanoes in the Cascade Range. *Science*, 150:1022-1025.

Davie, Ellen I.
1980 *The Geology and Petrology of Three-Fingered Jack, A High Cascade Volcano in Central Oregon.* Unpublished Master's Thesis, Department of Geology, University of Oregon: Eugene, Oregon, 137p.

Davis, Carl M.
1987 *Research Design and Data Recovery Plan for Three Prehistoric Lithic Scatter Sites Located in the High Cascades, Willamette National Forest, Western Oregon.* Report on file at the Willamette National Forest, Eugene, Oregon.

Davis, Jonathon O.
1978 *Quaternary Tephrochronology of the Lake Lahontan Area, Nevada and California.* Nevada Archaeological Survey Research Paper No.7: Reno, Nevada, 137p.

Davis, Jonathon O.
1985 Correlation of Late Quaternary Tephra Layers in a Long Pluvial Sequence Near Summer Lake, Oregon. *Quaternary Research*, 23(1):38-53.

Davis, Richard
1978 *U.S. Forest Service Site Report, Irish Camp Lake Archaeological Site (35LA392).* Report on file at the McKenzie District Office (Willamette National Forest), McKenzie Bridge, Oregon.

Diller, J.S. and H.B. Patton
1902 *The Geology and Petrography of Crater Lake National Park.* U.S. Geological Survey Professional Paper 3, 167p.

Doak, William H.
1969 *A Qualitative and Quantitative Characterization of a Volcanic Ash Soil.* Unpublished Master's Thesis, Oregon State University: Corvallis, Oregon, 90p.

Dudas, M.J.; M.E. Harward, and R.A. Schmitt
1973 Identification of Dacitic Tephra by Activation Analysis of Their Primary Mineral Phenocrysts. *Quaternary Research*, 3(2):307-315.

Easterbrook, D.J.
1969 Pleistocene Chronology of the Puget Lowland and San Juan Islands, Washington. *Geological Society of America Bulletin*, 80:2273-2286.

Fagan, John L.
1975 Obsidian Hydration Analysis of Three Sites in Western Oregon, in *Archaeological Studies in the Willamette Valley, Oregon*, ed. by C.M. Aikens. University of Oregon Anthropological Papers No.8: Eugene, Oregon, pp.505-520.

Fairhall, A.W.; A.W. Young, and J.L. Erickson
1976 University of Washington Radiocarbon Dates IV. *Radiocarbon*, 18(2).

Felitsyn, S.B. and V. Yu. Kir'yanov
1990 Areal Variability of Tephra Composition as Indicated by Bulk Silicate Analysis Data. *Volcanology and Seismology*, 9(1):1-20.

Fink, Jonathon H. and Curtis R. Manley
1987 Origin of Pumiceous and Glassy textures in Rhyolite Flows and Domes, in *The Emplacement of Silicic Domes and Lava Flows*, ed. by J. Fink. Geological Society of America Special Paper 212, pp.77-88.

Fisher, Richard V.
1961 Proposed Classification of Volcaniclastic Rocks and Sediments. *Geological Society of America Bulletin*, 72:1409-1414.

Fisher, Richard V.
1964 Maximum Size, Median Diameter, and Sorting of Tephra. *J. Geophysical Research*, 69(2):341-355.

Fisher, Richard V and Hans-Ulrich Schmincke
1984 *Pyroclastic Rocks*. Springer-Verlag: New York, New York, 472p.

Flenniken, J. Jeffrey and Terry L. Ozbun
1988 *Archaeological Data Recovery from the Cougar Ridge Way Trail #4 Site, 35LIN116, Willamette National Forest, Oregon*. Report prepared for the Willamette National Forest, Eugene, Oregon, by Lithic Analysts: Pullman, Washington, 115p.

Flenniken, J. Jeffrey; Terry L. Ozbun, and A. Catherine Fulkerson
1989a *Archaeological Test Excavations at Five Sites (35LA320, 35LA444, 35LA814, 35LA633, 35LA632) on the Lowell and Oakridge Ranger Districts, Willamette National Forest, Oregon*. Report prepared for the Willamette National Forest, Eugene, Oregon, by Lithic Analysts. Lithic Analysts Research Report No.8: Pullman, Washington, 185p.

Flenniken, J. Jeffrey; Terry L. Ozbun, and A. Catherine Fulkerson
1989b *Archaeological Test Excavations at the Warehouse Site, 35LA822, Blue Ridge Ranger District, Willamette National Forest, Oregon*. Report prepared for the Willamette National Forest, Eugene, Oregon. Lithic Analysts Research Report No.8: Pullman, Washington, 106p.

Flenniken, J. Jeffrey; Terry L. Ozbun; A. Catherine Fulkerson, and Carol J. Winkler
1990a *The Diamond Lil Deer Kill Site: A Data Recovery Project in the Western Oregon Cascade Mountains*. Report prepared for the Willamette National Forest, Eugene, Oregon. Lithic Analysts Research Report No.11: Pullman, Washington, 247p.

Flenniken, J. Jeffrey; Terry L. Ozbun, and Jeffrey A. Markos
1990b *Archaeological Testing and Evaluation of the Gate Creek #1 Site, 35LA295. Report prepared for the Willamette National Forest, Eugene, Oregon.* Lithic Analysts Research Report No.17: Pullman, Washington, 118p.

Flenniken, J. Jeffrey; Terry L. Ozbun, and Jeffrey A. Markos
1990c *Archaeological Testing and Evaluation of the Swamp Peak Way Trail One Site, 35LIN373.* Report prepared for the Willamette National Forest, Eugene, Oregon. Lithic Analysts research Report No.18: Pullman, Washington, 92p.

Gannon, Brian L.
1981 *Geology of a Volcanic Complex on the South Flank of Mount Jefferson, Oregon.* Unpublished Master's Thesis, Department of Geology, Portland State University: Portland, Oregon, 181p.

Glenn, Jerry L.
1965 *Late Quaternary Sedimentation and Geologic History of the North Willamette Valley, Oregon.* Unpublished Ph.D. Dissertation, Oregon State University: Corvallis, Oregon.

Goles, Gordon G.
1980 *A Study of the Geothermal Potential of the Santiam Pass and Austin Hot Springs Areas, Central Oregon Cascades, By Field and Geochemical Approaches.* Interim report in possession of the author, 16p.

Hansen, Henry P.
1942 A Pollen Study of Lake Sediments in the Lower Willamette Valley of Western Oregon. *Bulletin of the Torrey Botanical Club*, 69(4):262-280.

Harbottle, Garman
1982 Chemical Characterization in Archaeology, in *Contexts for Prehistoric Exchange*, ed. by J.E. Ericson and T.K. Earle. Academic Press: New York, New York, pp.13-51.

Hassan, Fekri
1990 Appendix A: Sediment Analysis, in *The Diamond Lil Recovery Site: A Data Recovery Project in the Western Cascade Mountains*, by J.J. Flenniken, T.L. Ozbun, A.C. Fulkerson, and C.J. Winkler. Report prepared for the Willamette National Forest, Eugene, Oregon. Lithic Analysts Research Report No.11: Pullman, Washington, pp.179-182.

Heiken, Grant H.
1972 Morphology and Petrography of Volcanic Ash. *Geological Society of America Bulletin*, 83:1461-1488.

Heiken, Grant H.
1974 *An Atlas of Volcanic Ash.* Smithsonian Contributions to the Earth Sciences No.12, 101p.

Heiken, Grant H. and Kenneth Wohletz
1985 *Volcanic Ash.* University of California Press: Berkeley, California, 246p.

Henn, Winfield
1975 The Indian Ridge Site, Lane County, Oregon, in *Archaeological Studies in the Willamette Valley, Oregon*, ed. by C.M. Aikens. University of Oregon Anthropological Papers No.8: Eugene, Oregon, pp.455-468.

Hibbert, Dennis M.
1979 *Pollen Analysis of Late-Quaternary Sediments from Two Lakes in the Southern Puget Lowland, Washington*. Unpublished Master's Thesis, University of Washington: Seattle, Washington, 37p.

Hinkley, Todd K.; Kathleen S. Smith; Joseph E. Taggart, Jr., and Julia T. Brown
1987 *Chemical and Mineralogic Aspects of Observed Fractionation of Ash from the May 18, 1980 Eruption of Mount St. Helens*. U.S. Geological Survey Professional Paper 1397-A, 22p.

Hodge, Edwin T.
1925a *Mount Multnomah: Ancient Ancestor of the Three Sisters*. University of Oregon: Eugene, Oregon, 160p.

Hodge, Edwin T.
1925b Geology of Mount Jefferson. *Mazama*, 7(2):25-58.

Holmes, Kenneth
1955 Mount St. Helens' Recent Eruptions. *Oregon Historical Society*, 56(3):197-210.

Jan, M. Quasim
1967 *Geology of the McKenzie River Valley Between the South Santiam Highway and the McKenzie Pass Highway, Oregon*. Unpublished Master's Thesis, Department of Geology, University of Oregon: Eugene, Oregon, 70p.

Jashemski, Wilhelmina F.
1979 Pompeii and Mount Vesuvius, A.D. 79, in *Volcanic Activity and Human Ecology*, ed. by P. Sheets and D. Grayson. Academic Press: New York, New York, pp.587-622.

Jenkins, Paul C.
1988 *Archaeological Evaluation of the Saddle Quarry Site*. Report prepared for the Willamette National Forest, Eugene, Oregon. Coastal Magnetic Search and Survey Report No.24, 67p.

Johnson, Wesley M. and John A. Maxwell
1981 *Rock and Mineral Analysis*. John Wiley and Sons: New York, New York, 489p.

Juvigne, Etienne and Stephen C. Porter
1985 Mineralogical Variations Within Two Widespread Holocene Tephra Layers from Cascade Range Volcanoes, U.S.A. *Geographie Physique et Quaternaire*, 36(1):7-12.

King, R.H.; M.S. Kingston, and R.L. Barnett
1982 A Numerical Approach Toward the Classification of Magnetites from Tephra in Southern Alberta. *Canadian J. Earth Sciences*, 19(10):2012-2019.

Kir'yanov, V. Yu; S.E. Zharinov, and A.B. Perepelov
1990 Possible Geochemical Differences of East Kamchatkan Volcanic Ashes. *Volcanology and Seismology*, 9(2):320-328.

Kittleman, Laurence
1973 Mineralogy, Correlation, and Grain-Size Distribution of Mazama Tephra and Other Postglacial Pyroclastic Layers, Pacific Northwest. *Geological Society of America Bulletin*, 84:2957-2980.

Kittleman, Laurence
1979 Geologic Methods in Studies of Quaternary Tephra, in *Volcanic Activity and Human Ecology*, ed. by P. Sheets and D. Grayson. Academic Press: New York, New York, pp.49-82.

Larsen, Gudrun
1981 Tephrochronology by Microprobe Glass Analysis, in *Tephra Studies*, ed. by S. Self and R.S.J. Sparks. D. Reidel Publishing Co.: Boston, Massachusetts, pp.95-102.

Leach, Foss; Atholl Anderson; Doug Suton; Roger Bird; Peter Duerden, and Eric Clayton
1986 The Origin of Prehistoric Obsidian Artefacts from the Chatham and Kermadec Islands. *New Zealand J. Archaeology*, 8:143-170.

LeBas, M.J.; R.W. LeMaitre; A. Streckeisen, and B. Zanettin
1986 A Chemical Classification of Volcanic Rocks Based on the Total Alkali-Silica Diagram. *J. Petrology*, 27(3):745-750.

Lemke, R.W.; M.R. Mudge; Ray E. Wilcox, and H.A. Powers
1975 Geologic Setting of the Glacier Peak and Mazama Ash-Bed Markers in West-Central Montana. *U.S. Geological Survey Bulletin 1395-H*, 31p.

Lidstrom, John W.
1972 *A New Model for the Formation of Crater Lake Caldera*. Unpublished Ph.D. Dissertation, Oregon State University: Corvallis, Oregon, 85p.

Lindberg-Muir, Catherine
1988 *Obsidian: Archaeological Implications for the Central Oregon Cascades*. Unpublished Master's Thesis, Interdisciplinary Studies, Oregon State University: Corvallis, Oregon, 239p.

Mack, Richard N.; Rose Okazaki, and Sam Valastro
1979 Bracketing Dates for Two Ash Falls from Mount Mazama. *Nature*, 279:228-229.

Malin, Michael C.; Daniel Dzurisin, and Robert P. Sharp
1983 Stripping of Keanakakoi Tephra on Kilauea Volcano. *Geological Society of America Bulletin*, 94(10):1148-1158.

Matz, Stephan
1987 *The Effects of the Mazama Tephra Falls: A Geoarchaeological Approach.* Master's Thesis, Interdisciplinary Studies, Oregon State University: Corvallis, Oregon, 235p.

McBirney, Alexander R.
1968 Compositional Variations of the Climactic Eruption of Mount Mazama, in *Andesite Conference Guidebook*, ed. by H. Dole. Oregon Department of Geology and Mineral Industries Bulletin 62: Portland, Oregon, pp.53-56.

McDowell, Patricia F.
1989 Appendix 3: Tephra Sample Examination, in *Archaeological Testing of the Dale Beam Site, 35LA793, on the McKenzie District of the Willamette National Forest, Lane County, Oregon*, by L. Spencer. Report prepared for the Willamette National Forest, Eugene, Oregon. Lee Spencer Archaeological Paper No. 1989-3: Eugene, Oregon, pp.176-177.

Mehringer, Peter J., Jr.; Eric Blinman, and Kenneth L. Peterson
1977 Pollen Influx and Volcanic Ash. *Science* , 198:257-261.

Minor, Rock
1987 *Cultural Resources Overview of the Willamette National Forest: A 10-Year Update.* Heritage Research Associates Report 60: Eugene, Oregon, 194p.

Minor, Rick and Audrey F. Pecor
1977 *Cultural Resource Overview of the Willamette National Forest, Western Oregon.* University of Oregon Anthropological Papers No.12: Eugene, Oregon, 218p.

Minto, John
1903 Minto Pass: Its History, and An Indian Tradition. *Oregon Historical Quarterly*, 4(3):241-250.

Morganstein, Maury and Thomas J. Riley
1975 Hydration-Rind Dating of Basaltic Glasses: A New Method for Archaeological Chronologies. *Asian Perspectives*, 17(2):145-159.

Mullineaux, D.R.
1986 Summary of Pre-1980 Tephra-Fall Deposits Erupted from Mount St. Helens, Washington State, USA. *Bulletin of Volcanology*, 48(1):17-26.

Mullineaux, D.R. and R.E. Wilcox
1980 Stratigraphic Subdivisions of Holocene Airfall Tephra from the Climactic Series of Eruptions of Mount Mazama, Oregon (Abstract). *EOS*, 61(5):66.

Mullineaux, D.R.; R.E. Wilcox; W.F. Ebaugh; R. Fryxell, and M. Rubin
1978 Age of the Last Major Scabland Flood of the Columbia River Plateau in Eastern Washington. *Quaternary Research*, 10:171-180.

Murdock, George P.
1980 The Tenino Indians. *Ethnology*, 19(2):129-149.

Mustard, Peter and Jean M. Richardson
1990 A Lotus 1-2-3 Template for Triangular Plots. *Geobyte*, 5(2):47-53.

Naeser, C.W.; N.D. Briggs; J.D. Obradovich, and G.A. Izett
1981 Geochronology of Quaternary Tephra Deposits, in *Tephra Studies*, ed. by S. Self and R.S.J. Sparks. D. Reidel Publishing Co.: Boston, Massachusetts, pp.13-47.

Nelson, C. Hans; Paul R. Carlson, and Charles R. Bacon
1988 The Mount Mazama Climactic Eruption (~6900 yr B.P.) and Resulting Convulsive Sedimentation on the Crater Lake Caldera Floor, Continent, and Ocean Basins, in *Sedimentary Consequences of Convulsive Geologic Events*, ed. by H.E. Clifton. Geological Society of America Special Paper 229, pp.37-57.

Newman, Thomas N.
1966 *Cascadia Cave*. Occasional Papers of the Idaho State University Museum 18: Pocatello, Idaho, 49p.

Nilsson, Elena
1989 *Archaeological Data Recovery Investigations at the Bear Saddle Site, 35LIN302, Willamette National Forest, Oregon*. Report prepared for the Willamette National Forest, Eugene, Oregon, by Mountain Anthropological Research: Redding, California, 156p.

Olsen, Thomas L.
1975 Baby Rock Shelter, in *Archaeological Studies in the Willamette Valley, Oregon*, ed. by C.M. Aikens. University of Oregon Anthropological Papers No.8: Eugene, Oregon, pp.469-494.

Oviatt, Charles G. and William P. Nash
1989 Late Pleistocene Volcanic Ash and Volcanic Eruptions in the Bonneville Basin, Utah. *Geological Society of America Bulletin*, 101(2):292-303.

Peterson, Norman V. and Edward A. Groh
1965 *Lunar Geological Field Conference Guidebook*. Oregon Department of Geology and Mineral Industries Bulletin 57: Portland, Oregon, 51p.

Pilles, Peter J.
1979 Sunset Crater and the Sinagua: A New Interpretation, in *Volcanic Activity and Human Ecology*, ed. by P. Sheets and D. Grayson. Academic Press: New York, New York, pp.459-485.

Porter, S.C.
1978 Glacier Peak Tephra in the North Cascade Range, Washington: Stratigraphy, Distribution, and Relationship to Late-Glacial Events. *Quaternary Research*, 10:30-41.

Powers, Howard A. and R. Wilcox
1964 Volcanic Ash from Mount Mazama (Crater Lake) and from Glacier Peak. *Science,* 144:1334-1336.

Preston, R.S.; Elaine Person, and E.S. Deevey
1955 Yale Natural Radiocarbon Measurements II. *Science*, 122:954-960.

Radosevich, Stefan C.
No Date *Soil Analysis of Irish Camp Lake Site (LA-392).* Unpublished report on file at the McKenzie District Ranger Station (Willamette National Forest), McKenzie Bridge, Oregon, 10p.

Radosevich, Stefan C.
1989 Appendix F: Soil Analysis,in *Archaeological Investigations of Pepper Rockshelter (35LA801) and Katz Rockshelter (35LA802)*, by T.E. Churchill and P.C. Jenkins. Report prepared for the Oakridge and Lowell Ranger Districts of the Willamette National Forest, Eugene, Oregon. Coastal Magnetic Search & Survey Report No.38, pp.123-144.

Rai, Dhanpat
1970 *Stratigraphy and Genesis of Soils from Volcanic Ash in the Blue Mountains of Eastern Oregon.* Unpublished Ph.D. Dissertation, Oregon State University: Corvallis, Oregon, 136p.

Randle, K.; G.G. Goles, and L.R. Kittleman, Jr.
1971 Geochemical and Petrological Characterization of Ash Samples from Cascade Range Volcanoes. *Quaternary Research*, 1(2):262-282.

Rarick, Theodore M.
1962 *Changing Landscapes in the McKenzie Valley, Oregon.* Unpublished Master's Thesis, Department of Geography, University of Oregon: Eugene, Oregon, 100p.

Ray, Verne F.
1932 *The Sanpoil and Nespalem.* University of Washington Publications in Anthropology No.5.

Renfrew, Colin
1979 The Eruption of Thera and Minoan Crete, in *Volcanic Activity and Human Ecology*, ed. by P. Sheets and D. Grayson. Academic Press: New York, New York, pp.565-585.

Retallack, Greg J.
1988 Field Recognition of Paleosols, in *Paleosols and Weathering Through Geologic Time: Principles and Applications*, ed. by J. Reinhardt and W.R. Sigleo. Geological Society of America Special Paper 216, pp.1-20.

Rollins, Anthony
1976 *Geology of the Bachelor Mountain Area, Linn and Marion Counties, Oregon.* Unpublished Master's Thesis, Department of Geology, Oregon State University: Corvallis, Oregon, 83p.

Romesburg, H. Charles
1984 *Cluster Analysis for Researchers.* Lifetime Learning Publication: Belmont, California, 334p.

Rubin, Meyer and Corrine Alexander
1960 U.S. Geological Survey Radiocarbon Dates V. *Radiocarbon*, 2:129-185.

Sarna-Wojcicki, Andrei M.; Harry W. Bowman, and Paul C. Russell
1979 *Chemical Correlation of Some Late Cenezoic Tuffs of Northern and Central California by Neutron Activation Analysis of Glass and Comparison With X-Ray Fluorescence Analysis.* U.S. Geological Survey Professional Paper 1147, 15p.

Sarna-Wojcicki, Andrei M.; Duane E. Champion, and Jonathon O. Davis
1983 Holocene Volcanism in the Conterminous United States and the Role of Silicic Volcanic Ash layers in Correlation of Latest-Pleistocene and Holocene Deposits, in *Late-Quaternary Environments of the United States*, Vol.2, ed. by H.E. Wright, Jr. University of Minnesota Press: Minneapolis, Minnesota, pp.52-77.

Sarna-Wojcicki, Andrei M.; S.D. Morrison; C.E. Meyer, and J.W. Hillhouse
1987 Correlation of Upper Cenezoic Tephra Layers Between Sediments of the Western United States and Eastern Pacific Ocean and Comparison With Biostratigraphic and Magnetostratigraphic Age Data. *Geological Society of America Bulletin*, 98(2):207-223.

Schmid, R.
1981 Descriptive Nomenclature and Classification of Pyroclastic Deposits and Fragments: Recommendations of the I.U.G.S. Subcommission on the Systematics of Igneous Rocks. *Geology*, 9:41-43.

Scott, William E.
1974 *Quaternary Glacial and Volcanic Environments, Metolius River Area, Oregon.* Unpublished Ph.D. Dissertation, University of Washington: Seattle, Washington, 95p.

Scott, William E.
1977 Quaternary Glaciation and Volcanism in the Metolius Area. *Geological Society of America Bulletin*, 88:113-124.

Scott, William E.
1987 Holocene Rhyodacite Eruptions on the Flanks of South Sister Volcano, Oregon, in *The Emplacement of Silicic Domes and Lava Flows*, ed. by J.H. Fink. Geological Society of America Special Paper 212, pp.35-53.

Scott, William E.
1990 Temporal Relations Between Eruptions of the Mount Bachelor Volcanic Chain and Fluctuations of Late Quaternary Glaciers. *Oregon Geology*, 52(5):114-117.

Scott, William E. and Cynthia A. Gardner
1990 Field Trip Guide to the Central Oregon Cascades, Part 1: Mount Bachelor-South Sister Area. *Oregon Geology*, 52(5):99-114.

Scott, William E.; Cynthia A. Gardner, and Andrei M. Sarna-Wojcicki, eds.
1989 *Guidebook for Field Trip to the Mount Bachelor-South-Sister-Bend Area, Central Oregon High Cascades*. U.S. Geological Survey Open-File Report 89-645, 66p.

Self, S. and R.S.J. Sparks, eds.
1981 *Tephra Studies*. D. Reidel Publishing Co.: Boston, Massachusetts, 477p.

Self, S.; R.S.J. Sparks; B. Booth, and G.P.L. Walker
1974 The 1973 Heimaey Strombolian Scoria Deposit. *Geological Magazine*, 111(6): 539-548.

Sheets, Payson D.
1983 Summary and Conclusions, in *Archaeology and Volcanism in Central America: The Zapotitan Valley of El Salvador*, ed. by P. Sheets. University of Texas Press: Austin, Texas, pp.275-293.

Sherrod, David R.
1986 *Geology, Petrology, and Volcanic History of a Portion of the Cascade Range Between Latitudes 43-44° N., Central Oregon, USA*. Unpublished Ph.D. Dissertation, University of California: Santa Barbara, California, 320p.

Silvermoon, Jon
1986 *Archaeological Evaluation and Mitigation Plan for the Frog Camp Site (35LA526) and the Obsidian Trailhead Relocation Project, Lane County, Oregon*. Report on file at the McKenzie Ranger District, Willamette National Forest, McKenzie Bridge, Oregon.

Silvermoon, Jon
1988 *Research Design for the Scott Mountain Plateau Study Unit, Upper McKenzie River Study Area, McKenzie Ranger District, Willamette National Forest, Western Oregon: Draft Version*. Unpublished manuscript in possession of the author, 31p.

Silvermoon, Jon and Tony Farque
1986 The Obsidian Cliff Quarries of the Three Sisters (Abstract). *Northwest Anthropological Research Notes*, 20(1):62.

Skinner, Craig E.
1990 *Holocene Volcanic Tephra in Oregon: A Bibliography and Hypertext Index for the IBM PC*. Geo-Anthropology Research Program, University of Oregon: Eugene, Oregon, 1 5-1/4" diskette.

Skinner, Craig E. and Stefan R. Radosevich
1989 The Source of the Mazama 'Mimic' Mystery Tephra: Geochemical Studies of Volcanic Tephra from Vine Rockshelter (35LA304): Central Western Cascades, Oregon (Abstract). *Current Archaeological Happenings in Oregon*, 14(4):15-16.

Smith, D.G.W. and J.A. Westgate
1969 Electron Probe Technique for Characterising Pyroclastic Deposits. *Earth and Planetary Science Letters*, 6(5):313-319.

Snyder, Sandra L.
1981 Medicine Creek: Pre- and Post-Mazama Occupation in the Cascades. *Tebiwa Miscellaneous Papers No.23*, 11p.

Soil Survey Staff
1975 *Soil Taxonomy*. U.S.D.A Handbook 436: Washington, D.C., 754p.

Spencer, Lee
1988 *Archaeological Testing of the Squaw Mountain North III Site and Canyon Owl Confluence Site: Two Middle Archaic Period Sites on the Sweet Home District of the Willamette National Forest*. Report prepared for the Willamette National Forest, Eugene, Oregon. Lee Spencer Archaeology paper 1988-2: Eugene, Oregon, 230p.

Spencer, Lee
1989a *Archaeological Testing of the Dale Beam Site, 35LA793, on the McKenzie District of the Willamette National Forest, Lane County, Oregon*. Report prepared for the Willamette National Forest, Eugene, Oregon. Lee Spencer Archaeological Paper No. 1989-3, 188p.

Spencer, Lee
1989b *Archaeological Testing of the Bee Bee Site, 35LIN302: A Low Density Site on the Detroit District of the Willamette National Forest*. Report prepared for the Willamette National Forest, Eugene, Oregon. Lee Spencer Archaeology Paper No.1989-1: Eugene, Oregon, 106p.

Steen, Virginia and Roald Fryxell
1965 Mazama and Glacier Peak Pumice Glass: Uniformity of Refractive Index After Weathering. *Science*, 150:878-880.

Steen-McIntyre, Virginia
1977 *A Manual for Tephrachronology*. Colorado School of Mines Press: Boulder, Colorado, 167p.

Steen-McIntyre, Virginia
1981 Approximate Dating of Tephra, in *Tephra Studies*, ed. by S. Self and R.S.J. Sparks. D. Reidel Publishing Co.: Boston, Massachusetts, pp.49-64.

Steen-McIntyre, Virginia
1985 Tephrochronology and Its Application to Archaeology, in *Archaeological Geology*, ed. by G. Rapp, Jr. and J.A. Gifford. Yale University Press: New Haven, Connecticut, pp.265-302.

Stokes, Stephen and David J. Lowe
1988 Discriminant Function Analysis of Late Quaternary Tephras from Five Volcanoes in New Zealand Using Glass Shard Major Element Chemistry. *Quaternary Research*, 30(3):270-283.

Stuiver, Minze and Paula J. Reimer
1986 A Computer Program for Radiocarbon Age Determination. *Radiocarbon*, 28(2B): 1022-1030.

Sutton, Kenneth G.
1974 *Geology of Mount Jefferson.* Unpublished Master's Thesis, Department of Geology, University of Oregon: Eugene, Oregon, 119p.

Swanson, Frederick J. and Michael E. James
1975 Geomorphic History of the Lower Blue River-Lookout Creek Area, Western Cascades, Oregon. *Northwest Science*, 49(1):1-11.

Taylor, Edward M.
1965 Recent Volcanism Between Three-Fingered Jack and North Sister, Oregon Cascade Range. *Ore Bin*, 27(7):121-147.

Taylor, Edward M.
1967 *Recent Vulcanism Between Three-Fingered Jack and North Sister, Oregon Cascade Range*. Unpublished Ph.D. Dissertation, Washington State University: Pullman, Washington, 84p.

Taylor, Edward M.
1968 Roadside Geology, Santiam and McKenzie Pass Highways, Oregon, in *Andesite Conference Guidebook*, ed. by H. Dole. Oregon Department of Geology and Mineral Industries Bulletin 62: Portland, Oregon, pp.3-33.

Taylor, Edward M.
1978 *Field Geology of S.W. Broken Top Quadrange, Oregon.* Oregon Department of Geology and Mineral Industries Special Paper 2: Portland, Oregon, 50p.

Taylor, Edward M.
1981 Central High Cascade Roadside Geology, Bend, Sisters, McKenzie Pass, and Santiam Pass, Oregon, in *Guides to Some Volcanic Terranes in Washington, Idaho, Oregon, and Northern California*, ed. by D. Johnston and J. Donnelly-Nolan. U.S. Geological Survey Circular 838, pp.55-83.

Taylor, Edward M.; Norman S. MacLeod; David R. Sherrod, and George W. Walker
1987 *Geologic Map of the Three Sisters Wilderness, Deschutes, Lane, and Linn Counties, Oregon*. U.S Geological Survey Miscellaneous Field Investigations Map MF-1954, scale 1:63,360.

Teit, James A.
1930 Salishan Tribes of the Western Plateaus. *Bureau of American Ethnology Annual Report*, 45:23-396.

Theisen, Arthur A.; Glenn A. Borchardt; Moyle E. Harward, and Romas A. Schmitt
1968 Neutron Activation for Distinguishing Cascade Range Pyroclastics. *Science*, 161: 1009-1011.

Thorarinsson, Sigurdur
1981 Tephra Studies and Tephrochronology: A Historical Review With Special Reference to Iceland, in *Tephra Studies*, ed. by S. Self and R.S.J. Sparks. D. Reidel Publishing Co.: Boston, Massachusetts, pp.1-12.

Tilling, Robert I.; Theodore J. Bornhorst; Joseph E. Taggart, Jr.; William I. Rose, and James J. McGee
1987 Inter-Laboratory Comparison of X-Ray Fluorescence Analyses of Eruptive Products of El Chicon Volcano, Chiapas, Mexico. *Applied Geochemistry*, 2(3):337-345.

Toepel, Kathryn A. and Rick Minor
1980 *Cultural Resources Survey of Proposed Developments at Hoodoo Ski Bowl, Linn County, Oregon*. Report prepared for Hoodoo Ski Bowl Developers, Inc. Heritage Research Associates: Eugene, Oregon, 39p.

Tucker, Glennda B.
1977 *Morphologic Parameters of Mount Mazama and Glacier Peak Tephras: A Scanning-Electron Microscope Study*. Unpublished Master's Thesis, University of Washington: Seattle, Washington, 108p.

Tukey, J.W.
1977 *Exploratory Data Analysis*. Addison-Wesley Publishing Co.: Reading, Massachusetts, 688p.

Valastro, S.; E. Mott Davis, and Craig T. Rightmire
1968 University of Texas at Austin Radiocarbon Dates VI. *Radiocarbon*, 10(2):384-401.

Verosub, Kenneth L.
1981 The Interrelationship Between Magnetostriagraphy and Tephrochronology, in *Tephra Studies*, ed. by S. Self and R.S.J. Sparks. D. Reidel Publ. Co.: Boston, Massachusetts, pp.65-72.

Waitt, Richard B., Jr.; Vicki L. Hansen; Andrei M. Sarna-Wojcicki, and Spencer H. Wood
1981 Proximal Air-Fall Deposits of Eruptions Between May 24 and August 7, 1980 - Stratigraphy and Field Sedimentology, in *The 1980 Eruptions of Mount St. Helens, Washington*, ed. by P.W. Lipman and D.R. Mullineux. U.S. Geological Survey Professional Paper 1250, pp.617-628.

Waitt, Richard B., Jr. and Daniel Dzurisin
1981 Proximal Air-Fall Deposits from the May 18 Eruption - Stratigraphy and Field Sedimentology, in *The 1980 Eruptions of Mount St. Helens, Washington*, ed. by P.W. Lipman and D.R. Mullineux. U.S. Geological Survey Professional Paper 1250, pp.601-616.

Walker, G.P.L.
1971 Grain-Size Characteristics of Pyroclastic Deposits. *J. Geology*, 79:696-714.

Walker, G.W.; R.C. Greene, and E.C. Pattee
1966 *Mineral Resources of the Mount Jefferson Primitive Area, Oregon*. U.S. Geological Survey Bulletin 1230-D, 32p.

Westgate, J.A. and N.D. Briggs
1980 Dating Methods of Pleistocene Deposits and Their problems: Tephrochronology and Fission-Track Dating". *Geoscience Canada*, 7:3-10.

Westgate, J.A. and A. Dreimanis
1967 Volcanic Ash Layers of Recent Age at Banff Park, Alberta, Canada. *Canadian J. Earth Sciences*, 4:155-161.

Westgate, J.A. and Michael P. Gorton
1981 Correlation Studies in Tephra Studies, in *Tephra Studies*, ed. by S. Self and R.S.J. Sparks. D. Reidel Publishing Co.: Boston, Massachusetts, pp.73-94.

Westgate, J.A.; D.G.W. Smith, and H. Nichols
1969 Late Quaternary Pyroclastic Layers in the Edmonton Area, Alberta, in *Pedology and Late Quaternary Research*, ed. by S. Pawluk. University of Alberta Printing Department: Edmonton, Canada, pp.179-186.

Wilcox, Ray E.
1965 Volcanic-Ash Chronology, in *The Quaternary of the United States*, ed. by H.E. Wright and D.G. Frey. Princeton University Press: Princeton, New Jersey, pp.807-816.

Williams, Howel
1942 *Geology of Crater Lake National Park, Oregon*. Carnegie Institute of Washington Publication 540, 162p.

Williams, Howel
1944 Volcanoes of the Three Sisters Region, Oregon Cascades. *University of California Department of Geological Sciences Bulletin*, 27(3):37-84.

Williams, Howel
1954 *Crater Lake: The Story of Its Origin.* University of California Press: Berkeley, California, 97p.

Williams, Howel and Gordon G. Goles
1968 Volume of the Mazama Ash-Fall and the Origin of Crater Lake Caldera, in *Andesite Conference Guidebook*, ed. by H.M. Dole. Oregon Department of Geology and Mineral Industries Bulletin 62: Portland, Oregon, pp.37-41.

Williams, Howel and Alexander R. McBirney
1979 *Volcanology.* Freeman, Cooper, and Co.: San Francisco, California, 397p.

Woller, Neil M. and Gerald A. Black
1983 Geology of the Waldo Lake-Swift Creek Area, Lane and Klamath Counties, Oregon, in *Geology and Geothermal Resources of the Central Oregon Cascade Range*, ed. by G.R. Priest and B.F. Vogt. Oregon Department of Geology and Mineral Industries Special Paper 15: Portland, Oregon, pp.57-68.

Wood, Charles A.
1980 Morphometric Evolution of Cinder Cones. *J. Volcanology and Geothermal Research*, 17(3-4):387-413.

Workman, William B.
1979 The Significance of Volcanism in the Prehistory of Subarctic Northwest North America, in *Volcanic Activity and Human Ecology*, ed. by P. Sheets and D. Grayson. Academic Press: New York, New York, pp.339-371.

Wozniak, Karl C.
1982 *Geology of the Northern Part of the Southeast Three Sisters Quadrangle, Oregon.* Unpublished Master's Thesis, Department of Geology, Oregon State University: Corvallis, Oregon, 98p.

Yellin, J.; I. Perlman; F. Asaro; H.V. Michel, and D.F. Mosier
1978 Comparison of Neutron Activation Analysis from the Lawrence Berkeley Laboratory and the Hebrew University. *Archaeometry*, 29(1):95-100.

Yoshido, Mio
1979 Identification of Tephras by Magnetic Measurement, Parts 1-3. *Rock Magnetism and Paleogeophysics*, 6:107-122.

Zielinski, Robert A.; Peter W. Lipman, and Hugh T. Millard, Jr.
1977 Minor-Element Abundances in Obsidian, Perlite, and Felsite of Calc-Alkalic Rhyolites. *American Mineralogist*, 62(5-6):426-437.

APPENDICES

APPENDIX ONE

Glossary of Terms

APPENDIX 1: GLOSSARY OF TERMS

Tephra and archaeological terms were adapted from: Steen-McIntyre, 1977; Williams and McBirney, 1979; Binford, 1981; Schmid, 1981; Fisher and Schmincke, 1984; Heiken and Wohletz, 1985; Bates and Jackson, 1987, and LeBas et al., 1986.

Aeolian Fractionation
Process of relative changes in tephra components during aeolian transport in an eruption cloud or plume.

AAS
Atomic absorption spectrophotometry.

Absolute Age
Age expressed in calendar years or radiocarbon years (see dendrochronologic calibration). Most so-called absolute ages have an associated statistical analytical uncertainty (for example, the $\pm$ of radiocarbon dates) and actually refer to a statistically-defined range of time.

Airfall Tephra
Tephra pyroclasts or deposits resulting from a shower of pyroclastic fragments from an eruption cloud. See fallout deposit.

Andesite/Andesitic
As used in this report, an igneous rock with a silica content lying between 57 and 63 percent. For a more detailed geochemical definition, see LaBas et al., 1986.

Ash
Pyroclasts with a diameter of 2 mm or less.

Ashfall
A rain of airborne volcanic ash falling from an eruption cloud plus the resulting deposit. Generally characterized by mantle bedding.

Ash Flow
The term correctly refers to pyroclastic flows with pyroclasts less than 2 mm in diameter but in practice is used as a synonym for pyroclastic flow.

Basalt/Basaltic
As used in this report, an igneous rock with a silica content lying between 48 and 53 percent. For a more detailed geochemical definition, see LeBas et al., 1986.

Basaltic Andesite
As used in this report, an igneous rock with a silica content lying between about 53 and 57 percent. For a more detailed geochemical definition, see Le Bas et al., 1986.

Basaltic Tephra
Volcanic tephra with a basaltic or basaltic andesite composition.

Base-Surge
Ring-shaped turbulent cloud that moves horizontally outward from the base of an eruption column at very high velocities.

Block
A pyroclast with a diameter greater than 64 mm that was solid when ejected.

Bomb
A pyroclast with a diameter greater than 64 mm that was still viscous when ejected.

Bulk Composition/Bulk Sample
Sample used for analysis in which no attempt is made to separate different components (other than to remove contaminants); for tephra, the vitric, lithic, and crystalline components are all analyzed together.

Characterization
Identification of a specific source on the basis of some distinguishing characteristic; "fingerprinting". See sourcing.

Chronstratigraphy/Chronostratigraphic
Branch of stratigraphy that deals with the age of strata and their time relations.

Cinder
Synonym for scoria. The term was used in ancient times when it was thought that volcanoes contained fire from combustible materials.

Cinder Cone
Conical hill formed by the accumulation of scoria and other pyroclasts, generally of basaltic to basaltic andesite composition.

Clastic
A fragmental rock that has been transported some distance from its source; termed a pyroclastic rock when formed by volcanic eruptions.

Coefficient of Variation
The product of the standard deviation of a data set divided by its arithmetic mean and multiplied by 100 (expressed as %); the result is a dimensionless figure that can be used as a measure of variability within a data set.

Contact Relationship
The relative stratigraphic placement or sequence of units is determined by exposures where direct contacts or contact relationships between units are observable.

Crystalline
As used in this report, the crystalline fraction of tephra; differentiated from the lithic and vitric fraction.

Dacite/Dacitic
As used in this report, an igneous rock with a silica content lying between 63 and 68 percent. For a more detailed geochemical definition, see LeBas et al., 1986.

Dendrochronologic Calibration
Because of variations in environmental ^{14}C over time, calendar ages and radiocarbon ages are not equivalent. Dendrochronologic calibration schemes based on radiocarbon-dated tree ring chronologies are used to convert radiocarbon to calendar dates (Stuiver and Reimer, 1986).

Distal-Source Tephra Facies
Tephra airfall deposits found in areas far from the source, much farther than lava or pyroclastic flows can travel. Tephra layers of distant-source facies are typically thin, have a small grain size, and are well-sorted.

EDA
Exploratory data analysis.

Ejecta
Material thrown out by a volcano; synonymous with pyroclast.

EPMA
Electron microprobe analysis.
Facies
Refers to physical, chemical, and biological variations of rocks deposited during a specific interval of time. See near-vent facies and distal facies.
Fallout Deposit
Deposit of airfall tephra.
Glass Separates
The vitric component of tephra; the chemical composition of this fraction of tephra is not affected by the distance from the vent and is often used to chemically characterize volcanic ash. The glass can be separated from the lithic and crystalline components through several means.
Glowing Avalanche
Synonym for pyroclastic flow; the term originated because of the high temperature of the flow during emplacement.
Holocene
An epoch of the Quaternary Period stretching from about 10,000 years ago (the end of the last major Pleistocene glacial period) to present times.
INAA
Instrumental Neutron Activation Analysis.
Intermediate-Source Facies
Tephra deposits that are intermediate between near-source and distal-source facies. All Willamette National Forest Holocene silicic tephra deposits can be placed in this category.
Isopach Map
Thickness contour map.
Isopleth Map
General term for any map showing the areal distribution of some variable in terms of lines or contours of constant value.
K-Ar Date
Age determined by the potassium-argon dating method, a technique based on the measurement of the ratio of radiogenic ^{40}Ar to ^{40}K and the known radioactive decay rate of ^{40}K to ^{40}Ar.
Kipuka
Hawaiian word meaning an area entirely surrounded by a lava flow; a younger island.
Lapilli
Pyroclasts with a diameter between 2 and 64 mm. A single lapilli is a lapillus.
Lithic
In this report, this refers to the non-crystalline, non-vitric fraction of tephra.
Magma
Naturally occurring molten rock material prior to eruption; magma stored in a relatively shallow reservoir is known as a magma chamber.
Major Elements
Elements found in abundances greater than 1000 parts per million.

Mantle Bedding
Stratigraphic unit that blankets thee existing topography rather than being deposited horizontally; typical of airfall tephra deposits.

Near-Source Tephra Facies
Tephra deposits in the immediate vicinity of the eruptive vent. Characterized by a large pyroclast grain size, thick tephra deposits, and poor sorting of pyroclasts. Synonym for near-vent facies.

Palagonite
General term to describe the alteration products of basaltic glass.

Paleomagnetic Age
Age determined through the measurement of the direction of remanent magnetization.

Paleosol
Buried soil.

Ped
A naturally formed unit of soil structure.

Pleistocene
An epoch of the Quaternary Period that immediately precedes the Holocene. Began two to three million years ago and ended about 10,000 years ago. Synonymous with the ice age or glacial period.

Plinian Eruption
Explosive ejection of large volumes of ash and pumice, typically of a silicic composition. The resulting tephra dispersal may cover large areas. The 6850 B.P. eruption of Mount Mazama was a classic Plinian eruption.

Pompeii Effect
The notion that archaeological sites, when excavated, are the result of prehistoric behavior preserved at a point in time, rather than being the result of the interplay of often complex and long-term natural and cultural site formation and site modification processes.

Porphyritic
Texture of an igneous rock in which larger crystals are set in a fine-grained or glassy groundmass.

Primary Tephra Deposit
Deposit of volcanic tephra located in its original context. An undisturbed deposit of airfall tephra, for example, would be a primary airfall tephra deposit.

Primary Tephra Source
Original volcanic vent and associated landform from which tephra originated.

Principle of Original Horizontality
A general geological law. Most sediments are deposited in strata that are horizontal or nearly horizontal, and parallel or nearly parallel to the earth's surface.

Pumice
Highly vesicular pyroclasts with very low density and thin vesicle walls. Generally associated with silicic eruptions.

Pumice Lapilli
Pumice pyroclasts with a diameter ranging from 2 to 64 mm.

Pyroclast
Any fragment ejected during an explosive volcanic eruption.

Pyroclastic
Referring to clastic rocks formed by volcanic eruptions.

Pyroclastic Flow
Eruption cloud consisting of hot pyroclasts and gas, driven by gravity and moving across the ground as a flow. Many pyroclastic flows are generated by the near-vent collapse of particle-laden eruption clouds. The flows are capable of traveling at high speeds for distances of many tens of kilometers.

Pyroclastic Stratum
A single bed or stratum of pyroclastic material that is visibly set apart from contiguous layers by distinctive structural, textural, or compositional qualities.

Radiocarbon Years
Ages determined by the radiocarbon dating method. Because of fluctuations in global ^{14}C throughout the Holocene, radiocarbon ages and calendar ages are not equivalent. Radiocarbon ages can, however, be converted to their approximate calendar equivalents through dendrochronologic calibration (see Stuiver and Reimer, 1986).

Relative Age
Concerned with ascertaining the correct order or sequence of chronologic events.

Reworked
Redeposited; displaced by natural processes from its original (primary) context.

Rhyodacite/Rhyodacitic
A term often encountered in the geological literature of the High Cascades. Refers to rhyolitic igneous rocks with a silica content greater than 68 percent and a K_2O content less than 4 percent. In this report, these rocks are treated as a subset of silicic rhyolitic rocks. For a more detailed geochemical classification, see LeBas et al., 1986.

Rhyolite/Rhyolitic
As used in this report, an igneous rock with a silica content greater than 68 percent. For a more detailed geochemical definition, see LeBas et al., 1986.

Scoria
Vesicular, coarse-grained (lapilli-sized or larger) pyroclastic of basaltic to basaltic andesite composition. Synonymous with cinders.

Secondary Tephra Deposit
Tephra deposit that has been reworked or transported from its original primary context.

SEM
Scanning Electron Microscope.

Set
Groups of tephra layers distinguishable from adjacent layers of other sets by mineralogical or geochemical characteristics or by evidence of elapsed time.

Shard
A glass fragment (vitric pyroclast) broken from a vesicle wall; it may be flat, curved, blocky, or y-shaped, depending on the bubble wall segment from which it was broken.

Sideromelane
Basaltic glass; the brown glass of basaltic ash.

Silica
SiO_2; the chemically resistant dioxide of silica, a major constituent of volcanic glasses.

Silicic
A silica-rich igneous rock. Though there is no general agreement among petrologists, the amount of silica is usually said to be at least 65 percent.

Sourcing
Grammatically-incorrect synonym for characterization.

Strombolian Eruption
Weak to violent explosive eruptions of basaltic or andesitic magma; cinder cones are constructed during this type of eruptive activity.

Tachylite
Basaltic to andesitic pyroclasts consisting of very fine-grained minerals separated by glass.

Tephra
Collective term for all materials, regardless of size, that are ejected during an explosive volcanic eruption. Includes airfall tephra, ash flow deposits, base surge deposits, etc. The term (from the Greek for volcanic ash) was reintroduced by Thorarinsson, an Icelandic volcanologist, in 1944.

Tephragenic
Volcanic eruptive styles that produce tephra.

Tephrochronology/Tephrochronologic
The use of tephra layers for correlation and dating. Often used synonymous with tephrostratigraphy.

Tephrostratigraphy/Tephrostratigraphic
Definition, description, and age relationships of tephra layers.

Trace Elements
Elements found in abundances of less than 1000 parts per million.

Tuff
A general term for all well-consolidated pyroclastic rocks.

Vesicle
A cavity within a volcanic rock that is formed by the exsolution of volatile phases during eruption.

Vesicular
Volcanic rock texture characterized by the presence of abundant vesicles.

Vitric
Glassy; glassy fraction of tephra.

XRF
X-ray fluorescence.

APPENDIX TWO

AAS Data

APPENDIX 2: AAS DATA

	BELKC-4	BELKC-5	BELKC-6	BELKC-7	BELKC-9	BNASH-1	BNASH-2	BNASH-3	CARLL-1	COLLC-1
SIO2	47.53	49.68	50.78	46.66	50.02	52.40	53.17	50.92	53.09	54.75
TIO2	1.54	1.41	1.37	1.27	1.26	1.22	1.15	1.34	0.86	1.05
AL203	18.59	16.82	16.77	18.86	17.89	17.84	17.44	18.10	19.04	17.31
FE203	3.60	3.46	3.55	5.55	3.47	3.28	5.15	3.63	2.69	4.08
FEO	5.36	5.68	5.41	3.62	4.76	5.36	3.57	5.31	3.76	3.94
MNO	0.16	0.15	0.15	0.13	0.14	0.14	0.12	0.15	0.11	0.14
MGO	5.85	7.60	6.28	3.18	5.70	6.23	4.43	6.26	2.73	5.51
CAO	8.20	7.92	8.27	4.50	7.83	8.13	7.58	7.92	5.30	7.89
NA20	3.21	3.25	3.25	3.19	3.38	3.64	3.26	3.50	4.31	3.87
K20	0.68	0.71	0.98	0.76	0.77	0.77	0.72	0.72	0.85	0.82
H20+	1.53	0.69	1.03	0.69	1.03	0.18	1.46	1.07	3.76	0.65
H20-	2.26	1.81	1.39	1.47	1.45	0.18	1.20	1.01	3.50	0.14
P205	0.40	0.34	0.34	0.36	0.22	0.37	0.40	0.38	0.40	0.19
TOTAL	98.83	99.52	99.57	90.24	97.92	99.74	99.65	100.31	100.40	100.34
FE *	9.49	9.70	9.50	9.53	8.70	9.17	9.08	9.47	6.83	8.41
BA	211	210	396	337	326	277	277	305	349	244
CO	39	36	32	19	28	38	26	36	18	33
CR	117	138	157	55	91	105	108	107	35	74
CU	56	64	54	62	56	53	47	63	33	54
NI	94	160	87	29	46	172	85	140	20	110
RB	11	12	15	18	13	11	11	11	18	13
SR	479	520	658	593	585	755	686	697	771	521
ZN	80	77	83	91	78	97	81	94	80	79

* TOTAL FE AS FE203
MAJOR ELEMENT ABUNDANCES REPORTED AS WEIGHT PERCENT OXIDES
TRACE ELEMENT ABUNDANCES REPORTED IN PARTS PER MILLION

Table 11. Results of atomic absorption spectrophotometry (AAS) analysis of tephra samples. These major element data were normalized to 100 percent (water-free) for analysis (see table 8). A Lotus 1-2-3 compatible spreadsheet file containing the AAS data (AAS.WKS) is located in the back pocket of the Tephra Overview. The data may be examined with As-Easy-As 4.0, a shareware spreadsheet included with the data files (see Appendix 5 for spreadsheet details).

	COLLC-2	COLLC-3	COLLC-4	FORKB-1	FORKB-2	FORKB-3	FORKB-4	LNASH-1	LNASH-2	LNASH-3
SIO2	55.64	52.78	53.70	48.32	45.83	48.58	46.96	49.51	51.89	52.04
TIO2	0.88	0.67	0.85	1.16	1.15	1.05	1.19	1.22	1.38	1.19
AL203	19.16	17.60	18.71	19.05	20.31	19.91	19.82	18.88	18.38	18.13
FE203	2.86	2.28	2.54	3.58	4.97	3.23	4.29	4.56	7.26	6.79
FEO	3.52	4.28	4.17	5.14	4.33	4.73	4.65	4.73	1.58	2.05
MNO	0.11	0.12	0.12	0.15	0.14	0.14	0.16	0.16	0.15	0.14
MGO	4.38	6.17	4.25	6.62	5.37	5.97	6.93	6.62	5.74	5.90
CAO	7.53	8.11	6.37	6.99	6.38	7.45	7.08	7.77	8.21	8.33
NA20	3.86	3.44	3.70	3.04	2.81	3.22	2.91	3.35	4.35	4.11
K20	0.88	0.76	0.90	0.64	0.59	0.63	0.50	0.70	0.87	0.88
H20+	0.73	0.67	1.39	2.34	3.45	3.30	1.97	2.02	0.10	0.18
H20-	0.31	0.36	1.44	1.86	3.54	1.78	1.54	1.33	0.16	0.15
P205	0.12	0.16	0.15	0.40	0.33	0.34	0.39	0.44	0.39	0.40
TOTAL	99.98	97.40	98.29	99.29	99.20	100.33	98.39	100.44	100.46	100.29
FE *	6.73	6.98	7.13	9.23	9.73	8.43	9.40	9.76	8.99	9.04
BA	238	244	227	186	177	250	186	294	360	344
CO	28	32	29	37	38	38	43	41	38	36
CR	61	60	55	226	141	170	207	108	109	105
CU	47	49	52	47	51	45	57	61	66	78
NI	85	160	101	159	112	127	164	134	134	125
RB	17	18	18	10	11	11	9	11	12	12
SR	533	489	473	543	530	561	574	695	700	716
ZN	65	69	67	72	79	74	71	96	95	92

* TOTAL FE AS FE203
MAJOR ELEMENT ABUNDANCES REPORTED AS WEIGHT PERCENT OXIDES
TRACE ELEMENT ABUNDANCES REPORTED IN PARTS PER MILLION

Table 11 (Continued). Results of AAS analysis of tephra samples.

	LNASH-5	LNASH-6	LOSTL-2	LOSTL-3	LOSTL-4	LOSTL-5	MAZA-2	MAZA-5	MAZA-8	MAZA-9
SIO2	50.05	46.23	45.35	49.80	48.88	49.69	56.80	67.36	62.69	62.69
TIO2	1.31	1.08	1.51	1.32	1.47	1.18	0.54	0.54	0.50	0.55
AL203	17.27	18.81	17.39	16.12	16.93	16.26	19.82	15.41	17.04	17.04
FE203	4.04	4.53	4.00	2.97	3.53	3.32	1.29	2.25	1.90	1.87
FEO	5.08	3.78	5.71	6.38	5.88	6.16	1.84	1.14	1.24	1.14
MNO	0.14	0.13	0.16	0.16	0.16	0.15	0.06	0.06	0.07	0.06
MGO	7.25	4.55	9.13	10.15	8.76	9.53	0.55	0.87	0.84	0.64
CAO	7.67	4.46	7.60	8.62	8.27	8.48	1.92	2.43	2.43	2.33
NA20	3.47	2.63	2.66	3.21	3.07	3.19	3.80	4.97	4.32	4.11
K20	0.74	0.64	0.55	0.77	0.64	0.78	1.78	2.40	2.03	1.98
H20+	1.63	3.81	3.63	0.26	1.23	0.54	5.46	2.01	4.67	3.35
H20-	1.39	8.55	2.04	0.26	1.27	0.63	5.58	0.63	2.41	4.04
P205	0.38	0.36	0.34	0.34	0.34	0.34	0.36	0.20	0.26	0.29
TOTAL	100.42	99.56	100.06	100.36	100.43	100.25	99.80	100.27	100.40	100.09
FE *	9.63	8.69	10.28	9.99	10.00	10.10	3.31	3.50	3.27	3.12
BA	337	256	294	288	272	291	512	698	629	593
CO	36	32	48	48	46	39	8	4	3	7
CR	116	100	164	165	175	162	15	15	15	19
CU	58	48	70	65	61	64	15	21	19	18
NI	171	85	222	238	202	181	4	7	6	7
RB	11	12	9	12	10	11	33	47	36	38
SR	757	422	624	665	637	701	266	404	335	376
ZN	87	93	83	82	83	77	46	50	51	48

* TOTAL FE AS FE203
MAJOR ELEMENT ABUNDANCES REPORTED AS WEIGHT PERCENT OXIDES
TRACE ELEMENT ABUNDANCES REPORTED IN PARTS PER MILLION

Table 11 (Continued). Results of AAS analysis of tephra samples.

	NEWBE-1	ROCKM-1	ROCKM-2	ROCKM-3	ROCKM-4	SANDM-1B	SANDM-2	SANDM-3	SANDM-5	SCINP-1
SIO2	70.79	71.28	70.65	70.07	70.70	48.94	52.22	49.70	50.66	47.30
TIO2	0.37	0.33	0.37	0.30	0.35	1.00	1.22	1.57	1.27	1.46
AL203	14.16	13.74	13.79	14.00	14.47	18.02	18.54	17.18	18.06	19.23
FE203	0.65	0.75	0.77	0.81	0.68	3.67	3.46	3.54	3.50	4.79
FEO	1.62	1.35	1.35	1.35	1.48	4.89	4.57	5.36	5.10	4.85
MNO	0.06	0.05	0.05	0.05	0.06	0.15	0.14	0.16	0.15	0.16
MGO	0.57	0.49	0.50	0.60	0.54	6.94	5.59	7.52	6.83	5.94
CAO	1.98	1.81	1.76	1.91	2.10	8.28	8.55	9.26	8.96	6.66
NA2O	4.37	4.21	4.14	4.23	4.48	3.24	3.62	3.17	3.29	2.86
K2O	2.97	3.14	3.15	3.10	2.97	0.66	0.76	0.75	0.79	0.62
H2O+	1.95	2.79	2.64	2.83	1.86	1.53	0.53	0.70	0.63	2.46
H2O-	0.72	0.15	0.45	0.31	0.30	2.21	0.57	0.90	0.85	3.66
P2O5	0.15	0.16	0.13	0.13	0.16	0.35	0.35	0.36	0.37	0.37
TOTAL	100.36	100.25	99.75	99.69	100.15	99.88	100.12	100.17	100.47	100.36
FE *	2.43	2.24	2.26	2.30	2.31	9.04	8.49	9.44	9.11	10.12
BA	756	756	756	756	745	305	366	266	311	244
CO	1	1	1	1	1	41	35	41	38	36
CR	18	15	16	15	16	134	97	148	127	139
CU	8	8	8	9	9	54	55	65	57	57
NI	4	2	4	4	6	130	83	134	108	122
RB	66	70	76	75	71	10	11	11	11	11
SR	211	187	202	205	222	895	909	781	897	511
ZN	42	40	42	38	42	83	115	79	81	76

* TOTAL FE AS FE203
MAJOR ELEMENT ABUNDANCES REPORTED AS WEIGHT PERCENT OXIDES
TRACE ELEMENT ABUNDANCES REPORTED IN PARTS PER MILLION

Table 11 (Continued). Results of AAS analysis of tephra samples.

	SCINP-2	SCINP-3	SCINP-4	SSDCH-1	SSDCH-3	SSDCH-6	YAPOA-1	YAPOA-3	YAPOA-4	YAPOA-6
SIO2	46.90	46.53	46.11	71.68	71.10	70.49	53.67	54.99	54.50	53.79
TIO2	1.47	1.49	1.57	0.36	0.34	0.35	1.04	0.99	0.90	0.98
AL203	18.80	18.41	20.03	14.33	14.49	14.38	18.01	18.00	18.86	18.32
FE203	4.58	4.32	4.69	0.86	0.79	0.91	2.45	3.10	2.37	3.27
FEO	4.81	4.94	4.84	1.43	1.41	1.41	4.42	4.74	4.21	4.26
MNO	0.17	0.17	0.16	0.06	0.06	0.06	0.13	0.15	0.12	0.13
MGO	6.37	6.38	6.25	0.61	0.53	0.64	5.08	4.92	5.06	5.24
CAO	7.12	6.99	7.14	1.97	2.01	2.06	6.98	7.41	7.49	7.08
NA2O	2.90	3.08	2.97	4.57	4.50	4.43	3.75	3.85	3.71	3.64
K2O	0.65	0.64	0.63	2.93	2.91	2.96	0.91	0.94	0.84	0.91
H2O+	2.34	2.56	2.60	1.30	1.78	1.95	0.76	1.02	0.81	1.20
H2O-	3.04	3.01	2.68	0.08	0.31	0.15	0.55	0.51	0.54	1.11
P2O5	0.37	0.40	0.42	0.11	0.14	0.13	0.19	0.28	0.14	0.25
TOTAL	99.52	98.92	100.09	100.29	100.37	100.24	97.94	100.47	99.55	100.18
FE *	9.87	9.76	10.01	2.45	2.34	2.46	7.31	8.31	7.00	7.95
BA	244	261	277	756	756	733	283	279	255	261
CO	37	38	42	TR	TR	TR	31	30	31	30
CR	128	126	140	14	15	14	55	78	57	68
CU	59	54	60	10	9	8	53	64	53	57
NI	144	130	150	0	2	2	105	41	110	75
RB	11	11	12	67	63	71	18	16	17	19
SR	535	573	596	225	214	207	514	510	521	530
ZN	79	103	91	40	42	37	69	72	68	73

* TOTAL FE AS FE203
MAJOR ELEMENT ABUNDANCES REPORTED AS WEIGHT PERCENT OXIDES
TRACE ELEMENT ABUNDANCES REPORTED IN PARTS PER MILLION

Table 11 (Continued). Results of AAS analysis of tephra samples.

	STANDARDS - THIS STUDY				STANDARDS - ACCEPTED VALUES			
	AGV-1	DNC-1	JG-1	W-2	AGV-1	DNC-1	JG-1	W-2
SIO2	59.09	47.20	72.30	52.27	59.00	47.15	72.30	52.68
TIO2	1.00	0.47	0.27	1.09	1.04	0.48	0.26	1.06
AL203	16.99	18.31	14.44	15.47	17.25	18.34	14.20	15.45
FE203	4.55	1.97	0.36	1.56	4.51	1.79	0.39	1.53
FEO	2.00	7.25	1.62	8.40	2.05	7.32	1.63	8.34
MNO	0.10	0.15	0.06	0.17	0.10	0.15	0.06	0.17
MGO	1.53	10.15	0.77	6.42	1.53	10.13	0.74	6.37
CAO	4.92	11.29	2.18	10.89	4.90	11.49	2.18	10.86
NA20	4.25	1.90	3.36	2.19	4.26	1.89	3.39	2.20
K20	2.90	0.23	3.96	0.63	2.89	0.23	3.95	0.63
H20+	0.78	0.65	0.28	0.45	0.81	0.73	0.48	0.55
H20-	1.18	0.44	0.16	0.33	1.03	0.29	0.07	0.25
P205	0.49	0.09	0.10	0.14	0.49	0.07	0.10	0.14
TOTAL	99.68	100.40	99.86	100.34	99.86	100.06	99.75	100.23
FE *	6.75	9.94	2.14	10.80	6.76	9.93	2.14	10.80
BA	1210	116	490	175	1208	118	462	174
CO	15	57	3	43	14	57	4	43
CR	21	267	47	97	12	270	53	92
CU	60	98	4	106	60	100	2	106
NI	13	247	7	70	19	247	6	70
RB	67	7	181	21	67	5	181	21
SR	657	144	178	198	657	144	184	192
ZN	89	67	43	79	86	70	41	80

* TOTAL FE AS FE203
MAJOR ELEMENT ABUNDANCES REPORTED AS WEIGHT PERCENT OXIDES
TRACE ELEMENT ABUNDANCES REPORTED IN PARTS PER MILLION

Table 11 (Continued). Results of AAS analysis of tephra samples.

APPENDIX THREE

EPMA Data

APPENDIX 3: EPMA DATA

Sample # Point #	BELKC-7 1	BELKC-7 2	BELKC-7 3	BELKC-7 4	BELKC-7 5	BELKC-7 6	AVERAGE BELKC-7	100% NORM BELKC-7 (A)	S.D. BELKC-7 (B)	CV% BELKC-7 (C)
SiO2	72.67	72.17	73.14	72.70	72.20	72.35	72.54	74.16	0.34	0.5
TiO2	0.40	0.43	0.36	0.43	0.44	0.36	0.40	0.41	0.03	8.2
Al2O3	13.99	14.55	14.10	14.45	14.23	14.54	14.31	14.63	0.22	1.5
MgO	0.37	0.47	0.43	0.43	0.49	0.45	0.44	0.45	0.04	8.5
CaO	1.42	1.52	1.35	1.59	1.59	1.58	1.51	1.54	0.09	6.0
MnO	0.07	0.07	0.06	0.08	0.04	0.09	0.07	0.07	0.02	23.4
FeO	1.67	1.85	1.87	1.93	1.92	1.94	1.86	1.90	0.09	4.9
Na2O	3.83	3.95	3.85	3.65	3.57	3.89	3.79	3.87	0.13	3.6
K2O	2.71	2.87	2.79	3.04	2.94	3.06	2.90	2.97	0.13	4.4
Total	97.12	97.87	97.95	98.29	97.41	98.25	97.81	100.00		
Si % Error	0.8	0.8	0.8	0.8	0.8	0.8				
Ti % Error	10.3	10.1	11.5	10.3	9.7	11.3				
Al % Error	0.9	0.9	0.9	0.9	0.9	0.9				
Mg % Error	7.2	5.9	6.3	6.6	6.1	6.4				
Ca % Error	2.8	2.7	2.9	2.7	2.6	2.6				
Mn % Error	35.5	35.6	42.4	31.8	66.8	31.0				
Fe % Error	7.2	7.0	7.0	6.6	6.6	6.5				
Na % Error	2.5	2.5	2.5	2.6	2.6	2.5				
K % Error	1.9	1.8	1.9	1.8	1.8	1.8				

• Major element abundances reported as weight percent oxides
(A) Average value normalized to 100 percent; this figure was used for visual and statistical analysis
(B) Standard deviation of all sample points
(C) Coefficient of variation = standard deviation / average x 100

Table 12a. Results of electron microprobe analysis of tephra shards from sample BELKC-7, a Mazama paleosol from the Belknap Crater area. Average values (normalized to 100 percent) of six analyzed points for each sample reported in this appendix were used for analysis in Section 6 (see table 10). A Lotus 1-2-3 compatible spreadsheet file containing the EPMA data (EPMA.WKS) is located in the back pocket of the Tephra Overview. These data may be examined with As-Easy-As 4.0, a shareware spreadsheet included with the data files (see Appendix 5 for spreadsheet details).

Sample # Point #	CARLL-1 1	CARLL-1 2	CARLL-1 3	CARLL-1 4	CARLL-1 5	CARLL-1 6	AVERAGE CARLL-1	100% NORM CARLL-1 (A)	S.D. CARLL-1 (B)	CV% CARLL-1 (C)
SiO2	73.30	72.89	72.27	72.78	72.03	67.82	71.85	73.33	1.85	2.6
TiO2	0.37	0.44	0.39	0.41	0.46	0.56	0.44	0.45	0.06	14.5
Al2O3	14.51	14.68	14.70	14.32	14.30	15.58	14.68	14.98	0.43	2.9
MgO	0.53	0.45	0.44	0.48	0.45	1.05	0.57	0.58	0.22	38.1
CaO	1.55	1.58	1.61	1.61	1.53	2.67	1.76	1.79	0.41	23.2
MnO	0.07	0.06	0.11	0.06	0.06	0.07	0.07	0.07	0.02	26.2
FeO	1.64	1.89	1.75	1.98	1.83	3.67	2.13	2.17	0.70	32.9
Na2O	3.88	3.70	3.76	3.75	3.59	4.34	3.84	3.92	0.24	6.2
K2O	2.75	2.76	2.70	2.78	2.68	2.23	2.65	2.71	0.19	7.2
Total	98.59	98.45	97.74	98.18	96.93	98.00	97.98	100.00		
Si % Error	0.8	0.8	0.8	0.8	0.8	0.8				
Ti % Error	10.9	9.9	10.5	10.5	9.2	8.4				
Al % Error	0.9	0.9	0.9	0.9	0.9	0.9				
Mg % Error	5.5	6.4	6.4	5.6	6.1	3.8				
Ca % Error	2.7	2.6	2.6	2.6	2.7	2.0				
Mn % Error	40.2	44.2	22.6	43.9	44.8	39.6				
Fe % Error	7.5	6.7	7.2	6.5	6.9	4.7				
Na % Error	2.5	2.6	2.5	2.6	2.6	2.4				
K % Error	1.9	1.9	1.9	1.9	1.9	2.1				

- Major element abundances reported as weight percent oxides

(A) Average value normalized to 100 percent; this figure was used for visual and statistical analysis
(B) Standard deviation of all sample points
(C) Coefficient of variation = standard deviation / average x 100

Table 12b (Continued). Results of electron microprobe analysis of tephra shards from sample CARLL-1, a Mazama paleosol from the Mount Jefferson area of the High Cascades.

Sample # Point #	LNASH-6 1	LNASH-6 2	LNASH-6 3	LNASH-6 4	LNASH-6 5	LNASH-6 6	AVERAGE LNASH-6	100% NORM LNASH-6 (A)	S.D. LNASH-6 (B)	CV% LNASH-6 (C)
SiO2	72.10	71.45	70.30	72.88	70.43	70.93	71.35	73.87	0.92	1.3
TiO2	0.39	0.38	0.39	0.45	0.45	0.36	0.40	0.41	0.03	8.6
Al2O3	14.38	14.48	14.21	14.61	14.13	14.05	14.31	14.81	0.20	1.4
MgO	0.53	0.47	0.45	0.46	0.51	0.49	0.49	0.50	0.03	5.9
CaO	1.70	1.60	1.64	1.72	1.71	1.64	1.67	1.73	0.04	2.6
MnO	0.07	0.06	0.06	0.05	0.07	0.06	0.06	0.06	0.01	9.8
FeO	1.91	1.64	1.72	1.84	2.10	2.01	1.87	1.94	0.16	8.4
Na2O	3.58	3.52	2.87	3.72	2.65	3.22	3.26	3.37	0.39	11.9
K2O	3.26	3.30	3.07	3.34	3.08	3.05	3.18	3.30	0.12	3.7
Total	97.91	96.90	94.71	99.06	95.13	95.81	96.59	100.00		
Si % Error	0.8	0.8	0.8	0.8	0.8	0.8				
Ti % Error	11.0	11.0	10.4	9.7	9.4	11.7				
Al % Error	0.9	0.9	0.9	0.9	0.9	0.9				
Mg % Error	5.4	6.1	6.5	6.2	5.7	5.8				
Ca % Error	2.5	2.6	2.6	2.5	2.5	2.6				
Mn % Error	37.2	45.3	42.6	51.8	37.7	45.1				
Fe % Error	6.8	7.6	7.4	6.7	6.3	6.6				
Na % Error	2.6	2.6	2.9	2.6	3.0	2.7				
K % Error	1.7	1.7	1.8	1.7	1.8	1.8				

* Major element abundances reported as weight percent oxides
(A) Average value normalized to 100 percent; this figure was used for visual and statistical analysis
(B) Standard deviation of all sample points
(C) Coefficient of variation = standard deviation / average x 100

Table 12c (Continued). Results of electron microprobe analysis of tephra shards from sample LNASH-6, a Mazama paleosol from the Little Nash Crater area of the Western Cascades.

Sample # Point #	MAZA-5 1	MAZA-5 2	MAZA-5 3	MAZA-5 4	MAZA-5 5	MAZA-5 6	AVERAGE MAZA-5	100% NORM MAZA-5 (A)	S.D. MAZA-5 (B)	CV% MAZA-5 (C)
SiO2	71.75	71.93	72.02	72.78	72.38	72.36	72.20	74.27	0.34	0.5
TiO2	0.32	0.41	0.40	0.43	0.43	0.37	0.39	0.40	0.04	10.1
Al2O3	14.26	13.84	13.93	14.21	14.19	13.95	14.06	14.47	0.16	1.1
MgO	0.47	0.44	0.43	0.42	0.44	0.45	0.44	0.45	0.01	3.3
CaO	1.42	1.47	1.53	1.46	1.57	1.48	1.49	1.53	0.05	3.1
MnO	0.04	0.05	0.10	0.09	0.06	0.03	0.06	0.06	0.03	44.0
FeO	1.98	1.78	1.78	1.70	1.92	1.91	1.85	1.90	0.10	5.3
Na2O	3.90	4.22	3.91	3.80	4.05	3.95	3.97	4.09	0.13	3.3
K2O	2.77	2.72	2.68	2.82	2.83	2.70	2.75	2.83	0.06	2.1
Total	96.92	96.85	96.78	97.72	97.85	97.19	97.22	100.00		
Si % Error	0.8	0.8	0.8	0.8	0.8	0.8				
Ti % Error	12.7	9.7	10.8	10.0	9.5	11.1				
Al % Error	1.0	1.0	1.0	1.0	1.0	1.0				
Mg % Error	6.3	6.5	6.3	6.7	6.4	6.3				
Ca % Error	2.9	2.8	2.8	2.8	2.7	2.8				
Mn % Error	63.9	49.2	25.0	29.9	42.4	97.5				
Fe % Error	6.8	7.2	7.2	7.5	7.0	6.8				
Na % Error	2.5	2.4	2.4	2.5	2.4	2.4				
K % Error	2.0	2.0	2.1	2.0	2.0	2.1				

- Major element abundances reported as weight percent oxides

(A) Average value normalized to 100 percent; this figure was used for visual and statistical analysis

(B) Standard deviation of all sample points

(C) Coefficient of variation = standard deviation / average x 100

Table 12d (Continued). Results of electron microprobe analysis of tephra shards from sample MAZA-5, a pumice lapillus originating from Mount Mazama.

Sample # / Point #	MAZA-8 1	MAZA-8 2	MAZA-8 3	MAZA-8 4	MAZA-8 5	MAZA-8 6	AVERAGE MAZA-8	100% NORM MAZA-8 (A)	S.D. MAZA-8 (B)	CV% MAZA-8 (C)
SiO2	72.70	72.98	72.50	72.05	72.26	72.64	72.52	74.08	0.30	0.4
TiO2	0.34	0.37	0.35	0.35	0.38	0.42	0.37	0.38	0.03	7.2
Al2O3	14.26	14.47	14.55	14.27	14.72	14.20	14.41	14.72	0.18	1.3
MgO	0.44	0.45	0.47	0.45	0.51	0.45	0.46	0.47	0.02	4.9
CaO	1.56	1.60	1.52	1.62	1.52	1.53	1.56	1.59	0.04	2.5
MnO	0.08	0.04	0.11	0.04	.00	0.00	0.05	0.05	0.04	88.2
FeO	1.93	1.82	1.87	1.85	1.93	2.15	1.93	1.97	0.11	5.7
Na2O	3.97	3.98	3.99	3.94	3.57	3.61	3.84	3.92	0.18	4.7
K2O	2.82	2.82	2.73	2.72	2.70	2.80	2.77	2.83	0.05	1.8
Total	98.10	98.53	98.09	97.28	97.59	97.79	97.90	100.00		
Si % Error	0.8	0.8	0.8	0.8	0.8	0.8				
Ti % Error	12.7	11.3	12.4	12.2	11.0	10.4				
Al % Error	1.0	1.0	1.0	1.0	1.0	1.0				
Mg % Error	6.7	6.7	6.2	6.2	5.8	6.2				
Ca % Error	2.7	2.7	2.8	2.7	2.8	2.8				
Mn % Error	32.8	61.2	23.9	67.6	-1.0	-1.0				
Fe % Error	6.8	7.2	7.1	7.1	6.9	6.5				
Na % Error	2.4	2.4	2.4	2.4	2.5	2.5				
K % Error	2.0	2.0	2.1	2.1	2.1	2.0				

- Major element abundances reported as weight percent oxides

(A) Average value normalized to 100 percent; this figure was used for visual and statistical analysis

(B) Standard deviation of all sample points

(C) Coefficient of variation = standard deviation / average x 100

Table 12e (Continued). Results of electron microprobe analysis of tephra shards from sample MAZA-8, a pumice lapillus originating from Mount Mazama.

Sample # / Point #	MAZA-9 1	MAZA-9 2	MAZA-9 3	MAZA-9 4	MAZA-9 5	MAZA-9 6	AVERAGE MAZA-9	100% NORM MAZA-9 (A)	S.D. MAZA-9 (B)	CV% MAZA-9 (C)
SiO2	70.67	71.80	73.01	73.97	71.50	71.69	72.11	74.66	1.08	1.5
TiO2	0.38	0.41	0.40	0.38	0.46	0.33	0.39	0.41	0.04	9.3
Al2O3	14.12	14.05	14.71	14.53	14.18	13.94	14.26	14.76	0.27	1.9
MgO	0.47	0.41	0.43	0.43	0.44	0.45	0.44	0.45	0.02	4.1
CaO	1.72	1.39	1.62	1.58	1.53	1.60	1.57	1.63	0.10	6.3
MnO	0.06	0.07	0.04	0.05	0.08	0.07	0.06	0.06	0.01	19.1
FeO	1.81	1.86	2.08	1.64	1.84	1.75	1.83	1.90	0.13	7.2
Na2O	3.71	2.29	3.91	1.92	3.67	3.39	3.15	3.26	0.76	24.2
K2O	2.78	2.81	2.77	2.88	2.70	2.71	2.77	2.87	0.06	2.2
Total	95.72	95.09	98.98	97.38	96.38	95.94	96.58	100.00		
Si % error	0.7	0.7	0.7	0.8	0.8	0.8				
Ti % error	13.6	13.1	13.6	10.8	9.4	12.9				
Al % error	1.0	1.0	1.0	1.0	1.0	1.0				
Mg % error	7.1	7.7	7.1	6.6	6.3	6.1				
Ca % error	3.5	4.0	3.6	2.7	2.8	2.7				
Mn % error	42.2	34.1	53.4	47.9	32.0	36.0				
Fe % error	6.7	6.6	6.2	7.6	7.1	7.3				
Na % error	2.6	3.3	2.5	3.3	2.5	2.6				
K % error	2.7	2.7	2.7	2.0	2.1	2.1				

* Major element abundances reported as weight percent oxides
(A) Average value normalized to 100 percent; this figure was used for visual and statistical analysis
(B) Standard deviation of all sample points
(C) Coefficient of variation = standard deviation / average x 100

Table 12f (Continued). Results of electron microprobe analysis of tephra shards from sample MAZA-9, a pumice lapillus originating from Mount Mazama.

	NEWBE-1 1	NEWBE-1 2	NEWBE-1 3	NEWBE-1 4	NEWBE-1 5	NEWBE-1 6	AVERAGE NEWBE-1	100% NORM NEWBE-1 (A)	S.D. NEWBE-1 (B)	CV% NEWBE-1 (C)
SiO2	68.90	69.88	71.51	65.74	71.42	67.46	69.15	71.05	2.07	3.0
TiO2	0.14	0.15	0.19	0.09	0.18	0.12	0.15	0.15	0.03	22.6
Al2O3	17.94	15.55	14.13	18.71	15.24	17.46	16.50	16.96	1.63	9.9
MgO	0.17	0.10	0.15	0.06	0.17	0.23	0.15	0.15	0.05	35.9
CaO	3.02	2.16	1.69	3.64	1.94	3.00	2.58	2.65	0.69	26.8
MnO	0.03	0.04	0.05	0.03	0.03	0.05	0.04	0.04	0.01	24.0
FeO	1.05	1.03	1.16	0.84	1.27	0.93	1.05	1.07	0.14	13.5
Na2O	5.96	4.92	4.12	6.12	4.44	6.15	5.28	5.43	0.83	15.6
K2O	2.09	2.69	2.99	1.71	3.02	2.09	2.43	2.50	0.50	20.4
Total	99.29	96.52	96.00	96.93	97.72	97.49	97.32	100.00		
Si % Error	0.8	0.8	0.8	0.8	0.8	0.8				
Ti % Error	24.3	22.3	18.4	30.5	19.4	27.4				
Al % Error	0.9	1.0	1.0	0.9	1.0	0.9				
Mg % Error	13.0	19.8	13.6	30.1	12.3	9.7				
Ca % Error	2.0	2.3	2.6	1.8	2.4	2.0				
Mn % Error	65.7	56.7	46.9	87.6	73.4	51.3				
Fe % Error	9.8	9.9	8.9	10.9	8.9	11.1				
Na % Error	2.1	2.2	2.4	2.1	2.3	2.0				
K % Error	2.3	2.1	2.0	2.5	2.0	2.3				

- Major element abundances reported as weight percent oxides

(A) Average value normalized to 100 percent; this figure was used for visual and statistical analysis

(B) Standard deviation of all sample points

(C) Coefficient of variation = standard deviation / average x 100

Table 12g (Continued). Results of electron microprobe analysis of tephra shards from sample NEWBE-1, a pumice lapillus originating from the Devils Hill Chain of Domes, South Sister volcano.

Sample # Point #	ROCKM-1 1	ROCKM-1 2	ROCKM-1 3	ROCKM-1 4	ROCKM-1 5	ROCKM-1 6	AVERAGE ROCKM-1	100% NORM ROCKM-1 (A)	S.D. ROCKM-1 (B)	CV% ROCKM-1 (C)
SiO2	74.65	74.88	75.08	74.76	75.50	75.06	74.99	77.40	0.28	0.4
TiO2	0.16	0.18	0.14	0.21	0.18	0.21	0.18	0.18	0.02	13.7
Al2O3	12.29	12.54	12.32	12.44	12.66	12.36	12.43	12.83	0.13	1.0
MgO	0.15	0.20	0.14	0.18	0.17	0.14	0.16	0.17	0.02	13.0
CaO	0.96	0.85	0.92	0.86	0.89	0.94	0.90	0.93	0.04	4.4
MnO	0.03	0.02	0.02	0.02	0.05	0.03	0.03	0.03	0.01	41.3
FeO	1.16	1.23	0.92	1.20	1.08	1.34	1.15	1.19	0.13	11.5
Na2O	3.10	3.34	3.27	3.16	3.33	3.44	3.27	3.38	0.11	3.5
K2O	3.77	3.83	3.70	3.75	3.86	3.68	3.77	3.89	0.06	1.7
Total	96.26	97.06	96.51	96.59	97.72	97.20	96.89	100.00		
Si % Error	0.8	0.8	0.8	0.8	0.8	0.8				
Ti % Error	20.8	18.7	25.0	16.9	18.6	16.1				
Al % Error	1.1	1.1	1.1	1.1	1.1	1.1				
Mg % Error	15.1	11.3	16.0	11.5	13.0	14.9				
Ca % Error	3.5	3.9	3.7	3.7	3.7	3.6				
Mn % Error	84.4	-1.0	-1.0	-1.0	48.9	83.9				
Fe % Error	9.3	8.8	11.1	8.9	9.6	8.5				
Na % Error	2.7	2.6	2.6	2.7	2.6	2.6				
K % Error	1.8	1.8	1.8	1.8	1.8	1.8				

- Major element abundances reported as weight percent oxides

(A) Average value normalized to 100 percent; this figure was used for visual and statistical analysis

(B) Standard deviation of all sample points

(C) Coefficient of variation = standard deviation / average x 100

Table 12h (Continued). Results of electron microprobe analysis of tephra shards from sample ROCKM-1, a pumice lapillus originating from the Devils Hill Chain of Domes, South Sister volcano.

Sample # / Point #	ROCKM-4 1	ROCKM-4 2	ROCKM-4 3	ROCKM-4 4	ROCKM-4 5	ROCKM-4 6	AVERAGE ROCKM-4	100% NORM ROCKM-4 (A)	S.D. ROCKM-4 (B)	CV% ROCKM-4 (C)
SiO2	76.48	76.01	77.41	77.10	76.96	75.59	76.59	77.05	0.64	0.8
TiO2	0.19	0.29	0.27	0.33	0.25	0.23	0.26	0.26	0.04	17.0
Al2O3	13.01	13.01	12.73	12.88	13.34	12.86	12.97	13.05	0.19	1.5
MgO	0.30	0.20	0.15	0.15	0.18	0.13	0.19	0.19	0.06	31.0
CaO	0.93	0.93	0.94	0.88	0.93	0.85	0.91	0.91	0.03	3.7
MnO	0.07	0.02	0.04	0.04	0.04	0.05	0.04	0.04	0.01	31.5
FeO	1.51	1.25	1.38	1.24	1.24	1.27	1.31	1.32	0.10	7.7
Na2O	3.39	3.49	3.44	3.35	3.33	3.28	3.38	3.40	0.07	2.0
K2O	3.70	3.79	3.81	3.74	3.74	3.77	3.76	3.78	0.03	0.9
Total	99.58	98.99	100.16	99.71	100.00	98.02	99.41	100.00		
Si % Error	0.8	0.8	0.8	0.8	0.8	0.8				
Ti % Error	18.8	13.4	13.8	11.2	14.6	15.9				
Al % Error	1.0	1.0	1.0	1.0	1.0	1.0				
Mg % Error	8.1	10.5	14.5	13.3	11.6	16.1				
Ca % Error	3.6	3.6	3.6	3.7	3.6	3.8				
Mn % Error	35.6	-1.0	59.1	62.8	56.1	45.1				
Fe % Error	7.9	9.3	8.3	8.8	9.0	9.0				
Na % Error	2.6	2.6	2.5	2.6	2.6	2.6				
K % Error	1.8	1.8	1.8	1.8	1.8	1.8				

* Major element abundances reported as weight percent oxides
(A) Average value normalized to 100 percent; this figure was used for visual and statistical analysis
(B) Standard deviation of all sample points
(C) Coefficient of variation = standard deviation / average x 100

Table 12i (Continued). Results of electron microprobe analysis of tephra shards from sample ROCKM-4, a pumice lapillus originating from the Devils Hill Chain of Domes, South Sister volcano.

APPENDIX FOUR

Tephra Sample Locations and Descriptions

APPENDIX 4: TEPHRA SAMPLE LOCATIONS AND DESCRIPTIONS

Samples described in this appendix were those that were used in the geochemical characterization studies reported in Section V. See figure 36 for the general location of all samples described in this appendix.

BELKC-4 BELKNAP CRATER TEPHRA

Location: Sec.20, T.15S., R.8E; Deschutes County.
USGS Map: Mt. Washington (1988)
Description: Fine basaltic ash from unit 1 of a test pit in a kipuka crossed by the Pacific Crest Trail immediately north of Highway 242 (McKenzie Pass Highway). Collected from the profile between 0-23 cm below the surface (see figure 35). Located about 3.4 km SE of Belknap Crater. From the same sampling location as BELKC-5, BELKC-6, and BELKC-7. Most Recent tephra surface is locally overlain by a lava flow from Yapoah Crater.

BELKC-5 BELKNAP CRATER TEPHRA

Location: Sec.20, T.15S., R.8E.; Deschutes County.
USGS Map: Mt. Washington (1988)
Description: Unconsolidated pea to gravel-sized basaltic scoria from unit 2 of the kipuka test pit. Collected from 23-30 cm below the surface (figure 35). Located about 3.4 km SE of Belknap Crater. Probably represents the early stages of the same eruptive event that produced the immediately overlying stratum of tephra (BELKC-4). From same sampling location as BELKC-4, BELKC-6, and BELKC-7.

BELKC-6 MAZAMA TEPHRA PALEOSOL

Location: Sec.20, T.15S., R.8E.; Deschutes County.
USGS Map: Mt. Washington (1988)
Description: Tephra-derived paleosol from unit 3 of the kipuka test pit. Collected from 30-50 cm below the surface (figure 35). This soil appears to be an A horizon developed on Mazama tephra. The paleosol was initially mistaken for an earlier eruptive unit from Belknap Crater. From the same sampling location as BELKC-4, BELKC-5, and BELKC-7.

BELKC-7 MAZAMA TEPHRA

Location: Sec.20, T.15S., R.8E.; Deschutes County.
USGS Map: Mt. Washington (1988)
Description: Tan-colored silicic tephra from unit 4 of the kipuka test pit. Collected from 50-61 cm below the surface (figure 35). The source of the tephra was presumed at the time of sampling to have been Mount Mazama. While AAS characterization of a bulk sample proved inconclusive, EPMA characterization of the tephra confirmed Mount Mazama as the original geologic source of the sampled tephra unit. The presence of numerous rootlets in the tephra unit suggests that this is a paleosol and is probably a B horizon (immediately underlies BELKC-6). The sample was heavily contaminated with organic matter, probably accounting for the low overall AAS totals (loss through ignition). From the same sample location as BELKC-4, BELKC-5, and BELKC-6.

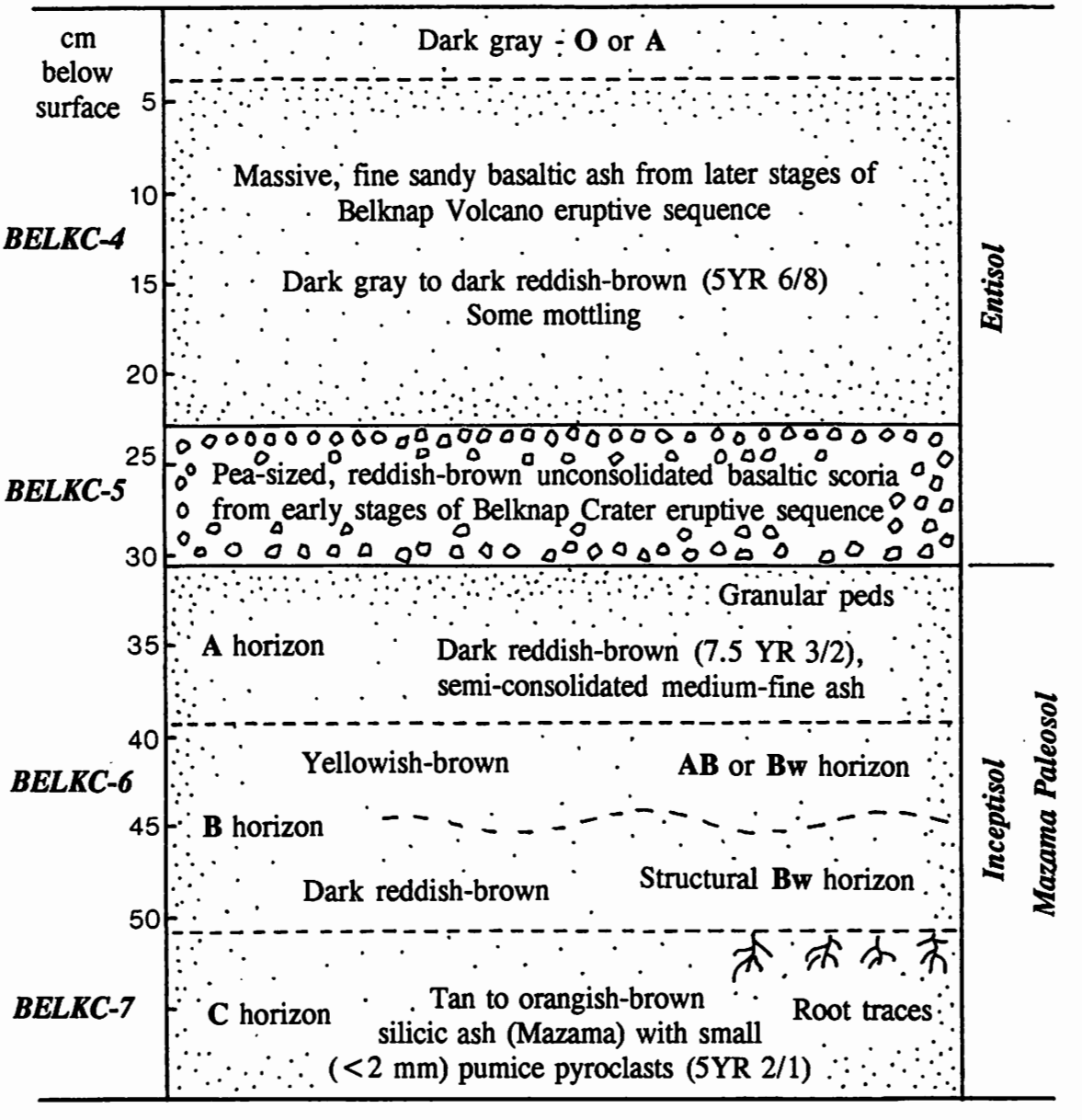

Figure 35. Test pit profile at the Belknap Volcano kipuka test pit. This kipuka, an earlier island surrounded by more recent basalt flows from Little Belknap Crater, is the southernmost of two kipukas crossed by the Pacific Crest Trail immediately north of the McKenzie Pass Highway.

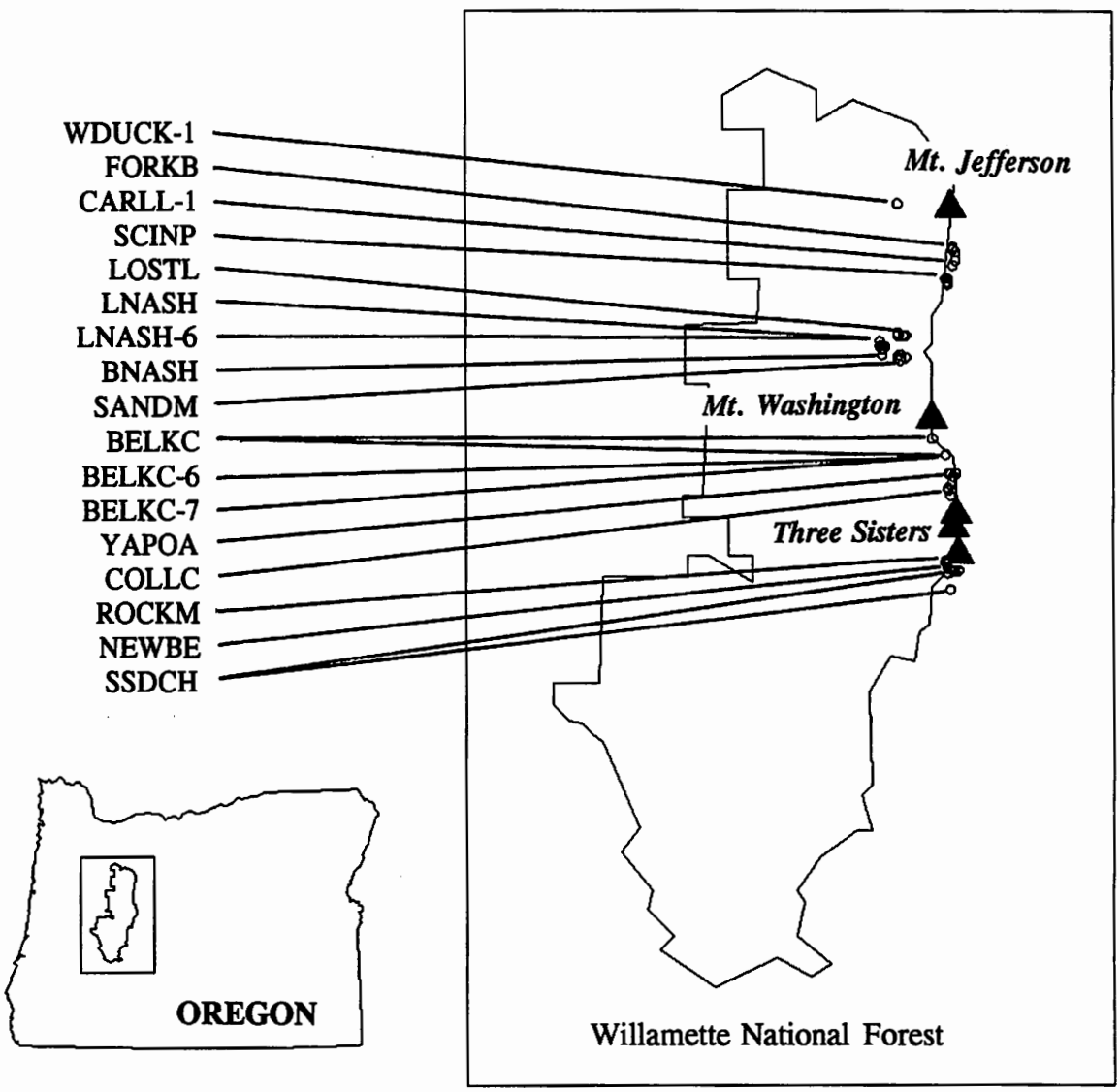

Figure 36. Location of tephra samples collected for geochemical characterization studies. Mazama sample localities are not shown.

BELKC-8 BELKNAP CRATER TEPHRA

Location: Sec.12, T.15S., R.7½E; Deschutes County.
USGS Map: Mt. Washington (1988)
Description: Basaltic ash and lapilli from a shallow test pit on the lower eastern slopes of Belknap Volcano. Located about 100 m west of and overlain by a lava flow from Little Belknap Crater.

BNASH-1 NASH CRATER SCORIA

Location: Sec.22, T.13S., R.7E.; Linn County.
USGS Map: Santiam Junction (1988)
Description: Basaltic ash and scoria collected from the south end of a roadcut in U.S. Forest Service Road #2676 at the northwestern base of Nash Crater.

BNASH-2 NASH CRATER SCORIA

Location: Sec.22, T.13S., R.7E.; Linn County.
USGS Map: Santiam Junction (1988)
Description: Basaltic ash and scoria collected at the north end of a roadcut on U.S. Forest Service Road #2676 at the northwestern base of Nash Crater.

BNASH-3 NASH CRATER TEPHRA

Location: Sec.22, T.13S., R.7E.; Linn County
USGS Map: Santiam Junction (1988)
Description: Basaltic ash and scoria collected about 0.5 km south of Highway 20-126 on U.S. Forest Service Road #2676. Probable Nash Crater source. Appears to be overlain by basaltic tephra from Little Nash Crater.

CARLL-1 MAZAMA TEPHRA

Location: Sec.28, T.11S, R.8E.; Deschutes County.
USGS Map: Marion Lake (1988)
Description: Tan to orange-colored silicic ash and small pumice lapilli exposed in a trail cut about 1 km northeast of Carl Lake. A 14 cm-thick deposit of this tephra, presumed to be from Mount Mazama when sampled, is exposed in the trail cut and overlies local colluvial deposits. The silicic tephra is overlain by about 20 cm of basaltic tephra from nearby Forked Butte. Later EPMA characterization of the ash confirmed Mount Mazama as the original source.

COLLC-1 COLLIER CONE TEPHRA

Location: Sec.17, T.16S., R.8½E.; Lane County.
USGS Map: North Sister (1988)
Description: Basaltic ash collected next to the Collier Glacier Viewpoint Trail directly west of Collier Cone.

COLLC-2 COLLIER CONE TEPHRA

Location: Sec.8, T.16S., R.8½E.; Lane County.
USGS Map: North Sister (1988)
Description: Basaltic ash collected from slightly reworked surficial deposits next to the Pacific Crest Trail between Collier Cone and Minnie Scott Spring. Located about 0.7 km northwest of Collier Cone.

COLLC-3 COLLIER CONE TEPHRA

Location: Sec.8, T.16S., R.8½E.; Lane County.
USGS Map: North Sister (1988)
Description: Basaltic ash collected from surficial deposits about 100 m east of the Pacific Crest Trail at Minnie Scott Springs. Located 1 km north-northwest of Collier Cone.

COLLC-4 COLLIER CONE TEPHRA

Location: Sec.8, T.16S., R.8½E.; Lane County.
USGS Map: North Sister (1988)
Description: Basaltic ash collected from surficial deposits about 100 m northeast of Minnie Scott Spring at an unnamed lake not shown on local maps. Located about 1.1 km north-northwest of Collier Cone.

FORKB-1 FORKED BUTTE TEPHRA

Location: Sec.21, T.11S., R.8E.; Deschutes County.
USGS Map: Marion Lake (1988)
Description: Basaltic ash collected from upper 5 cm of surficial deposits located at Junction Lake.

FORKB-2 FORKED BUTTE TEPHRA

Location: Sec.21, T.11S., R.8E.; Deschutes County.
USGS Map: Marion Lake (1988)
Description: Basaltic tephra collected from surficial cinder field deposits located about 1 km southwest of Forked Butte. Adjacent to and overlain by lava flows from Forked Butte.

FORKB-3 FORKED BUTTE TEPHRA

Location: Sec.21, T.11S., R.8E.; Deschutes County.
USGS Map: Marion Lake (1988)
Description: Basaltic tephra collected from surficial cinder field deposits located about 1 km west-southwest of Forked Butte. Adjacent to and overlain by lava flows from Forked Butte.

FORKB-4 FORKED BUTTE TEPHRA

Location: Sec.21, T.11S., R.8E.; Deschutes County.
USGS Map: Marion Lake (1988)
Description: Basaltic tephra collected from surficial cinder field deposits located about 0.5 km west of Forked Butte. Adjacent to and overlain by lava flows from Forked Butte.

LNASH-1 LITTLE NASH CRATER TEPHRA

Location: Sec.15, T.13S., R.7E.; Linn County.
USGS Map: Santiam Junction (1988)
Description: Basaltic ash and scoria lapilli collected from surficial deposits 50 m north of Highway 20-126 and about 200 m east of the base of Little Nash Crater.

LNASH-2 LITTLE NASH CRATER SCORIA

Location: Sec.15, T.13S., R.7E.; Linn County.
USGS Map: Santiam Junction (1988)
Description: Basaltic scoria lapilli collected from an intact section of the quarried crater of Little Nash Crater. Same sample location as LNASH-3.

LNASH-3 LITTLE NASH CRATER SCORIA

Location: Sec.15, T.13S., R.7E.; Linn County.
USGS Map: Santiam Junction (1988)
Description: Basaltic scoria lapilli collected from an intact section of the quarried crater of Little Nash Crater. Collected from about 5 m above LNASH-2.

LNASH-5 LITTLE NASH CRATER TEPHRA

Location: Sec.15, T.13S., R.7E.; Linn County.
USGS Map: Santiam Junction (1988)
Description: Basaltic ash collected from the top of a road cut on Highway 22 directly north of the exit from the Little Nash Crater cinder quarry. Overlies tephra from Nash Crater and Mount Mazama. Same sampling location as LNASH-6 (plate 11).

LNASH-6 MAZAMA TEPHRA

Location: Sec.15, T.13S., R.7E.; Linn County.
USGS Map: Santiam Junction (1988)
Description: Tan-colored silicic ash and small pumice lapilli collected from the center of a road cut directly across from the exit of the Little Nash Crater cinder quarry on Highway 22. Overlain by tephra from Little Nash Crater and Nash Crater. The tephra was shown through EPMA analysis to have originated from Mount Mazama. The Mazama tephra directly overlies glacial deposits. Same sampling location as LNASH-5 (plate 11).

LOSTL-2 LOST LAKE GROUP TEPHRA

Location: Sec.21, T.13S., R.8E.; Linn County.
USGS Map: Santiam Junction (1988)
Description: Basaltic ash and cinders collected from the southernmost Lost Lake cinder cone. From a roadcut adjacent to the Santiam Highway and directly across from Jackpine Road.

LOSTL-3 LOST LAKE GROUP TEPHRA

Location: Sec.21, T.13S., R.8E.; Linn County.
USGS Map: Santiam Junction (1988)
Description: Basaltic ash and cinders collected in a Santiam Highway roadcut across the highway from the southernmost cone in the Lost Lake Group. The sample site is located just east of Jackpine Road on the south side of the highway.

LOSTL-4 LOST LAKE GROUP TEPHRA

Location: Sec.21, T.13S., R.8E.; Linn County.
USGS Map: Santiam Junction (1988)
Description: Basaltic ash and lapilli collected about 1 m below the surface in a roadcut in the campground road on the north side of Lost Lake.

LOSTL-5 LOST LAKE GROUP TEPHRA

Location: Sec.21, T.13S., R.8E.; Linn County.
USGS Map: Santiam Junction (1988)
Description: Basaltic ash and lapilli collected 3-4 m below the surface in a roadcut on the Santiam Highway about 1 km east of the Lost Lake Campground turnoff.

MAZA-2 MAZAMA TEPHRA

Location: Sec.21, T.28S., R.6E.; Douglas County,
USGS Map: Diamond Lake (1985)
Description: Silicic airfall pumice lapillus collected on the surface adjacent to Highway 138 at the Mount Thielsen trailhead.

MAZA-5 MAZAMA TEPHRA

Location: Sec.25, T.32S., R.6E.; Jackson County.
USGS Map: Maklaks Crater (1985)
Description: Silicic airfall pumice lapillus collected on the surface adjacent to Highway 62.

MAZA-8 MAZAMA TEPHRA

Location: Sec.8, T.27S., R.8E.; Klamath County.
USGS Map: Muttonchop Butte (1967)

Description: Silicic airfall pumice lapillus collected on the surface near Highway 97 about 5 km north of Chemult.

MAZA-9 MAZAMA TEPHRA

Location: Sec.28, T.22S., R.10E.; Deschutes County.
USGS Map: La Pine (1981)
Description: Silicic airfall pumice lapilli collected on the surface adjacent to Highway 97 about 2 km south of La Pine.

NEWBE-1 NEWBERRY OBSIDIAN FLOW, DEVILS HILL DOME CHAIN

Location: Sec.24, T.17S., R.8E.; Deschutes County.
USGS Map: South Sister (1988)
Description: Silicic airfall pumice lapillus collected on the surface immediately east of the eastern margin of the Newberry Obsidian Flow. Collected on the east side of Fall Creek at the southern end of Green Lake.

ROCKM-1 ROCK MESA TEPHRA

Location: Sec.33, T.17S., R.8E.; Deschutes County.
USGS Map: South Sister (1988)
Description: Silicic airfall pumice lapillus collected on the surface about 0.5 km south of the Rock Mesa obsidian flow next to the Moraine Lake - Wickiup Plain Trail. The most vesicular airfall lapilli at this site were selected (co-occurred with obsidian, rhyodacite fragments, and microvesicular rhyolite).

ROCKM-2 ROCK MESA TEPHRA

Location: Sec.5, T.18S., R.8E; Deschutes County.
USGS Map: South Sister (1988)
Description: Silicic airfall pumice lapillus collected on the surface about 1 km south of LeConte Cone and 1.5 km southwest of the Rock Mesa obsidian flow.

ROCKM-3 ROCK MESA TEPHRA

Location: Sec.32, T.17S., R.8E.; Deschutes County.
USGS Map: South Sister (1988)
Description: Silicic airfall pumice lapillus collected on the surface of the southwestern base of LeConte Cone about 150 m west of the Rock Mesa obsidian flow.

ROCKM-4 ROCK MESA TEPHRA

Location: Sec.5, T.18S., R.8E.; Deschutes County.
USGS Map: South Sister (1988)
Description: Silicic airfall pumice lapillus collected on the surface next to the Moraine Lake - Wickiup Plain Trail about 1.1 km east of the Rock Mesa obsidian flow.

SANDM-1B SAND MOUNTAIN TEPHRA

Location: Sec.1, T.14S., R.7E.; Linn County.
USGS Map: Santiam Junction (1988)
Description: Basaltic ash collected from the C horizon in a shallow test pit next to the junction of the Old Santiam Wagon Road immediately northeast of Sand Mountain.

SANDM-2 SAND MOUNTAIN TEPHRA

Location: Sec.1, T.14S., R.7E.; Linn County.
USGS Map: Santiam Junction (1988)
Description: Basaltic ash collected from the C horizon in a shallow test pit next to the Forest Service road that runs north-south directly east of Sand Mountain.

SANDM-3 SAND MOUNTAIN TEPHRA

Location: Sec.3, T.14S., R.7½E.; Linn County.
USGS Map: Santiam Junction (1988)
Description: Basaltic ash collected from the C horizon in a shallow test pit next to an abandoned landing strip on the road from Big Lake to Sand Mountain.

SANDM-5 SAND MOUNTAIN TEPHRA

Location: Sec.26, T.13S., R.7½E.; Linn County.
USGS Map: Santiam Junction (1988)
Description: Basaltic ash collected from a road cut on the south side of the Santiam Highway at the Santiam Pass. Located directly across the road from the entrance road to the Pacific Crest Trail parking lot.

SCINP-1 SOUTH CINDER PEAK BREACHED CONE TEPHRA

Location: Sec.5, T.12S., R.8E.; Deschutes County.
USGS Map: Marion Lake (1988)
Description: Basaltic ash collected from the top few centimeters of the cinder field located immediately southeast of South Cinder Peak. Ash and cinders originated from a breached cinder cone located on the south flanks of South Cinder Peak. 16 cm of basaltic tephra overlies Mazama tephra at this location.

SCINP-2 SOUTH CINDER PEAK BREACHED CONE TEPHRA

Location: Sec.5, T.12S., R.8E.; Deschutes County.
USGS Map: Marion Lake (1988)
Description: Basaltic ash collected from the top few centimeters of the cinder field located southeast of South Cinder Peak. Located about 100 m southeast of SCINP-1 sample site.

SCINP-3 SOUTH CINDER PEAK BREACHED CONE TEPHRA

Location: Sec.5, T.12S., R.8E.; Deschutes County.
USGS Map: Marion Lake (1988)
Description: Basaltic ash collected from the top few centimeters of the cinder field located southeast of South Cinder Peak. Located about 100 m south of SCINP-2 sample site.

SCINP-4 SOUTH CINDER PEAK BREACHED CONE TEPHRA

Location: Sec.5, T.12S., R.8E.; Deschutes County.
USGS Map: Marion Lake (1988)
Description: Basaltic ash collected from the top few centimeters of the cinder field located southeast of South Cinder Peak. Located about 100 m southwest of SCINP-3 sample site.

SSDCH-1 DEVILS HILL DOME CHAIN TEPHRA

Location: Sec.35, T.17S., R.8E; Deschutes County.
USGS Map: Broken Top (1988)
Description: Silicic airfall pumice lapillus collected on the surface at the intersection of the Green Lake and Corral Lake trails.

SSDCH-3 DEVILS HILL DOME CHAIN TEPHRA

Location: Sec.35, T.17S., R.8E.; Deschutes County.
USGS Map: Broken Top (1988)
Description: Silicic airfall pumice lapillus collected on the surface at the intersection of the Green Lake and Moraine Lake trails.

SSDCH-6 DEVILS HILL DOME CHAIN TEPHRA

Location: Sec.11, T.18S., R.8E.; Deschutes County.
USGS Map: Broken Top (1988)
Description: Silicic airfall pumice lapillus collected at the top a roadcut on the Cascade Lakes Highway about 200 m east of the southernmost dome. An excellent exposure of near-vent deposits is also found at this location.

WDUCK-1 WOODDUCK SITE COMPLEX SOIL

Location: Sec.25, T.10S., R.7E.; Linn County.
USGS Map: Mt. Bruno (1988)
Description: Soil sample from a deposit 40-80 cm below the surface at the Woodduck archaeological Site Complex. The sample was collected about 50 cm below the surface. Small pumice lapilli (<2 mm) and silicic ash of Mazama origin are easily identifiable under low magnification (x15-x30). EPMA characterization of glass tephra shards in the soil confirmed Mount Mazama as the source of the pyroclasts.

YAPOA-1 YAPOAH CRATER TEPHRA

Location: Sec.4, T.15S., R.8E.; Deschutes County.
USGS Map: North Sister (1988)
Description: Ash to lapilli-sized basaltic tephra collected on the surface adjacent to the Pacific Crest Trail about 1 km northeast of Yapoah Crater. The tephra was originally thought to have originated from Yapoah Crater, though the ash overlies Yapoah Crater flows and may have come from the more recent Collier Cone eruptions. Chemical and mineralogical similarities between Collier Cone and samples initially attributed to Yapoah Crater support this conclusion.

YAPOA-3 YAPOAH CRATER TEPHRA

Location: Sec.4, T.16S., R.8½E.; Deschutes County.
USGS Map: North Sister (1988)
Description: Ash to lapilli-sized basaltic tephra collected on the surface adjacent to the Pacific Crest Trail and immediately west of Yapoah Crater. The tephra was originally thought to have originated from Yapoah Crater, though the ash overlies Yapoah Crater flows and may have come from the more recent Collier Cone eruptions. Chemical and mineralogical similarities between Collier Cone and samples initially attributed to Yapoah Crater support this conclusion.

YAPOA-4 YAPOAH CRATER TEPHRA

Location: Sec.4, T.16S., R.8½E.; Deschutes County.
USGS Map: North Sister (1988)
Description: Ash to lapilli-sized basaltic tephra mantling Yapoah Crater lava flows. Collected on the surface of the flows adjacent to the Pacific Crest Trail and about 0.5 km northeast of Yapoah Crater. The tephra was originally thought to have originated from Yapoah Crater, though the ash overlies the Yapoah Crater flows and may come from the more recent eruptions of Collier Cone. Chemical and mineralogical similarities between Collier Cone and samples initially attributed to Yapoah Crater support this conclusion.

YAPOA-6 YAPOAH CRATER TEPHRA

Location: Sec.33, T.15S., R.8E.; Deschutes County.
USGS Map: North Sister (1988)
Description: Basaltic ash collected about 1.2 km northeast of Yapoah Crater next to the Pacific Crest Trail where the trail drops off the Yapoah lava flows. The slightly reworked tephra was originally thought to have originated from Yapoah Crater, though the ash may also have been generated from the more recent Collier Cone eruptions. Chemical and mineralogical similarities between Collier Cone and samples initially attributed to Yapoah Crater support this conclusion.

	WET			DRY			GEOSOURCE
SAMPLE	*Hue*	*Value*	*Chroma*	*Hue*	*Value*	*Chroma*	*Geologic Source*
BELKC-4	5YR	2.5/	2	5YR	4/	4	Belknap Crater
BELKC-5	5YR	6/	8	5YR	5/	4	Belknap Crater (1)(7)
BELKC-6	5YR	3/	2	5YR	3/	3	Mazama
BELKC-7	7.5YR	5/	8	5YR	6/	6	Mazama (2)
BELKC-9	5YR	2.5/	1	5YR	5/	3	Belknap Crater
BNASH-1	7.5YR	2/	0	5YR	3/	1	Nash Crater
BNASH-2	5YR	3/	3	5YR	3/	2	Nash Crater
BNASH-3	7.5YR	2/	0	7.5YR	3/	2	Nash Crater
CARLL-1	5YR	5/	8	7.5YR	7/	6	Mazama (3)
COLLC-1	7.5YR	2/	0	5YR	3/	1	Collier Cone
COLLC-2	5YR	3/	1	5YR	4/	1	Collier Cone
COLLC-3	5YR	3/	2	5YR	4/	2	Collier Cone
COLLC-4	5YR	2.5/	2	7.5YR	3/	2	Collier Cone (4)
FORKB-1	5YR	4/	4	5YR	5/	6	Forked Butte (5)
FORKB-2	5YR	3/	4	5YR	5/	6	Forked Butte
FORKB-3	5YR	3/	3	5YR	4/	4	Forked Butte
FORKB-4	5YR	4/	4	5YR	5/	6	Forked Butte
LNASH-1	5YR	2.5/	2	5YR	3/	4	Little Nash C.
LNASH-2	5YR	3/	3	5YR	4/	3	Little Nash C.
LNASH-3	5YR	3/	4	5YR	4/	4	Little Nash C.
LNASH-5	5YR	3/	3	5YR	3/	2	Little Nash C. (5)(6)
LNASH-6	7.5YR	5/	6	7.5YR	6/	4	Mazama
LOSTL-2	5YR	3/	3	5YR	5/	6	Lost Lake Group
LOSTL-3	7.5YR	2/	0	7.5YR	2/	0	Lost Lake Group (7)
LOSTL-4	5YR	3/	2	5YR	3/	4	Lost Lake Group (5)
LOSTL-5	7.5YR	2/	0	7.5YR	3/	0	Lost Lake Group (8)
MAZA-2	7.5YR	6/	6	7.5YR	7/	4	Mazama
MAZA-5	7.5YR	4/	2	5YR	6/	1	Mazama
MAZA-8	7.5YR	6/	4	7.5YR	7/	3	Mazama
MAZA-9	7.5YR	7/	3	7.5YR	8/	2	Mazama
NEWBE-1	5YR	6/	1	5YR	7/	1	DH Dome Chain
ROCKM-1	7.5YR	6/	2	7.5YR	7/	2	Rock Mesa
ROCKM-2	7.5YR	7/	2	7.5YR	8/	2	Rock Mesa
ROCKM-3	7.5YR	7/	2	7.5YR	8/	2	Rock Mesa
ROCKM-4	7.5YR	6/	2	7.5YR	7/	2	Rock Mesa
SANDM-1B	5YR	3/	1	5YR	3/	3	Sand Mountain (9)
SANDM-2	5YR	2.5/	2	5YR	3/	2	Sand Mountain
SANDM-3	5YR	2.5/	1	5YR	3/	2	Sand Mountain
SANDM-5	5YR	2.5/	2	5YR	3/	2	Sand Mountain (10)
SCINP-1	5YR	3/	3	5YR	4/	4	South Cinder Peak
SCINP-2	5YR	3/	3	5YR	5/	4	South Cinder Peak

Table 13. Munsell soil color designations for geological and archaeological tephra samples.

	WET			DRY			GEOSOURCE
SAMPLE	*Hue*	*Value*	*Chroma*	*Hue*	*Value*	*Chroma*	*Geologic Source*
SCINP-3	5YR	3/	3	5YR	4/	4	South Cinder Peak
SCINP-4	5YR	3/	3	7.5YR	4/	4	South Cinder Peak
SSDCH-1	5YR	6/	1	5YR	6/	1	DH Dome Chain
SSDCH-3	5YR	6/	1	5YR	7/	2	DH Dome Chain
SSDCH-6	6YR	6/	1	5YR	7/	1	DH Dome Chain
WDUCK-1	7.5YR	7/	3	7.5YR	8/	2	Mazama (11)
YAPOA-1	5YR	2.5/	1	5YR	4/	1	Yapoah C. (12)
YAPOA-3	5YR	3/	2	5YR	4/	3	Yapoah C. (5)(12)
YAPOA-4	5YR	2.5/	2	5YR	4/	1	Yapoah C. (5)(12)
YAPOA-6	5YR	3/	3	5YR	4/	2	Yapoah C. (12)(13)

NOTES:

(1) Color represents dominant fraction; varies from 5YR 5/4 - 10YR 5/4 (dry)
(2) Color represents dominant fraction; varies from 5YR 6/6 - 7.5YR 7/6 (dry)
(3) Color represents dominant fraction; varies from 7.5YR 7/6 - 5YR 7/8 (dry)
(4) Color represents dominant fraction; varies from 7.5YR 3/2 - 5YR 3/3 (dry)
(5) Salt and pepper
(6) Color represents dominant fraction; varies from 5YR 3/2 - 5YR 4/4 (dry)
(7) Scoria
(8) Color represents dominant fraction; varies from 7.5YR 3/0 - 5YR 3/1 (dry)
(9) Color represents dominant fraction; varies from 5YR 3/3 - 5YR 3/4 (dry)
(10) Color represents dominant fraction only; varies from 5YR 3/2 - 7.5YR 3/3 (dry)
(11) Color of small pumice lapilli only
(12) May have originated from Collier Cone instead of Yapoah Crater
(13) Color represents dominant fraction; varies from 5YR 4/2 - 7.5 YR 4/2 (dry)

Table 13 (Continued). Munsell soil color designations.

APPENDIX FIVE

Microcomputer Software and Hardware

APPENDIX 5: MICROCOMPUTER SOFTWARE AND HARDWARE USED IN THE TEPHRA PROJECT

This appendix is a direct reflection of the increasing dependence of researchers on microcomputers and their related software. We couldn't have done it without the temperamental little marvels. All computer-based analysis of data, as well as the production of the Tephra Overview, was handled with an IBM XT-compatible equipped with a 65MB hard disk, an 8087 coprocessor, a mouse, and 1MB of extended memory. The overview was printed with an HPIIP LaserJet with 1MB RAM installed. Most of the photographs in the overview were scanned with an HP ScanJet and printed (with WordPerfect 5.1) on the HPIIP laser printer.

The following IBM PC software was used for the many computer-based phases of data analysis and report production:

AS-EASY-AS 4.0 *
Trius, Inc. ▪ 231 Sutton St., Suite 2D-31 ▪ North Andover, MA 01845

This spreadsheet is included with supplementary diskette files in the back pocket of the Tephra Overview. The following AS-EASY-AS files and worksheets are located on the supplementary data disk:

ASEASY.EXE	Main Program
ASEASY.MSG	Opening Message Screen
ASEASY.HLP	Help File
ASEASY.PRT	Printer Control File
HTREE.EXE	Runs Help File
LANDSCAPE.EXE	Sideways-Like Add-On
READ.ME	Start-Up Instructions
ZOOM.EXE	Add-On Accessory
AAS.WKS	AAS (Atomic Absorption) Geochemical Data
EPMA.WKS	EPMA (Electron Microprobe) Geochemical Data

To run the spreadsheet and load the data files:

1. Insert the Supplementary Data disk.
2. Type GO, then <RETURN>.
3. Type 2 at the introduction screen to load the spreadsheet.
4. Press the backslash (/) key to activate up the menu window.
5. Press F (for-File) to bring up the File Menu.
6. Press R (for Retrieve) - use the cursor to move the highlighted cell to the name of the worksheet you want to load (AAS.WKS or EPMA.WKS) and press <RETURN>.

To exit the spreadsheet, press the backslash key (/), then E (for Exit), then Y (for Yes). For help while in the spreadsheet, use the F1 key.

CALIB 2.0 (Quaternary Isotope Laboratories, University of Washington) *
Quaternary Isotope Laboratories ▪ University of Washington ▪ Seattle, WA
Dendrochronologic calibration of radiocarbon dates.

GPP (Geochemical Program Package)
Center for Volcanology ▪ University of Oregon ▪ Eugene, OR 97403
Exploratory data analysis of geochemical data.

MVSP (Multivariate Statistical Package) 2.0 *
Warren L. Kovach ▪ Institute of Earth Studies ▪ University College of Wales ▪ Aberystwyth, Wales SY23 3DB ▪ U.K.
Cluster analysis and dendrograms for geochemical data analysis.

NCSS (Number Cruncher Statistical System) 5.1
Jerry L. Hintze ▪ 865 East 400 North ▪ Kaysville, UT 84037
General statistical and exploratory data analysis of geochemical data.

PIZAZZ PLUS
Application Techniques, Inc. ▪ 10 Lomar Park Drive ▪ Pepperell, MA 01463
Rescaling and printing of captured screen images.

QUATTRO PRO 2.0
Borland ▪ 1800 Green Hills Road ▪ Scotts Valley, CA 95067
Spreadsheet used for the tabulation and basic statistical analysis of all geochemical data. The graphics capabilities of the spreadsheet were used for the production of many of the scatterplots and ternary plots (see TRIANGLE.WK1).

SIDEWAYS 3.21
Funk Software ▪ 222 Third St. ▪ Cambridge, MA 02142
Printing of spreadsheet tables with laser printer.

SURFER 4.05
Golden Software ▪ P.O. Box 281 ▪ Golden, CO 80402
Perspective diagrams (Crater Lake images).

TRIANGLE.WK1 *
Peter S. Mustard ▪ Geological Survey of Canada ▪ 100 West Pender Street ▪ Vancouver, B.C. ▪ Canada
Spreadsheet layout and macros used with Quattro Pro to produce ternary plots of chemical data (Mustard and Richardson, 1990).

WORDPERFECT 5.1
WordPerfect Corporation ▪ 1555 N. Technology Way ▪ Orem, UT ▪ 84057
Word processing and overall production of the overview (including the printing of all graphics images).

* Public domain or shareware software

Oregon Tephra Bibliography Information System

We have also included an on-disk indexed bibliography for Oregon tephra sources. This bibliography was developed independently from the investigation reported here and is included to provide an additional resource for Willamette National Forest tephra researchers (Skinner, 1990). The files for the Oregon Tephra Bibliography are located on the 3-1/2" supplementary data disk in the back of the Tephra Overview.

To use the Oregon Tephra Bibliography, insert the diskette, type GO, then <RETURN>. This will load a menu-driven shell from which the bibliography, as well as the supplementary data files previously described, can be loaded.

APPENDIX SIX

Interlaboratory Geochemical Data

APPENDIX 6: INTERLABORATORY GEOCHEMICAL COMPARISON

INTERLABORATORY AND INTER-TECHNIQUE COMPOSITIONAL VARIATION OF MAZAMA TEPHRA

Considerable major and trace element geochemical data for silicic volcanic tephra deposits found within the Willamette National Forest are available in the published literature (see Skinner, 1990, for a complete listing). This is particularly true for the long-studied and often-analyzed Mazama tephra. In the brief investigation reported in this appendix, we asked the following question: Can this already available geochemical database be used for comparison with geochemical values from future geochemical tephra studies? Or, do significant variations exist among different laboratories and analytical methods?

Our investigation of interlaboratory and inter-technique variations was not meant to be extensive or comprehensive, but was meant only to be exploratory in nature. In an attempt to provide us with enough information to answer these questions, we took a brief look at a relatively small data set from a single source of tephra, Mount Mazama.

Previous interlaboratory and intermethod comparisons of major and trace element data demonstrate that significant differences may exist in abundances determined by different analytical methods and different laboratories (Brenner et al., 1976; Yellin et al., 1978; Sarna-Wojcicki et al., 1979; Tilling et al., 1987). Only through empirical quantitative comparisons among laboratories and methods, though, can variations be determined. The correspondence between laboratories and methods is quite variable; some elements may show a high degree of correlation while other elements may not. In a recent interlaboratory comparison of X-ray fluorescence analyses of tephra from El Chicón Volcano, Mexico, variation between analytical results ranged from 0 to nearly 50 percent. Different sample preparation techniques and different calibration procedures are thought to be significant variables affecting the differences that may be present among laboratories.

Comparison of Mazama Literature Values

Our source of data for the comparison came from the results of the AAS and EPMA analyses reported in this project, from a previous INAA tephra study that we had carried out (Skinner and Radosevich, 1989), from an early INAA study of Mazama tephra (Theisen et al., 1968), from XRF studies (Westgate and Dreimanis, 1967; Bruggman et al., 1989; Carrara, 1989), and from several electron microprobe studies of Mazama tephra (Westgate et al., 1969; Smith and Westgate, 1969; Lemke et al., 1975; Davis, 1985; Federman, 1985; Bruggman et al., 1989). The data used in this analysis appear in table 15.

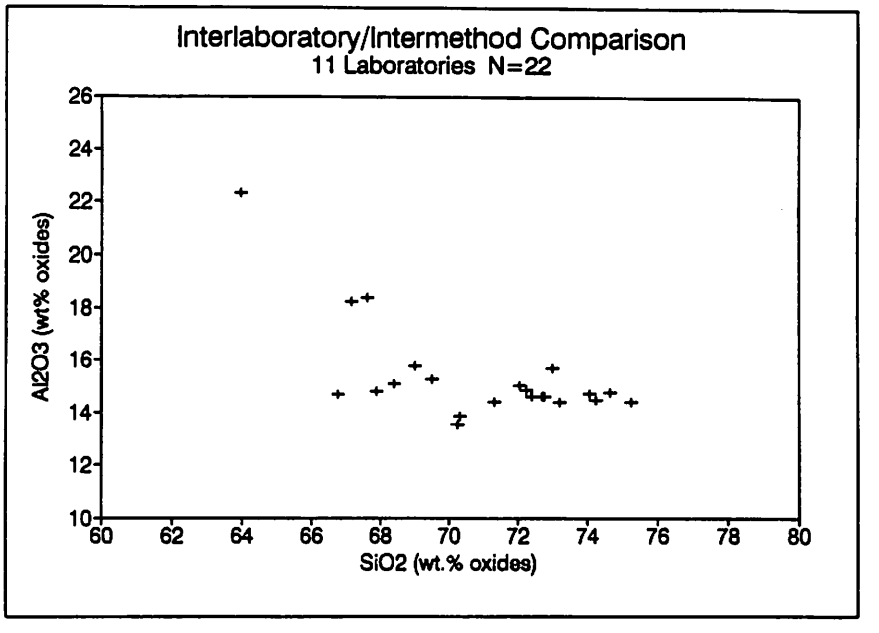

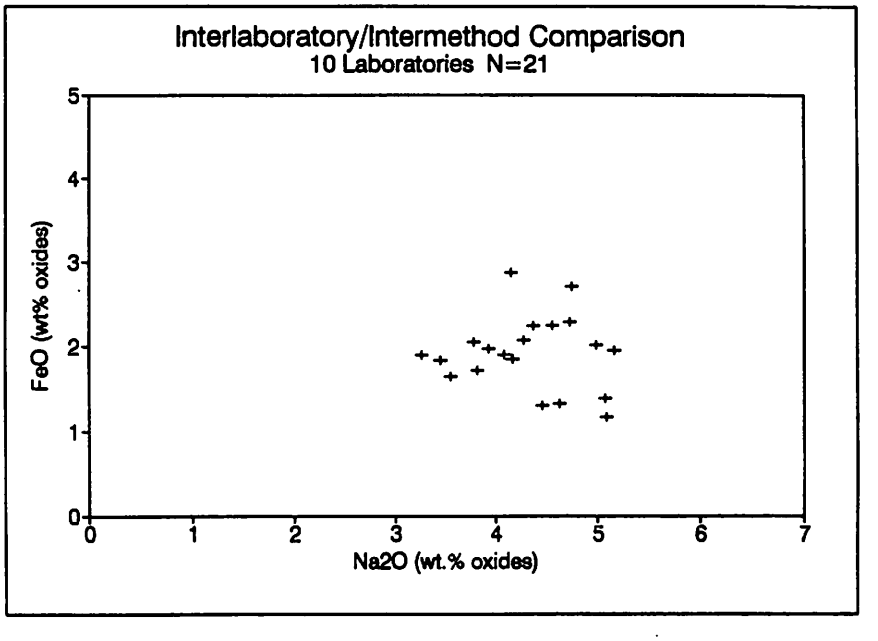

Figure 37. Scatterplots of major element abundances for Mazama tephra analyzed by different laboratories. The considerable chemical variation that is graphically illustrated in the scatterplots is introduced not by true chemical variation in the Mazama tephra but by interlaboratory variation.

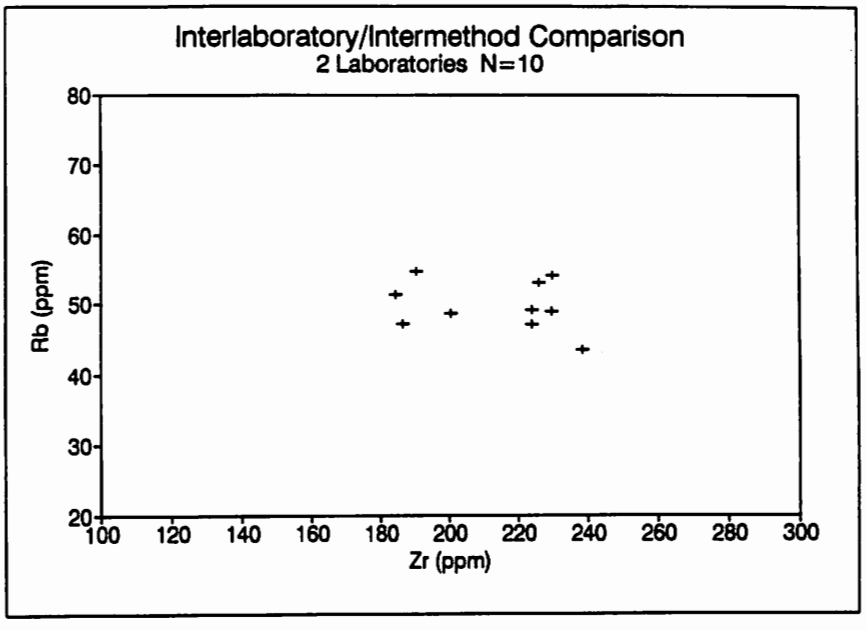

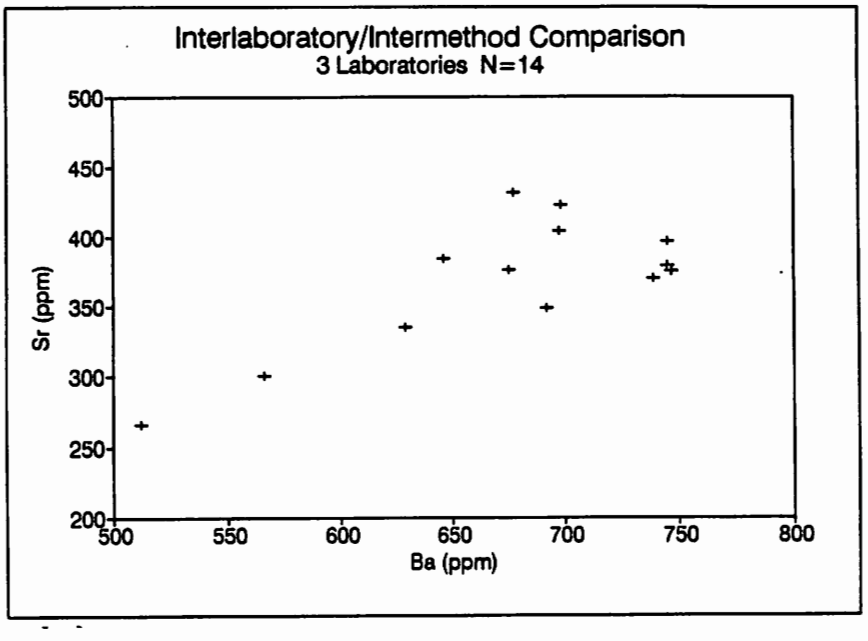

Figure 38: Scatterplots of Mazama tephra trace element values determined by multiple analytical laboratories). As with the major element results of the previous figure, significant compositional variability due to interlaboratory variation is illustrated.

Graphical comparison of major and trace element abundances indicates that considerable variation is found in literature values for volcanic tephra originating from a single source, Mount Mazama (figures 37 and 38). Differences in major and trace element values of 10 to 20 percent are common and even greater degrees of variability are found for some elements. These differences could present major problems when one attempts to correlate samples of unknown provenience with known sources and could easily lead to the source misidentification of samples. Any transformations of the data (such as normalization to 100 percent) must also be taken into account when comparing analytical results from different laboratories. Because of this demonstrable variation in analytical results, we recommend that the interlaboratory or intermethod comparison of geochemical data be undertaken only after systematic comparisons of results produced by participating laboratories.

Comparison of Oregon University Analytical Laboratories

We also compared results produced by three different analytical methods and three different laboratories at the University of Oregon and Oregon State University. INAA data from an earlier experiment conducted with a research grant from the Radiation Center, Oregon State University, was compared with AAS results from the Atomic Absorption Laboratory (Center for Volcanology, University of Oregon) and EPMA results from the Electron Microprobe Laboratory (Earth Sciences Department, University of Oregon). All data used for comparison can be found in table 15 and the the current report. Several of the analyzed samples were pumice lapilli collected at the same sampling site (these have identical sample numbers in table 15). This preliminary assessment (with an admittedly small sample size) was designed only to provide some initial guidelines for comparing geochemical data produced by the different Oregon laboratories.

The degree of interlaboratory and intermethod comparability was assessed by determining the CV% (coefficient of variation) for each combination of pairs of shared elements between laboratories (table 14). Data for only two elements were shared among all three data sets. A CV% of less than 10 indicates that results for the designated elements are highly comparable between the different Oregon university analytical laboratories and analytical techniques. A CV% of greater than 20 indicates fairly low comparability. The coefficient of variation works best, however, for comparing samples with similar geochemical values. As a result, more interlaboratory variation was observed for SiO_2 and Ba values than is reflected in their relatively low CV%.

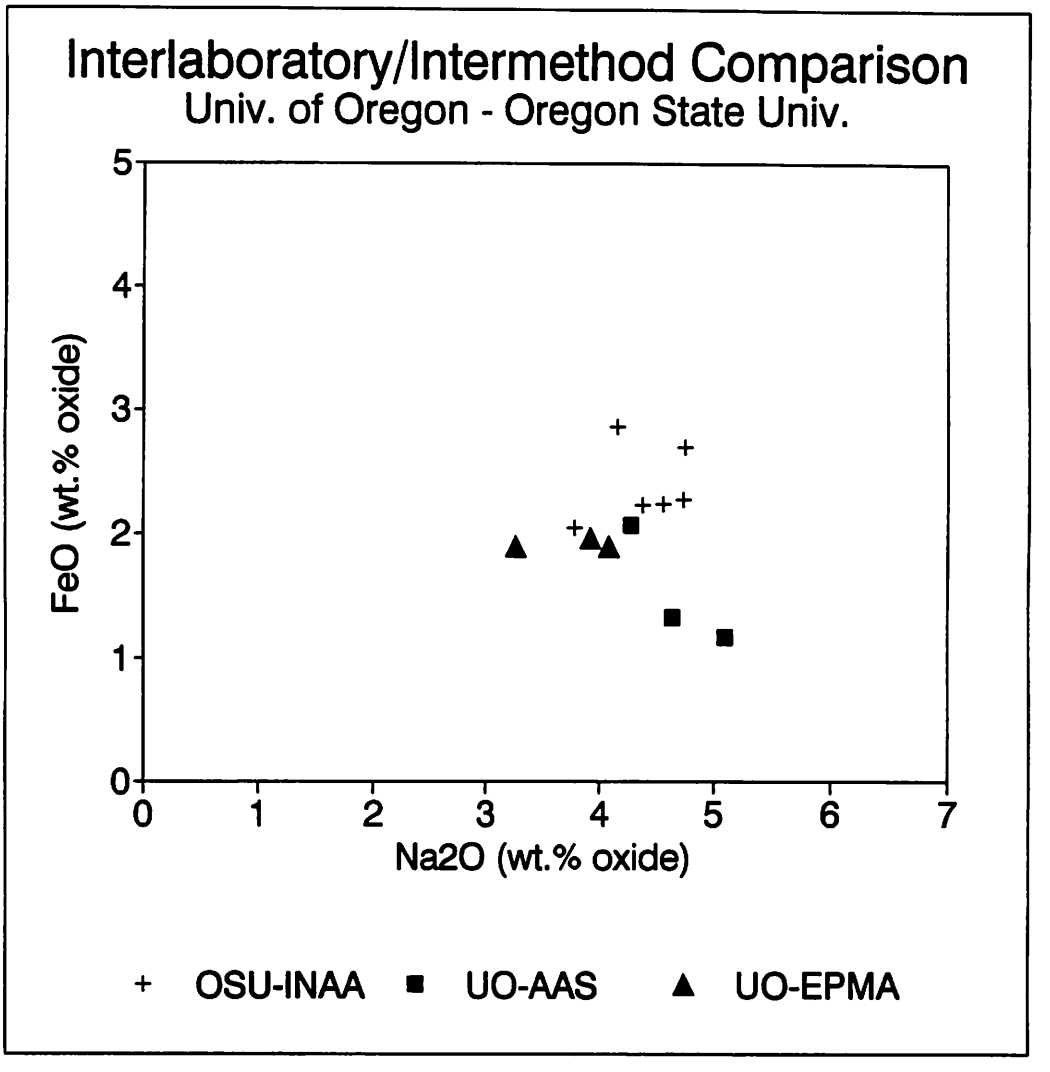

Figure 39. FeO plotted versus Na_2O in interlaboratory and intermethod comparison of Oregon university analytical laboratories. These two elements were the only ones shared by our tephra data sets from all three laboratories. While each technique individually produces internally consistent data (expected low intraunit variation), there is considerable variation among the different laboratories. See table 15 for original data.

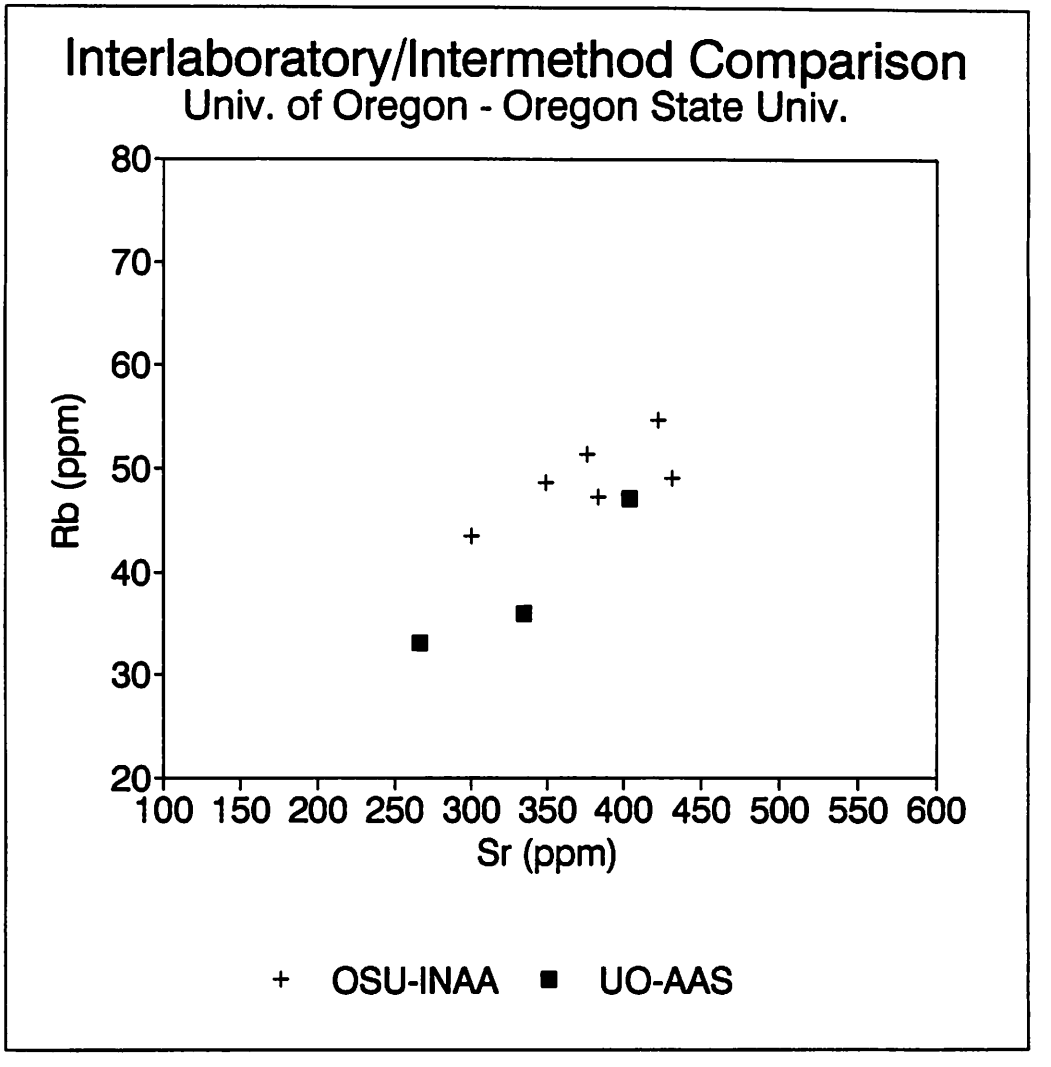

Figure 40: Rb plotted for Sr for Mazama tephra from Oregon university laboratories.

	OSU - INAA UO - AAS	OSU-INAA UO-EPMA	UO-AAS UO-EPMA	OSU-INAA UO-AAS UO-EPMA
SiO_2	-	-	5.6	-
Al_2O_3	-	-	15.8	-
FeO	28.4	14.5	22.6	25.3
MgO	-	-	30.3	-
CaO	-	-	21.3	-
Na_2O	8.6	11.0	14.1	11.6
K_2O	-	-	12.5	-
TiO_2	-	-	17.3	-
MnO	-	-	14.9	-
Co	32.9	-	-	-
Rb	13.8	-	-	-
Sr	14.0	-	-	-
Ba	9.3	-	-	-

Table 14. CV% for interlaboratory and intermethod comparison of geochemical analysis of Mazama Tephra from University of Oregon and Oregon State University laboratories.

Conclusions: Interlaboratory Comparison

We conclude that the use of geochemical data from different laboratories and different analytical techniques is an approach to avoid for most characterization studies. At its best, the amount of variation that is added by using multiple laboratory and technique sources is likely to make identification of discrete tephra sources difficult or uncertain. At its worst, tephra sources may be misidentified. The importance of controlling analytical intraunit variation is particularly important in geochemical characterization studies where the correlation of previously characterized sources with samples of unknown provenience is essential. We recommend that interlaboratory and intermethod data be used for characterization studies only when systematic studies of interlaboratory analytical variation have been conducted.

SAMPLE	MAZA-2	MAZA-4	MAZA-5	MAZA-7	MAZA-8	MAZA-9	MAZA-2	MAZA-5	MAZA-8	MAZA-9	MAZA-5	MAZA-8	MAZA-9	79C-012	79C-017
SIO2	-	-	-	-	-	-	63.99	69.00	67.18	67.63	74.27	74.08	74.66	68.40	69.50
AL203	-	-	-	-	-	-	22.33	15.78	18.26	18.38	14.47	14.72	14.76	15.10	15.30
FE203	-	-	-	-	-	-	1.45	2.30	2.30	2.04	-	-	-	2.85	2.81
FEO	2.86	2.05	2.28	2.70	2.24	2.23	2.07	1.17	1.17	1.33	1.90	1.97	1.90	-	-
MGO	-	-	-	-	-	-	0.62	0.89	0.89	0.90	0.45	0.47	0.45	0.84	0.79
CAO	-	-	-	-	-	-	2.16	2.49	2.49	2.60	1.53	1.59	1.63	2.39	2.10
NA20	4.15	3.78	4.73	4.75	4.56	4.37	4.28	5.09	5.09	4.63	4.09	3.92	3.26	5.18	5.07
K20	-	-	-	-	-	-	2.01	2.46	2.46	2.18	2.83	2.83	2.87	2.52	2.54
TIO2	-	-	-	-	-	-	0.61	0.55	0.55	0.54	0.40	0.38	0.41	0.47	0.48
P205	-	-	-	-	-	-	0.41	0.20	0.20	0.28	-	-	-	0.11	0.11
MNO	-	-	-	-	-	-	0.07	0.06	0.06	0.08	0.06	0.05	0.06	0.05	0.05
SC	8	6	6	7	7	7	-	-	-	-	-	-	-	7	6
CO	5	3	4	5	3	4	8	4	4	3	-	-	-	-	-
RB	43	51	55	49	49	47	33	47	47	36	-	-	-	53	54
CS	3	4	3	3	3	3	-	-	-	-	-	-	-	3	3
SR	300	376	422	431	349	384	266	404	404	335	-	-	-	396	370
BA	566	676	699	678	692	646	512	698	698	629	-	-	-	745	739
CE	43	40	40	46	45	45	-	-	-	-	-	-	-	42	40
ND	21	19	19	19	22	21	-	-	-	-	-	-	-	23	21
SM	5	4	4	5	5	5	-	-	-	-	-	-	-	5	5
YB	3	2	2	2	2	2	-	-	-	-	-	-	-	2	2
ZR	239	185	191	230	201	187	-	-	-	-	-	-	-	226	230
HF	7	6	6	6	6	6	-	-	-	-	-	-	-	5	6
TH	6	5	5	5	5	5	-	-	-	-	-	-	-	5	5
U	3	2	2	2	2	2	-	-	-	-	-	-	-	2	2
MAJOR	INAA	INAA	INAA	INAA	INAA	INAA	AAS	AAS	AAS	AAS	EPMA	EPMA	EPMA	EPMA	EPMA
TRACE	INAA	INAA	INAA	INAA	INAA	INAA	AAS	AAS	AAS	AAS	-	-	-	XRF/NAA	XRF/NAA
REFERENCE	1	1	1	1	1	1	2	2	2	2	3	3	3	4	4

REFERENCES:

1 SKINNER AND RADOSEVICH, 1989
2 CURRENT STUDY (AAS)
3 CURRENT STUDY (EPMA)
4 BRUGGMAN ET AL., 1989

AAS = ATOMIC ABSORPTION ANALYSIS
EPMA = ELECTRON PROBE MICROANALYSIS
INAA/NAA = INSTRUMENTAL NEUTRON ACTIVATION ANALYSIS
XRF = X-RAY FLUORESCENCE ANALYSIS

Table 15. Interlaboratory Geochemical Data for Mazama Tephra.

SAMPLE	79C-019	79C-025	1	EP 106	17	MAZAMA CX 1004	CX 9076	RM-5	CB-39	MAZAMA	MAZAMA	MAZAMA	60-7-29R
SIO2	67.90	66.80	72.07	75.25	73.20	- 71.34	70.26	70.35	72.40	72.27	72.80	72.70	73.00
AL203	14.80	14.70	15.04	14.40	14.40	- 14.40	13.55	13.88	14.60	14.85	14.60	14.60	15.70
FE203	2.76	2.74	1.18	-	-	- -	-	-	2.25	2.02	-	-	-
FEO	-	-	1.39	1.31	-	- 1.83	1.71	1.64	-	-	2.01	1.95	1.85
MGO	0.75	0.74	0.28	0.04	0.33	- 0.38	0.41	0.32	0.48	0.53	0.54	0.48	0.46
CAO	2.22	2.23	1.67	1.77	1.82	- 1.54	1.58	1.40	1.60	1.61	1.84	1.89	1.91
NA20	5.04	5.03	5.07	4.46	-	- 3.45	3.82	3.55	5.20	5.23	4.99	5.17	4.17
K20	2.48	2.47	2.72	2.04	2.96	- 2.69	2.62	2.60	2.70	2.67	2.75	2.73	2.79
TI02	0.46	0.46	0.48	0.15	0.57	- 0.44	0.37	0.34	0.44	0.49	0.43	0.41	0.38
P205	0.10	0.10	0.06	0.05	0.06	- -	-	-	-	0.06	-	-	-
MNO	0.05	0.05	0.03	0.03	-	- -	-	-	0.05	0.04	-	-	-
SC	6	6	-	-	-	13 -	-	-	-	-	-	-	-
CO	-	-	-	-	-	10 -	-	-	-	-	-	-	-
RB	47	49	-	-	-	39 -	-	-	-	-	-	-	-
CS	3	3	-	-	-	4 -	-	-	-	-	-	-	-
SR	379	375	-	-	-	- -	-	-	-	-	-	-	-
BA	745	747	-	-	-	837 -	-	-	-	-	-	-	-
CE	41	42	-	-	-	45 -	-	-	-	-	-	-	-
ND	23	22	-	-	-	16 -	-	-	-	-	-	-	-
SM	5	4	-	-	-	5 -	-	-	-	-	-	-	-
YB	2	2	-	-	-	3 -	-	-	-	-	-	-	-
ZR	224	224	-	-	-	- -	-	-	-	-	-	-	-
HF	6	6	-	-	-	6 -	-	-	-	-	-	-	-
TH	5	5	-	-	-	8 -	-	-	-	-	-	-	-
U	2	2	-	-	-	- -	-	-	-	-	-	-	-
MAJOR	EPMA	EPMA	-	EPMA	XRF	-	EPMA	EPMA	EPMA	EPMA	EPMA	XRF	XRF	EPMA
TRACE	XRF/NAA	XRF/NAA	-	-	-	INAA	-	-	-	-	-	-	-	-
REFERENCE	4	4	5	6	7	8	9	9	9	10	11	12	12	13

REFERENCES (CONTINUED):

5 MCBIRNEY, 1968
6 WESTGATE, SMITH AND NICHOLS, 1969; AVERAGE OF 58 SAMPLES
7 WESTGATE AND DREIMANIS, 1967
8 THEISEN ET AL., 1968
9 FEDERMAN, 1985
10 DAVIS, 1985
11 SMITH AND WESTGATE, 1969
12 CARRARA, 1989:61; AVERAGES OF SEVERAL ANALYSES
13 LEMKE ET AL., 1975

Table 15 (Continued). Interlaboratory Geochemical Data for Mazama Tephra.